INFORMATION TO USERS

This manuscript has been reproduced from the microfilm master. UMI films the text directly from the original or copy submitted. Thus, some thesis and dissertation copies are in typewriter face, while others may be from any type of computer printer.

The quality of this reproduction is dependent upon the quality of the copy submitted. Broken or indistinct print, colored or poor quality illustrations and photographs, print bleedthrough, substandard margins, and improper alignment can adversely affect reproduction.

In the unlikely event that the author did not send UMI a complete manuscript and there are missing pages, these will be noted. Also, if unauthorized copyright material had to be removed, a note will indicate the deletion.

Oversize materials (e.g., maps, drawings, charts) are reproduced by sectioning the original, beginning at the upper left-hand corner and continuing from left to right in equal sections with small overlaps.

ProQuest Information and Learning
300 North Zeeb Road, Ann Arbor, Mi 48106-1346 USA
800-521-0600

ESTIMATING THE FRESHWATER BUDGET OF HIGH-LATITUDE LAND AREAS

By

Laura C. Bowling

A dissertation submitted in partial fulfillment of the
requirements for the degree of

Doctor of Philosophy

University of Washington
2002

Program Authorized to Offer Degree:
Department of Civil and Environmental Engineering

UMI Number: 3072061

UMI Microform 3072061

ProQuest Information and Learning Company
300 North Zeeb Road
P.O. Box 1346
Ann Arbor, MI 48106-1346

In presenting this dissertation in partial fulfillment of the requirements for the Doctoral degree at the University of Washington, I agree that the Library shall make its copies freely available for inspection. I further agree that extensive copying of the dissertation is allowable only for scholarly purposes, consistent with "fair use" as prescribed in the U.S. Copyright Law. Requests for copying or reproduction of this dissertation may be referred to Proquest Information and Learning, 300 North Zeeb Road, Ann Arbor, MI 48106-1346, to whom the author has granted "the right to reproduce and sell (a) copies of the manuscript in microform and/or (b) printed copies of the manuscript made from microform."

Signature Laura C Bowling

Date 10-08-02

University of Washington
Graduate School

This is to certify that I have examined this copy of a doctoral dissertation by

Laura C. Bowling

and have found that it is complete and satisfactory in all respects,
and that any and all revisions required by the final
examining committee have been made.

Chair of Supervisory Committee:

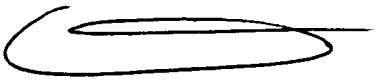

Dennis P. Lettenmaier

Reading Committee:

Dennis P. Lettenmaier

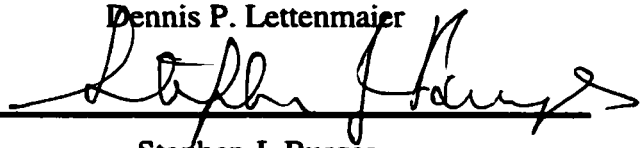

Stephen J. Burges

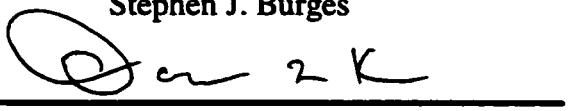

Douglas L. Kane

Date: 10-07-02

University of Washington

Abstract

ESTIMATING THE FRESHWATER BUDGET OF HIGH-LATITUDE LAND AREAS

by Laura C. Bowling

Chairperson of the Supervisory Committee

Professor Dennis P. Lettenmaier
Department of Civil and Environmental Engineering

As the most land-locked of the world's oceans, freshwater input from the land surface strongly controls the salinity of the Arctic Ocean, and subsequently the thermohaline circulation of the North Atlantic. There is mounting evidence of recent warming in the arctic, including thinning of sea ice, permafrost warming and increases in fall and winter streamflow in Siberia and Alaska. Such changes have the potential to feedback and further influence global climate through the modulation of fresh water inputs to the Arctic Ocean, and subsequently, the rate of deep water formation in the Greenland Sea. Based on observations alone we do not have the ability to close the water budget of the Arctic drainage basin, or make predictions regarding its response to warmer temperatures. This dissertation describes a course of research aimed at better estimating the arctic regional water budget, with a focus on the influence of lakes and wetlands and sublimation from blowing snow. In low-gradient arctic watersheds, permafrost contributes to the generation of extensive wetlands, ponds and lakes in a semi-arid region of precipitation. In the Putuligayuk catchment in northern Alaska, water balance calculations indicate that between 24 and 42 percent of snow melt water is not immediately available for runoff. This observed storage effect can be explained in large part by the excess of evapotranspiration over summer precipitation from open water areas which results in a seasonal reduction in the extent of surface water of 58 to 73 percent. A lake and wetland algorithm added to the Variable Infiltration Capacity (VIC) macroscale hydrology model is able to simulate this seasonal reduction in wetland extent. An algorithm to represent topographically induced sub-grid variability in wind

speed and blowing snow sublimation was designed for use within the VIC model. Annual average sublimation from blowing snow predicted by this model for a region on the Alaskan north slope varies from 55 mm in the foothills of the Brooks Range to approximately 25 mm on the Arctic coastal plain.

TABLE OF CONTENTS

LIST OF FIGURES

LIST OF TABLES

ACKNOWLEDGEMENTS

This research was improved by the guidance and support of the members of my supervisory committee, D. Lettenmaier (Chair), S. Burges and D. Battisti of the University of Washignton, D. Kane from the University of Alaska, Fairbanks and J. Pomeroy from the University of Wales. Their support is greatly appreciated. The field data used in this study, including snow survey results, meteorological data, and soil temperatures have been collected over several years by a number of investigators at the Water and Environmental Research Center at the University of Alaska Fairbanks, including J. Drage, R. Gieck, D. Kane, J. Mendez, B. Mueller, and L. Hinzman among others. In addition, the collection of ground truth data for the RADARSAT analysis presented in Chapter 3, and the pond data used in Chapters 3 and 4 would not have been possible without the generous support of D. Kane for providing access to these sites, and the assistance of J. Drage, R. Gieck and B. Mueller. The efforts of the Alaska SAR Facility at the University of Alaska Fairbanks in providing the RADARSAT images used in Chapter 3, and technical expertise, are greatly appreciated. Funding for this dissertation was provided by a National Aeronautics and Space Administration (NASA) Earth System Science Fellowship and NASA Grant No. NAG5-10092 to Dennis Lettenmaier at the University of Washington.

CHAPTER I: INTRODUCTION

BACKGROUND

Climate simulations predict that temperature changes associated with global warming will be most severe in high latitudes (Giorgi et al. 2001). This is primarily due to radiation feedbacks associated with a reduction in seasonal snow and ice cover (Manabe et al. 1991). Such sensitivity makes the Arctic a potential indicator of global change. There is mounting evidence of recent warming in the Arctic, including thinning and a decrease in the maximum extent of sea ice, permafrost warming and the northward migration of the tree-line (SEARCH 2001). Further evidence is seen in the increases in fall and winter streamflow that have been detected in Siberia and Alaska (Lammers et al. 2001,Yang et al. 2002). The observed increases are consistent with an increased portion of precipitation falling as rain and a shift forward in the timing of spring melt events (Lammers et al. 2001), and enhanced subsurface flow in the autumn due to later seasonal freezing of the active layer (Yang et al. 2002).

The strength of the coupling between the ocean, land and atmosphere in the Arctic is particularly important to the global climate due to their combined influence on the net transfer of heat northward and low-salinity ocean water southward. Freshwater input to the Arctic, along with sea-ice formation, controls the salinity of the polar ocean (Aagaard and Carmack 1989). The variability of freshwater fluxes to the Arctic Ocean controls the rate of outflow through the Fram Strait relative to the Canadian Archipelago (Stele 1996), and subsequently affects the thermohaline circulation of the world ocean, through control of convection in the gyres of the Greenland and Iceland seas (Aagaard and Carmack 1989, Broeker 1997). Andrews (1998) demonstrated that anomalously large influxes of freshwater to the Arctic Ocean have resulted in extreme changes in global ocean circulation in the past. Coupled ice-ocean models indicate that decadal trends in both arctic precipitation and river runoff have the potential to exert broad-scale impacts on the arctic sea ice regime (Weatherly and Walsh 1996) and to excite decadal and interdecadal oscillations of ocean circulation (Weaver et al. 1991).

By most estimates, runoff from the land surface represents the single largest input of freshwater to the Arctic Ocean. Alekseev and Buzuev (1973) estimated the total freshwater input to the Arctic Ocean to be between 4300 and 6475 km^3/year, based on ice formation data. Estimates of the portion of freshwater originating from the land surface are approximately 4000 to 4270 km^3/year (Grabs et al. 1999, Vuglinsky 1997). Treshnikov (1985) estimated the total freshwater flux from gauged land surface areas to be 3300 km^3/year, or 51 to 77 percent of the total from Alekseev and Buzuev (1973). Vuglinsky (1997) attributes 40 percent of the total land-surface derived freshwater flux to ungauged areas on the mainland and arctic islands. These estimates are based on the "Arctic Ocean Basin" as defined by Prowse and Flegg (2000) which does not include runoff into Hudson Bay or from the majority of Greenland.

Although extrapolation of observed streamflow to ungauged areas allows bulk estimates of land surface freshwater fluxes such as those cited above, the temporal and spatial variability of the evaporation and runoff response is largely unknown. Quantifying the magnitude and variability of evaporation from the land surface is important, not only because of its influence on river runoff volumes, but also because the flux of moisture and energy to the atmosphere through evaporation further influences atmospheric circulation patterns. The atmospheric moisture budget influences greenhouse warming, cloud cover and the surface radiation budget (Serreze et al. 1995). Low atmospheric moisture levels enhance longwave cooling of the surface, which may further suppress evaporation (Hinzman and Kane 1995). The efficiency with which energy is returned to the atmosphere in polar regions is controlled in part by the low rates of evaporation, sublimation and transpiration in arctic regions, limited by the low moisture holding capacity of the relatively cold arctic atmosphere (Hinzman and Kane 1995).

For these reasons, among others, characterization of the major features and natural variability of the pan-arctic water balance was posed as one of the central research themes in a recent report from the scientific community to the National Science Foundation Arctic System Science Program (Vörösmarty et al. 2001). Despite the importance of arctic land-surface freshwater fluxes to regional and global climate, the freshwater budget of the Arctic drainage basin on regional to circumpolar scales remains highly uncertain:

> "Overall, hydrologic data and our understanding of processes are both very poor. Data on energy and mass fluxes is meager, sometimes not continuous, not collected in the

optimum areas (but logistically the most convenient) and often collected with instrumentation that fails to accurately measure the variable of interest (Hinzman and Kane 1995)."

The dynamics of arctic land-surface hydrology are complicated by unique features such as the control of extreme seasonal runoff by snowmelt and ice break-up, large-scale redistribution of snow and the effects of ephemeral and permanently frozen soils. An important concern is the paucity of observed data and the difficulties associated with data collection. This makes closing the water balance in the Arctic based on observations problematic. Low-topography in some regions, and the influence of ice dams and snow drifts can obscure drainage divides (Rovansek et al. 1996, Moskvin 1989) and further disrupt discharge measurements. Furthermore, the number of stations for the operational monitoring of discharge throughout the Arctic declined by 40 percent between 1986 and 1999 (Shiklomonov et al. 2002). Perhaps most importantly, errors in the measurement of precipitation by standard networks in high-latitude countries can result in systematic underestimation of solid precipitation that can exceed 100 percent of true precipitation in high wind environments (Goodison et al. 1998). The lack of an apparent solution to the dilemma of accurate, measured precipitation has prompted some researchers to use other sources, such as output from retrospective runs of global climate assimilation models (reanalysis fields), for regional estimates of precipitation, despite their known problems (Bromwich 1997, Serreze and Hurst 2000). Walsh et al. (1998) found as part of the Atmospheric Model Intercomparison Project (AMIP) that the models overestimated arctic precipitation when compared to estimates based on the gauge-corrected gridded precipitation fields of Legates and Wilmott (1990) and monthly Russian maps (Khrol 1996). They suggest that the primary problem is likely the surface parameterization of evaporation, which controls the rate of moisture input to the atmosphere.

Land surface representations in most global climate models (GCMs) have historically treated cold region and cold season processes quite crudely. In recent years, much work has been done to improve the representation of cold region processes in land surface schemes that can be coupled to GCMs. Among the land surface schemes that participated in a recent model intercomparison over the Torne/Kalix river basin in northern Sweden and Finland (Bowling et al. 2002b), several have made significant changes to snow model structure (e.g. Shmakin 1998, Sud and Mocko 1999, Sun and Xue 2001, Viterbo et al. 1999, Boone and Etchevers 2001, Niu and Yang 2002,

and Cherkauer et al. 2002). Large differences in simulated runoff from LSSs have been attributed to differences in snow model parameterizations, including snow albedo and the treatment of partial coverage (Lynch et al. 1998, Mocko and Sud 2001). Soil freeze/thaw has also been an area of investigation (e.g. Cherkauer and Lettenmaier 1999, Viterbo et al. 1999, and Boone et al. 2000) and 12 of the 19 models participating in the intercomparison represent soil freezing through explicit calculation of the soil temperature profile.

Sublimation from blowing snow and the effects of lakes and wetlands remain largely neglected by the land surface models used in GCMs. Sublimation from blowing snow is difficult to observe directly and is often masked by the ability to quantify the other terms of the water budget, such as total snow precipitation (e.g. Kane et al. 1989). Although some effort has been made to address the effects of lakes in regional climate models, such efforts are primarily concerned with the simulation of atmospheric fluxes rather than the storage effects of lakes and wetlands (Goyette et al. 2000, Rummakainen et al. 2001). This neglect of surface storage is in large part because hydrologists have somewhat different motivations than climate modelers; i.e. the prediction of runoff versus surface fluxes. The focus of hydrologists has also traditionally been on much smaller scales.

OBJECTIVES AND DISSERTATION FORMAT

This dissertation describes a course of research aimed at improving the understanding of the role of land surface hydrology in the fresh water balance of the Arctic drainage basin. The primary objective of the research is to develop methods that will lead to improved predictions of the temporal and spatial variability of land-surface freshwater fluxes into the Arctic Ocean through the use of a macroscale hydrologic model appropriate for high-latitude runoff regimes, particularly those regions draining directly to the Arctic coast, which are currently ungauged. The specific objectives are:

1. To evaluate the performance of current generation macroscale hydrology models for the circumpolar arctic domain;
2. To improve representations of blowing snow sublimation losses from the regional water balance; and

3. To quantify the effects of storage and evaporation of water from lakes and wetlands in low-gradient arctic environments.

Nearly all of the ungauged portions of the circumpolar arctic drainage basin are north of 65° latitude (Bowling et al. 2000). Through the evaluation of the first objective, and in consideration of recent efforts to evaluate the capabilities and deficiencies of current land surface models as applied to high latitude hydrology (e.g., Bowling et al, 2002b), the second and third objectives were identified as having the greatest potential influence in the ability to estimate the water balance of these ungauged regions.

The physical and hydrologic characteristics of the arctic drainage basin are summarized briefly in Chapter 2. Preliminary research reported in Chapter 2 attempted to quantify the land-surface water budget of the Arctic from direct observations. Basin water balance calculations can provide bulk estimates of regional evaporation and runoff, but are not able to provide information on regional trends due to orography or latitudinal gradients. Nor can they provide estimates for the ungauged portions of the Arctic coastal plain.

For the reasons outlined above, the main objective of this dissertation was to improve certain parameterizations of hydrological models and hence their ability to represent runoff from the Arctic land areas. Chapter 2 describes a benchmark application of an early version of a macroscale hydrology model, the Variable Infiltration Capacity (VIC) model, to two large arctic drainage basins, the Mackenzie and Ob Rivers, in order to identify the strengths and weaknesses of land surface models in arctic environments. The application demonstrated the potential of such models to provide a continuous temporal and spatial diagnostic dataset of hydrologic variables not readily observed in data scarce regions, but identified some key weaknesses as well.

Analysis of the Ob and Mackenzie results suggested three processes of key importance to improving our understanding of the high-latitude water balance: 1) sublimation and re-distribution of snow by wind, 2) storage and evaporation of surface runoff by lakes, wetlands and fens and 3) reduction in infiltration by permafrost and seasonally frozen ground. The specific objectives of this research focus on the development of modeling tools to allow estimation of the role of lakes and wetlands, and sublimation from blowing snow in the regional water balance, through use of new parameterizations in land surface models that will be applicable over the pan-

Arctic domain. Representation of the hydrologic effects of permafrost and frozen ground in land surface models has been an active subject of research in recent years (e.g. Cherkauer and Lettenmaier 1999, Viterbo et al. 1999, and Boone et al. 2000) and is not an explicit subject of this research. As a first step towards these objectives, the influence of surface water in the numerous lakes and ponds of the Arctic coastal plain in Alaska on the annual and seasonal water budget was explored through field observations and synthetic aperture radar (SAR) imagery from the RADARSAT satellite. The results of this study are presented in Chapter 3. In Chapter 4, the insight gained from the Alaska results is used to aid in the development and testing of a lakes and wetland algorithm suitable for inclusion in a macroscale hydrology model. The relative influence of sublimation and redistribution of snow during wind events and the representation of this phenomenon at regional scales are explored in Chapter 5. Finally, the results of Chapters 2-5 are summarized in Chapter 6, along with conclusions and recommendations for further study.

CHAPTER II: THE ARCTIC DRAINAGE BASIN

The Arctic drainage basin refers to all land area draining to the Arctic Ocean. As discussed by Prowse and Flegg (2000), the domain of the Arctic drainage basin changes with perspective. The "Arctic Ocean Basin" as defined by Prowse and Flegg (2000) spans 37° of latitude, from 46° N in the headwaters of the Yenisei River to 83° N at the tip of Greenland, and several distinct vegetation and climate zones (see Figure 2.1). The entire Arctic drainage basin lies within one of three climate zones: 1) the arctic zone , which includes areas underlain by continuous permafrost, 2) the sub-arctic zone, defined by the limit of discontinuous permafrost or 3) the north temperate zone, which includes the zone of seasonally frozen ground (Woo and Winter 1993). The predominant vegetation class in the central Eurasian and North American portions of the Arctic drainage basin is boreal forest or taiga. The boreal region contains a mosaic of vegetation varying from closed coniferous canopies to sparsely vegetated clearings and numerous open lakes (Harding and Pomeroy 1996). Taiga transitions to steppe grassland in the south and to tundra in the north. In the mountainous regions, alpine forest and tundra represent another distinct class of vegetation. The alpine region typically contains dense conifers extending to the tree line, where shrubs and grasses give way to talus slope and bare rock (Storr and Golding 1974).

Much of what we know today about arctic hydrology comes from a rich tradition of field observations undertaken in frequently harsh conditions. Typically these campaigns focus on a single site or limited region and are limited in time. The most intensive observations are made during the spring and summer when climatic conditions are more favorable. Hydrologic models that simulate observed physical processes may prove a useful tool for extending the limited spatial and temporal coverage of such field observations. This chapter summarizes some of the relevant findings of observational field campaigns in the Arctic and uses them to identify weaknesses with a preliminary application of a hydrologic model to this area.

HYDROCLIMATOLOGY OF THE ARCTIC DRAINAGE BASIN

The temporal and spatial variability of fresh water fluxes entering the Arctic Ocean are controlled not only by space-time variability in precipitation and evapotranspiration but also by the storage of significant portions of annual precipitation on the land surface as snow, and in lakes and wetlands. Seasonally and permanently frozen ground also affects the interaction of surface and subsurface runoff storage with streamflow production. Interannual differences in the runoff response of northern rivers are in a large part due to changes in snow accumulation. Spatial variability is influenced by the distribution of permafrost, frozen ground, and lakes and wetlands. The effects of these mechanisms are discussed below.

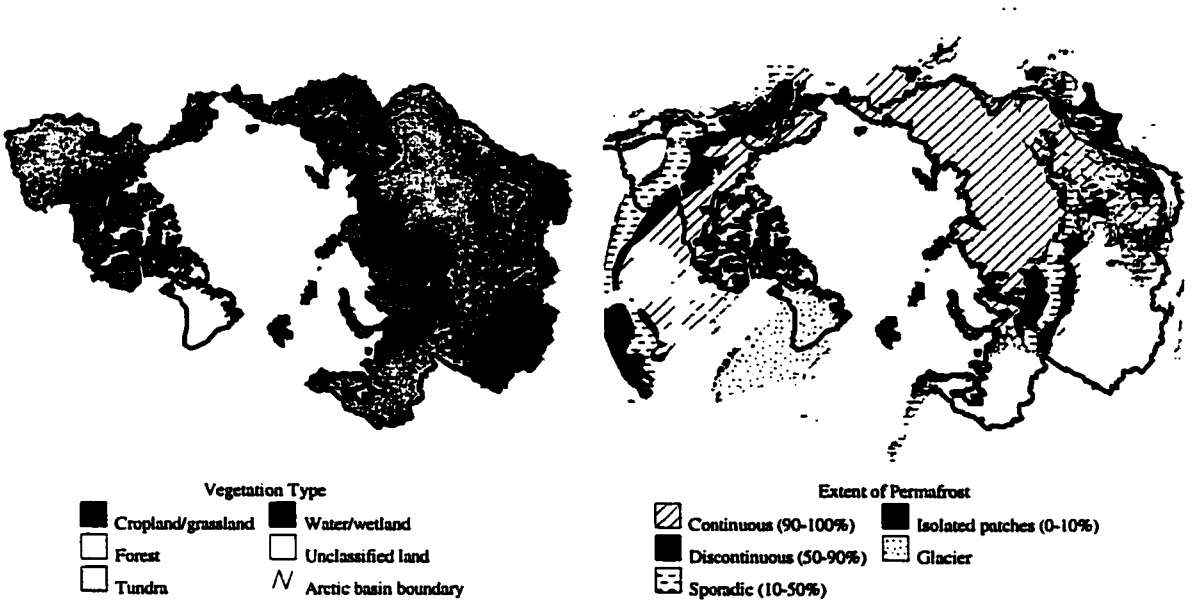

Figure 2.1. a) Vegetation of the Arctic drainage basin and b) Distribution of continuous and discontinuous permafrost in the Northern Hemisphere, adapted from the Circum-Arctic map of permafrost and ground-ice conditions (Brown et al. 1997).

Permafrost and Frozen Ground

The entire Arctic drainage basin is underlain by seasonally frozen ground or permafrost (soils that are below 0° C for a period of two years or longer). Percolation of snow melt water may raise soil surface temperatures to 0° C, but soils usually remain frozen until the snow cover is depleted (Woo and Steer 1983, Woo and Winter 1993). The presence of frozen water limits the infiltration rate into the soil and decreases the melt water storage capacity of the soils (Kane and Chaco

1990). Therefore, the dominance of surface flow is typical of both permafrost and many seasonally frozen regimes during snowmelt. One exception is very dry, seasonally frozen soil. The presence of the frost table severely restricts the storage capacity of permafrost soils throughout the snow-free season, resulting in a higher proportion of annual surface runoff (Woo and Steer 1983, Kane and Hinzman 1988). Uneven thawing of the active layer in permafrost areas in response to radiation exposure, melt water infiltration, and other heat transfer processes result in local regions with increased infiltration and storage capacity which may not reflect the overlying topography (Woo and Steer 1983).

Lakes and Wetlands

Numerous lowland lakes and bogs are characteristic of both the boreal forest zone and the low topography arctic coastal plain. Wetlands are areas having a water table near or above the mineral soil for most of the thaw season (Zoltai 1979). According to Church (1974), northern lakes and wetlands create a muskeg regime, in which high flows are attenuated by the absorption capacity of the muskeg (or peat bog) vegetation and resistance to flow by surface conditions. The storage capacity of wetlands, however, is often limited by frozen ground and high moisture content (Roulet and Woo 1986). Therefore, flow attenuation by wetlands is usually highest for summer rainfall after the peat is thawed (Roulet and Woo 1986, Woo 1988).

Evaporation from small lakes in the tundra region during the ice-free period often exceeds summer and even annual precipitation (Bigras 1990, Marsh and Bigras 1988, Rovansek et al. 1996). Lake and wetland storage is replenished each spring by runoff from the surrounding area. This is the case on the Alaskan coastal plain where Rovansek et al. (1996) observed that snowmelt runoff is delayed until the storage of ponds and wetlands is refilled.

Snow Hydrology

Snow cover accumulation, redistribution and ablation dominate the land surface hydrology of the Arctic. Although rain may account for a fairly large fraction of the annual precipitation, snow is proportionately more important to runoff due to low rates of winter evapotranspiration and the timing of melt water release. Snow accumulation and ablation processes are somewhat different for each of the four major arctic land classifications: boreal forest, grassland, tundra and alpine.

For example, Figure 2.2 shows the fraction of total precipitation falling as snow for stations across the Mackenzie River basin. A clear trend emerges in this figure, with proportionately more snow falling in the mountain and tundra regions than in the boreal forest zone, due to the longer winter period in the tundra and alpine zones. Sublimation during blowing snow events can be significant in the tundra as well as on the prairie (Hinzman et al. 1996, Kane et al. 1991, Pomeroy et al. 1993, Woo 1982).

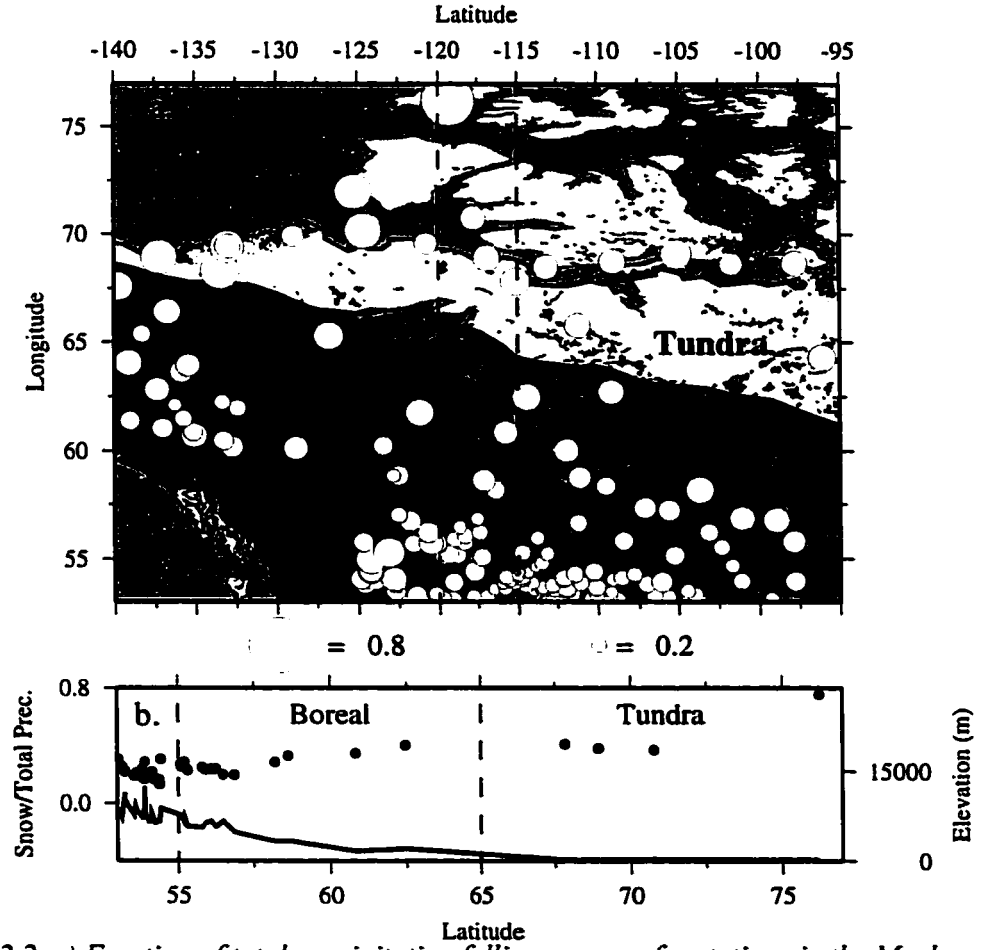

Figure 2.2 a) Fraction of total precipitation falling as snow for stations in the Mackenzie River basin and b) Transect of the snow fraction versus latitude for stations between 120°W and 115°W, station elevation is represented by the solid black line.

Interception of snow by boreal forest canopies can store up to 60 percent of the cumulative winter snowfall (Pomeroy and Gray 1995). Increased exposure and turbulent transfer in the canopy relative to the ground snowpack can result in sublimation losses from intercepted snow of

between 3 and 40 percent of annual snowfall (Krestovskiy et al. 1972, Pomeroy and Schmidt 1993).

The alpine zone contains elements of all of the preceding regions. However, it is further characterized by an increase in the snow accumulation season with elevation due to decreasing temperature. The gradient of snow depth versus elevation continues to steepen throughout the snow season as snow continues to accumulate at the highest elevations while differential melting occurs in the valleys. In the North American Rocky Mountains, snow generally melts at the highest elevations by late July (Storr and Golding 1974).

EXPOLORATORY SIMULATIONS OF ARCTIC HYDROLOGY

The variable infiltration capacity (VIC) model, developed at the University of Washington and Princeton University is a semi-distributed, grid-based hydrologic model that parameterizes the dominant hydrometeorological processes taking place at the land-atmosphere interface (Liang et al. 1994, 1996). The model has two modes of operation: a full water and energy balance mode, in which the surface energy budget is closed by iterating for surface temperature; and a water balance mode, in which the surface temperature is assumed to equal air temperature. This assumption is reasonable in many regions globally, but may be particularly problematic in regions with extremely cold snowpacks, for example. A mosaic representation of land surface cover, and sub-grid parameterizations for infiltration and baseflow, account for sub-grid scale heterogeneities in key hydrological processes. The VIC model incorporates a two-layer energy balance snow model (Cherkauer and Lettenmaier 1999). Frozen soil penetration is determined by solving for thermal fluxes through the soil column using a finite difference approximation of the general heat flux equation (Cherkauer and Lettenmaier 1999).

An application of the VIC model to the Ob and Mackenzie River basins is described here and in Appendix A. The frozen soil algorithm and improved snow energy balance were not fully implemented at the time of this application. The application utilized the model in water balance mode, which does not represent the effects of frozen ground but did use the energy balance snow model described above. The results of an earlier, unpublished, implementation using the Anderson (1973) temperature index snow model are also summarized here. The details of the meteorological forcings used for these applications are summarized in Table 2.1.

The key points derived from this model application can be summarized as follows:

- The average length of the snow season over the Ob River basin derived from weekly snow extent maps archived by the Earth Observing System (EOS) Distributed Active Archive Center (DAAC) is 190 days (Figure 2.3a). Weekly snow extent is estimated from visual satellite images, usually AVHRR and GOES, and gridded to a resolution of 25 km. The Anderson (1973) temperature index snow model, previously used in VIC, overpredicts the length of the snow season by 44 days, on average, relative to the satellite observations (Figure 2.3b). This is primarily due to an over-emphasis on hydrograph fit during calibration, at the expense of simulated snow cover. The energy balance model is closer to the observed (mean of 212 days for the Ob River), as shown in Figure 2.3c.

Table 2.1. Baseline VIC model setup

Model spatial resolution	2 degrees
Temporal resolution	Daily (hourly for the snow model)
Precipitation data	Daily time series produced from station data and stochastic models were scaled to match the mean monthly climatology of the Global Precipitation Climatology Project (GPCP) (Huffman et al. 1997), as described in Nijssen et al. (2001).
Minimum/maximum temperature	Daily time series produced from station data and stochastic models were scaled to match the mean monthly climatology of Jones (1994), as described in Nijssen et al. (2001).
Wind speed	Daily surface wind fields from NCEP/NCAR reanalysis
Incident shortwave radiation	Calculated using an adaptation of the method of Bristow and Campbell (1984).
Relative humidity	Calculated from minimum air temperature using the method of Kimball et al. (1997).
Longwave radiation	Calculated according to Bras (1990) as a function of air temperature and humidity.
Soil and vegetation	Based on the data set produced by the International Satellite Land Surface Climatology Project (ISLSCP)

- Using the Anderson (1973) temperature index snow model, which contains more adjustable parameters, it is possible to match the timing of observed hydrographs more closely (Figure 2.4a) than when the energy balance snow model is used (Figure 2.4b), despite the larger errors in snow cover. The scenario represented by Figure 2.4a, in which calibration was based on discharge

alone, masked other problems that are evident in the simulations that use the energy balance snow model.

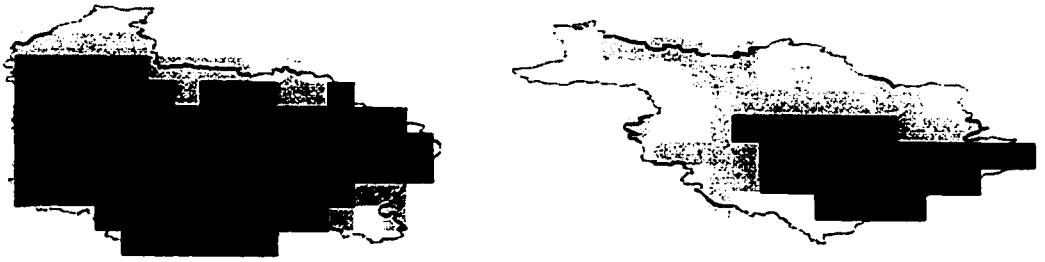

A) Remotely-sensed annual average days of snow cover (1979–1993): Ob River (left) and Mackenzie River (right)

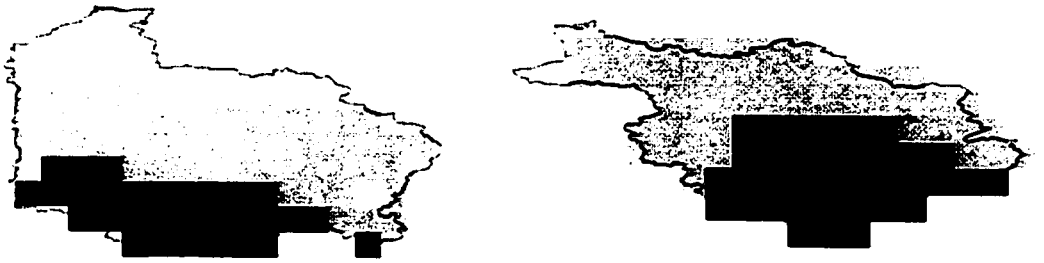

B) Simulated annual average days of snow cover (1979–1993), Anderson (1973) snow model: Ob River (left) and Mackenzie River (right)

C) Simulated annual average days of snow cover (1979–1993), Storck and Lettenmaier (1999) snow model: Ob River (left) and Mackenzie River (right)

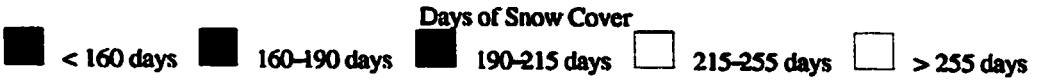

Figure 2.3. Snow cover extent for the Mackenzie and Ob River basins: A) remotely-sensed, B) temperature index snow model and C) energy-balance snow model

- The mean annual hydrographs for the Mackenzie and Ob Rivers shown in Figure 2.4b indicate that the VIC model with the energy balance snow algorithm is able to capture the volume of the snowmelt peak in both basins. However, both the rising and falling limb in

the annual hydrograph are too steep in the Ob basin. This may stem from a poor representation of surface storage effects in the top soil layer. The depth of the top soil layer adopted in this calibration (2 meters in the Ob and 1.5 meters in the Mackenzie) is realistic only if viewed as a surrogate for surface water storage, which is not represented by the model.

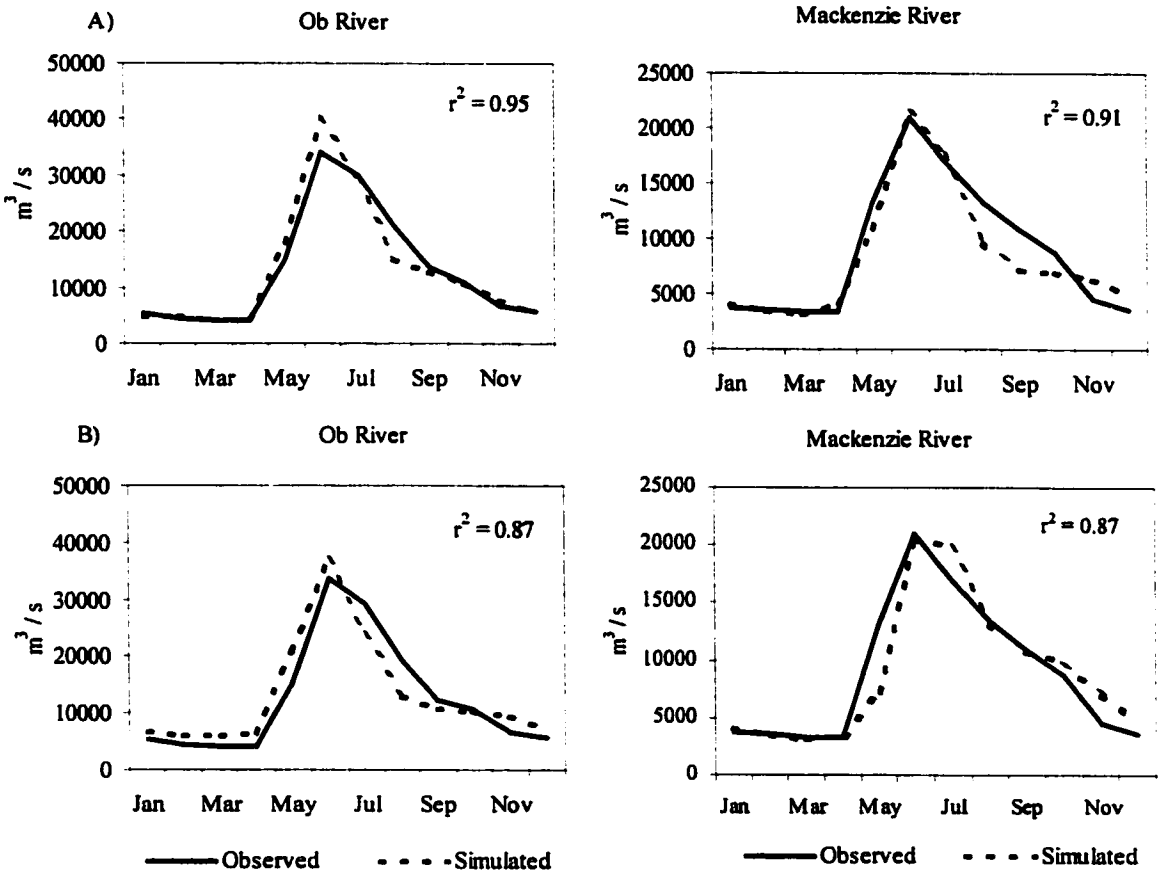

Figure 2.4. Simulated average annual hydrographs for the Ob (left) and Mackenzie (right) Rivers. a) using the Anderson (1973) temperature index snow model; b) using an energy balance snow model

- The calibrated parameters for the Ob basin were transferred without further calibration to the Yenesei and Lena Rivers, as shown in Figure 2.5. The timings of the snowmelt peaks correspond well, indicating that the energy balance snow model is reasonably transferable. However, large errors in peak flow volume and baseflow indicate that surface storage regulation is not adequately represented in the model by soil texture

parameters alone. In the Lena River, streamflow peaks are underpredicted and baseflow is over predicted. This is most likely due to the large soil depths that were necessary in the calibration of the Ob basin as a surrogate for the extensive wetlands in western Siberia. Lakes and wetlands are not as extensive in the Lena River, so this storage is over-represented.

Figure 2.6 shows the results of snow cover prediction for the circumpolar Arctic. While the length of the snow season in general is closely matched with the energy balance snow model, the length of the season tends to be over-predicted along the coastal plain.

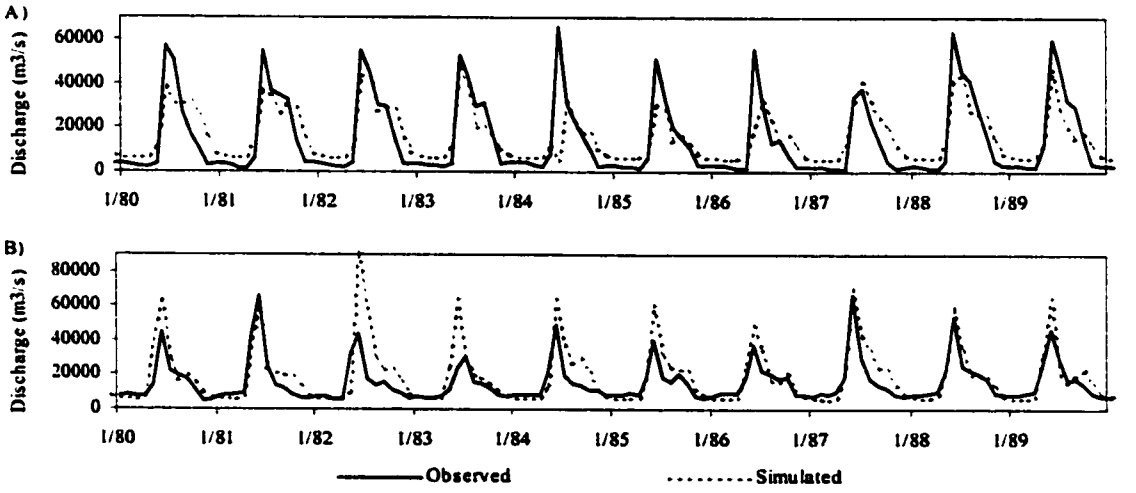

Figure 2.5. Simulated and observed discharge for A) the Lena River and B) the Yenesei River. Parameters for the simulation were transferred from the calibrated Ob River parameters without adjustment.

SUMMARY

Despite extremes in temperature and weather, and the remoteness of location, there is a rich tradition of field studies in the Arctic. Such field studies, though of necessity are limited in time and space, have provided a window to begin to understand the unique hydrology of the arctic. Based on scattered field investigations, a picture emerges of processes that we expect will be important at regional scales. These include the storage of a high proportion of annual precipitation as snow on the ground, that is released relatively quickly (often within 1 to 2 weeks) with the initiation of long solar days. Interception and sublimation of snow in the boreal forest

canopy and transport and sublimation of snow by wind in the tundra and plains, means that land-atmosphere water and energy exchange does not completely cease during the long, dark arctic winter. Surface runoff following snowmelt is intense due to the restriction of subsurface runoff and infiltration by seasonally and permanently frozen ground. In many regions, peatlands and the presence of extensive lakes and wetlands suppress the basin response to summer rain events, as surface storage is slowly decreased through evaporation.

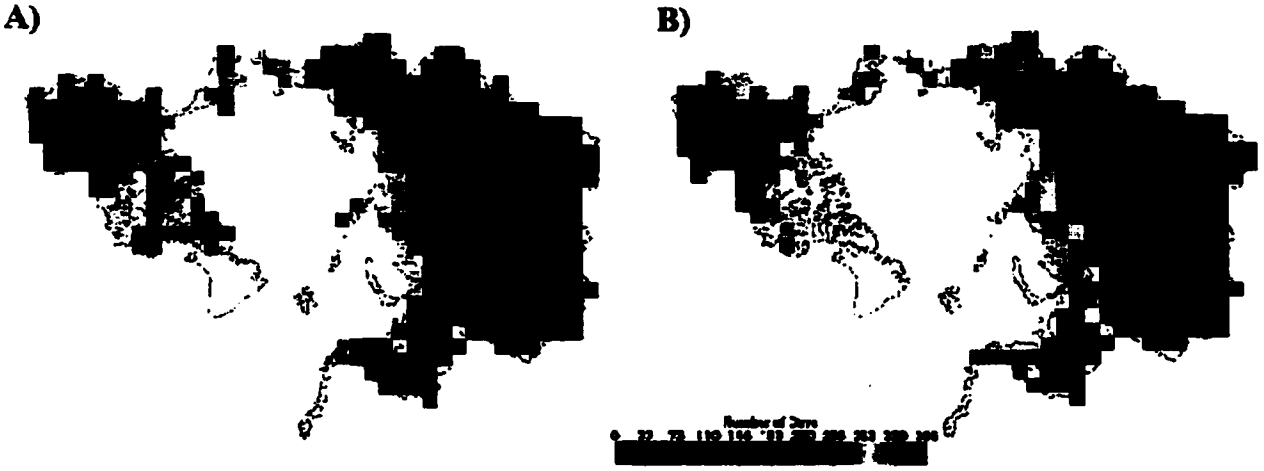

Figure 2.6. Circumpolar average annual days of snow cover a) from visual satellite data and b) simulated using the energy balance snow model

Applications of the VIC model to the Mackenzie and Ob River basins identified the largest shortcomings in the ability of a conventional macroscale hydrology models to represent the regional fluxes of water and energy in the Arctic. These include the following:

- Representation of surface storage effects in the top soil layer throughout the Mackenzie basin, which are actually due to storage in the large lakes of the lower Mackenzie, prevents quick runoff response from non-wetland areas. In addition, the simulated steepness in the rate of rise and recession in the Ob River appears to be due to a lack of representation of the extensive wetlands of the West Siberian Lowlands.

- Apparent over-estimation in the length of the simulated snow season, particularly on the Arctic coastal plain, may be related to both over-estimation of the end-of-season snow accumulation and under-estimation in the spatial variability of snow cover, since sublimation and redistribution by blowing snow is not represented by the model.

- Understanding of land surface processes in the Arctic, and hence model limitations, is constrained by the availability of reliable and continuous surface meteorological and solid precipitation data.

These findings suggest the importance of physical processes that are not represented by the current model generation to our ability to understand and estimate the regional water balance of the arctic land surface. These processes include the sublimation from blowing snow, surface storage in lakes and wetlands and infiltration limitation by frozen soils. Cherkauer and Lettenmaier (1999) and Cherkauer et al. (2002) studied the representation of the hydrologic effects of frozen soil. The remaining two processes will be explored in the following Chapters.

CHAPTER III: THE ROLE OF SURFACE STORAGE IN A LOW-GRADIENT ARCTIC WATERSHED

INTRODUCTION

The influences of contrasting land cover types on land-atmosphere moisture and energy exchanges is of great interest in climate studies (e.g. Adams et al. 2000, Brown and Arnold 1998, Goyette et al. 2000, Laurance and Williamson 2001, Peters-Lidard et al. 2001). The effects of small-scale heterogeneity in land surface characteristics (soils, vegetation, topography, etc.) on large-scale fluxes of water and energy have been a central focus of land-atmosphere field campaigns over the last decade (Wood 1995). The evolution of remotely sensed data and increased computational capabilities has motivated hydrologists to develop spatially distributed models that are capable of representing land surface characteristics more explicitly than the spatially lumped models that date to the early days of computerized hydrologic modeling. At the same time, hydrologists have been confronted with the challenge of predicting the response of land surface water and energy fluxes to changed climate and/or land cover, and the accurate representation of the interaction between the terrestrial and atmospheric components is the key to such predictions (e.g. Zhao et al. 2001). Simulation of land-atmosphere fluxes in arctic environments is complicated by many unusual environmental features such as permafrost, the presence of snow cover for much of the year, large seasonal variations in solar radiation, and extreme low winter air temperatures.

In low-gradient arctic watersheds, permafrost contributes to the generation of numerous landforms; many of which result in extensive wetlands, ponds and lakes in a semi-arid region of precipitation. Along the Arctic Ocean in Alaska, 83 percent of the coastal plain is classified as wetlands (Hall et al. 1994). Immediately following snowmelt in this region, surface wetness is near an annual maximum (Mendez et al. 1998). Low rates of evapotranspiration and continuous permafrost ensure saturated soils for much longer periods than are produced by similar snowmelt amounts in warmer climates. Although liquid water can move over short distances in frozen

soils, on seasonal and annual time scales this movement is insignificant compared to that in the unfrozen active layer.

The energy balances of arctic wetlands have been well studied (Rouse 2000, Mendez et al. 1998, Harazono et al. 1995 and Kane et al. 1990). Net radiation is partitioned into heat conduction into the active layer, and turbulent heat fluxes. Latent and sensible heat fluxes are large terms in the surface energy budget during the summer. During this period, 30 to 65 percent of net radiation is expended on evapotranspiration at the surface boundary (Harazono et al. 1995, Kane et al. 1990). In contrast, about 15 to 20 percent of the net radiation is used for melting and warming of the active layer (Kane et al. 1990, Rouse 1984). At wet sites, proportionately more energy goes into latent heat for evaporation (Eugster et al. 2000, Mendez et al. 1998). For example, the average monthly rates of water loss by evapotranspiration from a wetland near the Putuligayuk River in arctic Alaska ranged from 1.4 mm/day to 3.1 mm/day for a pond and 1.0 to 1.8 mm/day for a watershed (Mendez et al. 1998). Young and Woo (2000) observed daily evapotranspiration rates between 2.0 mm/day and 4.5 mm/day for a wetland site on Cornwallis Island, Canada. Generally the rates are greatest early in the summer near the solstice and decrease in late summer.

The majority of runoff from large, extensive arctic wetlands results from snowmelt in the late spring, and is followed by a nearly monotonic recession during summer (Rovansek et al. 1996, Woo 1988, Glenn and Woo 1997). During the summer months when evapotranspiration exceeds precipitation, there is a general drying of the watershed (Mendez et al. 1998, Rovansek et al. 1996). The drainage network of channels, lakes, ponds and wetlands becomes fragmented during relatively dry periods, limiting and delaying the runoff response of the watershed to precipitation events. Such watersheds are therefore poorly represented by traditional hydrology models that do not represent this lack of a continuous drainage network (Zhang et al. 2000).

When numerous lakes, ponds and wetlands dominate a catchment, it is nearly impossible to measure the amount of surface storage directly: estimation of the surface storage through direct measurement of the water balance components is a field intensive and time-consuming procedure. From a physical viewpoint, high quality digital elevation data could help to identify the physical characteristics of these surface storage reservoirs. In practice, the resolution of currently available digital topographic data are insufficient to define the drainage network in wetland areas, and to identify the many ponds and wetlands with small spatial dimension.

The use of synthetic aperture radar (SAR) data offers an alternative approach in which changes in surface water extent are estimated spatially. SAR imagery offers a unique opportunity for studying remote arctic landscapes, because SAR is not limited by cloud cover and low solar zenith angles, as is visible band imagery. SAR data have been used by a number of investigators for land use and wetland classification. Morrissey et al. (1996) used ERS-1 SAR data to delineate regions of wet and moist tundra near Barrow, Alaska. In particular, the HH–polarization C band of the RADARSAT satellite has been used successfully by several researchers to delineate inundated areas in general (Milne 1999, Pietroniro et al. 1999, Pope et al. 1997), and arctic wetlands in particular (Töyrä et al. 2001, Murphy et al. 2000).

This paper uses two independent methods to estimate the hydrologically active surface storage in the Putuligayuk catchment. The first method is based on direct use of field measurements to quantify surface storage during snowmelt over three melt periods. The second method uses a time series of synthetic aperture radar (SAR) imagery to map total inundated area over the course of two summers. The first method quantifies the total depression and reservoir storage available from all areas of the watershed at the end of the snow season; the second method determines to what extent this storage can be explained by cumulative evaporation less precipitation from the inundated areas of this low-gradient watershed.

SITE DESCRIPTION

The low-gradient Putuligayuk River catchment (~471 km^2), located on the Alaskan North Slope, drains north into Prudhoe Bay and the Arctic Ocean (Figure 3.1). It lies entirely within the coastal plain and is a patchwork of drained lakes and numerous other permafrost features, including: high and low centered polygons, Strangmoor ridges, frost boils, hummocky terrain and pingos. Almost all of these features physically impede drainage and result in extensive wetlands. The maximum thickness of the permafrost along the arctic coast is about 600 m, whereas the maximum depth of thaw of the active layer is about 35 to 55 cm (Hinzman et al. 1998). Vegetation is dominated by sedge tundra with shrubs along the riparian areas.

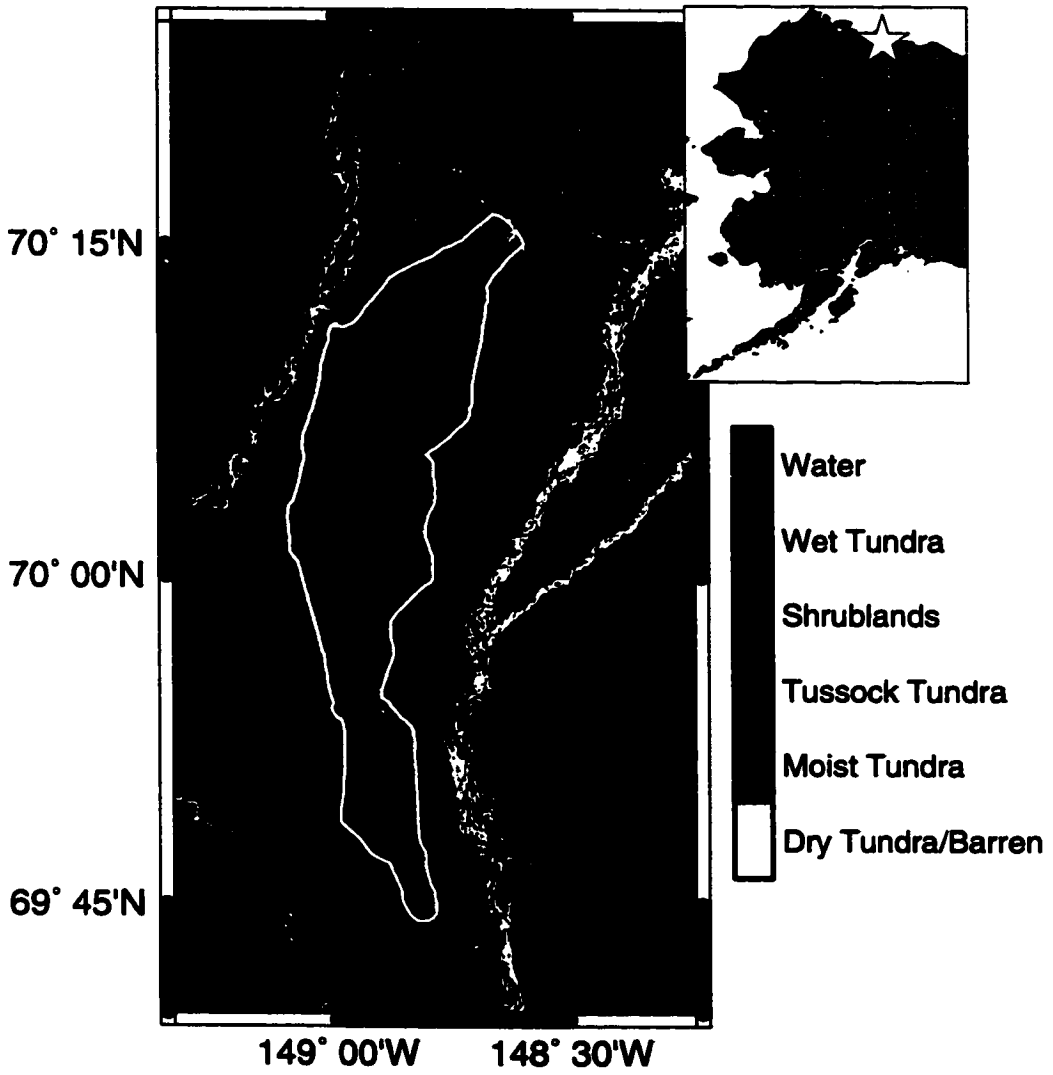

Figure 3.1. Location and vegetation of the Putuligayuk River on the Alaska North Slope. Vegetation classification from Landsat MSS images by Muller et al. (1999).

Discharge in the Putuligayuk River ceases during the winter months and the incised river channel is generally filled with drifted snow at the end of the winter. Snowmelt occurs during May and early June, as incoming solar radiation approaches the annual maximum, and typically lasts for about seven to ten days. Snowfall is approximately 40 percent of the annual precipitation total of over 200 mm of water (Kane et al. 2000). During snowmelt the river channel begins to fill, but discharge is impounded within the snow-filled channel. Eventually (usually about 6-7 days following the onset of melt) the channel opens up to drain freely. Measurable discharge does not

begin until almost all snow in the watershed melts. The U.S. Geological Survey gauged the Putuligayuk River for 15 years (1970-1979, 1982-1986). No other complementary hydrologic data were collected during this period. However, the runoff data are consistent with the observations of Rovansek et al. (1996) for a nearby wetland complex. First, there is a significant runoff event each spring from snowmelt. Second, only minimal runoff occurs during the summer in response to precipitation. Peak runoff events during snowmelt exceeded 100 m^3/sec, while peak runoff events during the summer were only about 4 m^3/sec. Figure 3.2 demonstrates the dominating effect of snowmelt runoff on the total volume of annual runoff.

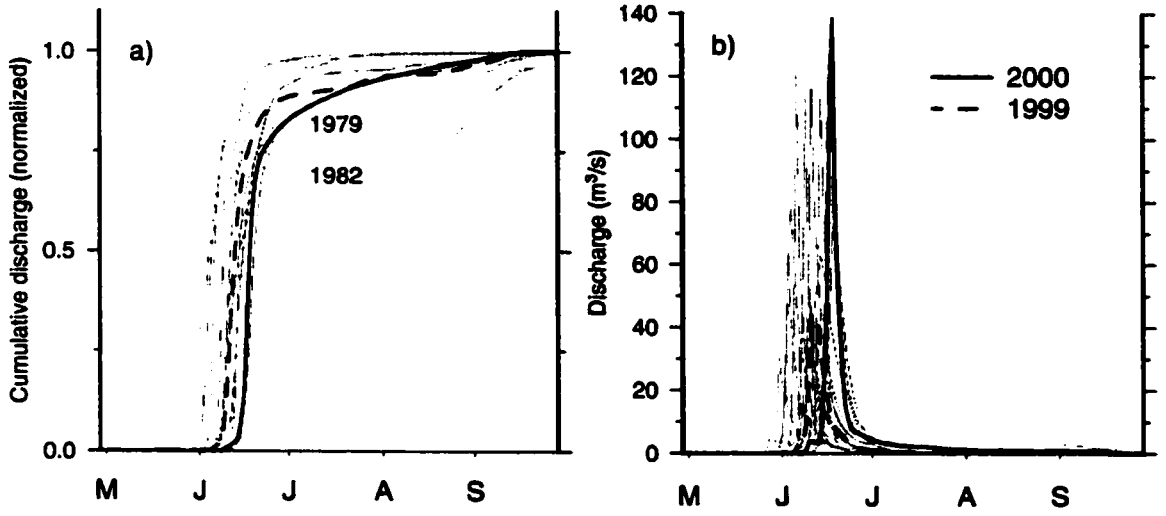

Figure 3.2. Discharge for the Putuligayuk River for the 17 years of record (1970-1985, 1999-2000): a) normalized cumulative discharge and b) total discharge.

METHODOLOGY

Field Data Collection

In order to estimate the volume of water entering storage during snowmelt, snow water equivalent (SWE) and stream discharge data were collected from the Putuligayuk catchment over the three-year period 1999 to 2001. The end-of-winter basin average SWE is determined each year through extensive snow surveys just prior to the onset of melt (surveys taken in late-April or early-May). Using snowmobiles, approximately nine sites were sampled for snow depth across the basin, with specific landforms targeted to obtain a representative distribution. At each snow survey site 50 depths and 5 densities were collected. Depths were measured using a snow probe. An

Adirondack snow tube and digital scale were used for collecting densities. Three snow survey sites were sampled daily during snowmelt for the Putuligayuk River watershed; Betty Pingo, West Dock and Franklin Bluffs. Franklin Bluffs is near the headwaters of the watershed while the Betty Pingo and West Dock sites are near the mouth (see Figure 3.1).

Continuous discharge monitoring of the Putuligayuk was re-initiated by researchers at the Water and Environmental Research Center (WERC) at the University of Alaska Fairbanks (UAF) in June 1999. Twice daily discharge measurements were taken in the spring from the start of flow in the channel, until the time at which the channel is free from snow and ice. Stage was monitored continuously at the pre-existing USGS station location for the remainder of the summer with some intermittent summer discharge measurements. At high stage, discharge was measured at a pipeline bridge 200 m downstream from the USGS cross-section using a bridge crane and 34 kg (75 lb) float. At low stage, discharge was measured by wading using a top setting rod and cup type current meter. The Putuligayuk River discharge peak on June 15, 2000 of 168 m^3/s (5920 cfs) was the maximum-recorded discharge on the river. The USGS recorded a peak discharge of 164 m^3/s (5800 cfs) on June 12, 1980.

Three thaw ponds on the Alaskan arctic coastal plain were selected for monitoring of evaporation processes throughout the spring and summer of 1999 and 2000. The wetland complex has been the site of on-going monitoring activities and meteorological observations by researchers at WERC since 1994 and has been previously studied by Rovansek et al. (1996) and Mendez et al. (1998). Net radiation, water temperature and water level were monitored continuously for each of the ponds from ice break-up through mid- September. The pond bathymetry was surveyed using a laser surveying station (total station) and inflatable raft, and depth-area relationships were determined for each pond using the Arc/Info® geographical information system.

Reference data collection and satellite image selection

To gain an understanding of the implications of summer season change in surface water extent across the Putuligayuk catchment for storage during snowmelt, a database of synthetic aperture radar (SAR) images was acquired, pre-processed and classified. A total of eighteen geo-referenced RADARSAT-1 full resolution ScanSAR beam images covering the Putuligayuk watershed over a two-year period were obtained from the Alaska SAR Facility (ASF) at UAF, as

summarized in Table 3.1. Five of the images were not used due to poor image quality over the region of interest. The ScanSAR beam has a pixel spacing of 50 m. This beam was chosen over the finer resolution standard beam because the much greater swath width (approximately 460 km) yielded much better temporal coverage of the Putuligayuk catchment in the archived images available from the ASF.

Table 3.1. RADARSAT ScanSAR SWB Images selected for analysis

Number	Date	Wind Speed (m/s)[a]	T_{avg} (°C)[b]	P_{cum} (mm)[c]
1	10-Jun-1999	6.3	2.1	5.8
2	20-Jun-2000	3.0	1.9	0.0
3	23-Jun-1999	3.0	3.5	0.0
4	30-Jun-1999	3.1	2.1	0.0
5	17-Jul-1999	3.0	5.2	13.2
6	14-Sep-1999	8.6	0.6	3.8
7	14-Jun-2000	2.5	1.8	0.0
8	21-Jun-2000	3.4	6.2	1.0
9	5-Jul-2000	9.7	8.3	13.0
10	22-Jul-2000	2.8	10.5	3.6
11	15-Aug-2000	2.5	-1.3	3.3
12	7-Sep-2000	1.7	1.0	0.0
13	15-Sep-2000	5.0	0.3	1.0

Notes:

[a]Hourly wind speed for hour of overpass measured at the Betty Pingo site.

[b]Average air temperature 12 hours prior to overpass.

[c]Cumulative precipitation for seven days prior to overpass.

The selected images were all from descending orbits and had overpass times between 7 and 8 am, Alaskan standard time. Wind-induced waves on open water areas increase the radar backscatter signal, making it more difficult to distinguish open water areas. Potential images were screened based on the hourly wind speed measured at the WERC Betty Pingo meteorological station at the time of overpass. Unfortunately, in some cases the lack of available images made it necessary to select images from periods with higher wind speeds, as summarized in Table 3.1. Four of the images were also selected to coincide with periods of field activity in June 1999 and 2000, August 1999 and September 2000.

To aid in classification of the images, a training dataset was surveyed in and around the Putuligayuk watershed in June and August 2000 using handheld GPS. A total of sixteen usable areas were surveyed and classified as open water, emergent vegetation, wet tundra and moist tundra. Photos of representative training areas are shown in Figure 3.3. Figure 3.4 shows the location of the training areas surveyed in the vicinity of Prudhoe Bay in June 2000 super-imposed on a June 14, 2000 ScanSAR image.

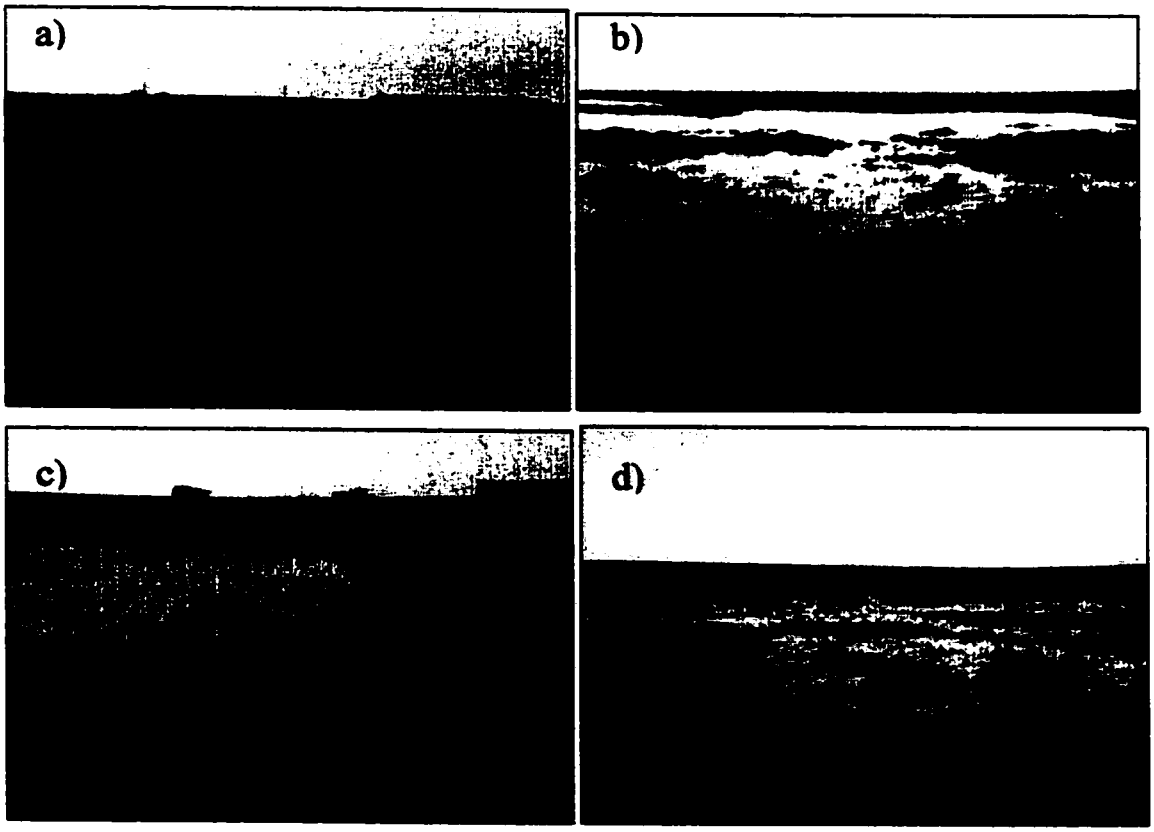

Figure 3.3. Photographs of characteristic classification training areas on the Alaskan North Slope, a) dry tundra, b) flooded tundra, c) emergent grasses and d) sparsely vegetated mud flats.

Image Preprocessing

After pre-processing at the ASF, the ScanSAR images were radiometrically calibrated to correct pixel intensity as a function of range using ASF software. The results of the radiometric calibration are pixel digital numbers (DN), which are related to radar backscatter (σ_o) as (DN/10 – 25.5). Correction for variation in local incidence angle with terrain (e.g. Goering et al. 1994)

was neglected due to the low gradient of topography in the Putuligayuk catchment and the lack of high quality digital elevation data.

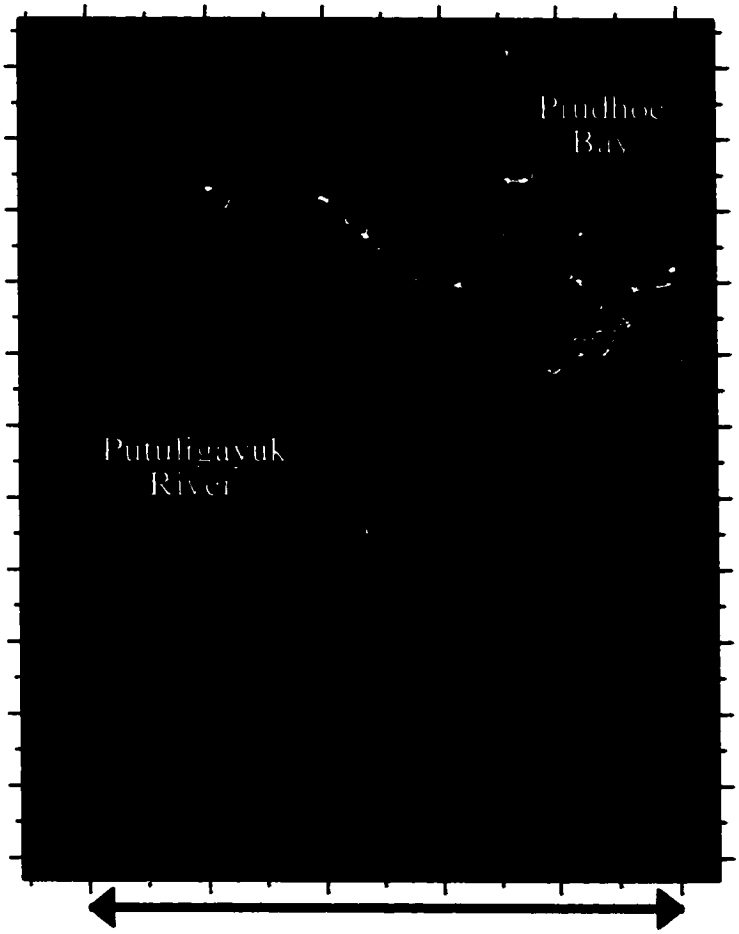

Figure 3.4. ScanSAR image of the Prudhoe Bay area from June 14, 2000. Red circles indicate the location of the training areas from GPS surveys and the green line indicates the Putuligayuk catchment boundary above the gauge location.

The calibrated images were converted to a universal transverse mercator (UTM) projection using ASF software and orthorectified using a Landsat TM land classification for tie points (Muller et al. 1999). Because multiple images are used in the classification procedure, it is imperative that they are registered precisely. The images for each season were therefore re-registered to one another using the high backscatter from buildings and other immobile man-made objects as ground control points. Finally, signal-dependent noise SAR speckling was reduced by application of a 7 by 7 pixel Lee filter (Lee 1981).

Image Processing

Figure 3.5 shows the time series of backscatter signal obtained from the filtered and registered SAR images from the summer of 2000 for each of the training areas. For the most part, the training samples fell into groups with characteristic backscatter signals, with the exception of one sample (dashed line, Figure 3.5b). This sample was taken from a flooded area of very sparse vegetation (see Figure 3.3d), with large areas of exposed mud at the end of summer.

Several interesting features are apparent in this backscatter time series. In the late summer, open water areas consistently have low backscatter response, as expected. The signal is confused immediately following melt, however. This is most likely due to the effect of floating and grounded ice. Jeffries et al. (1993) found that in mid-winter floating ice in small ponds near Barrow, Alaska tends to have a strong backscatter response, particularly in comparison to pond ice that is frozen to the bottom. During melt, they observed an unexplained increase in backscatter response from grounded ice. In this analysis, some ponds show a lower backscatter signal in the June 14, 2000 image, with a dramatic increase in the June 21, 2000 image, possibly due to the flotation of previously bottom-fast ice in flooded ponds during this time period.

Another striking feature of the backscatter time series is the decrease in backscatter between September 7th and 15th, 2000 for all cases. As shown in Figure 3.5a, the daily minimum temperature fell below 0° C in the time between these images. Surface freezing decreases the surface dielectric constant, hence lowering the backscatter signal (Villasenor et al. 1993, Kandus et al. 2001). The brief period of cold temperatures observed before these images is not sufficient to freeze the soil or open water areas, so the observed decrease in backscatter is likely the result of splash or water vapor condensing on vegetation that is below freezing. Such a decrease in backscatter is also visible in the August 15, 2000 image when the air temperature dropped below freezing.

Finally, the training samples for emergent grasses shows an increase in backscatter for the mid-summer (July 22, 2000) image that is not evident in the sedge tundra samples. Such an increase is typical of a double bounce signal between the vegetation and underlying water when the

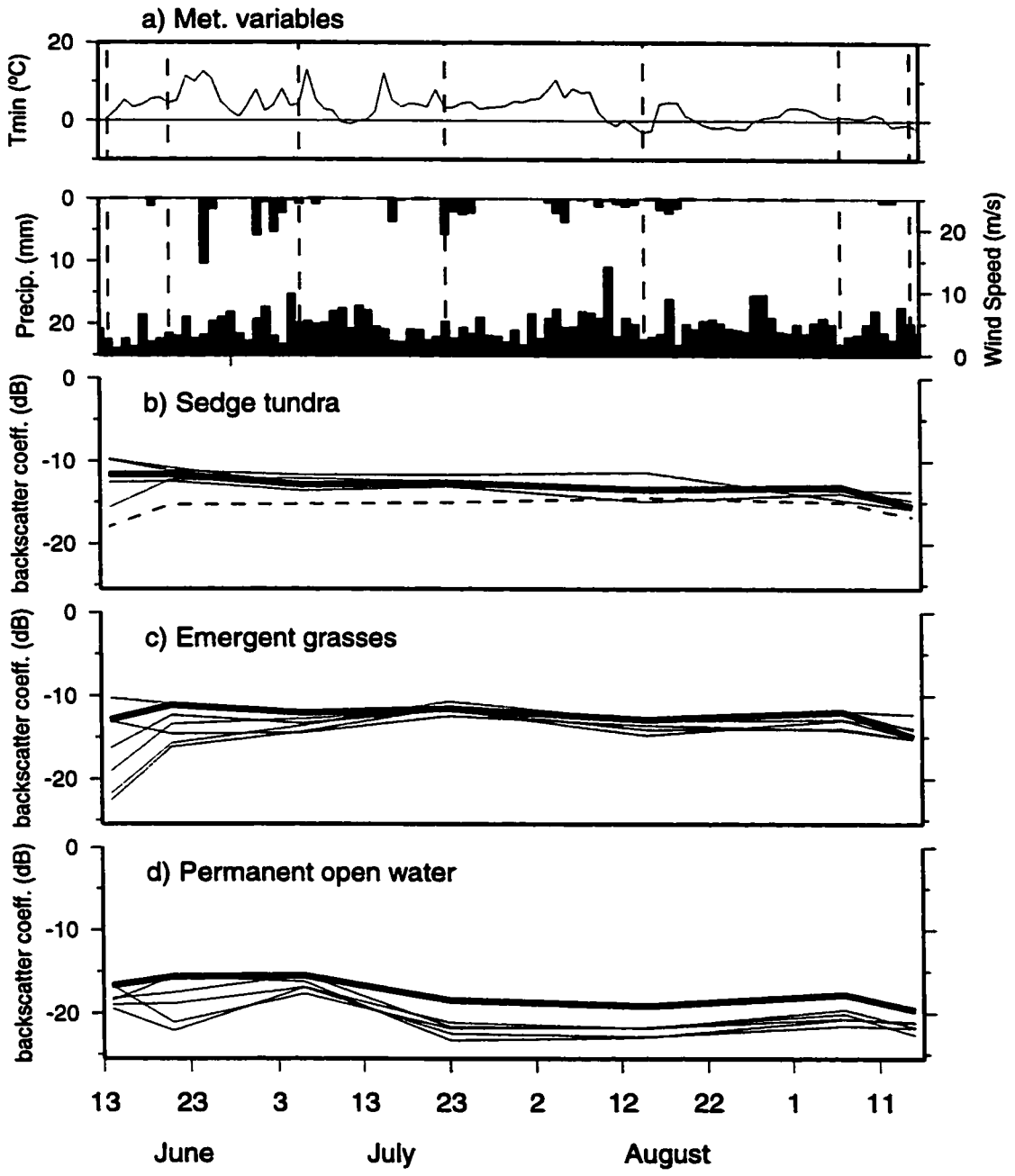

Figure 3.5. Time series of backscatter for training areas and meteorological conditions at the time of satellite overpass for summer 2000: a) Daily minimum air temperature, daily total precipitation, and mean hourly wind speed at the time of overpass; b) backscatter from sedge tundra, c) backscatter from emergent grasses and d) backscatter from open water areas. The dashed line in b) represents a training sample from a region of sparsely vegetated tundra. The average backscatter of each land surface type from the classified images (not the average of the shown training areas) is shown in bold.

vegetation is sufficiently dense (Pope et al. 1997). Many of the samples for both grasses and tundra show low backscatter immediately following snowmelt, typical of flooding of short vegetation (Pope et al. 1997) or flattened, dead grasses (Töyrä et al. 2001).

To make use of the unique temporal signature of each land class, a supervised classification algorithm in the Arc/Info geographical information system (GIS) was used with all seven images from 2000 combined. In this approach, each pixel is compared with the numerical description of the training areas and classified using a maximum likelihood estimator. The images were classified into open water, emergent vegetation (marshes), tundra, sparse vegetation (mud flats) and other (buildings, roads and barren).

In order to track the change in open water areas over time, a separate classification was done of each individual image. The open water area for each image was classified using a supervised classification scheme. Clearly delineated open water areas were used as training samples. This is similar to the previous classification, but pixels were classified only as water, non-water or other. The two images that were influenced by surface freezing (August 15th, 2000 and September 15th, 2000) were not included in this analysis. To prevent confusion of open water areas with floating ice, permanent open water areas as determined from the static land classification were masked out prior to classification.

RESULTS

Characterization of Surface Storage during Snowmelt

The change in storage (both surface water and moisture stored in the active layer) for any time period can be estimated as:

$$\Delta S = P + Q + ET \qquad (3.1)$$

where ΔS is the change in surface storage, P is precipitation, Q is runoff leaving the basin and ET is evapotranspiration when water is lost to the atmosphere (-) or condensation when water is gained from the atmosphere (+). To calculate the total change in storage from just prior to melt to the end of snowmelt-induced runoff, Q is measured by gauging, as described previously. In order to determine the proportion of Q that can be attributed to direct runoff originating from snowmelt, it is necessary to divide the observed streamflow into snowmelt runoff and drainage components.

The end of the snowmelt runoff period for purposes of this calculation was defined as the inflection point on the snowmelt hydrograph recession. The inflection point occurs on June 27, 1999, June 21, 2000 and June 23, 2001. Once temperatures drop below freezing in the fall (around mid-September), essentially all precipitation accumulates as snow. The end of winter SWE therefore represents total precipitation less sublimation for the winter months. Total evapotranspiration/condensation during the snowmelt period is estimated using an energy-balance snow model that has been calibrated for this region based on several years of hydrologic and meteorologic data, in the manner of Kane et al. (1997).

The results of this balance for the Putuligayuk basin are shown in Table 3.2. For the three years shown, the increase in surface storage during the snowmelt period, normalized by basin area, varied between 25 and 37 mm and 24 to 42 percent of the snowpack water equivalent over the watershed. These values represent the quantity of snowmelt water that goes into storage each spring and is not immediately available for runoff. The large range in percentage indicates that the volume of water that goes into storage is not directly dependent on the annual snowfall in the year of interest. It is likely, therefore, that it is dependent on the available surface or near-surface storage. The available storage at the time of melt is a function of the storage deficit created by evaporation from open water areas in excess of precipitation over the previous summer and the degree of saturation (and phase) of moisture in the active layer. These sources are explored further below.

Table 3.2. Spring water balance for the Putuligayuk watershed (471 km^2).

	1999	2000	2001
Snow Water Equivalent	+87 mm	+124 mm	+89 mm
Surface Runoff	-56 mm	-87 mm	-56 mm
Evapotranspiration (-)/ Condensation (+)	-6 mm	-7 mm	+4 mm
Change in Surface Storage	+25 mm	+30 mm	+37 mm

Temporal assessment of open water extent

The classified images of land surface type for 1999 and 2000 are shown in Figure 3.6 and summarized in Table 3.3. The classified images appear generally similar for the two years. As

expected, the total area of permanent open water was very similar for the two years (15 and 14 percent). The 2000 image classification shows an increase of the region classified as emergent vegetation wetlands (58 percent versus 43 percent), and a decrease in the area of upland tundra and exposed barrens. This is consistent with larger areas of flooding in 2000 resulting from snow accumulation that was substantially greater in 2000 than in 1999, (124 mm versus 87 mm) and may provide motivation for caution in interpretation of static land use classifications based on single years of data.

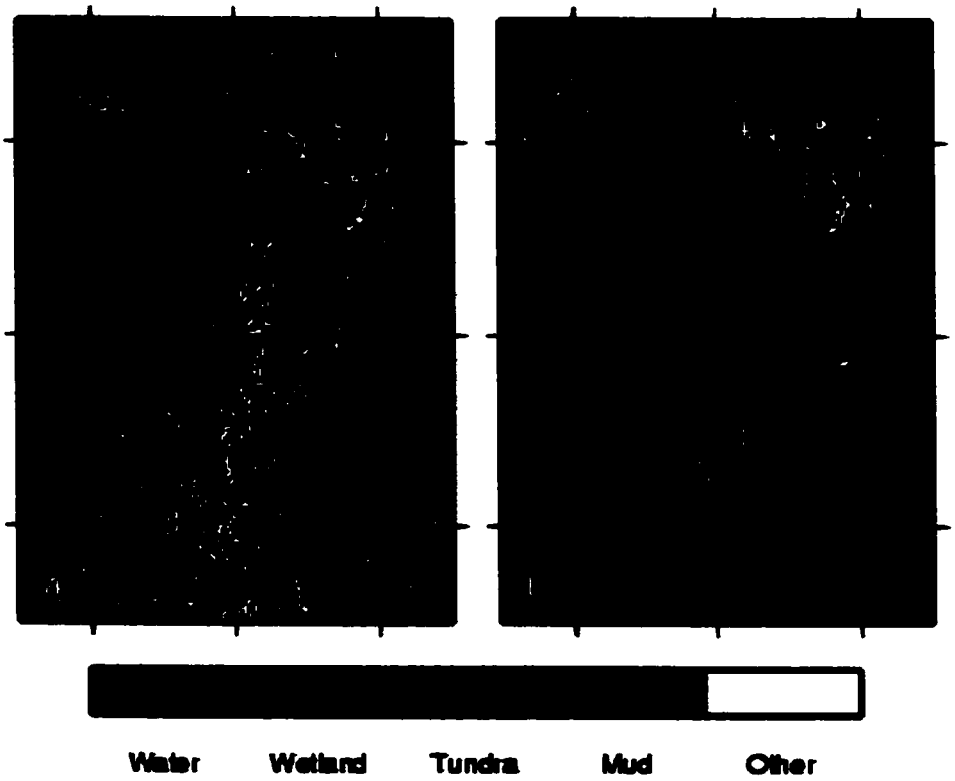

Figure 3.6. Land type classification from the temporal sequence of SAR images for a) 1999 and b) 2000.

The average temporal profiles of backscatter for each of the classified land surface types are shown in Figure 3.5 as bold lines. For both 1999 and 2000, the areas classified as emergent grasses have on average higher backscatter than the sedge tundra, and a slightly more pronounced mid-summer peak in backscatter. In 1999, the tundra, emergent grasses and sparsely vegetated areas all have low backscatter immediately following snowmelt. In 2000, the sedge tundra areas

do not have the initial low backscatter value characteristic of completely flooded vegetation. These areas may be exhibiting a double bounce due to partial flooding of the vegetation.

Table 3.3. Vegetation classifications of the Putuligayuk River basin for 1999 and 2000 from temporal sequences of ScanSAR images

Description	Percent of basin area	
	1999	2000
Water	14 %	15 %
Marsh (longer sedges and grasses)	43 %	58 %
Tundra (tussock sedges and mosses)	20 %	14 %
Sparsely vegetated (exposed mud)	13 %	12 %
Buildings, exposed rock and other	9 %	1 %

The time series of classified images for 2000 is shown in Figure 3.7. The change in saturated extent shows up quite clearly as a reduction of the black area, as summarized in Table 3.4 and Figure 3.8 for both years. There is a large reduction in saturated extent immediately following snowmelt, followed by a gradual reduction throughout June and July. In both years there is an apparent increase in saturated extent in the late fall, consistent with relatively heavy precipitation in mid- to late-August. Based on this classification, the total extent of open water in the Putuligayuk watershed changes by 58 and 73 percent over the course of the summer for 1999 and 2000 respectively.

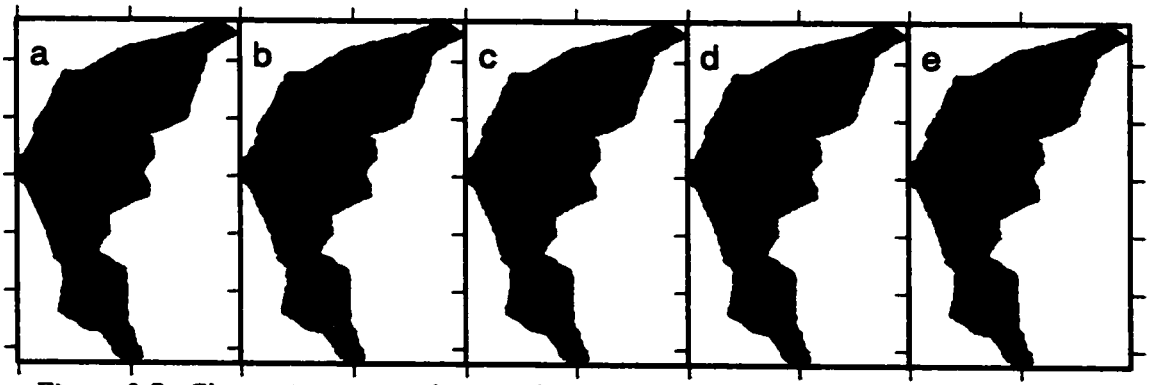

Figure 3.7. Change in saturated extent (black area) of the Putuligayuk River basin from classified SAR images: a) June 14, 2000, b) June 21, 2000, c) July 5, 2000, d) July 22, 2000 and e) September 7, 2000

Daily evaporation from open water areas

Point Estimates

The observed change in surface water storage in the three monitored ponds for the summers of 1999 and 2000 is summarized in Table 3.5. In order to divide the observed change in stage into drainage and evaporation components, an energy balance lake model was applied to each of the three ponds. Evaporation from the water surface is calculated in each hourly time step by solving a surface energy balance in the manner of Hostetler (1991) and Hostetler and Bartlein (1990). A more comprehensive description of this algorithm is provided in Chapter 4. Meteorological data to drive the lake model are taken from an adjacent station located within the wetland complex that includes the monitored ponds. Because the majority of the lakes on the coastal plain are of limited extent (diameter less than 1 km), thermodynamic feedbacks over the lakes themselves are neglected and the wetland meteorological measurements are considered representative of the conditions over the lakes. Outflow from the pond is computed using a stage-based rule curve, once the new stage is calculated based on the previous time step's balance of inflow, precipitation and/or melting of ice and overlying snow, and evaporation.

Table 3.4. Estimate of surface saturation and total storage deficit in the Putuligayuk River basin

Date	Sat. Extent	Change	Storage Deficit	Date	Sat. Extent	Change	Storage Deficit
6/10/99	228 km^2			6/14/00	315 km^2		
6/20/99	94	58 percent	16 mm	6/21/00	129	73 percent	15 mm
6/23/99	93			7/5/00	98		
6/30/99	83			7/22/00	72		
7/17/99	83			9/7/00	84		
9/14/99	96						

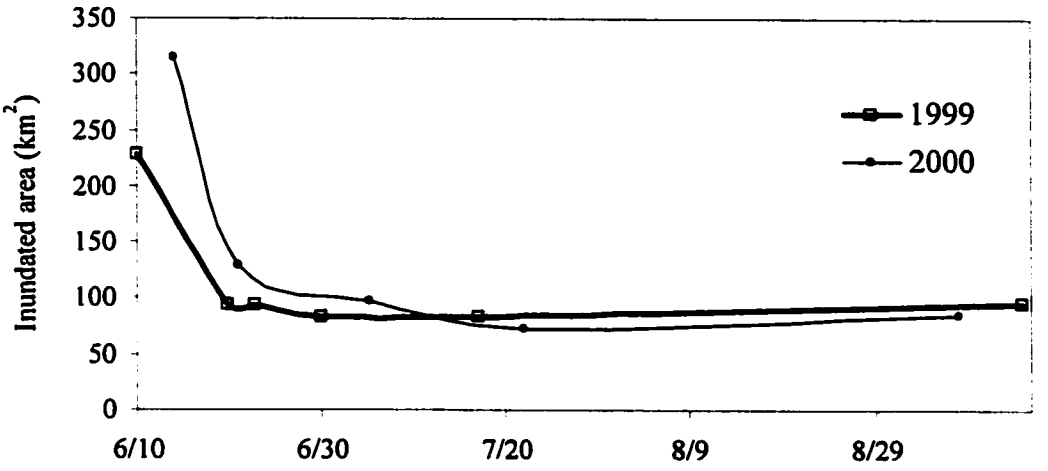

Figure 3.8. Time series of saturated extent of the Putuligayuk River basin for the summers of 1999 and 2000.

Results from the lake energy balance, compared with observations from the largest of the three monitored ponds, are shown in Figure 3.9. The model was initialized on June 18th, 2000 with zero degree water temperatures. The model is able to reproduce the observed decline in stage over the summer fairly well, including the fast drainage response prior to June 30th. Field observations verified that this pond drains through a culvert at high stage. After June 30th, the decline in stage is due to evaporation alone. The simulated change in stage and evaporation are also provided in Table 3.5. The simulated evaporation is less than the change in stage alone because drainage effects are included.

Table 3.5. Water balance for three water bodies, 1999 and 2000

Location	Area (m^2)	Change in stage[1] (mm)		Simulated evaporation[1] (mm)		Inferred runoff (mm)	
		1999	2000	1999	2000	1999	2000
Pond S2	5,100	-166	-154	-188	-161	-80	-95
Pond S11	6,700	-103	-80	-188	-161	-17	+21
Lake 1	57,000	-103	-81	-188	-161	-17	+20
Precipitation		+102	+60				

Notes:

[1]Values for 1999 are calculated for the time period 6/10/99 – 9/15/99. For 2000, the time period is 6/17/00 – 9/13/00.

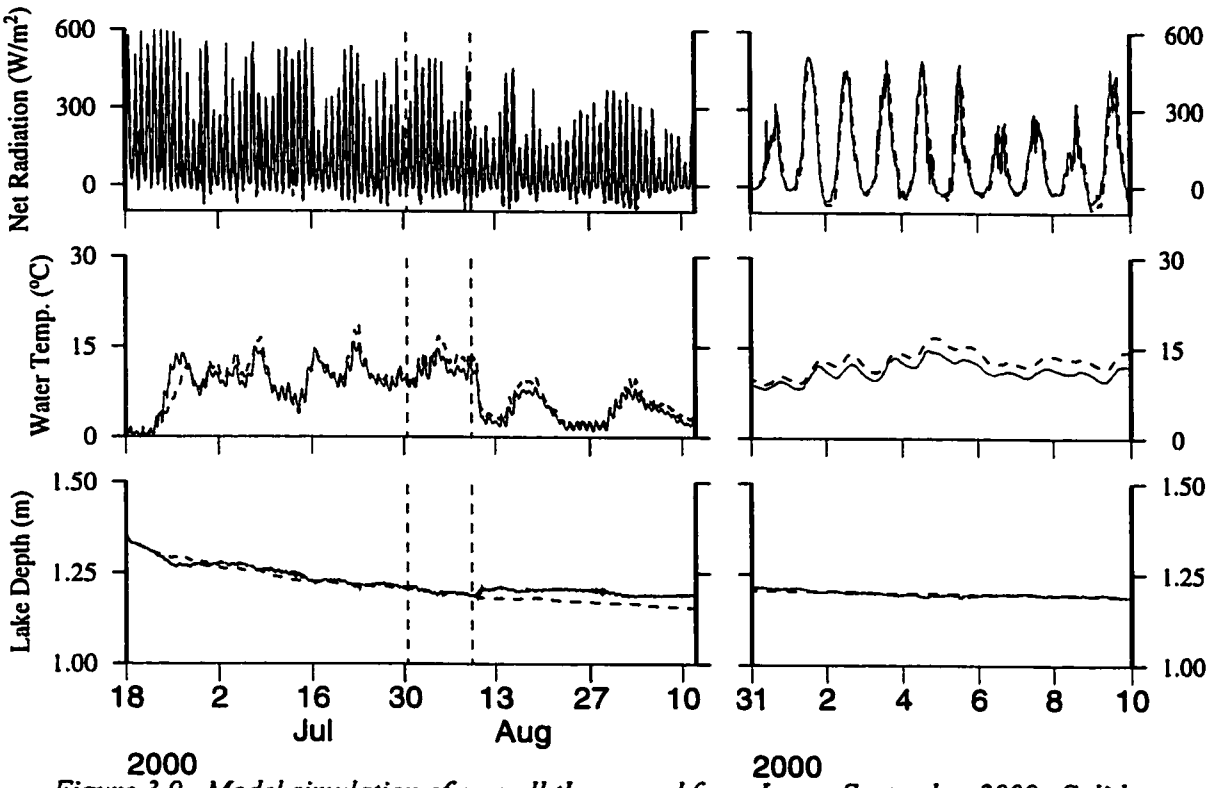

Figure 3.9. Model simulation of a small thaw pond from June – September 2000. Solid = observed, dashed = simulated: a) net radiation b) water temperature and c) lake level. The dashed lines indicate the boundaries of the time period shown in the figures on the right hand side.

Spatial Estimates

An estimate of the total storage change in the Putuligayuk watershed over the summer due to evaporation from open water areas can be calculated by multiplying the time series of saturated area obtained from the SAR images by the simulated daily lake evaporation rate, less the precipitation total. A time series of daily surface water area is calculated by linear interpolation of the classified area between dates (Figure 3.8). The estimated total change in catchment storage at the end of the summer due to open water evaporation is 16 mm for 1999 and 15 mm for 2000. This accounts for 64 (1999) and 50 (2000) percent of the storage observed during snowmelt of the previous spring.

SYNTHESIS AND DISCUSSION

The observations and results presented above provide a basis for evaluating the general role of surface storage in the functioning of the low-gradient Putuligayuk watershed. We approach the evaluation in three steps. First, insights provided by differences between the two summers of observations are explored in greater detail. Second, based on these insights, the balance of snow melt water in the Putuligayuk catchment for the period June 1999 – June 2001 is estimated. Finally, a hypothesis regarding the role of lakes and wetlands in modulating runoff response in this low-gradient Arctic catchment is formulated.

Effect of Climatalogical Differences

Differences in basin response to spring melt conditions can be seen via comparison of conditions in the spring of 1999 and 2000. Warm temperatures and clear skies dominated snowmelt in 2000, while snowmelt in 1999 was characterized by frequent cloud cover and near-freezing temperatures. Therefore, a snow pack that was 43 percent greater at the onset of melt in the spring of 2000 relative to 1999 melted in a shorter time period. The larger input of snow meltwater resulted in a runoff response that was 55 percent greater than 1999 and represents the largest flow recorded on the Putuligayuk River in seventeen years of record.

The maximum surface water extent was 38 percent larger in 2000 than in 1999 and total inundated area remained higher until approximately July 15th, when the inundated area became approximately equal for the two years (Figure 3.8). There was also a much larger rate of baseflow drainage over the summer of 2000 as compared to 1999 (Figure 3.2), as indicated by lower values of the normalized cumulative discharge in June and early July. The normalized cumulative discharge curves for 1999 and 2000 become approximately equal following July 18th.

As shown in Figure 3.10, the warmer temperatures and greater radiation input resulted in faster warming of the active layer during the melt period in 2000. Although surface soils remained frozen between the end of snowmelt and the date of peak flow in 1999, the active layer was thawed to approximately 6 cm by the end of the same period in 2000 (note that the end of the snowmelt period is defined here as the last day on which snow surveys could be performed at the Betty Pingo wetland complex).

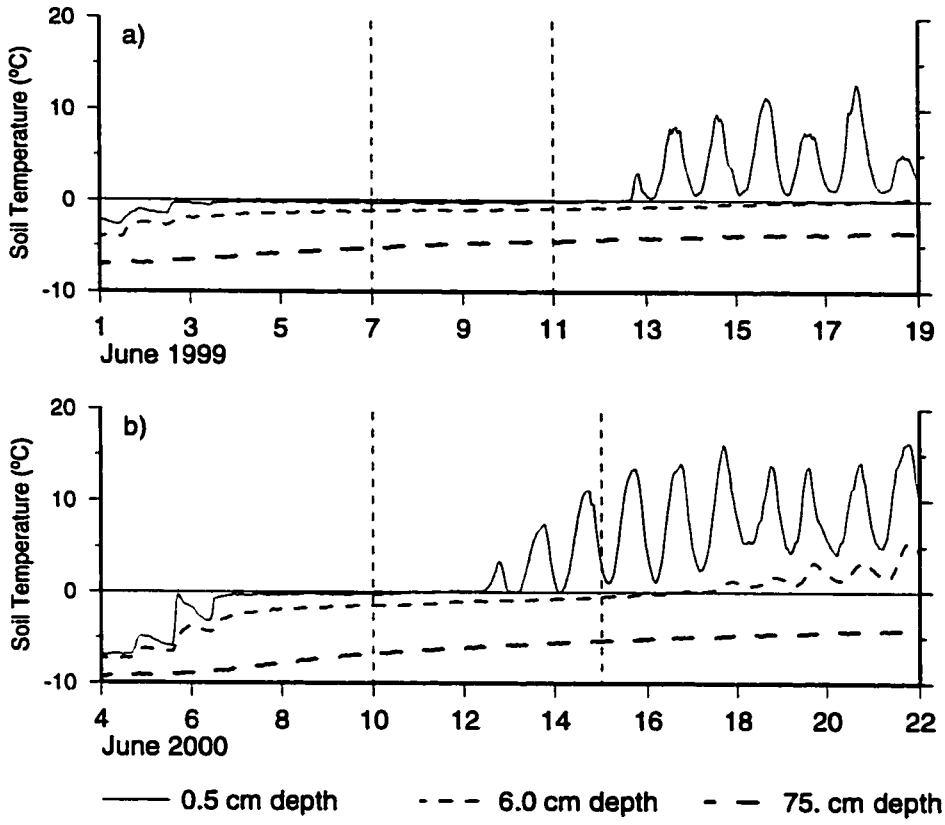

Figure 3.10. Soil temperature profiles for the wetland site in the time period surrounding snowmelt for a) 1999 and b) 2000. The first dashed vertical line indicates the date on which snow surveys ceased. The second dashed line indicates the date of peak discharge on the Putuligayuk River.

Given similar moisture conditions, the end-of-winter soil temperatures would be expected to be warmer in 2000 than in 1999 due to the insulating effects of the deep snowpack. This is not the case, as indicated by the beginning of the time series in Figure 3.10, which suggests that soils may also have been drier in 1999-2000 than in 1998-1999. Without the latent heat released by the freezing of soil moisture, soil temperatures would have been cooler.

Water Balance

Direct observations of the spring water balance for the Putuligayuk catchment for three years (1999 to 2001) indicate that 25, 30 and 37 mm, respectively, of snow meltwater did not contribute immediately to runoff. Based on the discussion above and neglecting measurement errors for the moment, there are four pathways that the stored "excess" meltwater could have followed: a)

evaporation from flooded tundra regions; b) release as baseflow drainage over the course of the summer; c) recharge of the active layer on regions that were not flooded during and immediately after snowmelt and d) contribution to interannual storage in the ponds and wetlands. The available observational data for this time-period does not allow complete closure of the meltwater balance to explicitly quantify each of these components, but qualitative estimates of the relative importance of each component can be made.

The RADARSAT imagery time series for the summers of 1999 and 2000 shows that areas of inundated tundra vary over the course of the summer from as much as 67 percent of the watershed, to as little as 15 percent. In conjunction with the estimates of point evaporation described above, this suggests that 16 and 15 mm of the stored meltwater evaporated from open water areas over the course of 1999 and 2000, respectively. That is, there are 16 and 15 mm of evaporation in excess of accumulated summer precipitation on inundated areas.

Cumulative discharge in the Putuligayuk River during the summer recession period, defined as all streamflow after the inflection in point in the annual snowmelt-induced peak, totaled 8 mm in 1999 and 36 mm in 2000. In general, the Putuligayuk River discharge is minimally affected by summer precipitation events (see e.g. Figure 3.2). The river discharge shows discernible runoff response to late summer precipitation events in only seven of the 17 years of record. The actual runoff response to summer rain events depends on the intensity and duration of the storm and the degree of saturation of the basin. To identify runoff events in response to summer precipitation, hydrographs for the summers of 1999 and 2000 were separated into baseflow and quickflow components using an exponential recession curve (see Figure 3.11). Based on the difference between the observed hydrograph and the fitted recession for the entire summer of 1999, a total of 87 mm of precipitation input resulted in only 5 mm of fast response runoff. The remaining 3 mm of discharge in 1999 is considered baseflow drainage. In 2000, there is little observable (1.3 mm) direct streamflow response to summer precipitation, and the remaining 35 mm of measured discharge appears to be baseflow.

The relative contribution of recharge to upland tundra areas is difficult to assess because no direct observations of tundra moisture content were made during this period. Instead, the contribution of recharge was estimated as follows. It is known that vapor flux into the colder snowpack from the underlying soil over the winter can result in desiccation of the surface soil layer in arctic

environments (Kane et al. 1989, Woo 1986). In addition, during mid-winter drops in temperature, cracks may form that can extend downward in excess of five meters (Mackay 1974). Higher than expected infiltration rates have been found in the early stages of melt as infiltration occurs into the cracked and desiccated soil (Kane et al. 1989, Mackay 1983, Woo 1986). Kane et al. (1989) estimated that 15 mm of moisture was needed to recharge the active layer in the Imnavait Creek watershed, located less than 200 km south of the Putuligayuk River in the foothills of the Brooks Range. Extensive cracking of the permafrost soils has not been observed in either Imanavait Creek or near the Putuligayuk River (Kane, personal communication), so it is assumed that drying of the soils through vapor flux is the main driving force for infiltration in the spring for both locations. Annual maximum precipitation occurs in the fall just prior to the basin freezing, so we assumed that the tundra was saturated in both years just before freeze-up. In that case, the only storage available for snowmelt in the surface soil layer is due to desiccation over the winter. Since this quantity has not been measured directly for the Putuligayuk River, a constant winter vapor flux of 15 mm is assumed. Under the assumption that 15 mm of snowmelt goes to re-wetting of the surface soils in the non-flooded regions of the tundra, approximately 8 mm of recharge would have occurred in 1999, and 5 mm in 2000, when normalized by the total basin area.

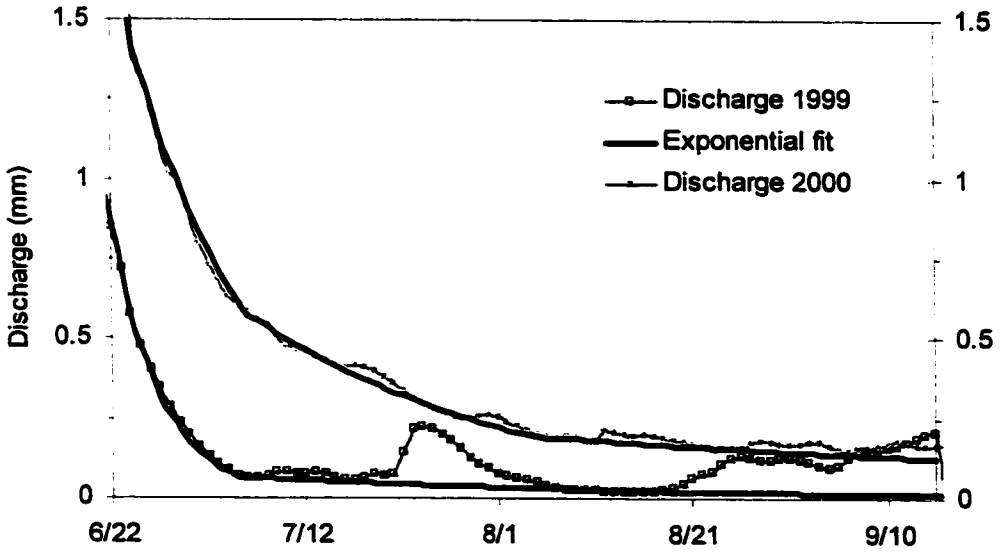

Figure 3.11. Separation of observed Putuligayuk River discharge into baseflow and quickflow components for 1999 and 2000.

The components of the snowmelt water balance described above are summarized in Table 3.6. The sum of the four components yields an estimate of the change in storage over the summer of –2 mm for 1999 and –25 mm for 2000. The influence of each component on total 'reservoir' storage in the catchment is shown graphically in Figure 3.12. The bars shown in Figure 3.12 correspond to each of the rows in Table 3.6, starting with the first bar that shows the initial storage conditions in the basin prior to snowmelt in 1999. The total height of the black column shows the evolution of storage depth in the basin following snowmelt input (bar 2) and the removal of storage due to runoff, recharge, drainage and lake evaporation (bars 3, 4, 5 and 6). Bar 7 represents the end-of-season storage for 1999 (corresponding to row 8 in Table 3.6). The difference in height between bar 1 and bar 7 reflects the change in storage over the summer of 1999 (row 9 of Table 3.6). The process repeats following recharge in the spring of 2000 (bar 8), which corresponds to row 3 of Table 3.6.

Table 3.6. Snow meltwater balance for the Putuligayuk watershed

		1999	2000	2001
1	Carry-over storage from previous year	27 mm[a]	25 mm[c]	0 mm
2	Snow melt inputs[b]	81 mm	117 mm	93 mm
3	Depth of recharge above base (1+2):	108 mm	142 mm	93 mm
4	Immediate runoff	-56 mm	-87 mm	-56 mm
5	Recharge to tundra	-8 mm	-5 mm	NA
6	Drainage	-3 mm	-35 mm	NA
7	P-E lakes	-16 mm	-15 mm	NA
8	End of season storage (3+4+5+6+7):	25 mm	0 mm	NA
9	Change in surface storage (8-1):	-2 mm	-25 mm	NA

Notes:

[a]This is an arbitrary initial condition, assumed to be 27 mm in order to avoid negative storage for this two year period.

[b]SWE plus evaporation/condensation from Table 3.2.

[c]From 1999, line 8.

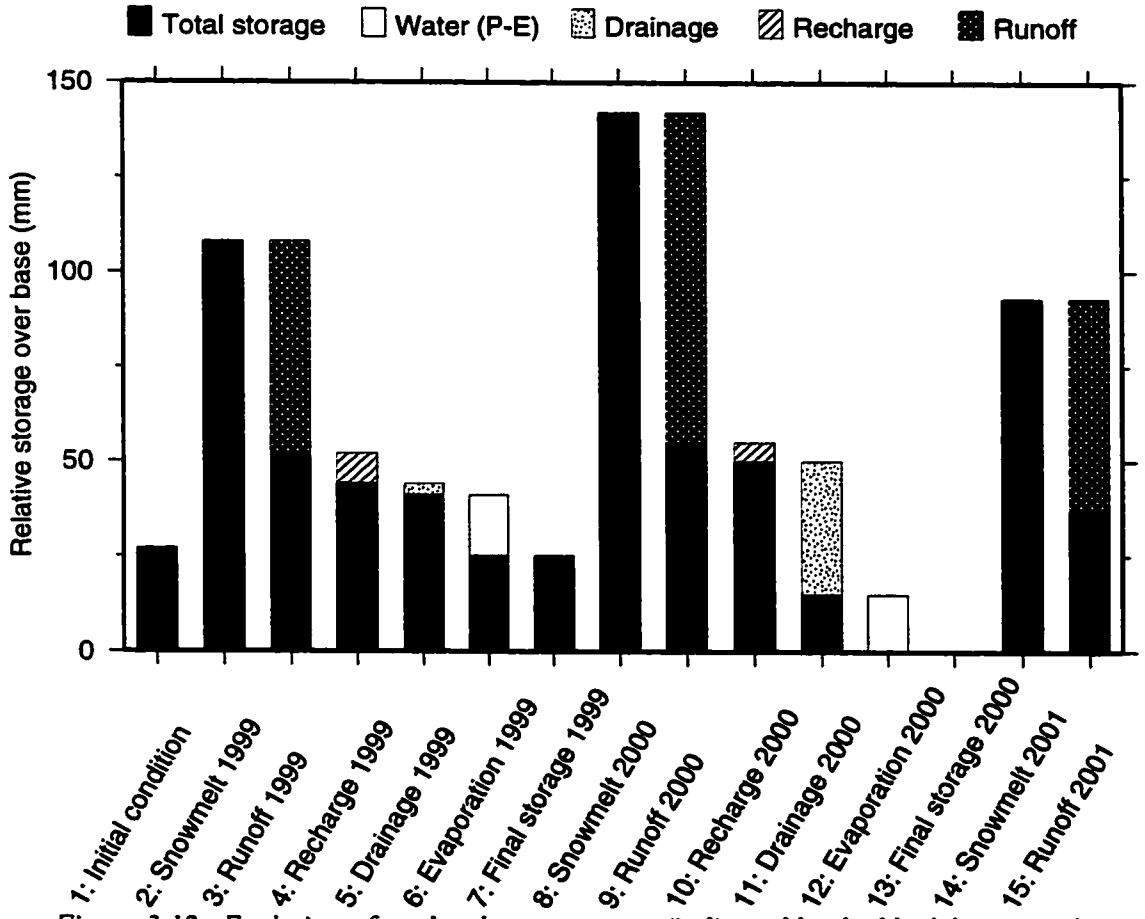

Figure 3.12. Evolution of total meltwater storage(indicated by the black bars) in the Putuligayuk catchment over the course of two summers and three snowmelt seasons as it is resolved into its five identified components: evaporation from open water areas, baseflow drainage, soil moisture recharge, direct runoff and interannual storage. The initial condition of 27 mm of storage carried over from 1998 was assumed to avoid negative storage in 2000 for plotting purposes. See the associated text for a further explanation.

Implications for influence of ponds on snowmelt runoff

The poorly defined drainage network of the low-gradient Putuligayuk catchment in many ways reflects the variable source area concept, as developed by Dunne et al. (1975). Precipitation and snowmelt inputs increase the total saturated area in the basin. As the saturated area increases, so does the connectivity of larger areas of the basin to the flow network and the effective contributing area. Because of this, surface runoff is prevalent in the Putuligayuk catchment immediately following snowmelt. From the SAR imagery we know that at least 50% of the catchment is flooded at the beginning of the summer. Surface flow takes place as these flooded

regions expand and connect. Due to the low topography and subsequent low drainage divides flow pathways may change when blocked by snow banks or other objects. As the floodwaters recede, this temporary network becomes fragmented. The decreasing connectivity of the Putuligayuk watershed with flood recession can be seen to some degree even at the coarse resolution of the ScanSAR data, as shown in Figure 3.13.

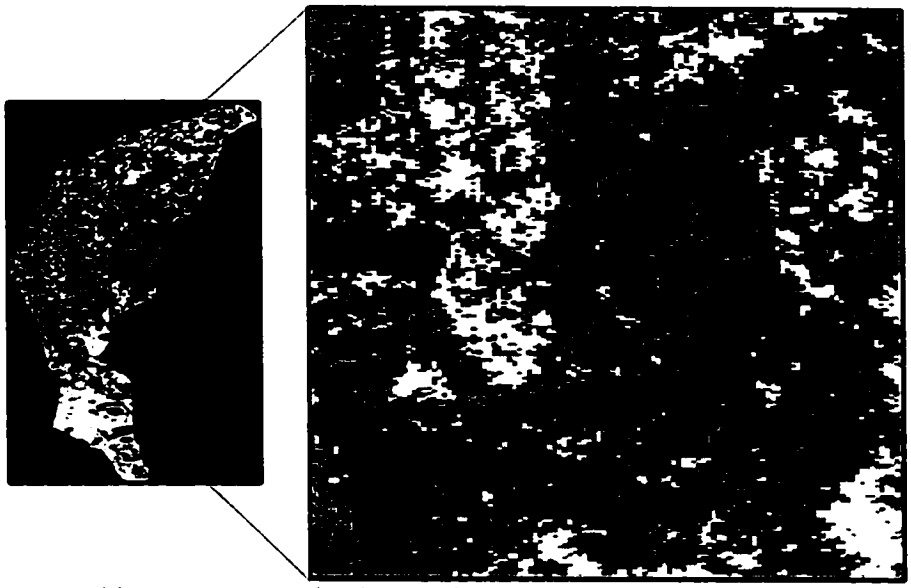

Figure 3.13. Variable source areas for the Putuligayuk catchment showing how the flow network expands and contracts. Gray shading represents the extent of the surface inundation for different storage levels, as determined from the summer 2000 ScanSAR images. White areas are never flooded in 2000.

Due to the low topographic gradients of the Putuligayuk catchment and the presence of continuous permafrost that restricts subsurface drainage, the variable source areas can also be compared to the filling of a surface reservoir. A larger saturated extent is directly related to a greater depth of water in the reservoir and the runoff rate is proportional to the depth of liquid water. This was observable in the summer of 2000, when a larger depth of stored surface water sustained a higher base flow rate throughout the summer (compare columns 5 and 11 in Figure 3.12).

There appears to be a minimum threshold below which precipitation and snowmelt inputs do not cause an increase in saturated extent or greater connectivity of the flow network, i.e. when the reservoir is drawn below its outflow point. For Imnavait Creek, in the foothills of the Brooks

Range, Kane et al. (1989) found that about 15 mm of water (precipitation or snowmelt) had to be added to the active layer before inducing a runoff response. A similar result is expected for the Putuligayuk, with potentially more input needed to generate a streamflow response due to the low topographic gradients and numerous ponds.

The total amount of snow meltwater that does not exit the basin immediately as runoff is therefore dependent both on evaporation from ponds over the previous summer and the snow water equivalent for the current year. As indicated in Table 3.6, the end of season storage is essentially the same in 1999 as that in 1998 (i.e., -2 mm difference). The large snowmelt pulse in 2000 was therefore able to fill surface reservoirs to greater heights than in 1999. However, the larger drainage component over the summer of 2000 depleted the surface reservoirs to 25 mm below their level at the end of summer 1999. This means that the maximum snowmelt storage in the spring of 2001 was considerably larger than in 1999 (37 mm vs. 25 mm), despite cumulative SWE very similar in 2001 and 1999 (89 mm vs. 87 mm).

We would expect that similar runoff rates would be generated for similar recharge depths. However, when we account for estimated interannual storage change in Table 3.6, the reservoir recharge depth following snowmelt in 2001 is substantially lower than in 1999 (93 mm vs 108 mm), but similar runoff volumes were generated (approximately 56 mm for both years). This discrepancy suggests either an error in the calculations, or that there is some term that has been missed. The most obvious error lies in the assumption that the 35 mm of drainage in 2000 derives entirely from stored snowmelt in inundated areas, with no baseflow drainage deriving from melting ground ice or precipitation on surrounding tundra areas. Thawing of the active layer over the course of the summer releases ground ice meltwater that could potentially augment summer baseflow. Young and Woo (2000) found that a valley-bottom wetland in the high Arctic was sustained over the summer in part by ground ice melt. However, the low-gradients and low hydraulic conductivity of the mineral soils in the Putuligayuk catchment, suggests that the mobility of the unfrozen groundwater may be too low to substantially influence summer baseflow.

The observed pond stage shown in Figure 3.9 indicates that there is some increase in pond depth in the first week of August, 2000, in response to summer precipitation events. Therefore, it seems likely that the baseflow drainage in 2000 was enhanced by precipitation on upland tundra areas

increasing storage in the lakes. Based on the runoff response in the spring of 2001, we expect the baseflow drainage due to snowmelt may be closer to 20 mm than the original estimate of 35 mm. This reduced estimate of drainage results in basin recharge levels in 2001 that are similar to those in 1999.

CONCLUSIONS

Wetlands are extensive in low gradient areas of the Arctic coastal plain. Large areas of the tundra are flooded immediately following snowmelt, at which point the surface drainage network is fully connected. The Putuligayuk catchment, located on the Alaskan North Slope, is characterized by a large snowmelt induced response that peaks between 7 to 10 days following ablation of the winter snowpack. Baseflow drops dramatically following snowmelt and there is little streamflow response to summer rain events. Whereas well-drained sites are dominated by sensible heat transfer and heat conduction into the ground (for primarily thawing of active layer), wetlands are dominated by latent heat fluxes. Analysis of seasonal water balances and a temporal series of SAR imagery leads to the following conclusions regarding the function of wetlands in low gradient areas of the Arctic coastal plain:

- Water balance calculations over three melt seasons indicate that between 25 and 37 mm of snow melt water is not immediately available for runoff.

- This observed storage effect can be explained in large part by baseflow drainage and the excess of evapotranspiration over summer precipitation from open water areas. Simulated daily evaporation rates coupled with a time series of surface water extent derived from RADARSAT imagery indicate that evaporation from open water areas accounts for 50 and 64 percent of the snowmelt storage in 1999 and 2000, respectively.

- The quantity of baseflow drainage of stored melt water is variable from year to year and appears to be dependent on the total depth of stored water.

- Evaporation and drainage result in a seasonal reduction of the extent of surface water bodies of 58 to 73 percent and a reduction of surface wetness over the summer period. The largest decrease in saturated extent takes place in the first one to two weeks following

snowmelt. After this point, the drainage network becomes disconnected, and the remaining decrease in surface water extent is primarily through evaporation.

- Some of the surface storage deficit is made up during the early fall period when precipitation is generally at an annual maximum while ET is rapidly shutting down. Late summer precipitation may result in runoff from upland tundra areas to partially recharge pond storage. The surface storage deficit carried over the winter must be satisfied the following spring before any runoff will be generated.

CHAPTER IV: A PREDICTIVE MODEL OF THE EFFECTS OF LAKES AND WETLANDS ON THE WATER BALANCE OF ARCTIC ENVIRONMENTS

INTRODUCTION

Lakes and wetlands are particularly prevalent in large regions of the Arctic, where the presence of permafrost and modest relief impedes the subsurface drainage of water (UNESCO 1978). Thousands of shallow thaw lakes cover up to 40 percent of the tundra on the Alaskan North Slope (Jeffries et al. 1999) and 30 to 50 percent of the central Mackenzie delta region (Marsh and Bigras 1988). Similarly, in the of western Siberia lowlands, tundra marshes compose up to 40 percent of the land area (Moskvin 1989). The predominance of surface water storage controls many aspects of the land surface water balance in these regions, through a tendency to suppress runoff and increase evaporation (UNESCO 1978). The presence of many lakes is often cited as a reason for lower interannual and seasonal variability in runoff from the lakes region of the Mackenzie River, relative to the large Eurasian arctic rivers (UNESCO 1978, Vuglinsky 1997, Cattle 1985).

Observations in arctic Canada and Alaska indicate that annual evaporation from lakes and wetlands exceeds annual precipitation (Roulet and Woo, 1986, Marsh and Bigras 1988, Rovansek et al. 1996, and Mendez et al. 1998). Rovansek et al. (1996) found that evaporation is the major cause of the observed drop in pond water levels during the snow-free period for a tundra wetland complex in northern Alaska. The wetlands therefore depend on a supply of water from the surrounding uplands that comes primarily from snowmelt (Bigras 1990, Rovansek et al. 1996) and in some cases by subsurface drainage and ground ice melt (Moskvin 1989, Young and Woo 2000).

Runoff from northern wetlands occurs as intensive surface flow following snowmelt (Rovansek et al. 1996, Moskvin 1989). The high ice content of poorly drained wetland soils makes them

slow to thaw, so infiltration may be delayed relative to drier soils (Roulet and Woo 1986, Woo and Xia 1996). Surface storage provides an initial control on runoff at the beginning of snowmelt (Glenn and Woo 1997, Rovansek et al. 1996). Lake volumes in the Mackenzie Delta, N.W.T., Canada have been observed to increase between 90 and 330 percent above mid-summer volumes with the influx of snow melt water (Bigras 1990). Lake water levels typically drop rapidly following spring melt (Bigras 1990, Bowling et al. 2002a). In the wetlands of northern Alaska and western Siberia, runoff often ceases in the summer and the active layer dries. Lake and wetland storage is gradually decreased through evaporation and becomes disconnected from the surrounding watershed (Moskvin 1989, Rovansek et al. 1996, and Bowling et al. 2002a).

Because of the high heat capacity of lakes and the availability of water for evaporation, lakes and wetlands act as surface heat reservoirs that can influence regional climate and the spatial distribution of energy fluxes. During the summer in northern Alaska, Mendez et al. (1998) found that 46 percent of net radiation went to latent heat of evaporation over wetlands, in contrast to 23 percent in a dryer upland tundra site. Jacobs and Grondin (1988) found that strongly positive sensible heat fluxes from two large lakes on south-central Baffin Island, N.W.T., Canada led to relatively warm (2° C above regional conditions) summer climate conditions in the interior lowlands relative to dry regions of the interior. Jeffries et al. (1999) found that conductive heat flow from water below the ice and snow layer near Barrow, Alaska provides a significant source of winter heat flux to the atmosphere.

The importance of the disparate heat fluxes from land and open water areas has led to the introduction of lake modules in regional climate models for the prediction of both past and present conditions (Goyette et al. 2000, Hostetler et al. 2000). Hostetler et al. (2000) used a regional climate model nested within a General Circulation Model (GCM) to simulate the effect of Lake Aggasiz on central North American climate 11,000 years ago. Goyette et al. (2000) included a mixed layer lake model within the Canadian Regional Climate Model (CRCM) to represent the evolution of water surface temperature and the initiation of lake ice cover, with the motivation of improving prediction of lake-induced winter precipitation downwind of the Laurentian Great Lakes.

Despite recent interest in representing the atmospheric effects of lakes in regional climate models, the hydrologic effects of lakes are largely neglected in the land surface schemes (LSS) of GCMs

used to predict the earth's climate. This is due in part to the scale differential: at the scale of current-generation GCM model grid cells, lakes rarely occupy an entire model grid cell, or even a major part of one. Seven of the 21 LSS that participated in the Project for Intercomparison of Land-surface Parameterization Schemes (PILPS) Phase 2(e) arctic model intercomparison (Bowling et al. 2002b) calculated evaporation from open water areas within the model grid cell. Only two of the models represented the storage retardation effect of lakes on the runoff hydrograph.

In this paper, we describe an algorithm to represent the evaporation and storage effects of lakes and wetlands within the variable infiltration capacity (VIC) macroscale hydrology model. The model is evaluated with respect to its ability to represent water temperatures, net radiation, ice freeze/thaw and runoff production for a variety of high-latitude locations. It is then used to investigate the influence of lake and wetlands on the spatial and temporal distribution of water and energy fluxes for the Putuligayuk River watershed, on the Alaskan Arctic coastal plain.

MODEL DESCRIPTION

The lake model is intended for use within the framework of the Variable Infiltration Capacity (VIC) macroscale hydrology model (Liang et al. 1994; 1996, Cherkauer and Lettenmaier 1999). VIC has been applied in many diverse environments, including a global application at 2° latitude/longitude resolution (Nijssen et al. 2001) and across the contiguous U.S. at 1/8° resolution (Maurer et al. 2002). Surface runoff is generated according to the variable infiltration curve, which represents the dependence of infiltration capacity on the spatial distribution of surface soil moisture (Liang et al. 1994). Baseflow is generated according to an empirically-based nonlinear soil moisture relationship (Liang et al. 1994). The effects of seasonally and permanently frozen soil on infiltration and runoff are represented using the method of Cherkauer and Lettemaier (1999) and Cherkauer et al. (2002). Once generated, surface runoff and baseflow are released from the model grid cell and are therefore no longer available for use within the grid cell. An independent routing model is used to route the runoff and baseflow to the basin outlet for prediction of streamflow hydrographs (Lohmann et al. 1998). The model is designed to be applied at scales sufficiently large that subsurface transfer of moisture between model grid cells

can be neglected, and all transfer of moisture between grid cells occurs via the runoff routing postprocessor.

The algorithm described here is intended to represent the effects of lakes and wetlands in the VIC model by creating a surface wetland land class that can be added to the grid cell mosaic, in addition to the vegetation and bare surface land classes. The wetland class represents seasonally flooded ground as well as permanent water bodies. Water and energy components of the combined lake and wetland are resolved at each model time step. The energy balance of the lake component builds on the work of Hostetler and Bartlien (1990), Hostetler (1991), and Patterson and Hamblin (1988), while that of the exposed wetland follows Cherkauer and Lettenmaier (1999).

Lake Algorithm Description

Evaporation from the water surface is calculated in each time step by solving a surface energy balance in the manner of Hostetler and Bartlien (1990) and Hostetler (1991). Energy exchange with the atmosphere takes place within a fixed depth surface water layer. Latent and sensible heat fluxes from the open water area are calculated based on an aerodynamic drag coefficient (e.g. Brutsaert 1982). Absorption of solar radiation by the surface layer is assumed to follow Beer's law. A two-band system is assumed, so radiation intensity as a function of depth, h, is given by (Patterson and Hamblin 1988):

$$I(h) = I_o\left[A_v \cdot \exp(-\lambda_v h) + A_{NIR} \cdot \exp(-\lambda_{NIR} h)\right] \qquad (4.1)$$

where I_o is the net shortwave radiation at the water surface, A_v and A_{NIR} are the fractions of total radiation in the visible and near-infrared bands, respectively, and $\lambda_{v \text{ and}}$ λ_{NIR} are the attenuation coefficients of the two bands.

Figures 4.1 and 4.2 compare model simulations and observations of net radiation and water temperature from the largest of three thaw ponds monitored on the Alaskan Arctic coastal plain for the summers of 1999 and 2000. Other meteorological components needed to run the VIC lake algorithm, including downward solar and longwave radiation, wind speed and humidity are monitored at a nearby meteorological tower maintained by the Water and Environmental Research Center (WERC) at the University of Alaska Fairbanks (UAF). Net radiation was

monitored using a Q-7.1 net radiometer from Campbell Scientific. Wind induced convective cooling as air moves over the sensors can cause a reduction in the measured net radiation of up to 6 percent for positive fluxes and 1 percent for negative fluxes. The observed net radiation was adjusted for this bias using observed wind speed from the UAF meteorological tower. Since the ponds are shallow (1 to 1.5 m), they are not affected by stratification and diffusive effects, and so provide a good evaluation of the surface energy balance alone. Figure 4.1 shows that the energy balance calculation is able to represent both the daily average surface water temperature and net radiation of the thaw pond (Figure 4.1). The mean diurnal cycle is also well represented, although the diurnal cycle of the simulated water temperatures is suppressed relative to the observations (Figure 4.2).

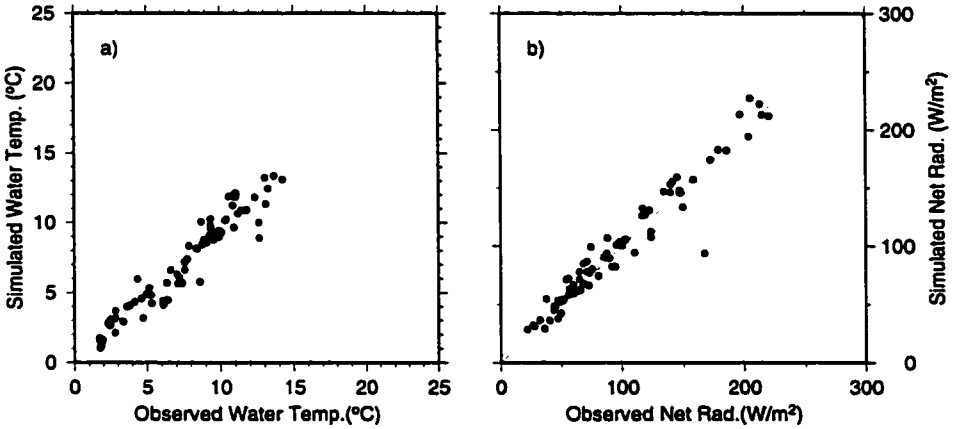

Figure 4.1. Simulated and observed daily average a) water temperature and b) net radiation for a thaw pond on the Alaskan Arctic coastal plain, June – August, 2000

In deeper lakes, the average temperature for each layer is resolved by solving a set of simultaneous equations. Included in these equations are the effects of radiation absorption by each layer and the eddy diffusion of heat from adjacent layers by molecular and wind-induced turbulent mixing (Hostetler and Bartlien 1990). Convective mixing due to temperature instabilities is also represented (Hostetler and Bartlien 1990). The number of computational layers in the lake is controlled by a user-specified number of nodes. Lake layer thickness is dynamic in response to changes in water level.

Figure 4.3a illustrates the average (1993-1999) observed water temperature profile of Toolik Lake, Alaska, for the ice-free period. Toolik Lake is a 1.5 km^2 kettle lake located in the foothills of the Brook's Range (68° 38' N, 149° 43' W). Its maximum depth is 25 m (7m average) and it is

ice-free from July through September. Periodic lake temperatures and ancillary meteorological data have been collected by researchers at the Marine Biological Laboratory of the Woods Hole Oceanographic Institution since 1975 as part of the Arctic Long-Term Ecological Research project at the Toolik Field Station. Figure 4.3b shows that the VIC lake algorithm captures several important features of the observed water temperature profile. One of these is the depth of the thermocline (approximately 5 to 7 m) which is controlled in part by the depth of penetration of solar radiation. Another is the gradual downward migration of heat driven by eddy diffusion. Finally, the influence of convective mixing is apparent in late August, when the lake completely overturns and becomes isothermal in both the simulated and observed profile.

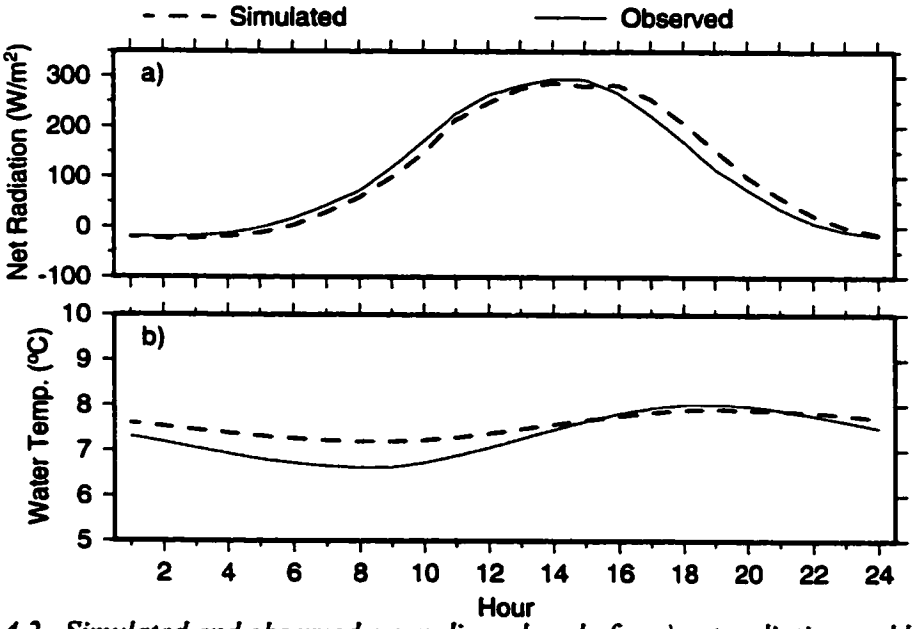

Figure 4.2. Simulated and observed mean diurnal cycle for a) net radiation and b) water temperature for a thaw pond on the Alaskan Arctic coastal plain, averaged for the period June – August, 2000

Freezing and thawing of the lake ice and snow accumulation over the frozen surface are represented in the VIC algorithm based on the method of Patterson and Hamblin (1988). A two-band solar radiation absorption model similar to equation (4.1) is assumed for the snow and ice layers. Exchange of energy with the atmosphere takes place at the snow and/or ice surface where the atmospheric fluxes must balance the heat flux out of the ice. Heat flux through the ice is driven by the temperature gradient, and must balance the heat flux from the lake and the energy of ice formation at the ice/water interface. Lake ice exists only if it exceeds a minimum

thickness. When the ice thickness falls below this threshold, ice fractional coverage is reduced until the minimum thickness can be maintained.

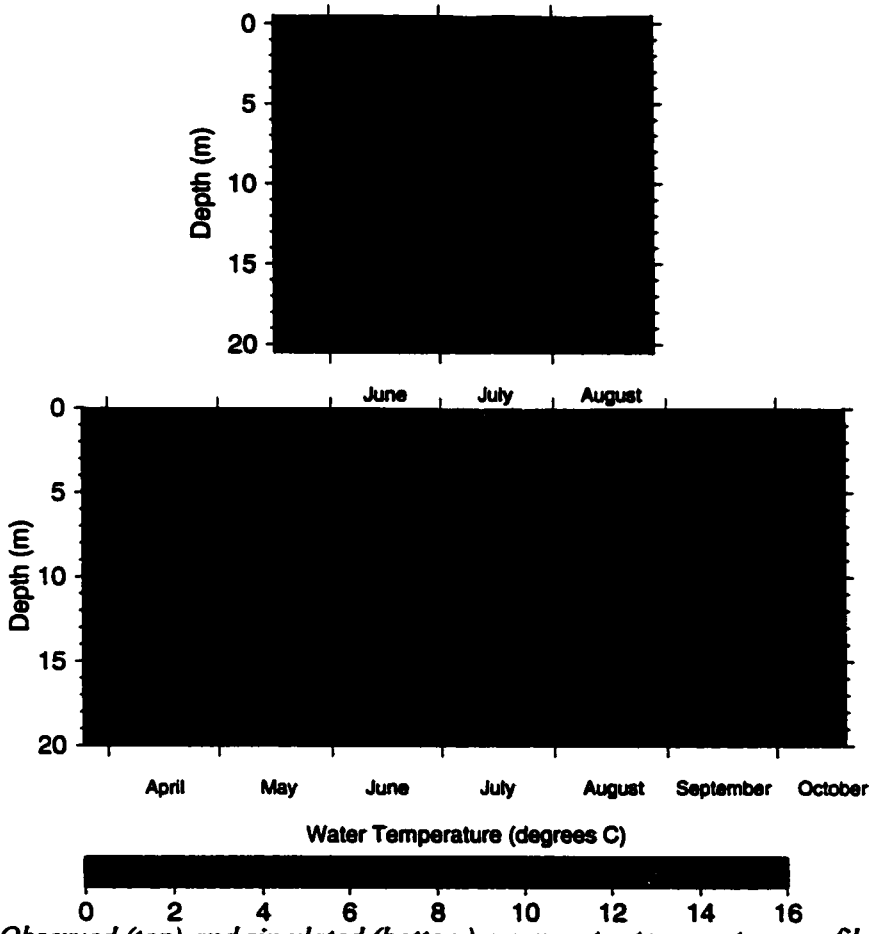

Figure 4.3. Observed (top) and simulated (bottom) mean water temperature profile (1993-1997) for the ice-free season for Toolik Lake in the foothills of the Brooks Range in northern Alaska.

The ability of the ice model to represent the depth and duration of ice cover for a range of arctic lakes was evaluated using data from northern Sweden. Figure 4.4 shows simulated and observed ice thickness on Torneträsk lake (68.1956° N, 19.9930° E) from January 1989 through December 1998. Torneträsk is a large glacial lake in the high mountain region of Sweden with a mean depth of approximately 150 meters. Ice thickness observations are collected weekly by the Swedish Meteorological and Hydrological Institute (SMHI). The simulated data represents a fraction of the VIC model grid cell closest to the observation location. Meteorological data for this simulation came from the PILPS 2(e) model intercomparison (Bowling et al. 2002b). Maximum ice depth and the timing of break-up are well represented, despite an apparent bias in

the initiation of ice-cover in the fall. This bias is likely due to the inability of the simple one-dimensional model to represent the impact of wind, which suppresses continuous ice formation. Despite similar observed ice thickness in 1997 and 1998, the simulated ice thickness is much shallower in 1997 than in 1998. Air temperatures are colder in early 1998 when compared to 1997, which may partially explain the difference. In addition, the simulated ice thickness in 1997 may reflect an over sensitivity to the insulating effects of early season snow precipitation in the fall of 1996.

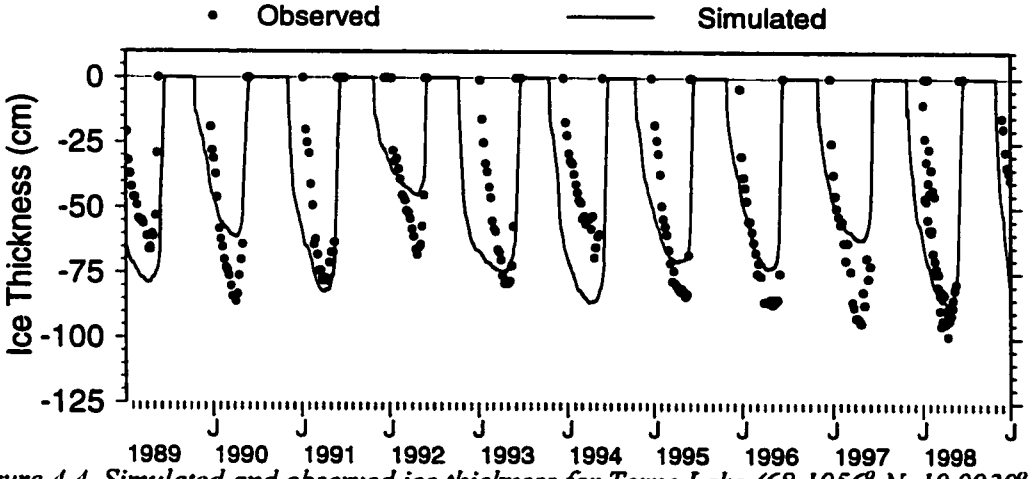

Figure 4.4 Simulated and observed ice thickness for Torne Lake (68.1956° N, 19.9930° E), northern Sweden, for the period 1989-1998.

The simulated dates of lake freeze-up and break-up for the period 1989 to 1998 on 14 lakes within the Torne-Kalix river basin in northern Sweden is shown in Figure 4.5. These dates are compared to observed dates of ice formation and break-up, which were collected by SMHI. For the simulated ice cover, the dates of freeze-up and break-up are defined, respectively, as the date on which the ice cover becomes continuous and the date on which the ice cover becomes fractional (for the "effective lake" in the 1/4° VIC model grid cell corresponding to the observation location). On average, the VIC algorithm is able to correctly represent the duration of the ice-covered period for these 14 lakes. The largest lakes (simulated lake area greater than 20 km^2) are indicated by open circles. There is a tendency for VIC to simulate a break-up date later than that observed for these lakes, which may be a function of river flow or other mechanical action not represented in the model which aids in the break-up of ice cover of most lakes.

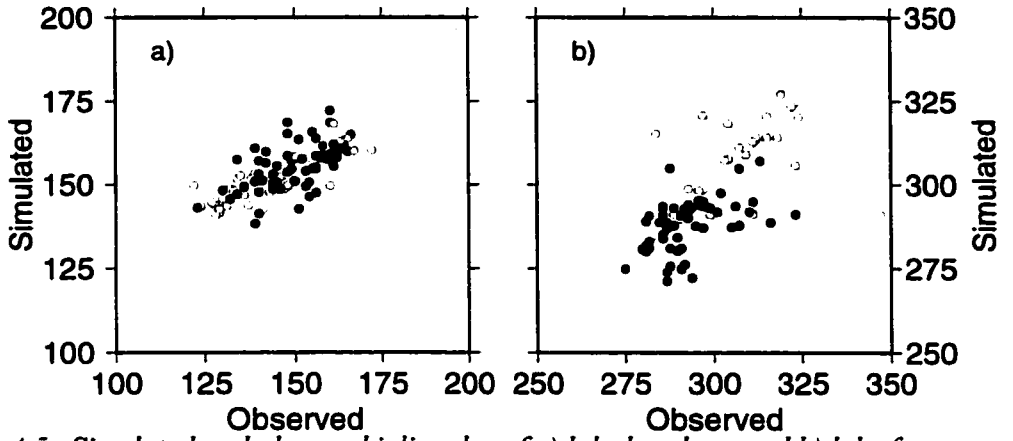

Figure 4.5. Simulated and observed julian day of a) lake break-up and b) lake freeze-up for the period 1989-1998 for 14 lakes in the Torne-Kalix basin, Sweden. Open circles indicate lakes greater than 20 km^2 in area.

Wetland Algorithm Description

Unique features of the VIC lakes and wetland algorithm include the interaction of the simulated lake with the VIC model grid cell and the ability to represent wetlands of varying size. The algorithm can be summarized as follows (see Figure 4.6):

- All open water areas within a VIC model grid cell are simulated together as an effective grid cell lake.
- A user-defined fraction of runoff from vegetated areas within the grid cell is diverted to the lake. This represents the storage retardation effect of lakes on spring melt.
- Once the new lake level is calculated, runoff is released from the lake according to a stage-based rule curve.
- Specification of a variable depth-area relationship allows for the representation of the reduction in surface water extent and the emergence of wetland vegetation following drainage of seasonally flooded wetlands.

Wetlands are defined as areas that are inundated for some portion of a year (Zoltai 1979). The tendency of a region to flood periodically can be represented within the VIC model by specifying a depth-area relationship for the maximum inundated fraction of the grid cell. For the clarity of subsequent discussion, 'wetland' fraction, C_{wet}, will be used to refer to the maximum fraction of the VIC model grid cell that can be flooded, while 'lake' fraction, f_{lake}, refers to the fraction of C_{wet} that is inundated for a given time step. As illustrated in Figure 4.7, as the stage of the

simulated lake drops, the open water area is recalculated and additional wetland area exposed. The energy and water balance of the newly exposed wetland is solved as an additional vegetation tile. The water balance of the wetland system can be represented as follows:

$$\Delta S = P - [E_w \cdot f_{lake} + E_v \cdot (1 - f_{lake})] + R_{veg} - D \qquad (4.2)$$

where ΔS is the change in soil moisture, lake and snow storage, P is precipitation, E_w and E_v are evaporation from the open water and wetland vegetation, respectively. R_{veg} is the runoff (and baseflow) into the lake from the non-wetland portion of the gridcell and D is the discharge out of the lake.

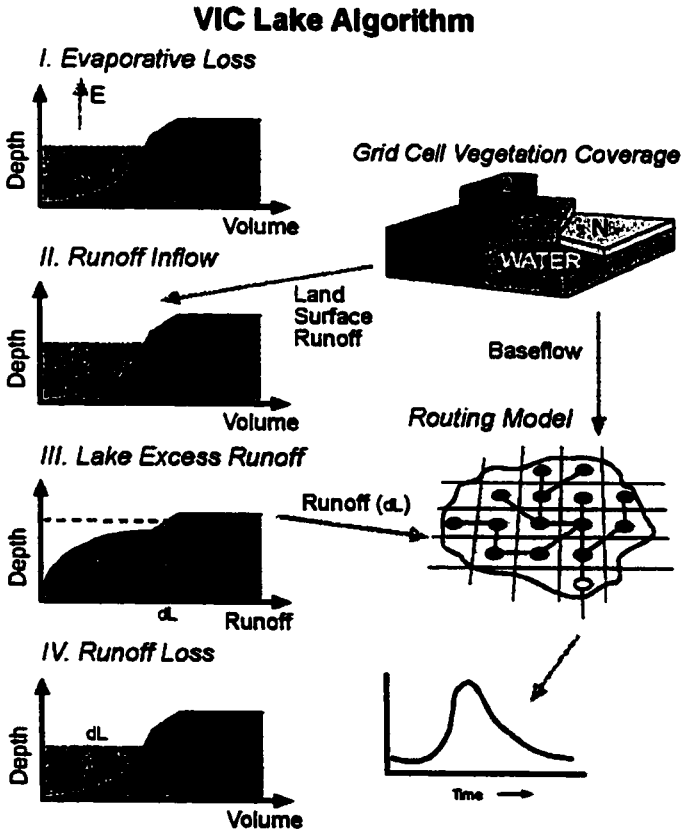

Figure 4.6. Schematic of the VIC lake algorithm. I: Evaporation from the lake is calculated via energy balance, II. Runoff enters the lake from the land surface, III: Runoff out of the lake is calculated based on the new stage, and IV: The stage is re-calculated.

The soil column under the lake is assumed to be saturated. As the lake area is reduced, the soil moisture of the non-lake area is updated to include the newly exposed fraction of saturated soil

(Figures 4.7b and c). Likewise, as the lake area expands, some of the lake volume must go to saturating the newly inundated soil (Figure 4.7d). The average soil moisture for the wetland fraction is therefore updated as follows:

$$\overline{W} = (1 - f_{lake}) \cdot W_v + f_{lake} \cdot W_{\max} \qquad f'_{lake} \le f_{lake} \qquad (4.3)$$

$$\overline{W} = (1 - f'_{lake}) \cdot W_v + f'_{lake} \cdot W_{\max} \qquad f'_{lake} > f_{lake}$$

where f'_{lake} and f_{lake} represent the new and old lake fraction, respectively. W_v is the wetland soil moisture for the current timestep and W_{max} is the total soil moisture storage capacity of the soil column. The volume of water (as mm per unit area) from the expanding lake used to recharge the wetland soil moisture is calculated as follows:

$$Recharge = (f'_{lake} - f_{lake}) \cdot (W_{\max} - W_v) \qquad f'_{lake} > f_{lake} \qquad (4.4)$$

Changes in lake stage are calculated via a water balance for the saturated lake area. Runoff into the lake is composed of all runoff and baseflow from the exposed wetland and a fraction of the runoff and baseflow from all other grid cell vegetation types, as follows:

$$R_{in} = R_{veg} + R_{wetland} = \alpha \cdot \sum_{i=1}^{N} (R_v(i) + B_v(i)) \cdot C_v(i) + (R_w + B_w) \cdot (1 - f_{lake}) \cdot C_{wet} \qquad (4.5)$$

where C_v is the fraction of the grid cell occupied by vegetation type i, and R_v and B_v are the runoff and baseflow from vegetation type i. α is a user-specified parameter controlling the portion of runoff from the vegetated areas that flows into the lake. R_w and B_w are the runoff and baseflow from the wetland.

To avoid the complications due to the variation of lake area with depth, lake volume is the state variable used for the water balance. A revised depth is calculated by piecewise integration of the volume and area curves. Discharge from the lake (mm/surface area) is calculated as a function of the new depth, as follows:

$$D(z) = \begin{cases} 0 & z < z_{\min} \\ \left(R_{\max} / (z_{\max} - z_{\min}) \right) \cdot (z - z_{\min}) & z_{\min} < z < z_{\max} \\ R_{\max} + (z - z_{\max}) & z > z_{\max} \end{cases} \qquad (4.6)$$

where R_{max} is the maximum runoff rate (in mm/timestep), z is the current lake depth, z_{max} is the depth at maximum areal extent (*i.e.* f_{lake} =1), and z_{min} is the minimum water level at which runoff is generated from the lake. Runoff and baseflow from the lake are calculated from $D(z)$, in proportion to their ratio in the inflow hydrograph. R_{max}, z_{min}, z_{max} and the depth-area curve are input parameters to the lake model. R_{max} is typically adjusted during calibration.

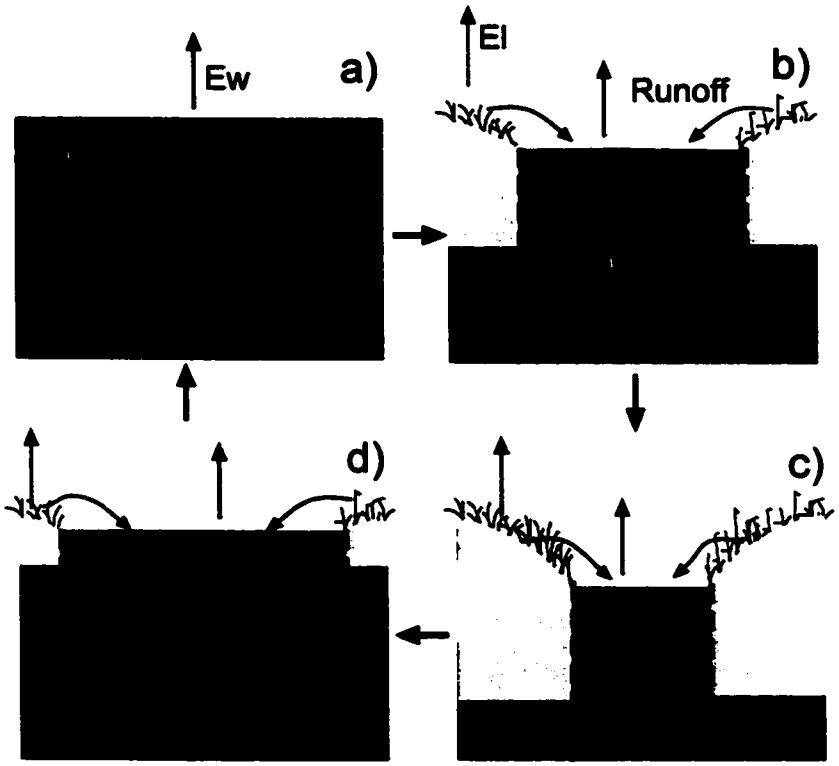

Figure 4.7. Schematic for the wetland algorithm: a) when the lake is at its maximum extent the soil column is saturated, b) as the lake shrinks runoff from the land surface enters the lake and c) evaporation from the land surface depletes soil moisture, d) as the lake grows, water from the lake recharges the wetland soil moisture

MODEL APPLICATION

Background

The Putuligayuk River is a 471 km^2 watershed located entirely on the Arctic coastal plain in northern Alaska (see Figure 4.8). The annual runoff hydrograph for the Putuligayuk River is

dominated by snowmelt and upwards of 90 percent of the annual discharge occurs in the two weeks following snowmelt. The watershed contains numerous thaw ponds and other permafrost features that impede drainage. As a result between 50 to 70 percent of the watershed is flooded seasonally (Bowling et al. 2002a). Bowling et al. (2002a) investigated the role of surface storage in ponds and wetlands on the hydrologic response of the Putuligayuk River and found that between 25 and 37 mm of snow melt water are not immediately available for runoff due to surface impoundment. Between 15 to 16 mm of the stored water is returned to the atmosphere by evaporation from open water areas, as determined from evaporation estimates and classification of RADARSAT ScanSAR imagery (Bowling et al. 2002a). The maximum extent of surface water was observed to decrease by 58 and 73 percent during the summer, in 1999 and 2000 respectively, due to the combined effects of evaporation and drainage. Following the large reduction in surface water extent, the drainage network becomes fragmented, and discharge from the watershed becomes near zero.

The Putuligayuk River was simulated using the VIC model with the lakes and wetlands algorithm at a grid cell resolution of 1/8° latitude by longitude (approximately 4.5 km by 7.5 km). Soil freezing and thawing is represented with a constant temperature lower boundary set to 0° C at a depth of 3 m using the algorithm of Cherkauer and Lettemaier (1999). Sublimation from blowing snow is also represented (see Chapter 5). Daily minimum and maximum temperature and daily total precipitation were obtained from two National Climatic Data Center (NCDC) Co-operative observer stations located on the Alaskan North Slope at the Prudhoe Bay and Kuparuk air fields (see Figure 4.8). Precipitation was corrected for gauge undercatch using the method of Yang et al. (1998) for an unshielded National Weather Service 8 inch standard gauge. The corrections for this wind swept environment resulted in a 70 percent increase in cumulative precipitation over the simulation period and are a major source of uncertainty in winter snow accumulation. Hourly water vapor pressure and wind speed were obtained from the Betty Pingo research site operated by the WERC at UAF. Incoming shortwave and longwave radiation are not monitored in this remote location during the winter months, so they were estimated internally to the model, using the method of Thornton and Running (1999).

The simulation period for the Putuligayuk was June 1994 through September 2000. Stream discharge measurements were re-initiated by UAF in 1999 after being discontinued by the USGS

in the 1980's. Observed discharge in the Putuligayuk River is therefore only available for 1999 through present. The period from September 1998 through September 1999 was used for calibration of the streamflow hydrograph. Calibration for streamflow primarily involved adjustment of the maximum runoff rate from lakes, and adjustment of the variable infiltration parameter, b_i and soil hydraulic paramters. The radiation extinction coefficients were adjusted slightly from published values (Patterson and Hamblin 1988) in order to obtain the best fit for the Toolik Lake profile, shown in Figure 4.3. The final radiation extinction coefficients and lake hydraulic parameters are listed in Table 4.1.

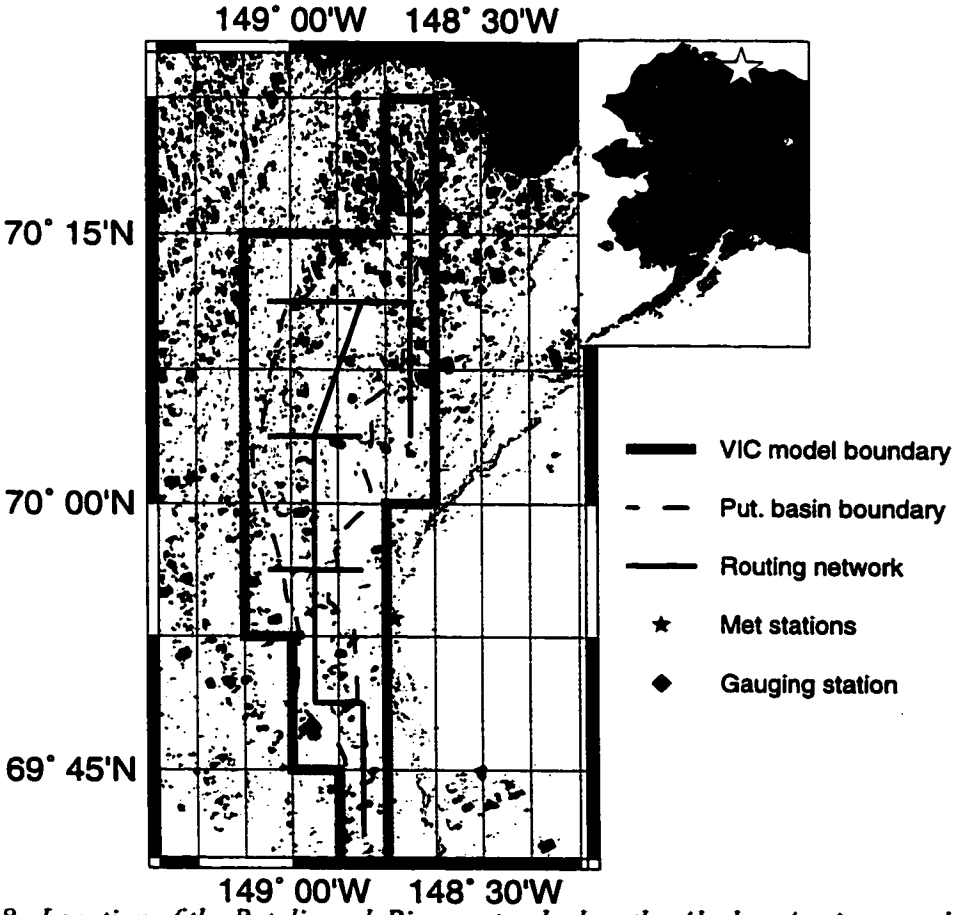

Figure 4.8. Location of the Putuligayuk River watershed on the Alaskan Arctic coastal plain and routing network for the VIC model at 1/8° resolution.

Lake Geometry

The physical description of the lake and wetland extent for each model grid cell was based on observations and consists of two primary components: the wetland extent and the extent of

permanent water areas. The depth-area relationship for the wetland portion of the watershed was derived from a time-series of classified RADARSAT ScanSAR images as described by Bowling et al (2002a). Bowling et al. (2002a) classified a sequence of images from the summers of 1999 and 2000 into water and non-water areas. From these classified images, it is possible to develop a time series of basin saturated extent, shown in Figure 4.9a. Simulated depth from the thaw pond simulations shown in Figures 4.1 and 4.2, yields a corresponding time series of lake depth (above the minimum depth of the largest monitored ponds), shown in Figure 4.9b. The combination of the saturated area and depth time series yields a plot of depth versus fractional saturated area shown as the black dots in Figure 4.9c. The lower range of the saturated extent (approximately 15 percent of the basin area) represents the point at which the wetlands are at their minimum extent. The remaining open water area corresponds to the location of permanent lakes and thaw ponds.

Table 4.1. Calibration parameters for the Putuligayuk River

Lake hydraulic parameters		
Max. runoff rate, R_{max}	0.0015 mm/hour	
Min. depth for runoff, D_{min}	1.15 to 1.4 m	
Max. allowable depth, D_{max}	1.54 m	
Coefficients for radiation attenuation	Visible	NIR
Ice, λ_{ice}	3.5	20
Water, λ_{water}	1.2	.1
Snow, λ_{snow}	12	20
Other		
New snow albedo	0.95	

The depth-area relationship for fractional areas below 15 percent is based on the bathymetry of the lakes themselves. The bathymetry of three typical thaw ponds on the coastal plain was determined using a laser-surveying station (total station) and inflatable raft. Three transects were made of each pond. The surveyed cross-sections were used to generate elevation contours within the Arc/Info geographical information system. The elevation contours were converted into a depth-area relationship for all three ponds, also shown in Figure 4.9c. The area was normalized and scaled such that the maximum percent area (the fractional basin area of permanent lakes and ponds) of each pond is 15 percent, as determined from the ScanSAR data. Although the three

ponds differ in maximum area (6,000, 7,000 and 16,000 m^2), the maximum depths are all between 1 and 1.5 meters, and the scaled depth-area relationships are all similar, due to the influence of the permafrost layer. It was therefore assumed that the average profile of pond fractional area versus depth is representative of the collective lakes and ponds of the coastal plain.

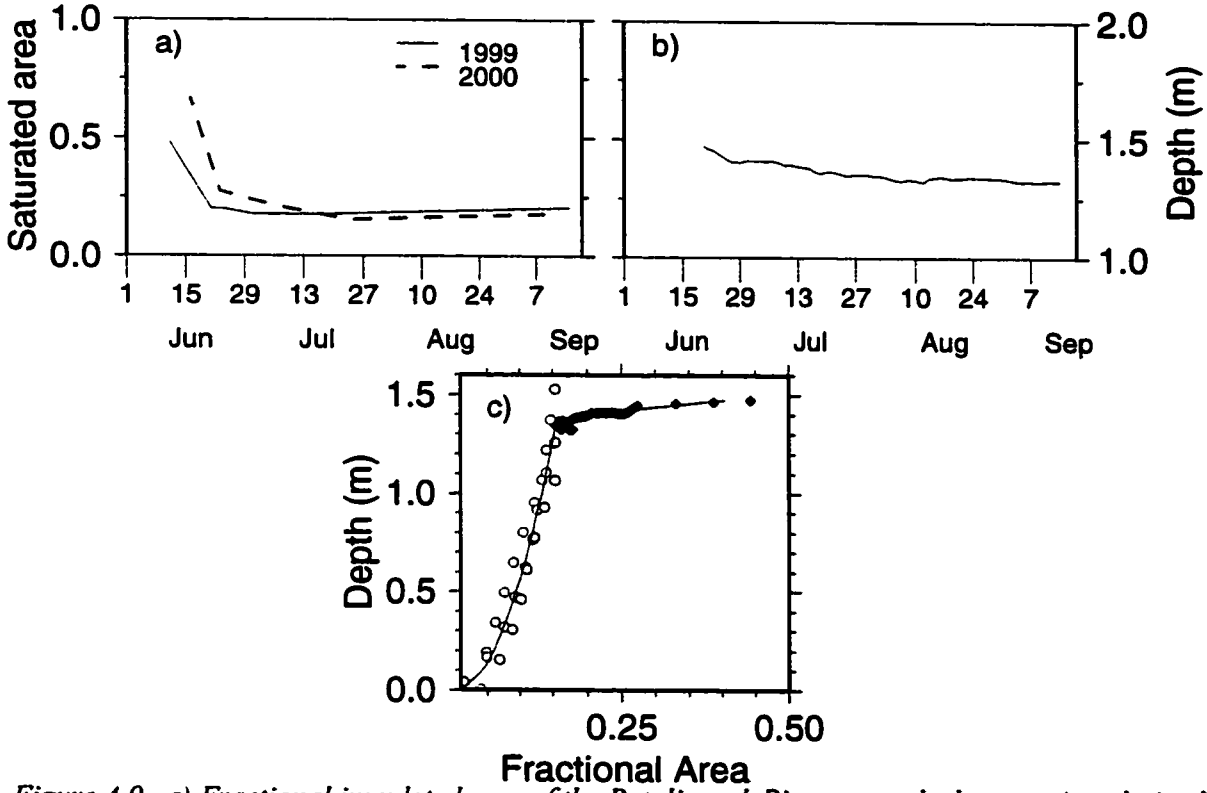

Figure 4.9. a) Fractional inundated area of the Putuligayuk River watershed versus time derived from RADARSAT ScanSAR imagery (from Bowling et al. 2002a), b) Simulated relative lake depth versus time for a monitored thaw pond on the coastal plain, and c) Derived depth-area relationship (line) using RADARSAT observations from wetlands (black diamonds) and surveyed depths for ponds (open circles).

Polynomial curves were fitted to both sets of data points shown in Figure 4.9c to derive a theoretical depth-area relationship for the lake and wetland portions of the Putuligayuk catchment, as follows:

$$A = \begin{cases} 11 \cdot (z - z_{\min})^2 + A_{\min} & A > A_{\min} \\ \left(z/56.5\right)^{\frac{1}{2}} & A < A_{\min} \end{cases} \tag{4.7}$$

where A is the fractional lake area, z is the water depth, and z_{min} is the relative depth at which A = A_{min}, the fractional area of permanent water bodies. The same profile shape was used for each grid cell in the Putuligayuk watershed, scaled according to actual wetland area. Maximum and minimum inundated fraction was determined for each grid cell, using classified RADARSAT images for 2000. That is, the maximum saturated area possible in the VIC model is set equal to that observed by RADARSAT in 2000. The depth corresponding to A_{max} (z_{max}) was assumed constant for each grid cell. Using A_{min}, A_{max} and z_{max}, z_{min} was calculated for each grid cell from equation (4.7). The observed wetland areas at maximum extent varied from 16 to 72 percent of the model grid cells, while at minimum extent wetland area varied from 2 to 9 percent of the model grid cells.

Results

The summer seasonal water balance on the Arctic coastal plain depends almost completely on the quantity of water entering the system as snowmelt. The end-of-winter basin average SWE as determined from surveys by UAF in early-May was 87 mm in 1999 and 124 mm in 2000. In comparison, the simulated average May SWE was 112 mm in 1999 and 114 mm in 2000. The predicted basin average end-of-water snow water equivalent (SWE) is based on the catch-corrected winter precipitation less sublimation/condensation from blowing snow and the surface snow pack. Errors in either of these quantities may account for the discrepancy in simulated SWE.

As shown in Figure 4.10, despite the errors in prediction of basin average SWE the timing of snowmelt is approximately correct. The observations of SWE in Figure 4.10 are from snow surveys at the monitored wetland complex adjacent to the Putuligayuk catchment. Simulated SWE from the closest corresponding model grid cell is shown from January 1998 through December 2000. Snowmelt typically occurs in late May and early June with the active layer beginning to thaw once the snow disappears. Observed active layer depth inferred from temperature profiles at both the wetland site and an adjacent upland site are also shown in Figure 4.10. Both sites thaw at approximately the same rate for the first 30 to 50 cm. Below this depth, the wetland site thaws more slowly due to the greater phase change energy required to thaw the saturated soils. The maximum depth of the active layer in the upland site is unknown for each of the three years shown, since the temperature exceeds zero at the lowest measurement point (60

cm). The active layer at the wetland site is typically more shallow, and varies between 50 and 70 cm (maximum measurement depth 75 cm). The VIC-simulated active layer depth represents an average of both the wetland and the upland portions of the grid cell and is consistent with the observations in both timing and the depth of thaw. The model appears to refreeze too rapidly in the fall, however this should not significantly effect predictions of the summer water balance. The sharp spike in active layer depth shown in August 2000 results from the simulated refreezing of the active layer in response to several days of below freezing temperatures. This appears to be the result of a model instability, and requires further investigation.

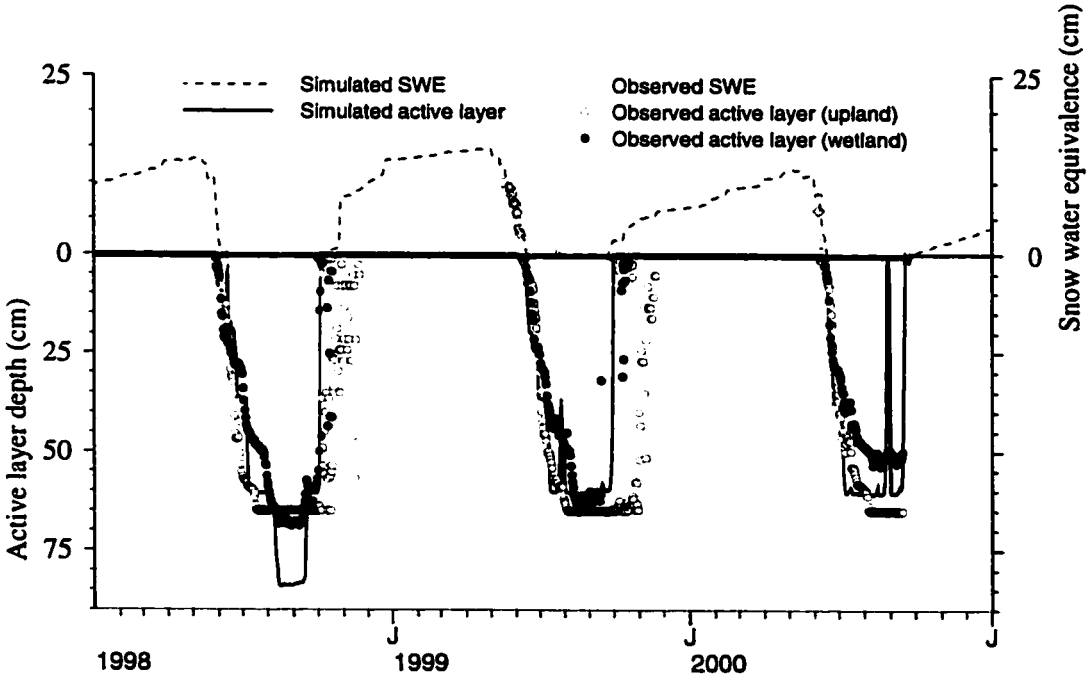

Figure 4.10. Simulated and observed SWE (top) and active layer depth (bottom) for the wetland study site adjacent to the Putuligayuk catchment. Simulated SWE and active layer are indicated by the blue lines, observations by the points.

Detailed observations of the duration of ice cover on the lakes and ponds are not available. The duration of ice cover varies with lake size and depth, with ice cover typically disappearing in the latter half of June (Kane, personal communication). The simulated last day of ice cover varied between June 6th and July 3rd amongst all grid cells and all years. For the simulated years 1995-2000, the difference in ice-free date between the first and the last grid cell to melt was as few as 5 days or as many as 18 days. Averaged over all of the grid cells, the ice melted earliest in 1998

(June 10th) and the latest in 1999 (June 24th). Simulated freeze-up dates (first date with 100 percent ice cover) varied between September 13th and October 29th. Averaged over all grid cells, the lakes froze earliest in 1996 (September 18th) and the latest in 2000 (October 20th).

The rapid snowmelt on top of frozen soils illustrated by Figure 4.10 results in extensive flooding of the low-gradient coastal plain. The simulated change in flooded area versus time for the years 1995 to 2000 is shown in Figure 4.11a. The model reflects the seasonal cycle inferred from previous field studies, with the saturated extent reaching an annual maximum immediately following snowmelt. The maximum surface water extent for the six years varies between approximately 50 and 75 percent of the total catchment area, which is within the range of observations. The saturated area frequently expands in the late summer in response to seasonal maximum precipitation. An increase in the saturated extent in late summer was noted by Bowling et al. (2002a), albeit of lesser magnitude. The simulated saturated extents for 1999 and 2000 are shown in comparison with the RADARSAT-based estimates of Bowling et al. (2002a) in Figure 4.11b. The magnitude of maximum saturated extent for both years matches well with that estimated from RADARSAT. The rate of recession in saturated area in 1999 is not as steep as the observations, indicating that the simulated lakes do not drain as rapidly as observed. In addition, the simulated saturated extent peaks early in 2000. Since the simulated maximum runoff rate appears to be too low during the recession, this suggests that the early peak is not because runoff is released from the lake too rapidly. The alternative is that runoff is getting to the lakes too rapidly, despite the fact that the simulated snowmelt appears to be well-timed. In addition, in 1999 both the simulated saturated area and the simulated discharge (see Figure 4.12) are too responsive to the late summer rain events. Both of these discrepancies suggest a problem in the representation of the overland flow hydraulics that requires further investigation of the interaction of the VIC runoff generation processes in a permafrost environment.

Observed discharge for the Putuligayuk River is shown in Figure 4.12, along with the discharge predicted by the VIC model with the lake algorithm. For both years, the predicted snowmelt hydrographs peak substantially earlier and lower than observed. The point observations of SWE equivalent, in conjunction with field observations that indicate these were typical of the area, suggests that simulated snowmelt did not occur early. In addition, the observations of saturated extent indicate that the stored snow meltwater drains from the lakes at an appropriate rate in the

simulations. To some extent, the problem with the hydrographs reflects the same problems with overland flow hydraulics observed in the dynamics of saturated area. Perhaps a larger influence is the damming effect of the snow-filled channel itself. The channel of the Putuligayuk River is incised into the flat tundra and large parts of the channel are filled with snow at the end of the winter. During snowmelt, the channel was observed to slowly fill with water for days before any measurable discharge was witnessed at the gauging location. Therefore, even if the VIC algorithm reasonably predicts the timing of runoff reaching the river channel, it cannot predict the delay in discharge created by the snow-filled channel. A similar result was found by Zhang et al. (2000) using the ARHYTHM distributed hydrology model to simulate runoff in two small snow-dominated catchments in the foothills of the Brooks Range.

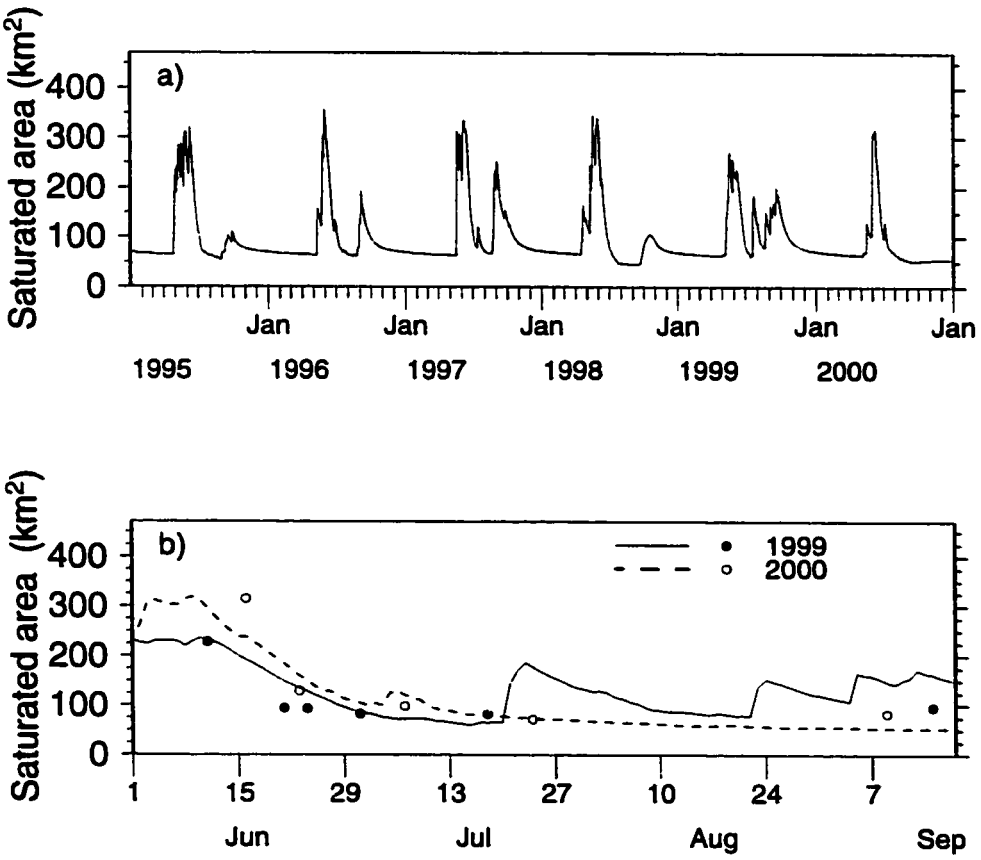

Figure 4.11. Simulated total saturated extent versus time for the Putuligayuk River watershed. a) 1995 through 2000 and b) 1999 through 2000 together with total inundated area on specific dates derived from RADARSAT ScanSAR imagery (Bowling et al. 2002a).

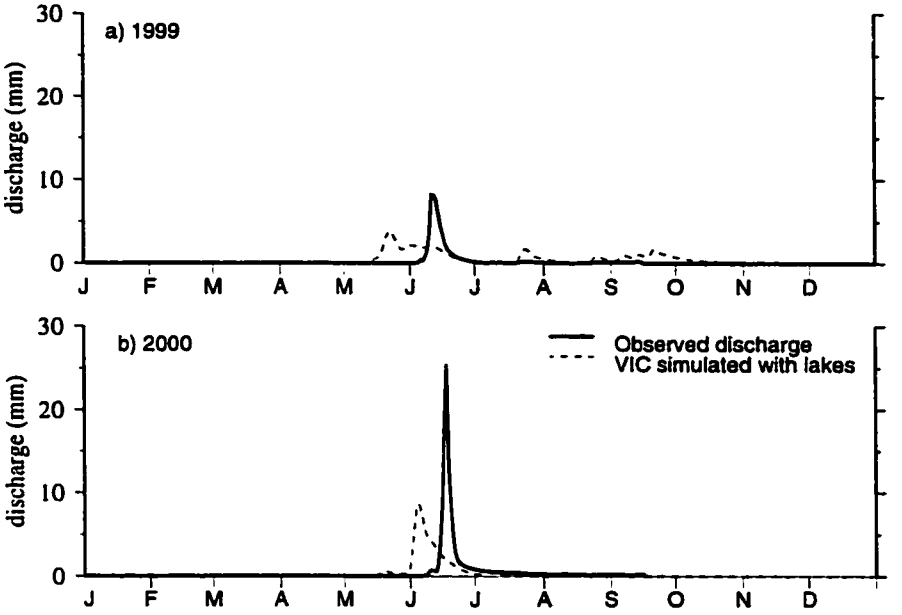

Figure 4.12. Simulated and observed discharge for the Putuligayuk catchment: a) 1999 and b) 2000.

Discussion

The volume of simulated runoff in response to snowmelt is larger than observed in 1999 (74 versus 56 mm, simulated versus observed, respectively), but matches well in 2000 (87 versus 87 mm). This 'immediate runoff' component is taken to be prior to June 27, 1999 and June 21, 2000 as in Bowling et al. (2002a) (Chapter 3). The overprediction in 1999 is presumably in response to the overprediction of SWE. The components of the simulated water balance for 1999 and 2000 are summarized in Table 4.2. In the simulated water balance, 53 percent of the recharge (initial moisture plus snowmelt) becomes immediate runoff in 1999 and 61 percent becomes immediate runoff in 2000. This corresponds well with the 52 percent and 61 percent for 1999 and 2000, respectively, inferred from the basin water balance. Similarly, the simulated change in storage (both soil moisture and lake volume) over the summer corresponds very well with the estimates in Bowling et al. (2002a), both in magnitude and percent. In 1999, the simulated change in storage was -3 mm (-2 mm previously) and in 2000, the simulated change in storage was –21 mm (versus –25 mm previously).

The storage deficit resulting from lake evaporation (P-E lakes) matches the previous estimate for 2000 well, both in magnitude and percent (12 percent versus 11 percent). The discrepancy in

1999 is due to different precipitation totals for this application. Despite differences in initialization, the evaporation from open water areas in this application is actually very similar to that calculated by Bowling et al. (2002a). In order to have a continuous precipitation record for the duration of the simulation, precipitation for the model runs is taken from NCDC Cooperative observer stations. In Bowling et al. (2002a) the summer precipitation was measured at the wetland study site. The summer precipitation used in the simulations is 19 mm higher in 1999 than that used previously and 4 mm lower in 2000. Such discrepancies further highlight the problems in precipitation measurement, particularly at automated stations in remote arctic areas and requires further investigation.

Table 4.2. Simulated snow meltwater balance for the Putuligayuk watershed

		1999	2000
1	Initial storage:	27 mm	31 mm
2	Snow melt inputs:	112 mm	114 mm
3	Depth of recharge above base (1+2):	139 mm	145 mm
4	Immediate runoff:	53 % (-74 mm)	60 % (-87 mm)
5	Recharge to tundra (3+4+6+7+9):	12 % (-16 mm)	13% (-19 mm)
6	Drainage:	14 % (-19 mm)	8% (-11 mm)
7	P-E lakes:	0 % (0 mm)	12% (-18 mm)
8	End of season storage:	22% (30 mm)	7% (10 mm)
9	Change in surface storage (8-1):	-3 mm	-21 mm

Notes:

Percentage shown is the percentage of recharge above base.

In the field-based study described by Bowling et al. (2002a), the highest degree of uncertainty was in the estimation of recharge to the tundra, which is assumed to be snowmelt input to the upland tundra that does not runoff. In Table 4.2 this term is calculated as the residual of the other components of the water balance. In 1999 and 2000, the simulated estimates (-16 and –19 mm) are larger than those estimated previously (-8 and -5 mm). The drainage portion of the hydrograph is also not well represented. In 1999, this is partially due to the difficulty in determining the drainage component of the simulated hydrograph since it is overly responsive to

the summer precipitation events. Both the drainage and the recharge components are likely influenced by the errors in representation of overland flow hydraulics mentioned earlier.

The effect of the simulated lakes on the spatial distribution of annual evaporation is shown in Figure 4.13. Evaporation from the lakes and wetlands increases the prediction of seasonal evaporation from individual grid cells between 9 and 39 mm depending on the total lake area of the grid cell, or 23 to 92 percent of the seasonal evaporation without lakes and wetlands. In addition to the magnitude of the differences, the greater heterogeneity represented by the lakes algorithm may be more significant in influencing the generation of summer convective storms and the position of the Arctic frontal zone.

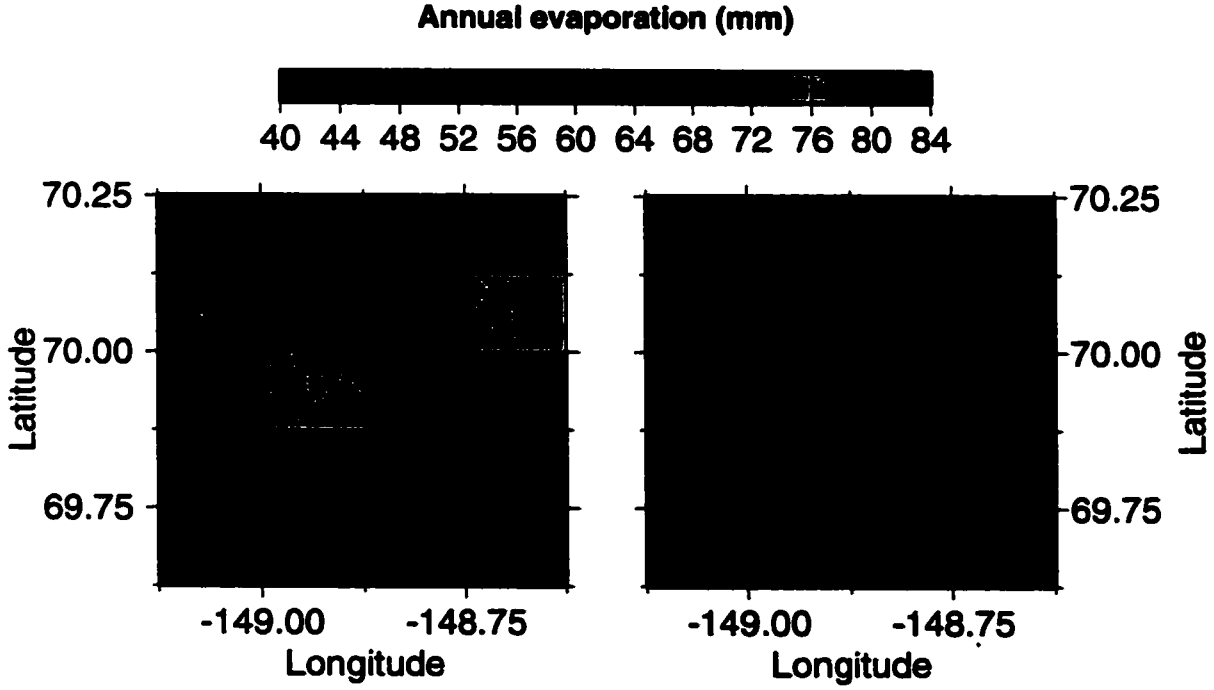

Figure 4.13. Annual average evaporation for the Putluligayuk catchment (1995-2000), a) using the VIC lakes and wetlands algorithm and b) without the lakes and wetlands algorithm

SUMMARY

This paper describes the development of an algorithm to represent the hydrologic effects of lakes and wetlands within a macroscale hydrology model. The algorithm allows for the growth and reduction of saturated area over time and the emergence of wetland vegetation. Although the

focus has been the representation of Arctic lakes, it is a potentially useful tool for studying the interaction of water fluxes between wetlands and adjacent surface water bodies in many climates and regions. Comparison of simulated and observed conditions for lakes in Alaska and Sweden indicate that the lake algorithm approximates the temperature and ice conditions of high-latitude lakes.

The Putuligayuk River watershed in northern Alaska was simulated from 1994 to 2000 as a case study to evaluate the wetland algorithm. This watershed is a dynamic system, in which the total basin saturated area varies by over 50 percent during the snow-free period. The combined influences of permafrost, low topographic gradients, snow cover and numerous ponds and wetlands make it a difficult system to represent with a traditional hydrology model. The depth-area relationship for the wetland portion of the watershed was derived from a time-series of classified RADARSAT ScanSAR images. The bathymetry of the lakes themselves was assumed based on surveys of three typical thaw ponds on the coastal plain. The wetland algorithm was able to reproduce the observed change in basin saturated area on a seasonal cycle. The simulated results suggest the following:

- The lakes and ponds of the coastal plain thaw between June 6th and July 3rd for the period 1994 to 2000. There is a wider range in the formation of complete ice cover, which varied between September 13th and October 29th.

- Surface runoff from the wetlands ceased following snowmelt by June 10, 1999 and June 3, 2000. After this point, discharge was sustained primarily by baseflow drainage in 2000. Surface runoff was generated in response to precipitation events in the summer of 1999. This is qualitatively consistent with the conclusions of Bowling et al. (2002a) based on hydrograph separation, however the surface runoff events are overpredicted in the simulation.

- The presence of extensive open water on the Arctic coastal plain effects the spatial distribution of evaporation. Estimated basin annual average evaporation is 60 percent higher (68 versus 42 mm) when the lakes are simulated, relative to the case with no lakes. Perhaps more significant is the large degree of heterogeneity in evaporation (and latent heat) represented by the lake model.

- The timing of the simulated runoff response is sensitive to the partitioning of surface and subsurface runoff, a distinction with questionable meaning in this low-gradient, permafrost catchment. Further investigation of the function of the VIC baseflow generating function in permafrost environments is required.

CHAPTER V: PARAMETERIZATION OF THE SUBLIMATION OF BLOWING SNOW IN A MACROSCALE HYDROLOGY MODEL

INTRODUCTION

The transport of snow by wind is prevalent over tundra, high to mid-latitude grasslands, high altitude steppes, alpine zones and ice sheets (Berg 1986, Petropavlovskaya and Kalyuzhnyi 1986, Groisman et al. 1997, Mann et al. 2000). Observations of the frequency of occurrence of blowing snow events range between 16 to 35 days a year in northern Kazahkhstan (Petropavlovskaya and Kalyuzhnyi 1986) to over 90 days a year along the Russian Arctic coastal plain and in the Colorado alpine region (Groisman et al. 1997, Berg 1986). Blowing snow events involve erosion, horizontal transport, deposition, and in-transit sublimation of snow and play an important role in the spatial and temporal distribution of water and energy fluxes in many high-latitude regions. Tabler (1975) estimated that over half of transported precipitation sublimates in the high plains of southeastern Wyoming. In the same region, Schmidt (1982) estimated that the sublimation flux rate was 39 percent of the mass rate of snow transported by suspension and saltation. Average monthly rates of sublimation calculated for Halley Station, Antarctica varied between 0.13 to .44 mm/day (King et al. 2001). Pomeroy and Essery (1999) measured maximum sublimation rates during blowing snow events of 0.05 – 0.075 mm/hour (1.2 to 1.8 mm/day) in the Canadian prairies.

Various studies indicate that sublimation during blowing snow events can represent a significant loss of moisture to the atmosphere over the winter in the tundra, alpine, and interior grasslands (Berg 1986, Dyunin 1959, Schmidt 1972, Pomeroy 1989, Kane et al. 1991, Hinzman et al. 1996, Hood et al. 1998). On the low end, estimates of total seasonal precipitation lost to blowing snow sublimation are around 15 percent in the Colorado Front Range and 10 percent at Halley Station, Antarctica (Hood et al. 1998, King et al. 2001). Such estimates increase to 23 to 41 percent of annual snowfall in the Canadian Prairies and 21 to 34 percent in arctic Alaska (Pomeroy 1989, Liston and Sturm 2002). However, the importance of snow sublimation at regional scales is not

well established. It is difficult to directly measure sublimation. Water budgets in wind swept environments are highly unreliable because of precipitation gauge undercatch, particularly where unshielded gauges are employed.

Adequate representation of sublimation is important not only for correct prediction of spring runoff, but also for determination of the spatial distribution of energy and water fluxes in mid-winter and their subsequent influence on atmospheric circulation. Many models have been developed that are applicable at point locations to predict the occurrence and quantity of mass transport and sublimation by blowing snow (e.g. Dery et al. 1998, Pomeroy et al. 1993, Bintanja 2001). All of these models calculate the mass rate of change of blowing snow particles based on the formulation of Thorpe and Mason (1966). Fundamental differences in the point blowing snow models are introduced in the representation of the distribution of suspended particles for a given wind speed and in the representation of thermodynamic feedbacks from sublimation on the temperature and moisture content of the near surface boundary layer.

There is some debate in the literature about whether blowing snow models tend to over-predict latent heat fluxes when negative thermodynamic feedbacks in the near surface boundary layer are neglected (Dery et al. 1998, Dery and Yau 2001, Xiao et al. 2000, Pomeroy and Li 2000). Based on work in Antarctica, King et al. (2001) and Mann et al. (2000) observed strong vapor pressure feedbacks following the initiation of blowing snow resulting in saturation of the air. Observations of saturation of the boundary layer during high wind speeds have not been widespread outside Antarctica (e.g. Schmidt 1982, Pomeroy and Li 2000). Pomeroy and Li (2000) argue that the observed record of humidity and temperature implicitly account for the large-scale advection and entrainment that should minimize saturation of the near surface layer in the natural system. Recent concerns regarding over measurement of humidity by Vaisala hygrothermometers also suggest that the case for humidity feedbacks may be overstated (Dery and Stieglitz 2002). In addition, simulation of the entrainment of drier air has been shown to overcome the thermodynamic suppression of sublimation (Bintanja 2001, Dery and Yau 2001).

In the past, macroscale hydrology models have accounted for sublimation from the ground snow pack, while neglecting the sublimation of snow during transport. Attempts have been made to create less computationally intensive versions of the point scale models for scaling to larger areas (e.g. Liston and Sturm 1998, Essery et al. 1999, Pomeroy et al. 1997, Dery and Yau 2001,

Bintanja 1998). However, snow transport, and hence sublimation, in the point scale models are sensitive to the path length, or fetch, over which the atmospheric boundary layer develops (Pomeroy et al. 1993, Pomeroy and Li 1997). Calculations of blowing snow fluxes over areas with varying fetch have used spatially distributed wind fields over gridded domains such that the fetch is calculated for each model grid cell (Essery et al. 1999, Liston and Sturm 1998). Alternatively, the mean fetch has been calculated for various landscape elements in a region as a pre-processing step (Pomeroy et al. 1997). The effect of the variation in fetch across the domain of a macroscale model grid cell (typically 1/8 – 2° latitude by longitude) on sublimation rates is an issue that remains to be quantified. In addition, the total sublimation rate during blowing snow events is sensitive to wind speed in a highly non-linear fashion (Essery et al. 1999, King et al. 2001, Mikhel and Rudneva 1967), and hence to topography (van den Broeke et al. 1999).

This chapter describes an algorithm that parameterizes the topographically induced sub-grid variability in wind speed, snow transport and sublimation in a blowing snow sublimation algorithm designed for use within macroscale hydrology models and other large scale land surface schemes. The algorithm is intended to provide consistent estimates of the relative influence of sublimation from blowing snow for continental-scale river basins, while balancing the land surface water and energy budget. In addition to the standard LSS inputs, the model requires specification of the standard deviation of terrain slope, the mean fetch and the lag one autocorrelation of terrain gradients for each model grid cell, as defined below. Sublimation fluxes are solved for each vegetation class, for each model grid cell. The model is compared with observed end-of-season snow water equivalent (SWE) and simulated estimates of sublimation from blowing snow for three tundra sites in North America, shown in Figure 5.1.

MODEL DESCRIPTION

The Variable Infiltration Capacity (VIC) model is a macroscale hydrology model that represents sub-grid variability in infiltration capacity through the variable infiltration curve (Liang et al. 1994). It includes a mosaic-type vegetation scheme, multiple soil layers and sub-grid representation of elevation zones. VIC has been applied in many diverse environments, including a global application at 2° latitude/longitude resolution (Nijssen et al. 2001) and across the contiguous U.S. at 1/8° resolution (Maurer et al. 2002). Recent work has focused on making the

model more representative of northern regions, including representation of frozen soils, spatial variability in snow and frost, and lakes and wetlands (Cherkauer and Lettenmaier 1999, Cherkauer et al. 2002).

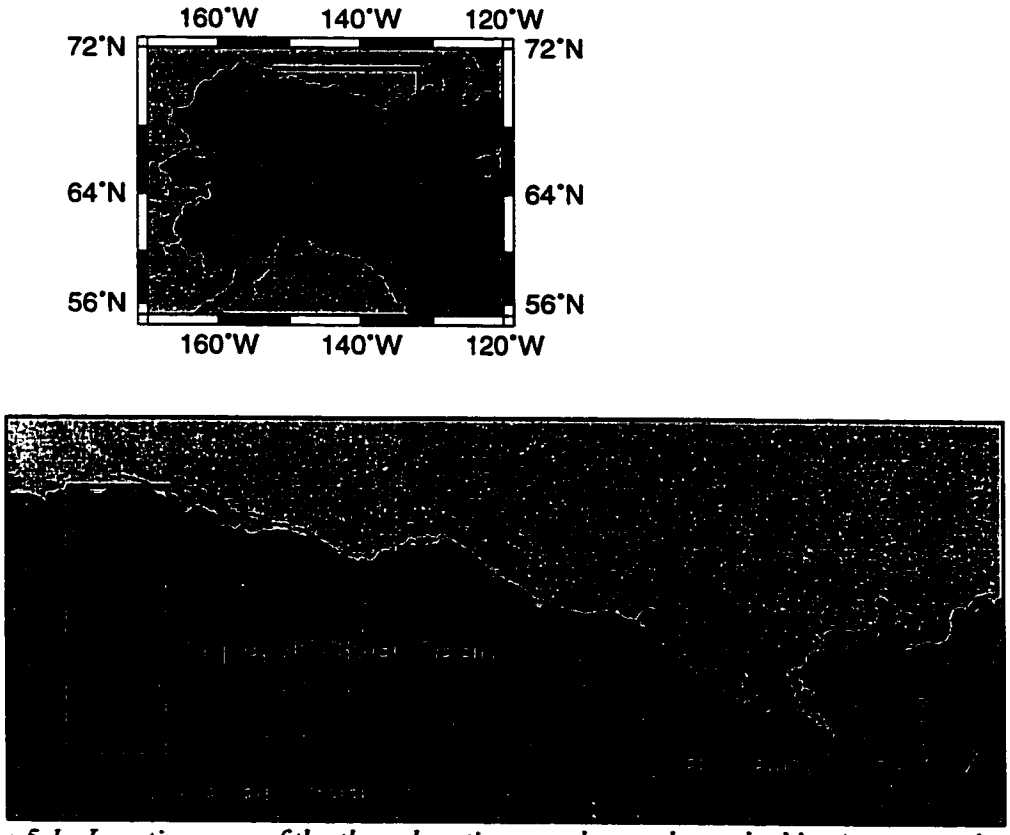

Figure 5.1. Location map of the three locations used to evaluate the blowing snow algorithm

The blowing snow algorithm described in this paper is designed to work within the structure of the existing mass and energy-balance equations in VIC, which describe the temporal variation of snow water equivalent and snow surface temperature within a model grid cell. For each vegetation fraction within the grid cell, the time rate of change of snow water (W_e) is:

$$\frac{dW_e}{dt} = P - M - p \cdot Q_v - Q_e \qquad (5.1)$$

where dW_e/dt is the rate of snow water accumulation, P is precipitation, M is snowmelt and drainage, and Q_e is evaporation and sublimation from the ground snow pack, for a time increment dt. All of the terms are in units of mm/timestep. Q_v is the sublimation from blowing snow and p

is the spatial probability of occurrence of blowing snow. To aggregate the fluxes from each landscape element to grid scale values, the fluxes are weighted by the respective area of the landscape element. Traditionally, the mass balance equation (5.1) would include a divergence term to represent the downwind transport of saltating and suspended snow out of (into) each landscape element. It is assumed that at the scale of application of the VIC model, transport of blowing snow between vegetation elements is negligible relative to the rate of sublimation of snow in transit within a vegetation element.

The method of calculating sublimation from blowing snow derives from existing column and small-scale distributed blowing snow models (e.g. Essery et al. 1999, Pomeroy et al. 1993, Liston and Sturm 1998). The model structure, shown in Figure 5.2, is summarized below. The maximum mass transport of blowing snow, Q_{t_max}, (in kg $m^{-1}s^{-1}$), is dependent on the mass concentration of saltating and suspended particles, as follows:

$$Q_{t\_max} = \int_0^{h_*} \phi_r \cdot u_r dz + \int_{h_*}^{z_t} \phi_s(z) \cdot u(z) dz \tag{5.2}$$

where u(z) is the height-dependent wind speed, assumed to follow a logarithmic profile, ϕ_r and u_r are the mass concentration and particle speed in the saltating layer, assumed constant with height, z, and ϕ_s is the vertical profile of mass concentration in the suspended layer. The height of the saltating layer, h_*, is estimated from wind shear (Greeley and Iversen 1985) and the height of the suspension layer, z_t, is found as the height at which ϕ_s reaches zero (Liston and Sturm 1998). The mass concentration of suspended transport is calculated according to the power-law relationship of Kind (1992), based on height and surface shear stress.

The maximum sublimation rate, Q_v (mm), is then based on the sublimation loss rate of the saltating and suspended particles, as follows:

$$Q_v = \left(\frac{\Delta t}{1000.}\right) \cdot \left[(\Psi_r \phi_r h_*) + \int_{h_*}^{z_t} \Psi_s(z) \phi_s(z) dz \right] \tag{5.3}$$

Here, Ψ_r and Ψ_s are the sublimation-loss rate of particles in the saltating and suspended layers, respectively, equal to the normalized time rate of change of the particle mass. The first term is a conversion factor in order to obtain units of mm for equation (5.1). The mean particle mass is

found by assuming that particle radii follow a two parameter gamma probability density function, based on the work of Schmidt (1982) and Pomeroy et al. (1993). The time rate of change of

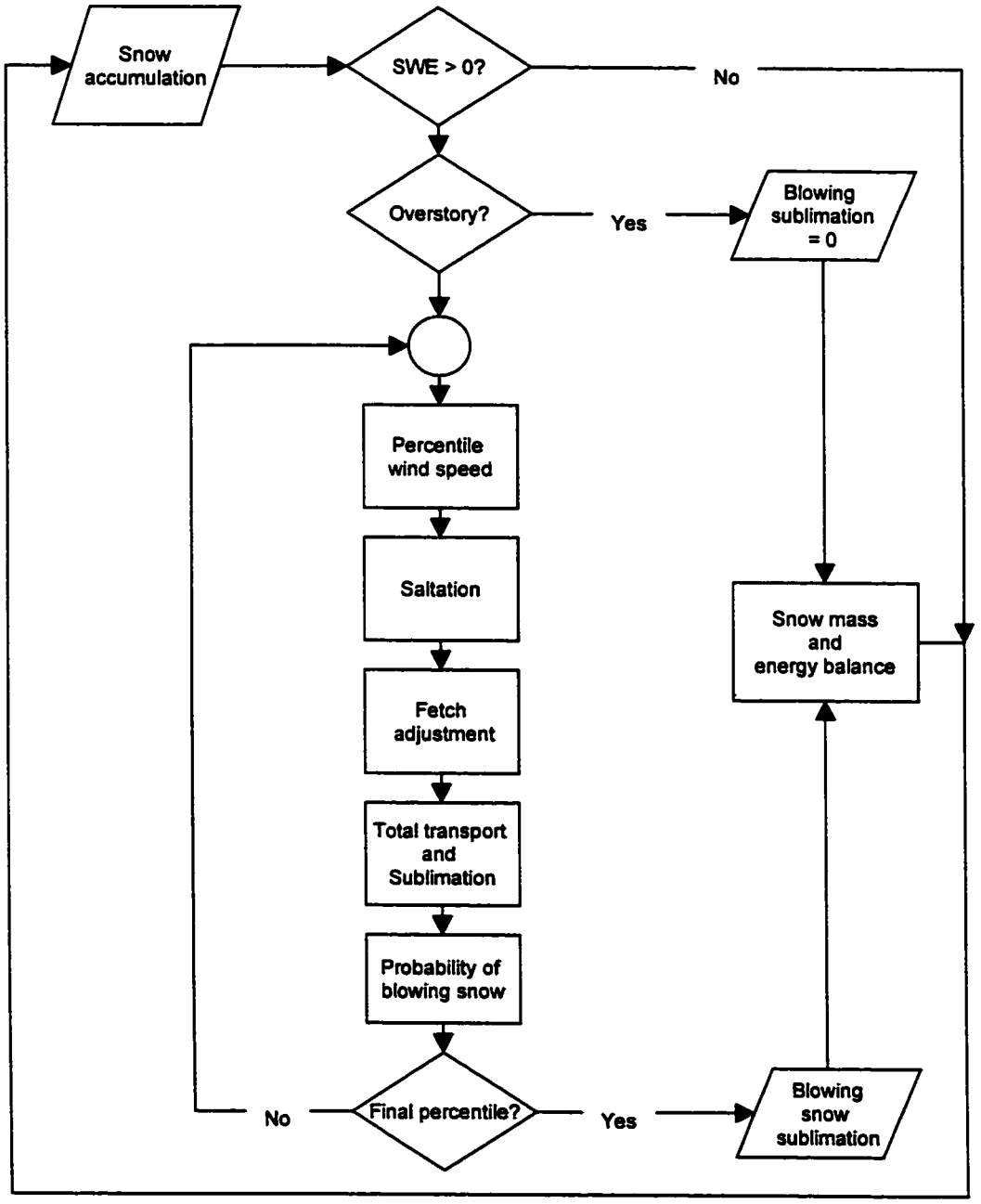

Figure 5.2. Schematic illustrating the calculation of sublimation from blowing snow and interaction with the existing VIC snow model

particle mass is calculated according the formulation of Thorpe and Mason (1966) and is proportional to the undersaturation of atmospheric water vapor with respect to ice, defined as the fractional atmospheric relative humidity minus one. The blowing snow algorithm occasionally results in extremely high sublimation rates that cannot be met by the available energy, leading to model instabilities. Therefore, the maximum sublimation rate in the model is capped at 0.1 mm/hr, based on the maximum rates of 0.05 – 0.075 mm/hr observed by Pomeroy and Essery (1999).

The probability of blowing snow occurrence over a uniform spatial area (i.e. fractional area experiencing snow transport for each time step) is calculated assuming to a normal probability distribution dependent on wind speed, snow age, exposed vegetation roughness and air temperature (Li and Pomeroy 1997, Pomeroy and Li 2000). By this method, the occurrence of blowing snow sublimation is restricted when vegetation height is high relative to the snow depth, so it is not necessary to suppress all transport when snow does not reach the vegetation holding capcity, in the manner of Liston and Sturm (1998).

For inclusion in the VIC model, the blowing snow algorithm must be applicable for grid cell resolutions on the order of 1/2 degree latitude by longitude (approximately 1000 to 2200 km^2 in area within the circumpolar arctic domain). In order to represent the large variation in wind speed in regions of complex terrain, the spatial distribution of wind speed within the model grid cell is represented by a Laplace distribution (Essery 2001). Parameters of the distribution are calculated from the distribution of terrain slopes within the grid cell calculated at an effective spatial resolution of 50 m, as described below. For large spatial domains, the parameters of the slope distribution are calculated at 30 arc second resolution (400 to 900 m) and re-scaled to be representative of the 50 m distribution using simple (monofractal) scaling relationships. The actual transport capacity of the boundary layer, that is, the mass flux of snow particles that can be carried through saltation and suspension, depends upon distance along a homogeneous fetch. The effective average fetch is calculated as a function of the variance of elevation, also described below.

Sub-grid variability in wind speed

Based on an assumed linear theory of wind flow over topography, Essery (2001) demonstrated that the probability distribution of wind speed must be the same as the probability distribution of terrain gradients. The Laplace (double exponential) distribution provides an approximation of the distribution of terrain gradients for two tundra catchments in North America with very different topographies: Imnavait Creek (calculated at 50 m resolution) and Trail Valley Creek (calculated at 40 m resolution), as shown in Figures 5.3 and 5.4. The Laplace distribution offers an advantage over other probability distributions because it relies on only two parameters and is easily integrated.

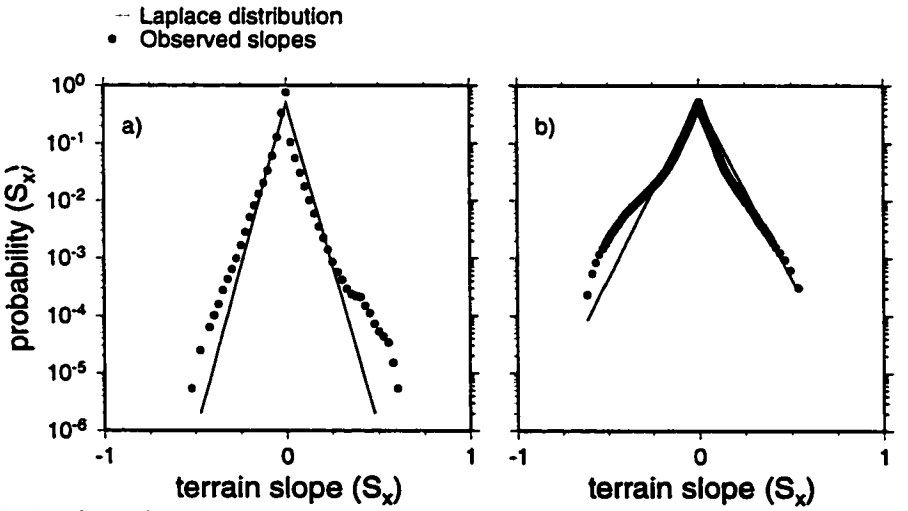

Figure 5.3. Laplace distribution fit to east-west terrain slopes for a) Trail Valley Creek, NWT and b) Imnavait Creek, Alaska

The probability distribution function of wind speed within a model grid cell is therefore assumed to be:

$$p(w) = \frac{1}{2\sigma_w} \cdot \exp\left(-|w - u_o|/\sigma_w\right) \tag{5.4}$$

where w is the spatially distributed wind speed. The grid cell mean (and median) wind speed is u_o. We assume that u_o is represented by the wind speed interpolated using least-distance squared from station observations to the grid cell centers. Because meteorological towers are located on flat fetches, the interpolated observations may be different than the mean.

As derived by Essery (2001), the standard deviation of wind speed, σ_w, is a function of u_o, the standard deviation of terrain gradient (σ_t), and the Fourier transform of the gradient autocorrelation function. The gradient autocorrelation is a measure of the extent to which the terrain gradient at distance x is related to the gradient at distance $x+n\Delta x$ for n = 1,2, etc., calculated as follows:

$$\rho(n) = \frac{\langle s(x) \cdot s(x+n\Delta x) \rangle}{\langle s^2 \rangle} \tag{5.5}$$

where s is the terrain gradient and $\langle\ \rangle$ denotes a spatial average. Lag-one refers to the value of the autocorrelation function for n=1.

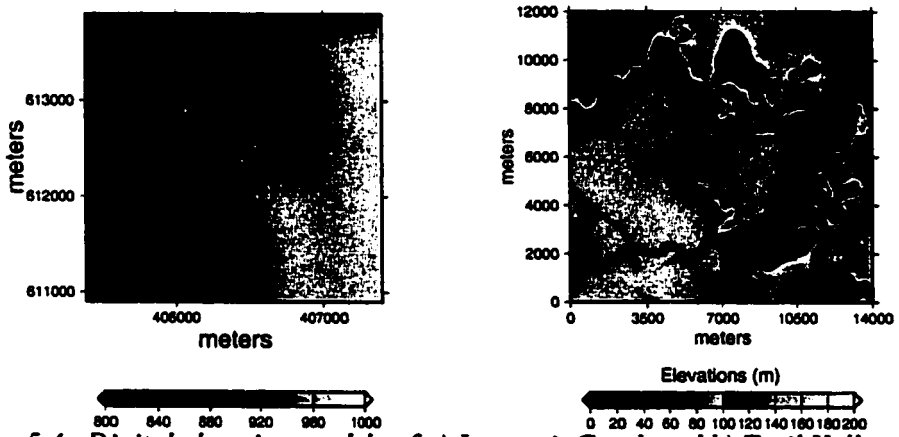

Figure 5.4. Digital elevation models of a) Imnavait Creek and b) Trail Valley Creek

In order to investigate the variation in wind speed (as predicted by a linear windflow model) with respect to topographies with a range of values in autocorrelation, Essery (2001) generated synthetic topographies of a specified autocorrelation. He found that the function describing σ_w is nearly linear for synthetic topographies with values of lag-one autocorrelation between 0.0 and 0.9 (Essery 2001). To avoid computationally intensive numerical integrations, the standard deviation of the wind speed is therefore estimated as:

$$\sigma_w = u_o \sigma_t (2.4 - 0.44\phi) \tag{5.6}$$

where ϕ is the lag-one gradient autocorrelation. For example, for the Trail Valley Creek watershed, Essery et al. computed a value of $\phi = 0.81$, and $\sigma_t = 0.044$, which yields a coefficient

of variation of wind speed, $\sigma_w/u_o = 0.09$. That is, the spatial variation in wind speed is low with respect to the mean.

The VIC wind parameterization requires the standard deviation of terrain gradients and the lag one gradient autocorrelation for each vegetation type and wind direction, for each model grid cell. For simplicity of model inputs, the standard deviation is calculated for the eight primary directions and then averaged to yield an effective value that varies with vegetation type. For limited testing in Alaska and the Northwest Territories the standard deviation of terrain gradients varied only slightly based on wind direction. In regions where this is not the case, the averaging has the potential to result in larger errors than when averaging of the results of the sublimation calculation for each wind direction (due to the highly non-linear dependence of sublimation on wind speed).

The total sublimation flux due to the spatially variable wind field is solved by summing the sublimation calculated for the average wind speed of ten equally probable intervals:

$$Q_v = \sum_{i=1}^{n} p_i \cdot Q_{vi}(u_i)$$

and

$$u_i = E[w] = \int_{z_i}^{z_{i+1}} p(w) \cdot w \cdot dw = \int_{z_i}^{z_{i+1}} \frac{1}{2} \cdot \frac{w}{\sigma_w} \exp\left(-\frac{|w-u_o|}{\sigma_w}\right) dw \qquad (5.7)$$

where Q_{vi} is the sublimation rate calculated for each wind speed u_i, n is the number of probability intervals to be solved and p_i (here equal to 1/n) is the probability that the spatially-varying wind speed falls within probability class i. The wind speed u_i is the expected value of the wind probability density function (equation 5.4) between limits calculated from p_i, as follows:

$$z_0 = 0$$

$$z_{i+1} = u_o + \sigma_w \cdot \ln\left(\exp\left(\frac{z_i - u_o}{\sigma_w}\right) + 2p_i\right) \qquad z_{i+1} \le u_o \qquad (5.8)$$

$$z_{i+1} = u_o - \sigma_w \cdot \ln\left(\exp\left(-\frac{z_i - u_o}{\sigma_w}\right) - 2p_i\right) \qquad z_{i+1} > u_o$$

Upscaling to large spatial domains

Application of the blowing snow algorithm to large spatial domains is complicated by the absence of digital elevation data at resolutions sufficient to derive the terrain gradient distributions. Therefore, the distribution of terrain slopes at 50 meter resolution must be derived from the GTOPO30, 30 arc second resolution digital elevation data, that is available globally.

Several researchers have investigated the (mono)fractal nature of topography (Klinkenberg and Goodchild 1992, Xu et al. 1993, Zhang et al. 1999) as well as the multifractal nature of topography (Lavalée et al. 1993, Lovejoy et al. 1995). The convenience of monofractal topography is that it indicates the applicability of simple scaling. That is, for re-scaled topography Z_l, such that (Gupta and Waymire 1990):

$$Z_l(x) = Z(lx) \tag{5.9}$$

a scaling function exists such that:

$$E\left[Z_l^h\right] = l^{h\theta} E\left[Z_1^h\right] \tag{5.10}$$

for all moments of order h. θ is the scaling constant, equal to 2 minus the fractal dimension, D, for a surface (Kono 1985).

Lovejoy et al. (1995) demonstrated that the topography of Deadman's Butte, Wyoming is multifractal in nature, which therefore requires a multiscaling approach when transforming between resolutions. For both simple and multiscaling processes, the statistical moments, m(h), should be linear with respect to the scale, l, in log-log space. A random field, Z, is considered wide sense multiscaling if the slopes of these linear functions, S(h), are nonlinear with respect to h (Gupta and Waymire 1990). The Upper Kuparuk River basin is a tributary to the Kuparuk River located in the foothills of the Brooks Range, Alaska, adjacent to the Imnavait Creek watershed (see Figure 5.1). A 50 meter resolution DEM is available for this basin (Walker 1996). A sampling of the statistical moments of terrain gradients for the Upper Kuparuk River basin is shown in Figure 5.5a, with respect to log (l). As indicated by the black dots, the moments are found to be linear with respect to l for several grid resolutions (50, 100, 200, 400, 800,and 1600 m), calculated from the 50 m DEM. The corresponding GTOPO30 DEM was transformed to the universal transverse mercator (UTM) projection at 800 m resolution (grid cell distances in the

geographic projection vary between 600 and 900 m at this latitude). The moments for this DEM (shown in red in Figure 5.5a) for resolutions of 800 and 1600 m indicate good correspondence between the 50 m and 800 m DEMs. For resolutions above 1600 m, the moments become increasingly nonlinear for both DEMs. Lovejoy et al. (1995) noticed the same nonlinearity for course resolution grids and attributed it to the small sample size at these resolutions. The linear best fit lines for the 50 m DEM are therefore calculated from the first 6 values of l for each moment. Unfortunately, with only two points available from the 800 m DEM from which to fit a line, it is not possible to recover the same slopes from the 800 m and 50 m DEMs, as indicated in Figure 5.5b. The empirically derived lines in Figure 5.5b are convex downward with respect to the straight line expected from simple scaling, indicating that the multiscaling model is more appropriate for this terrain. However, the difference is very small for moments up to two (the variance), so we conclude that simple scaling is appropriate for recovering the variance at 50 m resolution from the 800 m DEM.

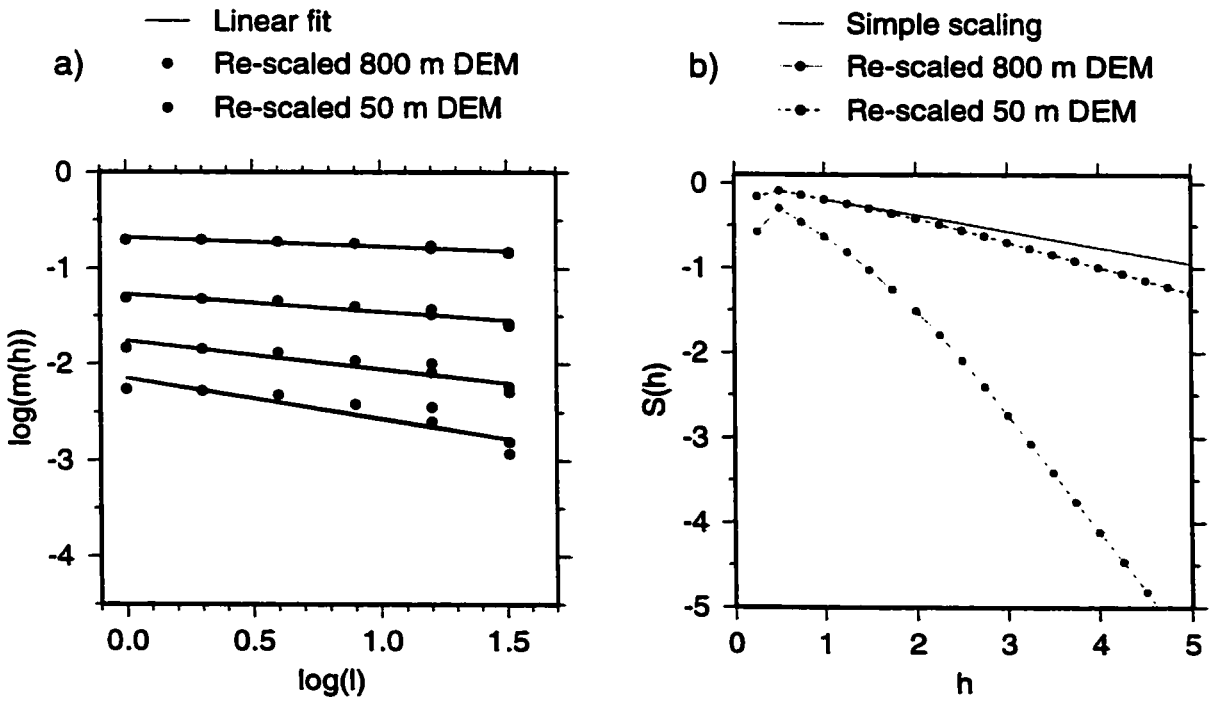

Figure 5.5. Procedure for estimating terrain parameters from coarse resolution DEMs using data from the Kuparuk River basin: a) the log of the moments, m(h), of the distribution of terrain slopes versus the log of the scale, l. The moment order is from top to bottom: h= 0.5, 1.0, 1.5 and 2.0. b) the slopes, S(h), of the fitted lines in a)versus the moment order, h. The solid black line indicates the relationship expected from simple scaling.

Since the slopes of the moments cannot be recovered from the 800 m DEM, an alternative method is used to calculate the fractal dimension of the surface, and therefore the scaling constant, θ. The surface fractal dimension for the region spanned by one model grid cell is calculated using the variogram technique as described by Xu et al. (1993), including all elevation pairs from the GTOPO30 DEM within a VIC model grid cell. This involves plotting the log of the average elevation difference of all pairs separated by an incremental distance. The fractal dimension is calculated as the slope of the first linear portion of this graph. For the Upper Kuparuk data, this yields an estimate of the fractal dimension of 2.18, so $\theta = 2\text{-}D = -0.18$. For comparison, the estimate of θ taken from the 50 m data in Figure 5.5b is $\theta = \left.\frac{dS(h)}{dh}\right|_{h=1} = -0.19$.

To determine the standard deviation of the distribution of terrain slopes for each VIC model grid cell, the variance of the terrain slope is first calculated for each VIC model grid cell. The GTOPO30 variance is re-scaled according to equation 5.10, where θ is calculated from the fractal dimension of the corresponding VIC grid cell estimated using the variogram method. The scale, l, is equal to 16 (800 m/50 m) and the moment, h, equals 2, corresponding to the variance. Using this approach for the Upper Kuparuk basin, the estimate of the standard deviation of terrain gradients from the 30 arcsec DEM (0.048 m/m), is rescaled to 0.079 m/m. This is within 6.8 % of the original estimate from the 50 m DEM (0.074 m/m, mean = 0.49 m/m).

Non-Equilibrium Transport

The total mass of downwind transport and sublimation of blowing snow depends upon the length of downwind development of the boundary layer, or fetch, from a point where blowing snow transport does not occur (Pomeroy et al. 1993). The observations of Takeuchi (1980) and Pomeroy et al. (1993) indicate that the increasing downwind transport of snow over a region of homogeneous vegetation and wind speed a distance, x, from the initiation of transport follows an exponential profile of the form:

$$Q_t(x) = Q_{t\_max}\left[1 - \exp\left(-\mu x / f_{max}\right)\right] \qquad (5.11)$$

where Q_{t_max} is the maximum rate of transport for fully-developed flow given in equation 5.2, f_{max}, is the fetch length for fully-developed flow and μ is a scaling factor. The scaling factor is set to 3.0 following Liston and Sturm (1998) and Essery et al. (1999).

For any parcel of the grid cell defined by homogeneous vegetation and wind speed, the average transport rate will be the integral of equation (5.11). Since the maximum transport rate is zero by definition at the edge of each of these parcels, the lower boundary of the integration is zero. The upper limit of integration is the average downwind distance for each parcel. The challenge lies in defining this distance as an effective average to be used at large scale.

In the remote Arctic, breaks in fetch can most often be related to terrain features such as river incisions, escarpments and divergence in slope and aspect, or relatively tall vegetation that serves to inhibit blowing snow transport. Man-made features such as roads, pipelines and snow fences may also be important locally, although they have minimal extent. In Trail Valley Creek, N.W.T., Pomeroy et al. (1997) calculated the average fetch for dominant vegetation classes. Although the difference in vegetation alone may not be the cause of a break in fetch, it is often a useful surrogate for fine scale topographic features, since vegetation is often closely correlated with terrain and the related drainage. Muller et al. (1999) developed a 50 m resolution land cover dataset for the Kuparuk River basin in northern Alaska based on Landsat imagery. From the descriptions, it is clear that these classifications are closely tied to topography, with moist tundra occurring on the coastal plain and river terraces, tussock tundra on moist hillslopes, and shrublands along rivers and water tracks. Since this dataset is of finer resolution and presumably higher quality than the available corresponding terrain data, the spatially-distributed average fetch for the Kuparuk is first estimated from the vegetation. The eight vegetation classes in the Muller et al. (1999) dataset were re-grouped into three dominant classes: 1) dry tundra and barrens, shadows and low-shrub tundra, which show up primarily as gravel river beds and roads on the coastal plain, and sometimes as exposed ridges in the foothills, 2) moist prostrate-shrub tundra, wet tundra, open water and clouds and ice, found primarily on the coastal plain and valley bottoms, and 3) moist dwarf shrub tussock tundra, most often found on hillslopes. For each VIC model grid cell, the average fetch of each land class was found automatically, using the following algorithm:

- The 50 m vegetation grid corresponding to each 1/8° VIC model grid cell is sampled for each of the four primary wind directions: N-S, E-W, NE-SW and NW-SE.
- For each vegetation grid cell, the distance that can be stepped in each of four directions while remaining within the same land class is calculated.
- The four direction values are averaged to obtain the average fetch for all directions.
- This fetch is then averaged over all vegetation grid cells in the same class to obtain an average fetch for each land class.
- Finally, the fetch is averaged over all vegetation classes, to obtain the average fetch for each VIC model grid cell.

The final average fetch for each VIC model grid cell calculated by this method is shown in Figure 5.6a. The pattern generally corresponds to expectations, with fetch lengths less than 500 m in the foothills, and between 1000 to 3000 m on the coastal plain.

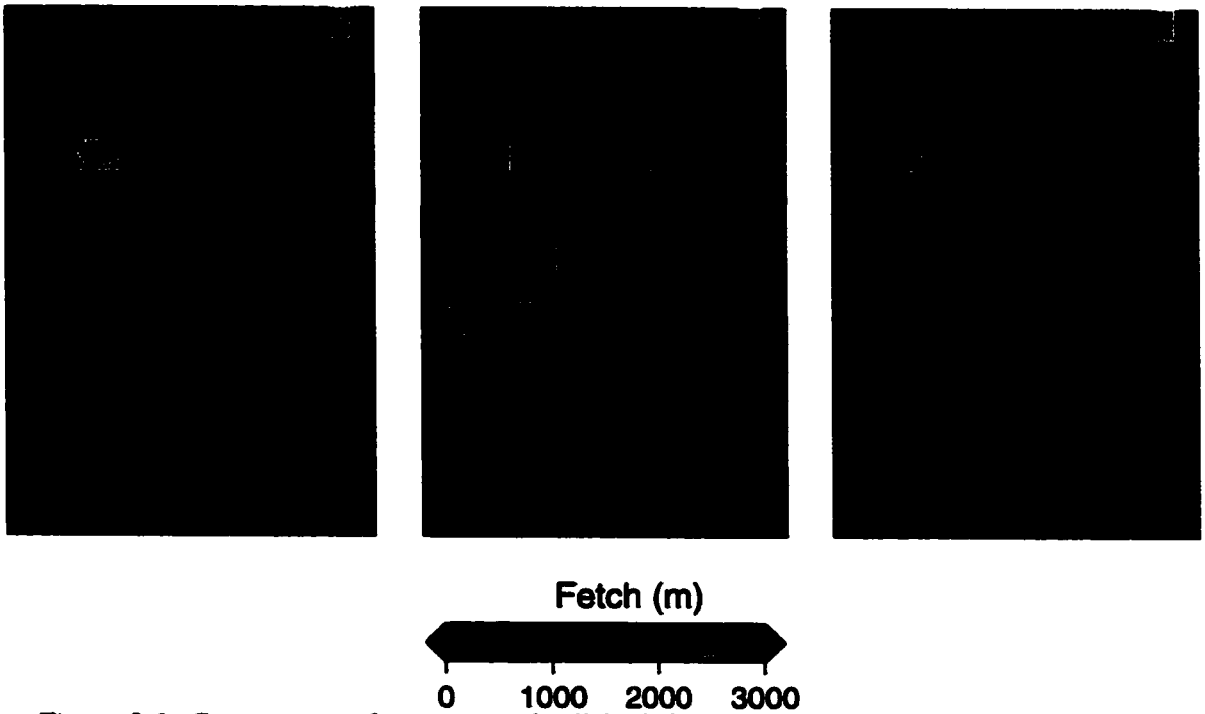

Figure 5.6. Comparison of average grid cell fetch for the Kuparuk River basin calculated by three methods: a) based on vegetation type, b) based on the magnitude of terrain slope and c) combined estimate using the minimum fetch estimated from terrain or vegetation.

High-quality, fine resolution vegetation data is not always available, so it would be useful to obtain the average fetch directly from the 30 arcsec DEM for regions of topographic control of fetch. However, identification of the topographic classes that correspond to breaks in fetch is not straightforward. Tabler (1975) predicted profiles of snowdrifts based on topographic slope along a transect. Consistent with this approach, grid cells were assigned to different topographic classes based on a difference of 0.5 percent slope, and the average fetch was calculated as described above (shown in Figure 5.6b). The topographic classes yield a spatial pattern consistent with the vegetation, although with generally longer fetches.

The control of fetch by either topography or vegetation will change depending on which factor limits the fetch length. For example, in regions of flat terrain, fetch is most often controlled by changes in vegetation. In regions with reduced vegetation diversity, however, such as the high arctic, topography controls fetch. Figure 5.6c shows a combined measure of fetch for the Kuparuk River basin calculated as the minimum of either the vegetation-based or the topography-based estimate of fetch. This figure indicates that for much of the basin, the fetch length calculated from vegetation is shorter than that calculated from topographic slope. This may indicate that fetch is predominantly controlled by vegetation throughout the Kuparuk River basin, although the calculated fetch lengths are also influenced by the coarseness of the DEM data. In addition, since the vegetation classes are closely correlated with terrain, the short fetch lengths calculated from the vegetation dataset may reflect the dual-control of vegetation and terrain.

The measure of fetch obtained from topography contains a region of high fetch in the western part of the basin, with a contrasting region of low fetch to the north and east. The vegetation measure shows the reverse signal. The region of low fetch in Figure 5.6b corresponds to a region of complex terrain (the White Hills) and may indicate a region where fetch is limited by topography that is not reflected in the uniform vegetation coverage. The effect of each of these measures of fetch on estimated blowing snow sublimation is explored further below.

TEST APPLICATIONS OF THE VIC BLOWING SNOW ALGORITHM

Imnavait Creek, Alaska, USA

Imnavait Creek is a 2.2 km^2 catchment located in the foothills of the Brooks Range in northern Alaska. Low-growing grasses and sedges are the dominant forms of vegetation, with taller willow shrubs occurring in valley-bottoms. Shallow soils and exposed rock are present on the ridges (Liston and Sturm 1998). The topography of Imnavait Creek (shown in Figure 5.4 a) is gently rolling, with north-sound trending ridges spaced approximately 1-2 km apart.

The catchment was represented by one VIC model grid cell with five fractional vegetation types, including dry, moist and wet tundras, shrubland and bare ground. Hourly observations of wind speed, relative humidity and air temperature for the VIC application were obtained from two meteorological towers operated in the basin by the Water and Environment Research Center (WERC), University of Alaska Fairbanks (UAF). Daily precipitation was obtained from a Wyoming snow gage operated at the same site. The Wyoming gauge utilizes a double fence shield and is more accurate than the 8" standard National Weather Service gauges, so no gauge catch correction was performed on this record. Averaged over four sites, Yang et al. (2000) found that the Wyoming snow gauge captured 91 percent of the precipitation measured by a double-fenced reference gauge, so gauge undercatch can still be a problem during windy events and is a source of uncertainty in this analysis. The simulation was conducted hourly from October 1986 through October 1993. October 1986 through October 1987 was used for model spin-up and these results are not presented. The terrain distribution and autocorrelation were calculated from a 50 m DEM of the area, so no fractal scaling was needed for this application. The example of fractal scaling shown in Figure 5.5 is for this region, however.

Time series of basin-averaged snow water equivalent and cumulative sublimation simulated by the VIC model with and without the blowing snow sublimation algorithm are shown in Figure 5.7 for the period October 1987 through October 1990. Figure 5.7 illustrates the relative influence of estimated sublimation in this environment; no observations are available for comparison. Simulated seasonal sublimation from blowing snow varies between 12 and 49 mm for the six year period (1987 through 1993). Vapor flux from the ground snow pack results in net evaporation

from the snowpack for five of the six years that averages 9.6 mm when blowing snow is represented.

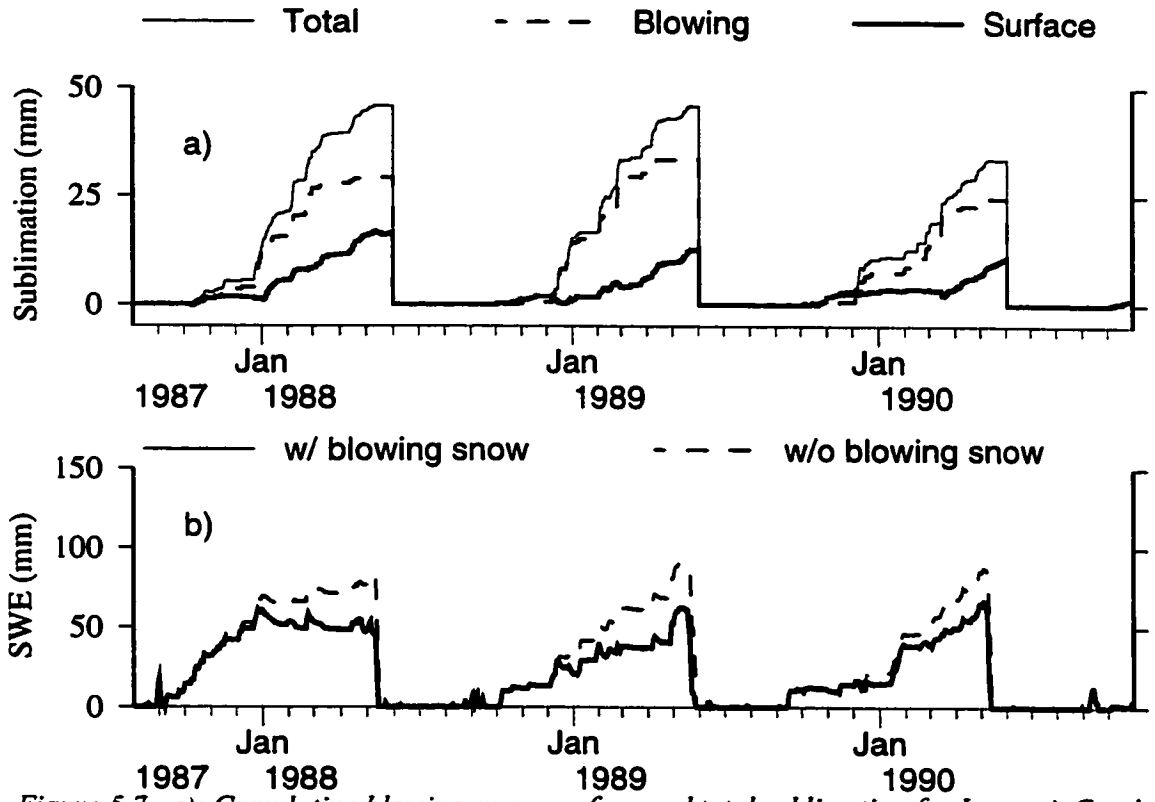

Figure 5.7. a): Cumulative blowing snow, surface and total sublimation for Imnavait Creek predicted using the VIC algorithm with the blowing snow algorithm (surface sublimation is slightly higher without the blowing snow algorithm) and b): Basin average snow water equivalent for Imnavait Creek predicted using the VIC algorithm with and without the blowing snow algorithm.

Sublimation and redistribution of snow by wind was simulated for the Imnavait Creek watershed for the period September 1985 through May 1990 by Liston and Sturm (1998) using the SnowTran-3d snow transport model. SnowTran-3d is fully distributed; wind speeds in the model were resolved for each 20 m pixel via an empirical wind weighting scheme based on terrain slope and curvature. The transport of snow from cell-to-cell in the direction of the wind is calculated in each time step, along with sublimation, erosion and deposition. SnowTran-3d therefore explicitly represents the small scale variations in wind speed and fetch that are parameterized in the VIC algorithm, however, it has not been extensively evaluated with respect to observations. Comparison of the VIC results with the distributed model results therefore allows assessment of the ability of the VIC algorithm to parameterize sub-grid variability in wind speed and fetch, but

provides only a qualitative evaluation of the magnitude of the sublimation fluxes. A daily time step was used for the simulation by Liston and Sturm (1998) and may have introduced errors to the simulation as the blowing snow model physics are based on sub-hourly relationships between wind speed and transport (Pomeroy and Gray 1990, Pomeroy et al. 1993).

VIC-simulated maximum accumulated snow water equivalence (SWE) is shown versus observations of the domain-averaged end-of-winter SWE for the three years of complete overlap (1987-88, 1988-89 and 1989-90) in Figure 5.8a. The observed SWE comes from unpublished data by Benson, as reported by Liston and Sturm (1998). VIC underpredicts SWE for all three years. This appears to be due to an underrepresentation of precipitation. As shown in Figures 5.8 a and b, the accumulated snowfall measured by the Wyoming gauge that was used in the VIC model is approximately equal to the snow on the ground in 1988 (measured precipitation is 101% of observed SWE) and is less than the observed SWE in 1989 and 1990 (measured precipitation is 85% and 72% of observed SWE for 1989 and 1990, respectively). Liston and Sturm (1998) used an iterative data assimilation approach in order to estimate total snow precipitation based on the observed SWE and simulated sublimation. Their precipitation estimates are shown in Figure 5.8a along with the Wyoming gauge measurements used in the VIC simulations.

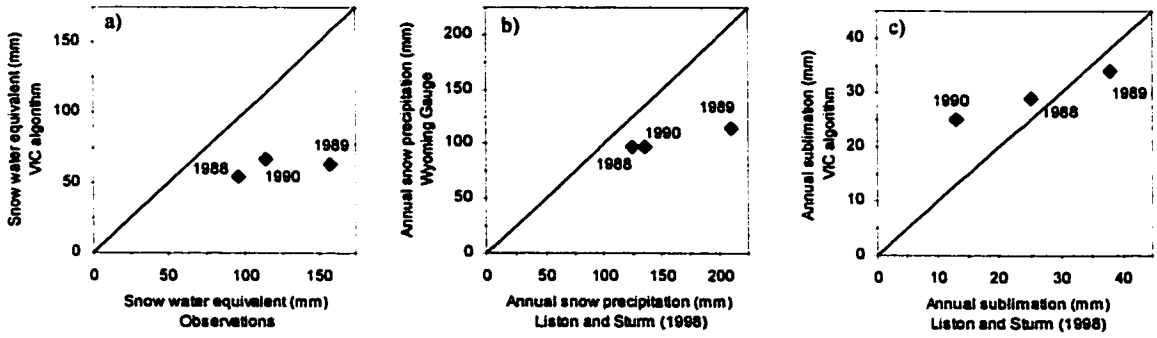

Figure 5.8. Comparision of basin average annual quantities for Imnavait Creek: a) snow water equivalent predicted by the VIC blowing snow algorithm versus observations, b) gauge-measured precipitation versus precipitation predicted by Liston and Sturm (1998) and c) blowing snow sublimation predicted by the VIC blowing snow algorithm versus sublimation predicted by Liston and Sturm (1998).

VIC-simulated annual sublimation is compared with the estimates of Liston and Sturm (1998) in Figure 5.8c. Despite the differences in precipitation, both models show similar estimates in total sublimation values. Liston and Sturm (1998) predict much lower rates of total sublimation in

1990 than in the other two years. The lower sublimation rates in 1990 are due primarily to lower sustained wind speeds in 1990 than in 1988 and 1989 (Liston and Sturm 1998). The relationship between sublimation and wind speed is highly non-linear (e.g. Essery et al. 1999). Due to this non-linear nature, the daily average wind speed will not reproduce the same total sublimation flux as the observed hourly average wind speed. The higher estimate from the VIC model may reflect an underprediction in blowing snow occurrence by Liston and Sturm (1998) due to the choice of a daily time step.

Trail Valley Creek, Northwest Territories, Canada

Trail Valley Creek is a 68 km^2 research basin located 50 km north of Inuvik, NWT on the Canadian Arctic coastal plain. Dominant vegetation includes sparse moss and lichen tundra in the upland regions and alder or willow shrub tundra on moister hillslopes and valley bottoms (Pomeroy et al. 1997). Open water and black spruce forest make up less than 5 percent of the basin area. The topography is characterized by an east-west trending valley that is incised into a raised plateau, resulting in more complex topography than that of Imnavait Creek (Figure 5.4). The catchment was represented by one VIC model grid cell with four fractional vegetation types. Half-hourly observations of wind speed, relative humidity, air temperature and gauge-corrected precipitation were obtained from a meteorological tower operated in the basin by the National Hydrology Research Institute (Essery et al. 1999). Half-hourly observations were aggregated to hourly for the VIC application, which was run from September 1996 through April 1997. The terrain distribution and autocorrelation were calculated from a 40 m DEM of the area, so no fractal scaling was needed for this application. The 40 m DEM was digitized from a 1:50000 topographic map (Pomeroy et al. 1997).

The time series of basin-averaged snow accumulation, snowfall and cumulative sublimation simulated by the VIC model with the blowing snow sublimation algorithm are shown in Figure 5.9. Sublimation during blowing snow events was simulated in the Trail Valley Creek watershed from 11 September 1996 through 8 April 1997 by Essery et al. (1999) using an empirical adaptation of the physically-based Prairie Blowing Snow Model (Pomeroy et al. 1993). This Distributed Blowing Snow Model (DBSM), operates similarly to SnowTran-3d. In this case, wind speeds for each grid cell were calculated for each of the 8 primary directions using the MS3DJH/3R linear windflow model (Walmsley et al. 1982).

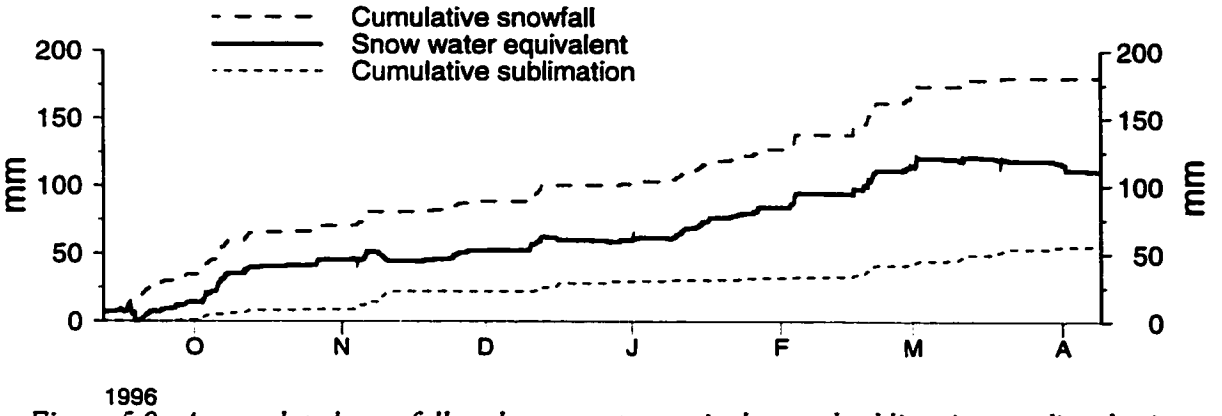

Figure 5.9. Accumulated snowfall and snow water equivalent and sublimation predicted using the VIC blowing snow algorithm for Trail Valley Creek

Basin-average total sublimation from blowing snow for the simulated period was 56 mm for VIC as compared with 73 mm estimated by Essery et al. (1999). The simulated SWE for each vegetation class are compared with observations in Figure 5.10a (the lakes were not sampled). The total SWE for open tundra is fairly well represented; however, total accumulation in the shrub tundra and forest are underpredicted by VIC by approximately 60 mm. Observed SWE in the forest and shrubs (215 and 219 mm, respectively) actually exceeds total precipitation (180 mm). This illustrates that for regions with intermixed vegetation, snow transport from one vegetation class to another can be important to representing the spatial distribution of SWE. Differences between observed and simulated SWE in the shrub tundra and forest is likely because this redistribution of snow from shorter to taller vegetation is not represented by VIC. The lack of representation of snow redistribution between vegetation types also affects the estimation of sublimation, as shown in Figure 5.10b. The VIC algorithm duplicates the general trend in differences between vegetation types, but total sublimation from the shrubs and forests are lower in the VIC simulations than in Essery et al. (1999). Essery et al. (1999) represented snow transport into the shrub and forests from the upwind lake and open tundra areas. This additional snow input meant that vegetation roughness elements were filled earlier in the snow season, thus increasing the calculated probability of blowing snow.

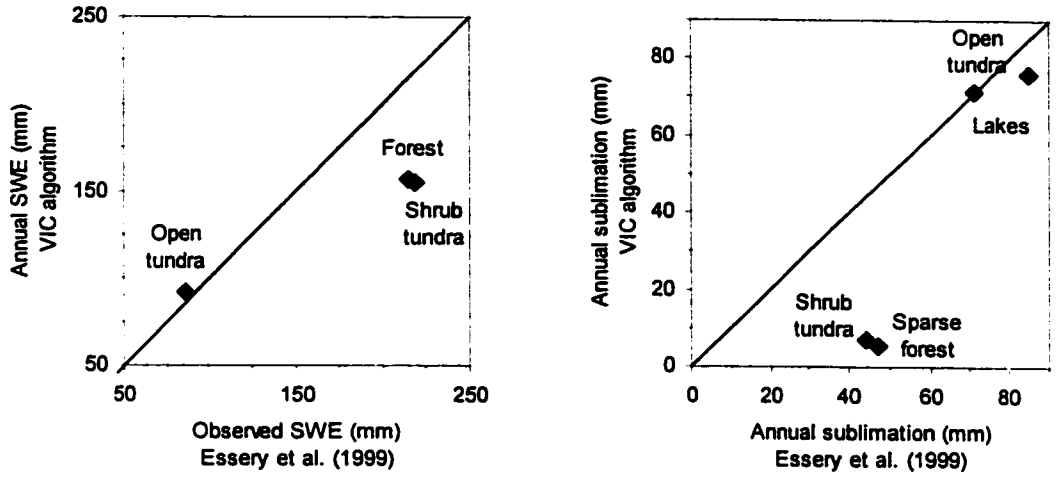

Figure 5.10. Comparision of average sublimation for each vegetation type for Trail Valley Creek predicted by Essery et al. (1999) with the Distributed Blowing Snow Model and using the VIC blowing snow algorithm

Kuparuk River, Alaska

The full capabilities of the VIC blowing snow algorithm, including scaling of the terrain slope distribution and simplified representation of large spatial domains were employed on the ~8000 km^2 Kuparuk River in northern Alaska (see Figure 5.1). The Kuparuk River drains north from the foothills of the Brooks Range to the Arctic Ocean. Imnavait Creek is located in the headwaters of the Kuparuk River. As shown by the elevations in Figure 5.11, moving northward from Imnavait Creek, the topography transitions to the relatively flat Arctic coastal plain. Vegetation of the coastal plain consists primarily of tussock tundra and wetlands. Meteorological conditions also have a strong north-south gradient, as shown in Figure 5.12. Hourly relative humidity, air temperature and wind speed were obtained from eight meteorological stations in the basin operated by WERC. Daily rainfall was also obtained from the WERC stations. Daily snow precipitation was obtained from two National Climate Data Center cooperative observer stations operated near the basin (Prudhoe Bay and Kuparuk) and two Natural Resource Conservation Service snow telemetry sites (Imanavait Creek and Sagwon). Meteorological inputs were interpolated to the resolution of the VIC model grid (1/8° latitude by longitude) using a least-distance squared interpolation routine (the SYMAP algorithm; Shepard 1984). Precipitation was corrected for wind-induced gauge undercatch using a correction devised for the 8" standard U.S.

National Weather Service gauge as part of the World Meteorological Organization (WMO) precipitation gauge intercomparison project (Yang et al. 1998). Precipitation bias adjustment is often approximate, particularly for liquid and mixed precipitation, so the true precipitation quantity remains a large source of uncertainty. The average fetch for each grid cell was taken from the combined topography/vegetation calculation illustrated in Figure 5.6 c). The variances of terrain slopes were scaled according to equation 5.10 with θ calculated from the fractal dimension of each grid cell.

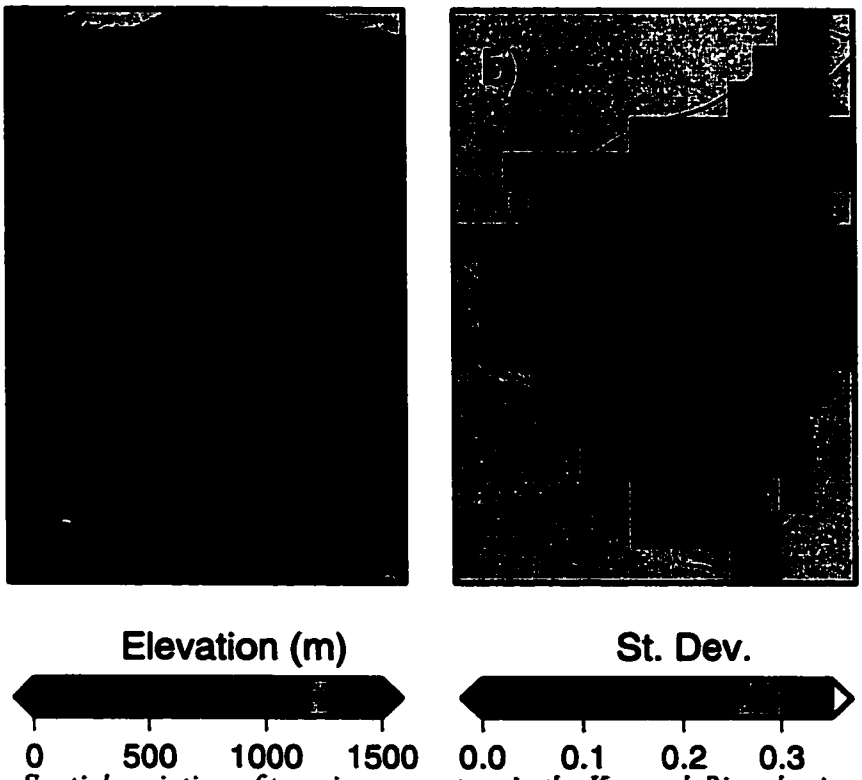

Figure 5.11. Spatial variation of terrain parameters in the Kuparuk River basin: a) 30 arcsec elevations and b) standard deviation of terrain slope.

Wind speeds and average relative humidity tend to increase along the exposed coastal plain. The corrected, gauge-measured precipitation also drops with the transition to the coastal plain. The Kuparuk River was simulated as 153 VIC model grid cells at 1/8° resolution. Average modeled seasonal sublimation from blowing snow (for the winters 1994-95, 1995-96 and 1996-97) is shown in Figure 5.13 for a north-south transect of the Kuparuk basin. The modeled seasonal average varies from a high of 55 mm in the foothills to a low of 14 mm in the central portion of the basin. Average simulated sublimation on the coastal plain is approximately 30 mm.

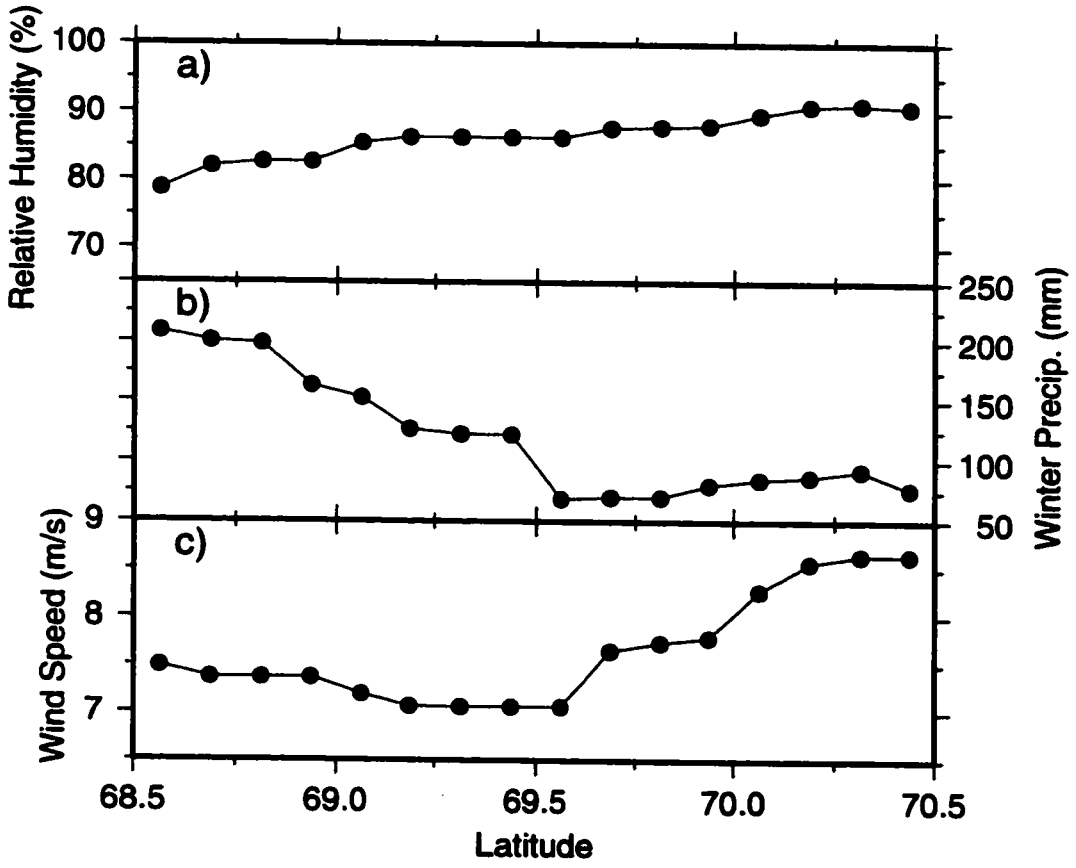

Figure 5.12. Gridded winter average meteorological inputs for the Kuparuk River basin, averaged over all longitudes to create and average north-south transect a) relative humidity, b) wind speed and c) total precipitation. Wind speed averages were calculated only for days on which the average daily wind speed exceeded 5 m/s, for more direct comparison with Listion and Sturm (2002).

Liston and Sturm (2002) simulated sublimation from blowing snow using the SnowTran-3d model for an 85 x 230 km region centered on the Kuparuk River. Their application utilized a 100 m x 100 m horizontal grid and daily time step and simulations were performed for the same three winters (1994 to 1997). Both VIC and SnowTran-3d estimate a region of low sublimation in the central portion of the basin, with increasing sublimation towards both the foothills and the coastal plain (see Figure 5.13). However, Liston and Sturm simulate the highest rates of sublimation on the coastal plain, while the VIC algorithm estimates the greatest rates in the foothills. On average, the VIC estimates are approximately 21 percent less than Liston and Sturm in the uplands (southern two thirds of the basin), while they are about 50 percent smaller on the coastal plain (northern one third of the basin). Largely due to the differences on the coastal plain, Liston

and Sturm (2002) predict 13 mm more sublimation from blowing snow averaged over the entire domain for the three years, than does the VIC algorithm (37 versus 24 mm).

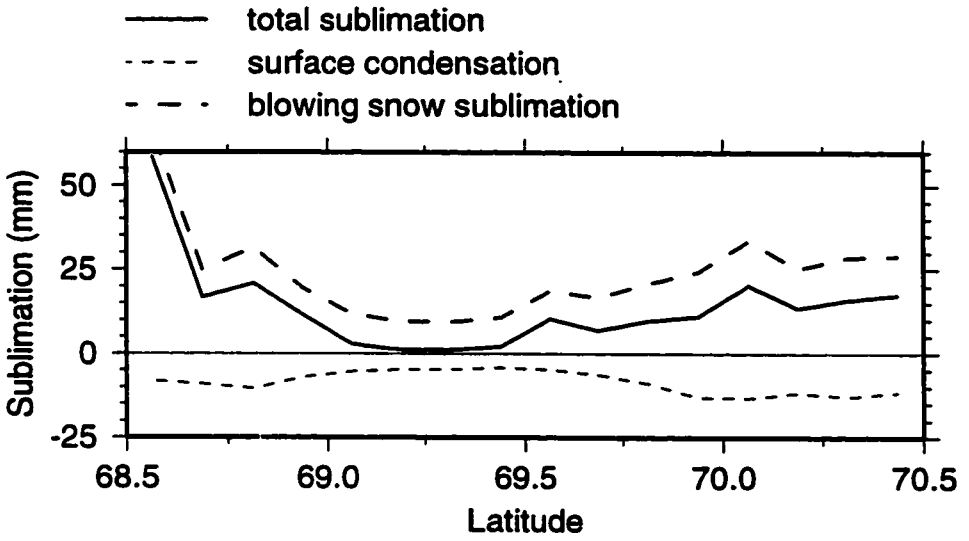

Figure 5.13. Average sublimation (positive) during blowing snow, average condensation (negative) from the surface snow pack and total sublimation for the Kuparuk River basin. Sublimation was averaged over all longitudes to create an average north-south transect.

One clear difference between the two model applications is that the precipitation inputs are fundamentally different. As described above, precipitation input for the VIC application was obtained by gridding catch-corrected station data. Liston and Sturm (2002) used extensive snow surveys to determine the end-of-winter distribution of snow water equivalent in April of 1995, 1996 and 1997. They then used an iterative process with the blowing snow model to estimate the precipitation inputs necessary to yield the observed north-south transect of snow water equivalent. The assimilation method of Liston and Sturm yielded estimates of annual average precipitation similar to the corrected gauge data at its maximum in the foothills (approximately 200-210 mm average for water years 1994 through 1996). However, although the trend in precipitation for the upland-coastal plain transition and the coastal plain is similar between the two methods, the maximum precipitation predicted on the coastal plain by Liston and Sturm is substantially higher than the corrected gauge data (approximately 153 mm versus 82 mm). The differences need to be verified through continued monitoring of both gauge precipitation and the ground snow pack along the arctic coastal plain.

The total sublimation from blowing snow is tied to both the timing and quantity of precipitation. Transport of snow by wind cannot be initiated in SnowTran-3D until the snow holding capacity of vegetation is satisfied. The calculation is different in VIC, but the effect is essentially the same. Therefore, if snow precipitation is underestimated, it reduces the length of the season over which blowing snow sublimation can occur. In addition, increasing time since the last snowfall decreases the probability of occurrence of blowing snow, as parameterized in VIC using the formulation of Li and Pomeroy (1997). So if the frequency of precipitation events is underestimated (i.e. from unrecorded trace events), blowing snow transport will be simulated to occur less frequently. Even with the relatively low sublimation rates predicted by the VIC model for the coastal plain region (26 mm/year, on average), total end-of-winter SWE is lower than that observed by Liston and Sturm (2002). Therefore, it appears that the estimates of precipitation (and hence sublimation) in the VIC model are underestimated for this application.

DISCUSSION AND SENSITIVITY

Surface sublimation from the ground snow pack and total sublimation (blowing snow sublimation plus surface sublimation) are also shown in Figure 5.13. Along the entire length of the basin, the simulated seasonal surface sublimation results in net condensation to the snowpack. Although net seasonal condensation to the snow surface is not anticipated from the literature, estimates of this quantity in isolation from blowing snow over an entire arctic winter are rare. Liston and Sturm (2002) do not simulate vapor exchange with the ground snowpack. Simulated surface sublimation is driven by the vapor pressure gradient between the atmosphere and the snow surface, with a correction for atmospheric stability. Snow surface vapor pressure is assumed to equal the saturation vapor pressure with respect to ice at the snow surface temperature. Snow surface temperature is solved by iteration in order to close the surface energy balance. In mid-winter, low snow surface temperatures result in a negative vapor pressure gradient even at times when the atmospheric relative humidity is less than 100 percent. In a comparison of three turbulent transfer schemes with observations near Saskatoon, Canada for a two-day period in March, 1996, Pomeroy et al. (1998) found that the downward turbulent energies were overestimated by all three models. The simulated rate of condensation by the VIC model for the Kuparuk basin may be due in part to inadequate dampening of turbulent mixing during stable conditions by the VIC snow algorithm.

The latent heat consumed by blowing snow sublimation further reduces the snow surface temperature, so surface condensation is slightly higher for the VIC model runs with blowing snow than those without (not shown). In contrast, as derived by Thorpe and Mason (1966), sublimation from a suspended ice particle is independent of the temperature of the particle surface, it is dependent only on the atmospheric relative humidity. Therefore, in the VIC model sublimation from suspended snow particles can be maintained at times when surface sublimation cannot.

For this application, the atmospheric water vapor pressure is calculated from interpolated station observations of relative humidity. Humidity measurements in arctic environments are frequently unreliable due to ice accumulation on the gauge. Dery and Stieglitz (2002) recently documented the tendency of the Vaisala hygrothermomenters to overpredict vapor saturation. In addition, it is frequently unclear whether such instruments measure relative humidity for water vapor in equilibrium with a liquid of frozen surface. For the reasons described above, the simulated surface sublimation is sensitive to small absolute changes in winter vapor pressure. Uncertainty in the measured relative humidity is undoubtedly influential in the estimates of net surface condensation in this region.

The influence of the VIC parameterizations on estimated blowing snow sublimation rates is shown in Figure 5.14. A north-south transect of predicted blowing snow sublimation is shown, together with similar estimates for the case of unlimited fetch. The unlimited fetch scenario results in a 65 percent increase in sublimation rates in the foothills where the complex terrain results in areas of limited fetch. The difference virtually disappears on the coastal plain, where the calculated average fetch is sufficiently large (1 to 2 km) that it does not impose a significant limitation on sublimation rates. The effect of fetch is further explored in Figure 5.15, which shows the seasonal sublimation from blowing snow in response to the three methods of fetch calculation shown in Figure 5.6. For the average north-south transect, estimates of blowing snow sublimation for fetch lengths calculated from vegetation are indistinguishable from the combined vegetation/topography fetch lengths. Once again, the estimates of blowing snow sublimation on the coastal plain are insensitive to small variations in fetch.

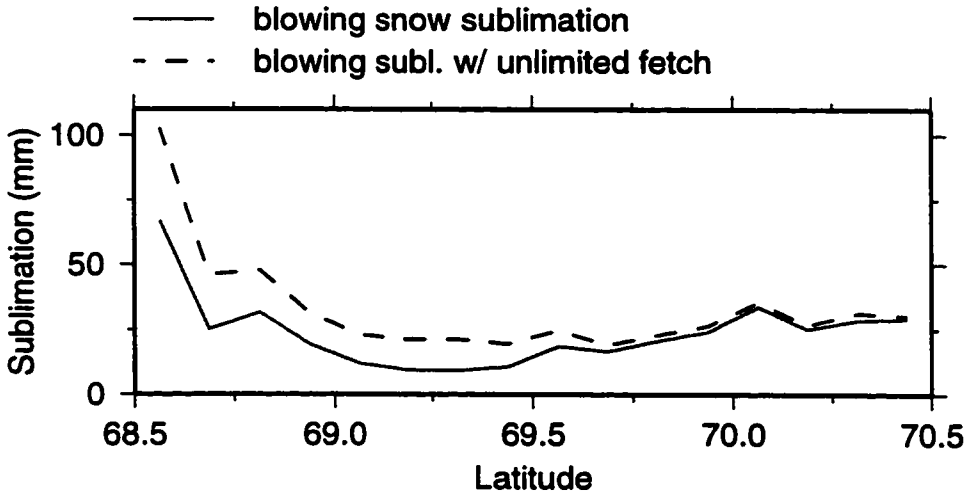

Figure 5.14. Comparision of average sublimation from blowing snow computed with and without spatially varying fetch.

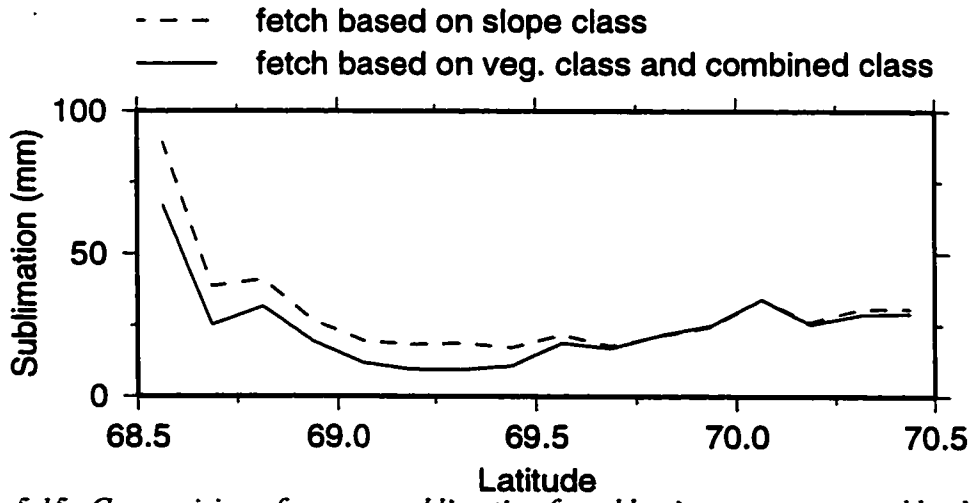

Figure 5.15. Comparision of average sublimation from blowing snow computed by the three estimates of average fetch shown in Figure 5.6.

The simulated sublimation from blowing snow is essentially zero when wind speed is assumed constant across the grid cell (equal to the value interpolated from meteorological stations). This is because with the smoothing of the wind profile that results from interpolating sparse observations, wind speeds are frequently not high enough to initiate blowing snow. This is consistent with previous observations that it is not possible to represent blowing snow transport at large scale without some parameterization of sub-grid variability in wind speed. The effect of the re-scaling of the terrain distribution on the simulated blowing snow sublimation is shown in

Figure 5.16. Using the variance in terrain slope calculated directly from the 30 arcsec DEM results in 24 percent less sublimation in the foothills and 7 percent less on the coastal plain. A larger effect in the foothills is expected. The complex topography of the foothills results in a greater spread of the spatial wind distribution, as reflected in the standard deviation of terrain gradient in Figure 5.11b. The relationship of sublimation to wind speed is extremely nonlinear (King et al. 2001, Essery et al. 1999, Mikhel and Rudneva 1967), so greater spread in the distribution results in a higher mean sublimation. The insensitivity of sublimation to the wind parameterization on the coastal plain is further evidence that blowing snow sublimation in this region is limited by snow availability for transport, rather than transport capacity.

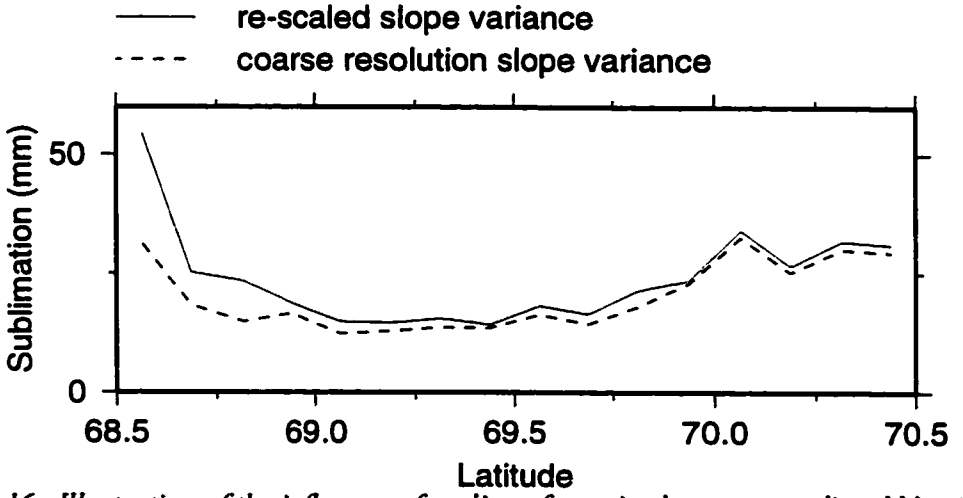

Figure 5.16. Illustration of the influence of scaling of terrain slopes on predicted blowing snow sublimation.

CONCLUSIONS AND RECOMMENDATIONS

This article describes an approximation of topographically induced sub-grid variability in wind speed, snow transport and sublimation in a blowing snow sublimation algorithm designed for use within the Variable Infiltration Capacity (VIC) macroscale hydrology model. A sensitivity analysis has shown that it is essential to represent the sub-grid variability in wind speed in order to generate blowing snow transport at the mesoscale. The algorithm provides an estimate of sublimation from blowing snow at the mesoscale, while simultaneously tracking the other land surface components of the water and energy balance. In addition to standard meteorological inputs, the model requires specification of three new parameters: the standard deviation of terrain slope, the standard deviation of terrain elevations and the lag one gradient autocorrelation for

each model grid cell. These are calculated in advance using global digital elevation databases. Sublimation fluxes are solved for each sub-grid vegetation class, for each model grid cell.

Model results are compared to simulated estimates of sublimation from blowing snow for two small tundra watersheds: Imnavait Creek, Alaska and Trail Valley Creek, Northwest Territories, produced by two different small-scale distributed blowing snow algorithms (Liston and Sturm 1998, Essery et al. 1999). Based on this comparison, the VIC algorithm reproduces some aspects of the variability between years and between vegetation types predicted by the other models.

The VIC blowing snow algorithm was subsequently used to estimate sublimation from blowing snow and the ground snow pack for the 8000 km^2 Kuparuk River watershed in northern Alaska. Based on these (currently unverifiable) model simulations:

- Annual average sublimation from blowing snow varies from 55 mm in the foothills to approximately 25 mm on the coastal plain. A regional low in blowing snow sublimation of approximately 14 mm occurs in the central portion of the basin.

- Simulated sublimation from blowing snow on the coastal plain is lower than previously reported

- Vapor flux from the ground snow pack results in net condensation for the winter between 5 and 20 mm throughout the basin. The combined fluxes therefore yield an estimate of total sublimation over the winter between 5 and 45 mm. The cause and validity of the estimated condensation requires further analysis.

The blowing snow algorithm is sensitive to estimations of average upwind fetch in regions of complex terrain. A simple parameterization based on the standard deviation of elevation as determined from a 30 arcsec DEM shows promise in reproducing the average fetch as calculated from a 50 m resolution vegetation classification. Transport of snow between vegetation classes, which is not represented by the VIC algorithm, may prove essential for estimates of spatial snow distributions at local scale.

CHAPTER VI: CONCLUSIONS

SUMMARY

The three papers that constitute this dissertation evaluate two key land surface hydrologic processes in the Arctic: the effect of lakes and wetlands on the surface water and energy budget, and the role of sublimation of blowing snow on snow accumulation subsequently available for runoff. Preliminary attempts to simulate the water budget of two large arctic rivers, the Mackenzie and the Ob, with an existing macroscale hydrology model suggested the importance of these processes to representation of the land surface water budget. The first study is based primarily on field observations, supplemented by remote-sensing, in the Putuligayuk River watershed, in the arctic of northern Alaska. Results of this study showed that:

- Evaporation and drainage result in a seasonal reduction of the extent of surface water bodies of 58 to 73 percent and a reduction of surface wetness over the summer period. The largest decrease in saturated extent takes place in the first one to two weeks following snowmelt. After this point, the drainage network becomes disconnected, and the remaining decrease in surface water extent is primarily through evaporation.

- Some of the surface storage deficit is made up during the early fall period when precipitation is generally at an annual maximum while ET is minimal to negligible. Late summer precipitation may result in runoff from upland tundra areas to partially recharge pond storage.

- The surface storage deficit carried over the winter must be satisfied the following spring before any runoff will be generated. Between 24 to 42 percent of the snowpack water equivalent was not immediately available for runoff because it filled the ponds and wetlands.

- This observed storage effect can be explained in large part by baseflow drainage and the excess of evapotranspiration over summer precipitation from open water areas. Model

estimated evaporation from open water areas accounts for 50 and 64 percent of the snowmelt storage in 1999 and 2000, respectively.

These observations led to the development of an algorithm to represent the effects of lakes and wetlands within the VIC hydrology model. The unique feature of this algorithm is its ability to represent seasonally inundated areas by allowing the lake area to expand and contract over time. The lake expands in area in response to inflow from upland regions of vegetation. Wetland vegetation emerges as the lake area contracts in response to evaporation and runoff outflow. Runoff ceases when the lake falls below a specified minimum depth, in order to represent the disconnection of the drainage network observed for many arctic lakes and wetlands. Simulation of the Putuligayuk River watershed using the lakes and wetlands algorithm indicated that the model was able to represent the large seasonal change in inundated area of the Putuligayuk watershed and the relative size of the components of the summer water budget, although problems remain in the simulation of outflow hydrographs. Analysis of the simulated system provides the following insights:

- Simulated surface runoff from the wetlands ceased within days of peak snowmelt. After this point, discharge is sustained primarily by baseflow drainage. Isolated summer precipitation events can result in occasional surface runoff events that are also evident in the observed record.

- The lakes and ponds of the coastal plain thaw in the latter part of June (between June 6th and July 3rd for the period 1995 to 2000). There is a wider range in variability in the timing of complete ice cover, which varied between September 13th and October 29th.

- The presence of extensive open water on the Arctic coastal plain effects the spatial distribution of evaporation. Basin annual average evaporation is 60 percent higher (68 versus 42 mm) when the lakes are simulated, relative to the case with no lakes. Perhaps more significant is the large degree of heterogeneity in evaporation (and latent heat) represented by the lake model.

- The timing of the simulated runoff response is sensitive to the partitioning of surface and subsurface runoff, a distinction with questionable meaning in this low-gradient, permafrost

catchment. Further investigation of the function of the VIC baseflow generating function in permafrost environments is required.

Examination of the mean simulated snow water equivalent (SWE) for May 1999 and May 2000 indicates that total SWE is overestimated in VIC in 1999 and underestimated in 2000. Initial simulations using catch-corrected winter precipitation resulted in overestimation of the end-of-season SWE for both years. This discrepancy led to a closer examination of the importance of sublimation from blowing snow events on the Arctic coastal plain and other wind-swept environments in the Arctic drainage basin.

This third study resulted in the development of an algorithm to parameterize the transport and sublimation of blowing snow within the VIC model. The model represents the spatial distribution of wind speed statistically within a VIC grid cell using the Laplace distribution of terrain slopes. The grid cell average fetch over which the boundary layer can develop is calculated as a function of the inverse of the terrain variance for the domain of each model grid cell. The algorithm was used to simulate the accumulation and ablation of the seasonal snow pack within the Kuparuk River basin in northern Alaska, including sublimation during blowing snow events. This study led to the following conclusions:

- Annual average sublimation from blowing snow varies from 55 mm in the foothills to approximately 25 mm on the coastal plain. A regional low in blowing snow sublimation of approximately 14 mm occurs in the central portion of the basin.

- Simulated sublimation from blowing snow on the coastal plain is lower than previously reported

- Vapor flux from the ground snow pack results in net condensation for the winter between 5 and 20 mm throughout the basin. The combined fluxes therefore yield an estimate of total sublimation over the winter between 5 and 45 mm. The cause and validity of the estimated condensation requires further analysis.

The blowing snow algorithm is sensitive to estimations of average upwind fetch in regions of complex terrain. A simple parameterization based on the standard deviation of elevation as determined from a 30 arcsec DEM shows promise in reproducing the average fetch as calculated

from a 50 m resolution vegetation classification. Transport of snow between vegetation classes, which is not represented by the VIC algorithm, may prove essential for estimates of spatial snow distributions at local scale.

These studies have resulted in changes in our estimates of evaporation from Arctic land areas. On the Alaskan Arctic coastal plain, the representation of surface storage and the sublimation from blowing snow results in an increase in the estimation of average annual evaporation in the VIC model on the order of 93 mm or approximately 34 percent of the gauge-corrected annual precipitation. It is difficult to verify this estimate based on careful measurements alone because of the difficulty in conducting a simple water balance in this extreme environment. There is the potential for even greater changes in total evaporation volume for more southerly reaches of the Arctic drainage basin where radiation inputs are larger. The Alaskan coastal plain environment studied in this research is typical of a large portion of the ungauged portion of the circumpolar Arctic drainage basin. The increased predictions of evaporation from these areas effects estimates freshwater fluxes from the land surface to both the atmosphere and the Arctic Ocean, with important implications for our understanding of the broad scale impacts of land-atmosphere-ocean interactions in the Arctic and their role in global climate.

RECOMMENDATIONS

The ability to evaluate the model algorithms developed here was limited by the quality of observed precipitation in the selected study areas, and throughout the Arctic. Quantification of precipitation, as well as other terms in the land surface water balance, remains a fundamental research question for Arctic system science. Underestimation of precipitation by the standard gauges in operation in high-latitude countries by wind, wetting and evaporation losses is a well-documented phenomenon (Sevruk and Hamon 1984, Goodison et al. 1998).

The solution to the problem is not apparent. Detailed field studies such as the Solid Precipitation Intercomparison sponsored by the World Meteorological Organization (Goodison et al 1998) have attempted to develop correction equations for standard precipitation gauges based on wind speed and gauge exposure statistics. Several researchers have developed adjusted historic datasets based on these corrections (Adam and Lettenmaier 2002, Mekis and Hogg 1999, Groisman et al. 1991, Yang et al. 1999). This is a good start, but even these attempts have proved

controversial within the scientific community due to disagreements over the nature of the field studies and application of the corrections. The quality of the correction also depends upon the availability of gauge metadata detailing gauge exposure, which in many cases is not available. Finally, it is not possible to correct nonexistent data. The network of existing precipitation stations in the Arctic is sparse, and is generally concentrated along the coasts and at low elevations along major river valleys. Nor does the future situation look better as the network of manned stations is decreasing throughout the former Soviet Union and Canada (SEARCH 2001). Recognition of the problem has yet to yield an agreed upon best method of measuring true precipitation, nor is it clear that such a method exists.

In the near future, new and novel approaches may offer the best hope of precipitation estimation. For example, Liston and Sturm (1998, 2002) used observed distributions of snow on the ground, in conjunction with a blowing snow model to represent snow redistribution and sublimation, to back-calculate total winter snow precipitation. Serreze et al. (2002) created a blended product of observed gauge precipitation and analysis fields from the European Centre for Medium-Range Weather Forecasting (ECMWF) model, to take advantage of the spatial resolution of the simulated product, while preserving the statistics of the observations. Such approaches show potential as creative solutions to the critical problem of winter precipitation estimation in the Arctic, however, the resulting precipitation fields are highly model dependent and the techniques may be premature. For example, Liston and Sturm (1998) describe the original development and testing of the SnowTran-3d blowing snow model in the same application that makes use of back-calculated winter snow precipitation. It is impossible to evaluate the interdependent, simulated snow precipitation and sublimation fields unless the blowing snow sublimation model is first tested using a best-quality, adjusted precipitation dataset.

In addition to the question of solid precipitation estimation, the results from this study present a number of more specific challenges and opportunities for future research. The assessment of the snowmelt water balance of the Putuligayuk River could be improved by a better understanding of the role of recharge to the upland tundra areas and the pathways of water exchange from the tundra to the wetlands in both the physical and the simulated system. Kane et al. (1989) used runoff plots to investigate tundra recharge of the Imnavait Creek watershed in the foothills of the

Brook's Range. The low topographic gradients of the coastal plain may limit the usefulness of this approach.

Finally, this study reveals some important questions regarding the representativeness of winter micrometeorological measurements in the Arctic. The two-layer energy balance snow model in VIC predicts net condensation to the ground snow pack over the winter. This appears to contradict numerous field observations in the Arctic, although mid-winter vapor exchange with the snowpack is not a quantity that is well observed. Measurements of humidity in cold regions are difficult to conduct. Dery and Stieglitz (2002) documented that humidity observations collected by the Vaisala HMP35CF sensors in use at many Canadian automated weather stations are frequently biased towards the ice saturation point due to persistent icing of the instrument. Such a bias in the observed data could lead to an excess of condensation in the VIC model simulations.

REFERENCES

Aagaard and Carmack, The role of sea ice and other freshwater in the Arctic circulation, *Journal of Geophysical Research, 94c*, 14485-14498, 1989.

Adam, J.C. and D.P. Lettenmaier, Bias correction of global gridded precipitation for solid precipitation undercatch, *Journal of Geophysical Research*, submitted, 2002.

Adams, J.M., N.A. Bond and J.E. Overland, Regional variability of the Arctic heat budget in fall and winter, *Journal of Climate, 13*(19), 3500-3510, 2000.

Alekseev, G. and Buzuev, A., On the evolution of the ice-surface layer of the ocean system in the region of drift of the Severniya Polyus-16 station, *Problems of the Arctic and Antarctic* 42, 37-43, 1973.

Anderson, E.A., National weather service river forecast system – snow accumulation and ablation model, NOAA Technical Memorandum NWS HYDRO-17, Silver Spring, MD, 1973.

Andrews, J.T., Abrupt changes (Heinrich events) in late Quaternary North Atlantic marine environments: A history and review of data and concepts, *J. Quatern. Sci., 13*, 3-16, 1998.

Berg, N.H., Blowing snow at a Colorado alpine site: measurements and implications, *Arctic and Alpine Research, 18* (2), 147-161, 1986.

Bigras, S.C., Hydrological regime of lakes in the Mackenzie delta, Northwest Territories, Canada, *Arctic and Alpine Research*, 22, 163-174, 1990

Bintanja, R., The contribution of snowdrift sublimation to the surface mass balance of Antarctica, *Annals of Glaciology, 27*, 251-259, 1998

Bintanja,R., Modelling snowdrift sublimation and its effects on the moisture budget of the atmospheric boundary layer, *Tellus, 53A*, 215-232, 2001.

Boone, A. and P. Etchevers,. An inter-comparison of three snow schemes of varying complexity coupled to the same land surface and macro-scale hydrologic models. *J. Hydrometeor., 2*(4): 374-394, 2001.

Boone, A., V. Masson, T. Meyers and J. Noilhan, The influence of the inclusion of soil freezing on simulation by a soil-atmosphere-transfer scheme, *J. Applied Meteor., 9*, 1544-1569, 2000.

Bowling, L.C., D.P. Lettenmaier and B.V. Matheussen, The hydroclimatology of the Arctic drainage basin, in *The Freshwater Budget of the Arctic Ocean*, E.L. Lewis, *ed.*, NAT0 Science Series 2. 70, Kluwer Academic Publishers, Dordrecht, The Netherlands, 2000.

Bowling, L.C., D.L. Kane, R.E. Gieck, L.D. Hinzman and D.P. Lettenmaier, The role of surface storage in a low-gradient Arctic watershed, *Water Resources Research*, in review, 2002a.

Bowling, L.C., D.P. Lettenmaier, B. Nijssen, L.P. Graham, D.B. Clark, M. El Maayar, R. Essery, S. Goers, Y.M. Gusev, F. Habets, B. van den Hurk, J. Jin, D. Kahan, D. Lohmann, X. Ma, S. Mahanama, D. Mocko, O. Nasonova, G. Niu, P. Samuelsson, A.B. Shmakin, K. Takata, D. Verseghy, P. Viterbo, Y. Xia, Y. Xue and Z. Yang, Simulation of high-latitude processes in the Torne-Kalix basin: PILPS Phase 2(e) 1: Experiment description and summary intercomparisons, *Global and Planetary Change*, in press, 2002b.

Bras, R.L., Hydrology, An Introduction to hydrological science, Addison-Wesley publishing Company, Reading, Mass., 1990.

Bristow, K.L. and G.S. Campbell, On the relationship between incoming solar radiation and daily maximum and minimum temperature, *Agric-Forest-Meteorol., 31*(2), 159-166, 1984.

Broecker, W.S., Thermohaline circulation, the Achilles heel of our climate system: will man-made CO_2 upset the current balance? *Science, 278*, 1582-1588, 1997.

van den Broeke, M.R., J.G. Winther, E. Isaksson, J.F. Pinglot, L. Karlof, T. Eiken, and L. Conrads, Climate variables along a traverse line in Dronning Maud Land, East Antarctica, *Journal of Glaciology, 45*(150), 295-302, 1999.

Bromwich, D.H., The atmospheric moisture budget of the Arctic and Antarctic from atmospheric numerical analyses, Proceedings, Conference on Polar Processes and Global Climate, Part I of II, 30-32, 1997.

Brown, M.E. and D.L. Arnold, Land-surface-atmosphere interactions associated with deep convection in Illinois, *International Journal of Climatology, 18*(15), 1637-1653, 1998.

Brown, J., Ferrians, O.J. Jr., Heginbottom, J.A. and Melnikov, E.S., Circum-Arctic map of permafrost and ground-ice conditions, United States Geological Survey, Circum-Pacific Map Series, CP-45, Reston, VA, U.S.A., 1997.

Brutsaert, W., Evaporation into the atmosphere. D. Reidel, Dordrecht, 1982.

Cattle, H., Diverting Soviet rivers: some possible repercussions for the Arctic Ocean, *Polar Record, 22*, 485-498, 1985.

Cherkauer, K. A. and D. P. Lettenmaier, Hydrologic effects of frozen soils in the upper Mississippi River basin, *J. Geophys. Res., 104*(D16), 19,599-19,610, 1999.

Cherkauer, K. A., L. C. Bowling and D. P. Lettenmaier, Variable Infiltration Capacity (VIC) Cold Land Process Model Updates, *Global and Planetary Change*, in press, 2002.

Church, M., Hydrology and permafrost with reference to northern North America, in *Proceedings Workshop Seminar on Permafrost Hydrology*, Can. Nat. Comm., IHD, Ottawa, pp. 7-20, 1974.

Dery, S.J., P.A. Taylor and J. Xiao, The thermodynamic effects of sublimating, blowing snow in the atmospheric boundary layer, *Boundary-Layer Meteorology, 89*, 251-283, 1998.

Dery, S.J. and M.K. Yau, Simulation of blowing snow in the Canadian Arctic using a double-moment model, *Boundary Layer Meteorology, 99*(2), 297-316, 2001.

Dery, S.J. and M. Stieglitz, A note on surface humidity measurements in the cold Canadian Environment, *Boundary Layer Meteorology, 102*(3), 491-497, 2002.

Dunne, T., T.R. Moore, and C.H. Taylor, Recognition and prediction of runoff producing zones in humid regions, *Hydrol. Sci. Bull., 20*(3), 305-327, 1975.

Dyunin, A.K., Fundamentals of the theory of snow drifting, Izvest. Sibirsk, Otdel, Akad. Nauk. USSR, 12, 11-24. [English translation by Belkov, G. 1961 Technical Translation 952, National Research Council of Canada, Ottawa.], 1959.

Essery, R., Spatial statistics of windflow and blowing-snow fluxes over complex topography, *Boundary-Layer Meteorology, 100*, 131-147, 2001.

Essery, R., L. Li and J. Pomeroy, A distributed model of blowing snow over complex terrain, *Hydrological Processes, 13*, 2423-2438, 1999.

Eugster, W., W.R. Rouse, R.A. Pielke Sr., J.P. McFadden, D.D. Baldocchi, T.G.F. Kittel, F.S. Chapin III, G.E. Liston, P.L. Vidale, E. Vaganov and S. Chambers, Land-atmosphere energy exchange in arctic tundra and boreal forest: available data and feedbacks to climate, *Global Change Biology, 6*, 84-115, 2000.

Giorgi, F., B. Hewitson, J. Christenson, M. Hulme, H. von Storch, P. Whetton, R. Jones, L. Mearns and C. Fu, Regional climate information-evaluation and projects. In: Climate Change 2001: The scientific basis. Contribution of working group I to the third assessment report of the intergovernmental panel on climate change [Houghton, J.D., Y. Ding, D.J. Griggs, M. Noguer, P.J. van der Linden, X. Dai, K. Maskell and C.A. Johnson (eds.)]. Cambridge University Press, Cambridge, United Kingdom and New York, NY, USA, 881 pp., 2001.

Glenn, M.S. and M.K. Woo, Spring and summer hydrology of a valley-bottom wetland, Ellesmere Island, Northwest Territories, Canada, *Wetlands, 17*(2), 321-329, 1997.

Goering, D.J., H. Chen, L.D. Hinzman, and D.L. Kane, Terrain correction of SAR satellite imagery of Alaska tundra, *IEEE Transactions on Geoscience and Remote Sensing, 33*(1), 185-194.

Goodison, B.E., P.Y.T. Louie, and D. Yang, WMO Solid precipitation intercomparison: final report, WMO/TD-872, 212 pp., World Meteorol. Organ., Geneva, 1998.

Goyette, S., N.A. McFarlane, and G.M. Flato, Application of the Canadian Regional Climate Model to the Laurentian Great Lakes region: Implementation of a lake model, *Atmosphere-Ocean, 38*(3), 481-503, 2000.

Grabs, W.E., Portmann, F., de Couet, T., Discharge observation networks in Arctic regions: computation of the river runoff into the Arctic Ocean, its seasonality and variability, in *The Freshwater Budget of the Arctic Ocean*, E.L. Lewis, ed., 1999.

Greeley, R. and J.D. Iversen, Wind as a geological process on Earth, Mars, Venus and Titan. Cambridge, Cambridge University Press, 1985.

Groisman, P., V. Koknaeva, T. Belokylova and T. Karl, Overcoming biases of precipitaiton measurement: A history of the USSR experience, *Bulletin of American Meteorological Society, 75*(2), 215-227, 1991.

Groisman, P.Y., Golubev, V.S., Genikhovich, E.L. and Bomin, S., Evaporation from snow cover: an empirical study, in Proceedings, Conference on Polar Processes and Global Climate, Part I of II, 72-73, 1997.

Gupta, V.K. and E. Waymire, Multiscaling properties of spatial rainfall and river flow distributions, *Journal of Geophysical Research, 95*(D3), 1999-2009, 1990.

Hall, J.V., W.E. Frayer and B.O. Wilen, Status of Alaska Wetlands, U.S. Fish and Wildlife Service, Alaska Region, Anchorage AK, 32pp, 1994.

Harazono, Y., M. Yoshimoto, A. Miyata, Y. Uchida, G.L. Vourlitis and W.C. Oechel, Micrometeorological data and their characteristics over the arctic tundra at Barrow, Alaska during the summer of 1993, Misc. Pub. of the National Institute, Agro-Environmental Sciences, 16, 1-215, 1995.

Harding, R.J. and Pomeroy, J.W., The energy balance of the winter boreal landscape, *Journal of Climate, 9*, 2778-2787, 1996.

Hinzman, L.D. and D.L. Kane, The role of hydrology in arctic atmospheric and oceanic processes, in Workshop to Define Research Priorities for Russian Arctic Land-Shelf Systems (abstracts), January 10-12, 1995. *Byrd Polar Research Center Miscellaneous Series M-335*, Byrd Polar Research Center, The Ohio State University, Columbus, Ohio, 132 pages, 1995.

Hinzman, L.D., D.J. Goering and D.L. Kane, A distributed thermal model for calculating soil temperature profiles and the depth of thaw in permafrost regions, *Journal of Geophysical Research, 103* (D22), 28975-28991, 1998.

Hinzman, L.D., Kane, D.L., Benson, C.S. and Everett, K.R., Energy balance and hydrological processes in an Arctic watershed, *Ecological Studies, 120*, 131-154, 1996.

Hood, E.W., M.W. Williams and D. Cline, Sublimation from a seasonal snowpack at a continental, mid-latitude alpine site, International conference on Snow Hydrology: The Integration of Physical, Chemical and Biological Systems, Brownsville, VT, 6-9 Oct 1998, p. 50, 1998.

Hostetler, S.W., Simulation of lake ice and its effects on the late-Pleistocene evaporation rate of Lake Lahontan, *Climate Dynamics, 6*, 43-48, 1991.

Hostetler, S.W. and P.J. Bartlein, Simulation of lake evaporation with application to modeling lake level variations of Harney-Malheur Lake, Oregon, *Water Resources Research, 26*(10), 2603-2612, 1990.

Hostetler, S.W., P.J. Bartlein, P.U. Clarke, E.E. Small and A.M. Soloman, Simulated influences of Lake Agassiz on the climate of central North America 11,000 years ago, *Nature, 405*, 334-337, 2000.

Huffman, G.J., Adler, R.F., Arkin, P.A., Chang, A., Ferraro, R., Gruber, A., Janowiak, J., Joyce, R.J., McNab, A., Rudolf, B., Schnieder, U. and Xie, P., The Global Precipitation Climatology Project (GPCP) Combined Precipitation data set, *Bulletin of the American Meteorological Society, 78*, 5-20, 1997.

Jacobs, J.D. and L.D. Grondin, The influence of an Arctic large-lakes system on mesoclimate in south-central Baffin Island, N.W.T., Canada, *Arctic and Alpine Research, 20*(2), 212-219, 1988.

Jeffries, M. O., H. Wakabayashi and W. F. Weeks, ERS-1 SAR backscatter changes associated with ice growing on shallow lakes in Arctic Alaska, *Proceedings of the 1993 International Geoscience and Remote Sensing Symposium (IGARSS '93)*, Tokyo, Japan, 18-21 August, 1993.

Jeffries, M.O., T. Zhang, K. Frey and N. Kozlenko, Estimating late-winter heat flow to the atmosphere from the lake-dominated Alaskan North Slope, *Journal of Glaciology, 45*(150): 315-324, 1999.

Jones, P. D., Hemispheric surface air temperature variations: A reanalysis and an update to 1993, *Journal of Climate, 7*, 1794-1802, 1994.

Kandus, P., H. Karszenbaum, T. Pultz, G. Parmuchi, and J.Bava, Influence of flood conditions and vegetation status on the radar backscatter of wetland ecosystems, *Canadian Journal of Remote Sensing, 27*(6), 651-662, 2001.

Kane, D.L. and E.F. Chaco, Frozen ground effects on infiltration and runoff, in Cold Regions Hydrology and Hydraulics, pp. 259-300, American Society of Civil Engineers, New York, 1990.

Kane, D.L. and L.D. Hinzman, Permafrost hydrology of a small Arctic watershed, In: B.A. Senneset-Kaare (Ed), *Permafrost; fifth international conference* 1, International Conference on Permafrost, Proceedings, 590-595, 1988.

Kane, D.L., L.D. Hinzman, C.S. Benson and K.R. Everett, Hydrology of Imnavait Creek, an arctic watershed, *Holarctic Ecology, 12*, 262-269, 1989.

Kane, D.L., L.D. Hinzman, C.S. Benson and G.E. Liston, Snow hydrology of a headwater Arctic basin, I, *Water Resources Research, 27*, 1099-1109, 1991.

Kane, D.L., L.D. Hinzman, J.P. McNamara, Z. Zhang and C.S. Benson, An overview of a nested watershed study in arctic Alaska, *Nordic Hydrology, 31*(4/5), 245-266, 2000.

Kane, D.L., R.E. Gieck, and L.D. Hinzman, Snowmelt modeling at a small Alaskan arctic watershed, *Journal of Hydrologic Engineering, 2*(4), 204-210, 1997.

Kane, D.L., R.E. Gieck and L.D. Hinzman, Evapotranspiration from a small Alaskan arctic watershed, *Nordic Hydrology, 21*, 253-272, 1990.

Khrol, V.P., Ed., Atlas of water balance of the northern polar area, Gidrometeozdat, 81 pp., 1996.

Kimball, J.S., S.W. Running, and R. Nemani, An improved method for estimating surface humidity from daily minimum temperature, *Agricultural and Forest Meteorology, 85*(1-2), 87-98, 1997.

Kind, R.J., One-dimensional aeolian suspension above beds of loose particles - a new concentration-profile equation, *Atmos. Environ., 26*A (5), 927-931, 1992.

King, J.C., P.S. Anderson and G.W. Mann, The seasonal cycle of sublimation at Halley, Antarctica, *Journal of Glaciology, 47* (156), 1-8, 2001.

Klinkenberg, B. and M.F. Goodchild, The fractal properties of topography: a comparison of methods, *Earth Surface Processes and Landforms, 17*, 217-234, 1992.

Kono, N., Hausdorff dimension of sample paths for self-similar processes, In: Dependence in Probability and Statistics, E. Berlein and M. Taqqu, eds., Birkhauser, Boston, 1985.

Krestovskiy, O.I., Postnikov, A.N. and Sergeyeva, A.G., Evaporation during the snow melting and flood period in spring, *Soviet Hydrology, 5,* 439-451, 1972.

Lammers, R.B., A.I. Shiklomanov, C.J. Vorosmarty, B.M. Fekete and B.J. Peterson, Assessment of contemporary Arctic river runoff based on observational discharge records, *Journal of Geophysical Research, 106* (D4), 3321-3334, 2001.

Laurance, W.F. and G.B. Williamson, Positive feedbacks among forest fragmentation, drought, and climate change in the Amazon, *Conservation Biology, 15*(6), 1529-1535, 2001.

Lavalée, D., S. Lovejoy, D. Schertzer and P. Ladoy, Nonlinear variability of landscape topography, in: Multifractal analysis and simulation, Eds. N. Lam, L. DeCola, Prentice-Hall, 171-205, 1993.

Lee, J-S, Speckle analysis and smoothing of synthetic aperture radar images, *Computer Graphics and Image Processing, 17*, 24-32, 1981.

Legates, D.R. and C.J. Wilmott, Mean seasonal and spatial variability in gage-corrected global precipitation, *Int. J. Climatol., 10*, 111-133, 1990.

Li, L. and J.W. Pomeroy, Probability of occurrence of blowing snow, *J. Geophys. Res., 102*(D18), 21,955-21,964, 1997.

Liang, X., D. P. Lettenmaier, E. F. Wood, and S. J. Burges, A Simple hydrologically-based model of land surface water and energy fluxes for GSMs, *J. Geophys. Res., 99*(D7), 14,415-14,428, 1994.

Liang, X., Lettenmaier, D.P. and Wood, E.F., One-dimensional statistical dynamic representation of subgrid spatial variability of precipitation in the two-layer Variable Infiltration Capacity model, *Journal of Geophysical Research, 101d*, 403-21,422, 1996.

Liston, G. and M. Sturm, A snow-transport model for complex terrain, *Journal of Glaciology, 44*(148), 498-516, 1998.

Liston, G. and M. Sturm, Winter precipitation patterns in Arctic Alaska determined from a blowing-snow model and snow-depth observations, *Journal of Hydrometeorology*, in press, 2002.

Lohmann, D., Raschke, E., Nijssen, B. and Lettenmaier, D.P., Regional scale hydrology: I. Formulation of the VIC-2L model coupled to a routing model, *Hydrological Sciences Journal, 43*, 131-141, 1998.

Lovejoy, S., D. Lavallee, D. Schertzer and P. Ladoy, The $l^{1/2}$ law and multifractal topography: theory and analysis, *Nonlinear Processes in Geophysics, 2*, 16-22, 1995.

Lynch, A., D. McGinnis and D. Bailey, Snow-albedo feedback and the spring transition in a regional climate system model: Influence of land surface model, *Journal of Geophysical Research, 103*(D22): 29037-29049, 1998.

Mackay, J.R., Ice-wedge cracks, Garry Island, Northwest Territories, *Canadian Journal of Earth Sciences, 11*(10), 1366-83, 1974.

Mackay, J.R., Downward water movement into frozen ground, western arctic coast, Canada, *Canadian Journal of Earth Sciences, 20*(1), 120-34, 1983.

Manabe, S., M.J. Spelman, and R.J. Stouffer, Transient responses of a coupled ocean-atmosphere model to gradual changes of atmospheric CO2 II. Seasonal response, Journal of Climate, 5(2), 105-26, 1992.

Mann, G.W., P.S. Anderson and S.D. Mobbs, Profile measurements of blowing snow at Halley, Antarctica, *Journal of Geophysical Research, 105*(D19), 24491-24508, 2000.

Marsh, P. and Bigras, S.C., Evaporation from Mackenzie delta lakes, N.W.T., Canada, *Arctic and Alpine Research, 20*(2), 220-229, 1988.

Maurer, E.P., A.W. Wood, J.C. Adam, D.P. Lettenmaier and B. Nijssen, A long-term hydrologically-based data set of land surface fluxes and states for the continental United States, *J. Climate*, in press, 2002.

Mendez, J., L.D. Hinzman and D.L. Kane, Evapotranspiration from a wetland complex on the Arctic coastal plain of Alaska, *Nordic Hydrology, 29* (4/5), 303-330, 1998.

Mekis, E. and W. Hogg, Rehabilitation and analysis of Canadian daily precipitaiton time series, *Atmosphere-Ocean, 37*(1), 53-85, 1999.

Milne, A.K., A comparative evaluation of multiband radar for detecting and mapping wetland inundation, IEEE International Geoscience and Remote Sensing Symposium, Piscataway, NJ, 4, 1883-1885, 1999.

Mikhel, V.M. and Rudneva, A.V., Regionalization of the USSR according to the transport of snow, *Soviet Hydrology, 5*, 441-449, 1967.

Mocko, D.M. and Y.C. Sud, Refinements to SSiB with an emphasis on snow-physics: Evaluation and validation using GSWP and Valdai data, *Earth Interactions, 5*(5-001), 31 pp, 2001.

Morrissey, L.A., S.L. Durden, G.P. Livingston, J.A. Stearn and L.S. Guild, Differentiating methane source areas in Arctic environments with multitemporal ERS-1 SAR Data, *IEEE Transactions on Geoscience and Remote Sensing, 34*(3), 667-672, 1996.

Moskvin, Y.P., Runoff from hummocky marshes of western Siberia, *Soviet Meteorology and Hydrology, 3*, 73-80, 1989.

Muller, S.V., A.E. Racoviteanu, and D.A. Walker, Landsat-MSS-derived land-cover map of northern Alaska: extrapolation methods and comparison with photo-interpreted and AVHRR-derived maps, *International Journal of Remote Sensing, 20*, 2921-2946, 1999.

Murphy, M.A., L.P. Martini and R. Protz, Seasonal changes in subarctic wetlands and river ice breakup detectable on RADARSAT images, southern Hudson Bay Lowland , Ontario, Canada, *Canadian Journal of Remote Sensing, 27*(2), 143-158, 2000.

Nijssen, B., R. Schnur, and D. Lettenmaier, Global retrospective estimation of soil moisture using the variable infiltration capacity land surface model, 1980-1993, *Journal of Climate, 14*(8), 1790-1808, 2001.

Niu, G.Y. and Z.L. Yang, A physically based multi-layer snow parameterization for the NCAR CCM3/LSM, Part I: validation and sensitivity tests in stand-alone experiments, *Journal of Climate*, in review, 2002.

Patterson, J.C. and P.F. Hamblin, Thermal simulation of a lake with winter ice cover, *Limnol. Oceanogr., 33*(3), 323-338, 1988.

Peters-Lidard, C.D., F. Pan and E.F. Wood, A re-examination of modeled and measured soil moisture spatial variability and its implications for land surface modeling, *Advances in Water Resources, 24*(9-10), 1069-1083, 2001.

Petropavlovskaya, M.S. and I.L. Kalyuzhnyi, Drifting of Snow in Northern Kazakhstan, *Soviet Meteorology and Hydrology, 2*, 67-74, 1986.

Pietroniro, A., T. Prowse and D. Peters, Hydrological assessment of an inland freshwater delta using multi-temporal satellite remote sensing, *Hydrological Processes, 13*(16), 2483-2498, 1999.

Pomeroy, J.W., A process-based model of snow drifting, *Ann. Glaciol., 13*, 237-240, 1989.

Pomeroy, J.W., D.M. Gray, K.R. Shook, B. Toth, R.L.H. Essery, A. Pietroniro and N. Hedstrom, An evaluation of snow accumulation and ablation processes for land surface modeling, *Hydrological Processes, 12*, 2339-2367, 1998.

Pomeroy, J.W. and D.M. Gray, Saltation of snow, *Water Resources Research, 26*(7), 1583-1594, 1990.

Pomeroy, J.W. and D.M. Gray, Snowcover accumulation, relocation and management, *National Hydrology Research Institute Science Report No. 7*, NHRI Environment Canada, Saskatoon, 144 pp, 1995.

Pomeroy, J.W. and L. Li, Development of the Prairie Blowing Snow Model for application in climatological and hydrological models, Proceedings, 65th Annual Western Snow conference, May 4-8, Banff, Alberta, Canada, 1997.

Pomeroy, J.W. and L. Li, Prairie and arctic areal snow cover mass balance using a blowing snow model, *Journal of Geophysical Research, 105*(D21), 26629-26634, 2000.

Pomeroy, J.W. and R.J. Schmidt, The use of fractal geometry in modelling intercepted snow accumulation and sublimation, in *Proc. Eastern Snow Conference, 50*, 1-10, 1993.

Pomeroy, J.W. and R.L.H. Essery, Turbulent fluxes during blowing snow: Field tests of model sublimation predictions, *Hydrological Processes, 13*(18), 2963-2975, 1999.

Pomeroy, J.W., D.M. Gray and P.G. Landine, The Prairie Blowing Snow Model: characteristics, validation, operation, *Journal of Hydrology, 144*, 165-192, 1993.

Pomeroy, J.W., P. Marsh and D.M. Gray, Application of a distributed blowing snow model to the Arctic, *Hydrological Processes, 11*, 1451-1464, 1997.

Pope, K., E. Rejmankova, J. Paris and R. Woodruff, Detecting seasonal flooding cycles in marshes of the Yucatan Peninsula with SIR-C polarimetric radar imagery, *Remote Sensing of the Environment, 59*(2), 157-166, 1997.

Prowse, T.D. and P.O. Flegg, Arctic river flow: a review of contributing areas, in *The Freshwater Budget of the Arctic Ocean*, E.L. Lewis, *ed.*, NATO Science Series 2. 70, Kluwer Academic Publishers, Dordrecht, The Netherlands, 2000.

Roulet, N.T. and Woo, M.K., Hydrology of a wetland in the continuous permafrost region, *Journal of Hydrology, 89*, 73-91, 1986.

Rouse, W.R., The energy and water balance of high-latitude: controls and extrapolation, *Global Change Biology, 6*, 59-68, 2000.

Rouse, W.R., Microclimate at Arctic tree line: 3. the effects of regional advection on the surface energy balance of upland tundra, *Water Resources Research, 20*(1), 74-78, 1984.

Rovansek, R.J., Hinzman, L.D. and Kane, D.L., Hydrology of a tundra wetland complex in the Alaskan Arctic coastal plain, U.S.A., *Arctic and Alpine Research, 28*, 311-317, 1996.

Rummukainen, M., J. Raisanen, B. Bringfelt, A. Ullerstig, A. Omstedt, U. Willen, U. Hansson and C. Jones, A regional climate model for northern Europe: model description and results from the downscaling of two GCM control simulations, *Climate Dynamics, 17*(5-6), 339-359, 2001.

Schmidt, R.A., Sublimation of wind-transported snow – a model, USDA Res. Paper RM-90, USDA Forestry Service, Rocky Mountain Forest and Range Experimental station, Fort Collins, Colorado, 24 pp., 1972

Schmidt, R.A., Vertical profiles of wind speed, snow concentration, and humidity in blowing snow, *Boundary Layer Meteorology, 23*, 223-246, 1982

SEARCH SSC, SEARCH: Study of Environmental Arctic Change, Science Plan, Polar Science Center, Applied Physics Laboratory, University of Washington, Seattle, 91 pp., 2001.

Serreze, M.C., M.C. Rehder, R.G. Barry, J.D. Kahl, and N.A. Zaitseva, The distribution and transport of atmospheric water vapour over the Arctic basin, International Journal of Climatology, 15(7), 709-27, 1995.

Serreze, M.C. and C.M. Hurst, Representation of mean Arctic precipitation from NCEP/NCAR and ERA Reanalyses, *J. Climate, 13*, 182-201, 2000.

Serreze, M.C., M.P. Clark and D.H. Bromwich, Monitoring precipitation over the Arctic terrestrial drainage: Applications of the NCEP/NCAR Reanalysis, *Journal of Hydrometeorology*, in review, 2002.

Sevruk, B. and W.R. Hamon, International comparison of national precipitation gauges with a reference pit gauge. WMO instrument and observing methods report No. 17, WMO, Geneva, 111 p., 1984.

Shepard, D.S., Computer mapping: the SYMAP interpolation algorithm, Spatial Statistics and Models, 133-145, Reidel Publishing Company, 1984.

Shiklomanov, A.I., R.B. Lammers, and C.J. Vörösmarty, Widespread decline in hydrological monitoring threatens pan-arctic research, EOS, Transactions, American Geophysical Union, 83 (2), 13-16, 2002.

Shmakin, A.B., The updated version of SPONSOR land surface scheme: PILPS-influenced improvements. *Global and Planetary Change, 19*(1-4): 49-62, 1998.

Stele, M., A simple model of the Arctic Ocean freshwater balance, 1979-1985, *Journal of Geophysical Research, 101c*, 20833-20848, 1996.

Storck, P. and Lettenmaier, D.P., Predicting the effect of a forest canopy on ground snow accumulation and ablation in maritime climates, in C. Troendle (ed), 67th Western Snow Conference, Colorado State University, 1999.

Storr, D. and Golding, D.L., A preliminary water balance evaluation of an intensive snow survey in a mountainous watershed, in *Advanced Concepts and Techniques in the Study of Snow and Ice Resources*, Nat. Acad. Sci., Washington, D.C., 294-303, 1974.

Sud, Y.C. and D.M. Mocko, New snow-physics to complement SSiB. Part I: Design and evaluation with ISLSCP Initiative I datasets. *J. Meteor. Soc. Japan, 77* (1B): 335-348, 1999.

Sun, S. and Y. Xue, Implementing a new snow scheme in Simplified Simple Biosphere Model (SSiB). *Advances in Atmospheric Sciences, 18*: 335-354, 2001.

Tabler, R.D., Estimating the transport and evaporation of blowing snow, In: Symposium on snow management on the Great Plains, Bismarck, North Dakota, July 29, 1975, Great Plains Agricultural Council Publication 73, 85-104, 1975.

Tabler, R.D., Predicting profiles of snowdrifts in topographic catchments, Proceedings of the Western Snow Conference, 43rd annual meeting, Coronado, California, April 23-25, 1975, 87-97, 1975.

Takeuchi, M., Vertical profile and horizontal increase of drift-snow transport, *Journal of Glaciology, 26*(94), 481-492, 1980.

Thornton, P.E., and S.W. Running, An improved algorithm for estimating incident daily solar radiation from measurements of temperature, humidity and precipitation, *Agricultural and Forest Meteorology, 93*, 211-228, 1999.

Thorpe, A.D. and B.J. Mason, The evaporation of ice spheres and ice crystals, *Brit. J. Appl. Phys., 17*, 541-548, 1966.

Töyrä, J., A. Pietroniro, and L.W. Martz, Multisensor hydrologic assessment of a freshwater wetland, *Remote Sensing of Environment, 75*, 162-173, 2001.

Treshnikov, A.F., Main stages and prospects of study in the polar regions of the Earth, in *Problems of the Arctic and the Antarctic, Collection of Articles*, 57, 1-19, 1985.

UNESCO, World water balance and water resources of the earth, United Nations Educational, Scientific and Cultural Organization, 1978.

Villasenor, J.D., D.R. Fatland and L.D. Hinzman, Change detection on Alaska's north slope using repeat-pass ERS-1 SAR Images, *IEEE Transactions on Geoscience and Remote Sensing, 31* (1), 227-236, 1993.

Viterbo, P., A. Beljaars, J. Mahfouf and J. Teixeira, The representation of soil moisture freezing and its impact on the stable boundary layer, *Quarterly Journal of the Royal Meteorological Society, 125*, 2401-2426, 1999.

Vörösmarty, C.J., L.D. Hinzman, B.J.Peterson, D.H. Bromwich, L.C. Hamilton, J. Morison, V.E. Romanovsky, M.Sturm, and R.S. Webb, The hydrologic cycle and its role in the Arctic and global environmental change: a rationale and strategy for synthesis study. Fairbanks, Alaska: Arctic Research Consortium of the U.S., 84 pp., 2001.

Vuglinsky, V.S., River inflow to the Arctic Ocean: Conditions of formation, time variability and forecasts, in polar Processes and Global Climate, ACSYS, Orcas Island, Washington, 275-276, 1997.

Walker, D.A., *GIS data from the Alaska North Slope.* Boulder, CO: National Snow and Ice Data Center. Digital media, 1996.

Walmsley, J.L., J.R. Salmon and P.A. Taylor, On the application of a model of boundary-layer flow over low hills to real terrain, *Boundary Layer Meteorology, 23*, 17-46, 1982

Walsh, J.E., V. Kattsov, D. Portis, and V. Meleshko, Arctic precipitation and evaporation: model results and observational estimates, *Journal of Climate, 11*, 72-87, 1998

Weatherly, J.W. and J.E. Walsh, The effects of precipitation and river runoff in a coupled ice-ocean model of the Arctic, *Climate Dynamics, 12*(1), 785-798, 1996.

Weaver, A.J., E.S. Sarachik, and J. Marotze, Fresh-water flux forcing of decadal and interdecadal oceanic variability, *Nature, 353*(6347), 836-838, 1991.

Woo, M.K., Snow hydrology in the high Arctic, presented at the western Snow Conference, Reno, Nevada, April 20-23, 63-74, 1982.

Woo, M.K., Permafrost hydrology in North America, *Atmos. Ocean, 24* (3), 201-234, 1986.

Woo, M.K., Wetland runoff regime in northern Canada, in *Permafrost: fifth international conference* 1, Proceedings, International conference on permafrost, 644-649, 1988.

Woo, M.K. and Winter, T.C., The role of permafrost and seasonal frost in the hydrology of northern wetlands in North America, *Journal of Hydrology, 141*, 5-31, 1993.

Woo, M.K. and Steer, P., Slope hydrology as influenced by thawing of the active layer, Resolute, N.W.T., *Canadian Journal of Earth Sciences, 20*, 978-86, 1983.

Woo, M.K. and Xia, Z., Effects of hydrology on the thermal conditions of the active layer, *Nordic Hydrology, 27,* 129-142, 1996.

Wood, E.F., Heterogeneity and scaling of land-atmosphere water and energy fluxes in climate systems. In: Space and Time Scale Variability and Interdependencies in Hydrological processes, R.A. Feddes, ed., Cambridge University Press, 3-20, 1995.

Xiao, J., R. Bintanja, S. Dery, G. Mann and P. Taylor, An intercomparison among four models of blowing snow, *Boundary-Layer Meteorology, 97,* 109-135, 2000.

Xu, T., I.D. Moore, and J.C. Gallant, Fractals, fractal dimensions and landscapes – a review, *Geomorphology, 8,* 245-262, 1993.

Yang, D., B.E. Goodison and S. Ishida, Adjustment of daily precipitation data at 10 climate stations in Alaska: Application of World Meteorological Organization intercomparison results, *Water Resources Research, 34*(2), 241-256, 1998.

Yang, D., D.L. Kane, L.D. Hinzman, B.E. Goodison, J.R. Metcalfe, P.Y.T. Louie, G.H. Leavesley, D.G. Emerson and C.L. Hanson, An evaluation of the Wyoming gauge system for snowfall measurement, *Water Resources Research, 36*(9), 2665-2677, 2000.

Yang, D., L.D. Hinzman, X. Zhang and T. Ohata, Siberian major river streamflow regime and recent change, *Water Resources Research,* in review, 2002.

Yang, D., S. Ishida, B.E. Goodison, T. Gunther, Bias correction of daily precipitation measurements for Greenland, *J. Geophysical Research, 105*(D6), 6171-6182, 1999.

Young, K.L. and M.K. Woo, Hydrological response of a patchy high Arctic wetland, *Nordic Hydrology, 31*(4/5), 317-338, 2000.

Zhang, Z., D.L. Kane and L.D. Hinzman, Development and application of a spatially-distributed Arctic hydrological and thermal process model (ARHYTHM), *Hydrological Processes, 14,* 1017-1044, 2000.

Zhang, X., N.A. Drake, J. Wainwright and M. Mulligan, Comparison of slope estimates from low resolution DEMS: scaling issues and a fractal method for their solution, *Earth Surface Processes and Landforms, 24,* 763-779, 1999.

Zhao, M., A.J. Pitman and T. Chase, The impact of land cover change on the atmospheric circulation, *Climate Dynamics, 17*(5-6), 2001.

Zoltai, S.C., An outline of the wetland regions of Canada, in *Proc. Workshop on Canadian Wetlands, 12,* Environ. Can., Lands Dir., Ecol. Land Classif. Ser., 1-8, 1979.

APPENDIX A: HYDROCLIMATOLOGY OF THE ARCTIC DRAINAGE BASIN

L.C. Bowling, D.P. Lettenmaier, and B.V. Matheussen, 2000,
The hydroclimatology of the Arctic drainage basin, in *The Freshwater Budget of the Arctic Ocean*, E.L. Lewis, *ed.*, NATO Science Series, 2, Kluwer Academic Publishers, Dordrecht, The Netherlands, p. 57-90.

1. Introduction

By most estimates, runoff from the land surface represents the single largest input of freshwater to the Arctic Ocean. Alekseev and Buzuev [1] estimated the total freshwater input to the Arctic Ocean to be between 4300 and 6475 km^3/year based on ice formation data. Treshnikov [2] (reported in [3]) estimated the total freshwater flux from gauged land surface areas to be 3300 km^3/yr, or 51 to 77 percent of the total from [1]. Grabs et al. [4] report that the accumulated sum of mean annual flow from the 35 largest gauged Arctic basins is approximately 202 mm/yr (2603 km^3/yr). When extrapolated to the entire land area draining to the Arctic (approximately 19.3 million km^2), this yields a total annual freshwater flux from the land surface of approximately 4000 km^3, or between 62 and 93% of the total freshwater input as estimated from [1]. Another estimate of total freshwater flux from land areas into the Arctic Ocean is 4269 km^3/year, with 17 and 24% attributed to ungauged discharge from islands and mainland, respectively [5].

Despite the importance of Arctic land-surface freshwater fluxes to global ocean circulation and the global heat balance, hydrologists have shied from large-scale studies of the hydrology of the Arctic basin. The dynamics of land-surface hydrology in the Arctic basin are not well understood due to their dependence on unique features such as the control of extreme seasonal runoff by snowmelt and ice break-up, large-scale redistribution of snow and the effects of ephemeral and permanently frozen soils. An important complication is the paucity of observed data and the difficulties associated with data collection. Although extrapolation of observed streamflow to ungauged areas allows bulk estimates of land surface freshwater fluxes such as those cited above, the temporal and spatial variability of runoff response from approximately 30% of the Arctic drainage area is unknown. Hydrologic models offer the most feasible option for estimating runoff in these ungauged areas. In recognition of this fact, the hydrological program of the Arctic Climate System Study (ACSYS) has as one of its specific objectives "the development of mathematical models of the hydrological cycle under specific Arctic climate conditions..." [6].

Land surface models that can represent unique northern hydrologic features are in their infancy. Coupled land-atmosphere-ocean models are an important tool for studies of the interaction of land, atmosphere and ocean processes as they affect climate. However, land surface representations in most such models treat cold season and cold

region processes quite crudely. For instance, most general circulation models (GCMs) do not simulate frozen soils, nor do they represent the sub-grid variability of snow. Nevertheless, some early efforts have been made to incorporate cold regions processes into land-surface models. Anisimov and Nelson [7] simulated permafrost extent in conjunction with three global GCMs, using a dimensionless "frost index". Foster et al. [8] compared snow output from seven GCMs with passive-microwave observations of snow depth. The U.S. Air Force snow depth climatology and National Oceanic and Atmospheric Administration (NOAA) satellite observations of snow extent were used as the standard of reference. Although seasonal and interannual snow distributions were simulated fairly well, transition season simulations (spring and fall) were susceptible to large errors.

The relatively crude representation of cold-regions land surface processes in GCMs can result in over-estimation of peak runoff, as well as errors in timing. For instance, Arctic river runoff predictions are too early by up to two months in both the Canadian Climate Centre and the National Aeronautic and Space Administration (NASA)/Goddard GCMs [9, 10]. Kite et al. [9] hypothesized that one factor in these discrepancies may be the lack of model representation of storage of snowmelt in surface depressions, which allow greater evapotranspiration. They found that partial coupling of GCM runoff output with a simple land surface hydrological model corrected volume and phase deficiencies of the GCM simulation.

Although some conventional hydrology models may have more detailed cold-regions process representations, they are generally applicable to small regions and suffer from the paucity of observational data over high latitude land areas with which to force these models. Typical data requirements for hydrology models include the downward components of the water and energy budgets at the land surface, namely precipitation, shortwave and longwave radiation, air temperature, humidity, and wind speed. Land surface characteristics, including soil, topography and vegetation are also needed. The single most important variable for streamflow prediction is precipitation.

The scarcity of precipitation data and the inconsistency of gauge observations due to variation in gauge catch efficiencies in northern regions have led some researchers to perform climatological studies using precipitation predicted by retrospective runs of numerical weather prediction models, so-called reanalysis data fields [11, 12, 13, 14, 15, 16]. Three major modeling centers have completed multi-decade reanalysis runs using a fixed version of their respective forecast models; the European Center for Medium Range Weather Forecasting (ECMWF), the (U.S.) National Centers for Environmental Prediction (NCEP), and the NASA Data Assimilation Office (DAO). Unfortunately, the mean climates of the reanalysis models are inextricably linked to not only the accuracy of the physical parameterizations, but also to the data assimilation systems. In areas of sparse data such as the Arctic, the assimilation system must rely heavily on the model-simulated fields especially for surface variables [17], therefore the process of updating the model state to match observations is not constrained to a water or energy balance and can result in physically unrealistic fields (see Section 3.1). In particular, the NCEP reanalysis tends to underpredict precipitation over the Atlantic Ocean and overpredict precipitation over land and the central Arctic Ocean, particularly during summer [11, 13, 15, 18]. These biases can strongly affect water (and energy) budgets that use reanalysis

fields for some or all of the budget components, and the reanalysis data are unfortunately not a panacea for the sparseness of surface observations over the Arctic land areas.

The opportunities and limitations presented by observational and model-derived data sets for understanding the freshwater balance of the Arctic basin are reviewed in this paper, from a land surface hydrological perspective. The paper is organized into three sections. The first describes the hydroclimatic zones within the Arctic drainage basin and the cold-regions hydrologic processes that dominate the major Arctic river systems. In the second section, the space-time variability of these processes is examined through large-scale surface water and energy budget analyses. Finally, in the third section, the ability of a state-of-art macroscale hydrologic model to reproduce the observed regime is explored for the Mackenzie and Ob River basins.

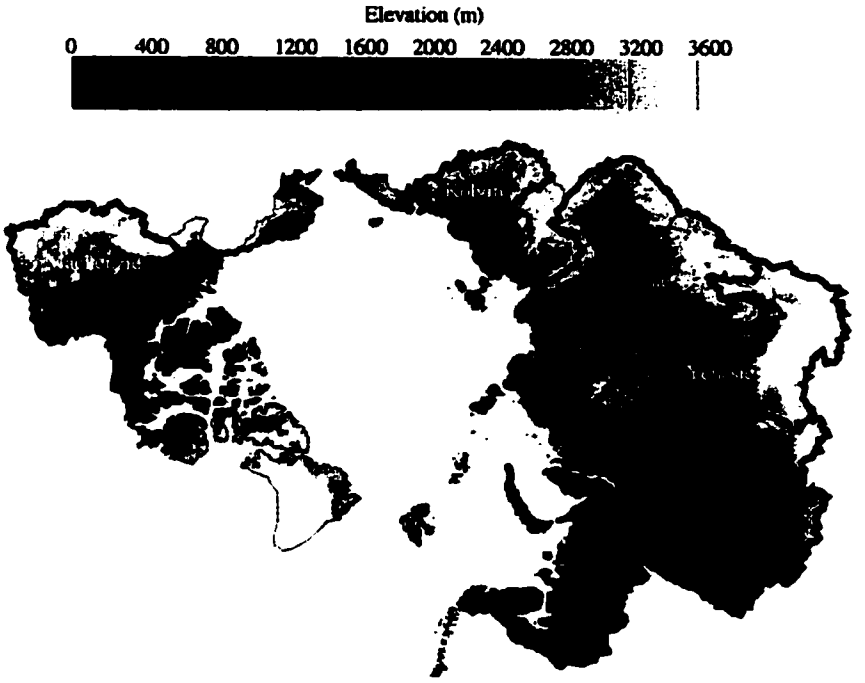

Figure 1. Digital elevation model of the Arctic drainage basin.

2. Background

Runoff from high-latitude rivers represents a significant source of freshwater to the Arctic Ocean. The temporal and spatial variability of fresh water fluxes to the Arctic Ocean are controlled not only by space-time variability in precipitation and evapotranspiration, but by the storage of significant portions of annual precipitation as snow, and in lake and wetlands. The influence of seasonally frozen ground also affects

the interaction of surface and subsurface runoff storage with streamflow production. Much of the available data that would allow examination of processes such as snow accumulation and ablation is from small-scale field observations. However, by combining observations from various field studies, a picture of trends at the large-scale begins to emerge.

2.1. REGIONAL CHARACTERISTICS

The Arctic drainage basin, defined here as the land area draining to the Arctic Ocean, spans 37° of latitude, from 46° N in the Yenisei Basin to 83° N at the tip of Greenland (Figure 1), and several distinct vegetation and climate zones (Figure 2). For simplicity, we will adopt the climate zone definition of Woo and Winter [19] in which arctic refers to those areas underlain by continuous permafrost; sub-arctic is defined by the limit of discontinuous permafrost and the north temperate zone includes the zone of seasonally frozen ground (see Figure 3). The entire Arctic drainage basin lies within one of these three zones.

Figure 2. General vegetation classes of the Arctic drainage basin (adapted from the USGS Global Land Cover Characterization [20]).

All three climate zones contain multiple landforms and vegetation types [20], as shown in Figures 2 and 3. The four major regions will be described here: boreal forest, interior continental grass and cropland, arctic tundra, and maritime alpine. The largest vegetation class in both the Eurasian and North American portions of the Arctic

drainage basin is boreal forest (or taiga), composed of mixed cool coniferous and deciduous forest. In the south-central Ob and Mackenzie basins, the boreal forest transitions into steppe grassland and cropland at the southern extremes. Extensive swamp and marshland within the low altitude taiga forest dominate the central lowlands of the Ob River basin. There is a lesser, but still significant, distribution of wetlands throughout the Lena and Kolyma basins in Eurasia and to a similar extent in the Mackenzie basin in North America. There are negligible wetlands in the Pechora and Yenisei basins.

True arctic tundra represents a relatively small portion of the land area of the Arctic basin, primarily consisting of the Canadian Archipelago and the coastal plains of both North America and Eurasia. Tundra vegetation tends to transition northward from wooded and shrub tundra to low-lying moss and lichens. Wetlands and thaw ponds dominate the low-topography coastal plain.

Both the Eurasian and the North American portions of the Arctic basin contain alpine zones. In the Mackenzie Basin, this includes a moderate maritime zone of coastal and alpine forest along the Rocky Mountains, as well as high elevation alpine tundra. Pockets of alpine tundra are also located in the Ural Mountains in the western Ob basin and in the Altai Mountains and Aldan Plateau in the headwaters of the Lena and Yenisei Rivers.

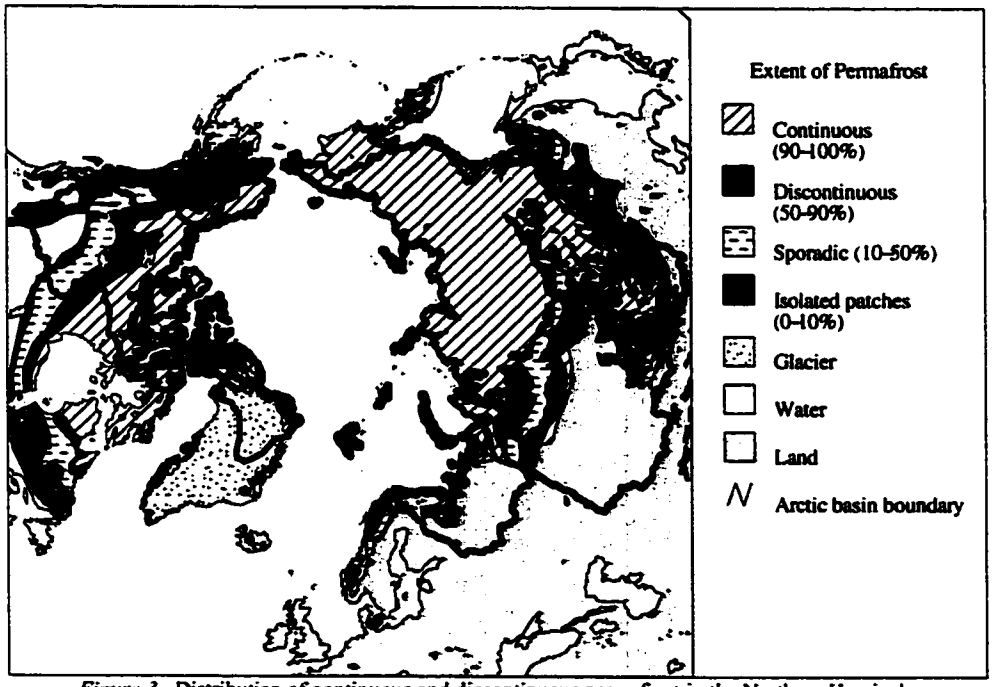

Figure 3. Distribution of continuous and discontinuous permafrost in the Northern Hemisphere (adapted from Circum-Arctic map of permafrost and ground-ice conditions [27])

2.2. PRECIPITATION AND EVAPORATION

The spatial and temporal distribution of runoff source areas can be explored through analysis of the land surface and atmospheric water balances. The distribution of atmospheric convergence (which, in the long term, must be balanced by precipitation, P less evapotranspiration, E) can be calculated from a network of radiosonde observations (e.g., as a line integral) or as the spatial integral of the convergence field produced from atmospheric model analysis (e.g., resulting from data assimilation). By using atmospheric soundings, Serreze et al. [21] found that specific humidity generally decreases poleward for all seasons and precipitable water decreases poleward for winter, spring, and autumn on the Atlantic side of the Arctic. Precipitable water ranged from winter lows of 1.8 and 3.8 mm (for 80-90° N and 65-70° N, respectively) to summer maxima of 12.5 and 18.2 mm [19]. However, there was large spatial variability independent of latitude. Land surface water balance calculations from experimental sites also show a decrease in P-E poleward, as summarized in Table 1. Due to the greater availability of data, this table is biased towards North American trends. Although moisture availability decreases with latitude, there is still a positive net flux of atmospheric fresh water towards the polar region.

TABLE 1. Experimental measurements of P-E

Location	Latitude	Longitude	P-E (mm)	Reference
Imnavait Creek	68°30' N	149°15' W	170	[22]
Siksik Creek	68°45' N	133°30' W	90	[23]
Western Siberia	-	-	311	[24]
Marmot Creek	50°57' N	115°10' W	460	[25]

High-latitude vapor convergence reaches a maximum over the pole in late summer, coinciding with a minimum over the Mackenzie basin which sometimes becomes negative due to proportionately larger evapotranspiration over the Mackenzie River as compared with the central Arctic [26]. An 18-year mean of convergence calculated from radiosonde data implies a mean evaporative fraction (evapotranspiration/precipitation) over the Mackenzie River of 0.26 [26]. This contrasts with water balance estimates, which suggest a much larger evaporative fraction (see Section 2.3).

The temporal variability of vapor convergence correlates well with both precipitation and discharge, but only explains about 50 % of the variability in discharge [26]. Bjornsson [28] found that spring runoff in the Mackenzie River is highly correlated with total precipitation from fall to spring. An analysis of interannual variability of runoff from the 15 largest rivers draining to the Arctic from 1950-1990 indicates that a maximum of mean annual total river runoff occurred in the 1970s. However, the maximum runoff rates for rivers of the Kara, East-Siberian and Beaufort Seas (Ob, Yenisei, Kolyma and Mackenzie Rivers, among others) were accompanied by minimum values in land surface runoff to the Barents and Laptev Seas (Pechora and Lena Rivers, among others) [29]. Based on ocean salinity data, discharge into the western Arctic Ocean is more variable than discharge into the eastern Arctic Ocean [31]. Coefficients of variation (C_v, standard deviation divided by mean) for the large river basins are on the order of 0.08 to 0.28 [2, 31]. In particular, the Yenisei, Lena,

Mackenzie and Ob Rivers have C_v's of 0.08, 0.12, 0.10 and 0.15 respectively [4]. A more detailed discussion of the variability of these rivers is provided in [4].

2.3. RUNOFF RESPONSE

The seasonal cycle of runoff from northern rivers is strongly controlled by the storage of precipitation as snow during all but the summer season. Large northern rivers tend to have a relatively short period (2 to 4 months) of sustained high flow in late spring/early summer followed by an extended seasonal dry down [31]. Flow may stop completely during the winter. In catchments of up to 100-200 km^2, the annual maximum runoff rate is often associated with rainfall events, because over such small areas the rainfall rate may exceed the maximum rate of snowmelt [32]. With increasing catchment area, this effect is reduced due to the relatively small scale of high-intensity rainfall. Additionally, the likelihood of rain floods exceeding snow floods decreases with latitude, due to the progressive reduction in the length of the rain season [32]. Interannual differences in the runoff response of northern rivers are in large part due to changes in snow accumulation, but spatial differences are often controlled by the distribution of permafrost, frozen ground, lakes and wetlands. The effects of these mechanisms are discussed below.

2.3.1. Permafrost and frozen ground

As shown in Figure 3, the entire Arctic drainage basin is underlain by seasonally frozen ground and permafrost (soils in which the water content is perennially frozen). This results in similar early spring surface water responses for the entire basin. Although meltwater percolation may raise soil surface temperatures to 0° C, soils usually remain frozen until the snow cover is depleted [19, 33]. The presence of frozen water limits infiltration into the soil, and decreases the melt water storage capacity of the soils. Several researchers have found that the upward flux of water vapor from the soil throughout the winter increases the ice-free void space at the soil surface by winter's end, allowing some infiltration of meltwater [33, 34, 35]. However, the initial meltwater refreezes in the soil, completely filling void spaces and preventing any further infiltration [33]. Therefore, the dominance of surface flow is typical of both permafrost and seasonally frozen regimes during snowmelt.

In contrast to seasonally frozen soil, the presence of permafrost continues to inhibit ground water recharge and movement, and restricts plant growth throughout the growing season [36]. All surface and subsurface groundwater interaction will occur in the active layer, the top 1 to 3 m of soil that thaws annually [36]. The uneven thawing of the active layer in response to radiation exposure, meltwater infiltration, and other heat transfer processes results in changes to basin storage capacity which may not reflect the overlying topography [33]. As the depth of thaw increases, non-saturated areas may develop, however the presence of the frost table continues to severely restrict the storage capacity of permafrost soils, resulting in a higher proportion of annual surface runoff [33, 34].

Untersteiner [36] suggested that differences in the amplitude of the seasonal hydrograph of major north flowing rivers might be due in part to the presence of permafrost. Runoff ratios (annual discharge/precipitation) reported for some of the largest Arctic rivers are summarized in Table 2 [10, 16, 31]. Presumably, the different

ratios reported by the three studies result from using different sources of precipitation data. In general, the Yenisei, Lena and Kolyma Rivers tend to have the highest runoff ratios. These rivers are underlain by continuous or discontinuous permafrost for 88% (Yenisei River) to 100% (Kolyma and Lena Rivers) of their length. In contrast, the Ob and Mackenzie rivers traverse permafrost for 27 and 83% of their length [36]. The Pechora River is an anomaly as it traverses discontinuous permafrost for only 50% of its length but it is also characterized by fewer wetlands than the other major north flowing rivers.

TABLE 2. Runoff Ratios of Major Arctic Rivers

River	Oki et al. [16]	Kuhl and Miller [10]	Vuglinsky [31]
Yenisei	0.52	0.54	0.47
Kolyma	0.53	0.39	0.49
Lena	0.53	0.61	0.46
Ob	0.29	0.33	0.25
Mackenzie	0.46	0.41	0.30
Pechora	0.73	ND	0.58
Severnaya Dvina	ND	0.60	0.43

Notes: Kuhl and Miller [10] used precipitation from Shea [37]. Oki et al. [16] used precipitation from [38]. The source of precipitation for Vuglinsky [31] is unknown. ND indicates no data was provided for that river

2.3.2. Lakes and wetlands

Seasonal variability is dramatically different between large Eurasian and North American rivers [31, 39]. Eurasian rivers tend to have a short period (2-3 months) of sustained high flow in late spring and early summer that exceeds the mean low flow discharge by 7 to 10 times [31], although exceedances as high as 40 times have been recorded in the Yenisei and Lena Rivers [39]. North American rivers tend to have an extended seasonal cycle, with one to two more months of sustained high flow. Mean high flow discharge exceeds mean low flow discharge by factors of 4 to 5 in North American rivers [31, 39]. This attenuation is generally thought to be due to storage in lakes and wetlands, which cover a much larger portion of North American as opposed to Eurasian river basins.

Evaporation from small lakes during the ice-free period often exceeds summer and even annual precipitation [40, 41, 42]. This is also the case on the Alaskan coastal plane where Rovansek et al. [41] observed that snowmelt runoff is delayed until the entire storage of ponds and wetlands is refilled.

Wetlands are areas having a water table near or above the mineral soil for most of the thaw season [43]. According to Church [44], northern lakes and wetlands create a muskeg regime, in which high flows are attenuated by the absorption capacity of the muskeg vegetation and resistance to flow by surface conditions. However, the storage capacity of wetlands is often limited by frozen ground [35]. Therefore, flow attenuation by wetlands is usually highest for summer rainfall after the peat is thawed [35, 45].

High ice content wetland soils are slow to thaw due to the large energy inputs required to melt the ice. Meltwater infiltration is delayed longer, thus the presence of frozen wetlands can actually accentuate the surface water response of frozen ground [19, 35, 46]. These wetlands are often poorly drained, remaining saturated through the summer and refreezing with a high ice content the next winter [46]. In the north

temperate zone, the feedback between wetlands and frozen ground can actually be reversed as winter flooding of wetlands can prevent or limit frost formation [19].

The presence of thousands of small thaw lakes on the coastal plain and river delta regions can also have a profound impact on heat and energy exchange. Conductive heat flow from a lake system can serve as a significant source of heat flow to the atmosphere, maintaining locally moderate temperatures [47, 48].

2.4. SNOW HYDROLOGY

Snow cover accumulation, redistribution and ablation dominate the land surface hydrology of the Arctic. Although rain may account for a fairly large fraction of the annual precipitation, even at high latitude, snow is proportionately more important to runoff due to low rates of winter evapotranspiration and the timing of meltwater release. Snow accumulation and ablation processes are somewhat different for each of the four major Arctic land classifications (Section 2.1) and are discussed separately.

The snow-covered period extends from 6 to 10 months in the tundra zone. Spring melt releases between 35-60% of annual precipitation [49]. Negligible mid-winter melt occurs and winter sublimation in the tundra zone is generally energy limited [22, 50, 51]. However, sublimation during blowing snow events can represent a significant loss of snow over the winter [22, 50]. Pomeroy et al. [52] found that 28% of annual snowfall sublimated from tundra surfaces in a low Arctic catchment in northwestern Canada. The initiation and movement of blowing snow depends on wind velocity and duration, vegetation and snow structure. Therefore, the likelihood of transport decreases with increasing air temperature and snow age [53, 54]. The absence of tall vegetation in moss-lichen tundra regions and the presence of a dry snowpack facilitates significant wind redistribution of snow, creating a fairly consistent snow spatial structure with respect to topography [22, 52, 55, 56, 57]. Despite this wind redistribution, snow cover is nearly continuous at the start of melt. Initially, melt energy is dominated by net radiation, with sensible and latent heat fluxes contributing to a lesser degree [49]. As melt progresses, faster melt will occur in locally thinner snowpacks, in part due to lower albedo, longwave emittance from protruding plants and increased absorption of shortwave radiation penetrating to the underlying surface [22, 49]. Longwave radiation and sensible heat from the snow-free ground warms the overlying air and accelerates the melting of surrounding snow, resulting in large spatial variation in snowmelt rates [22, 49].

During snowmelt, evapotranspiration is bounded by the vapor pressure gradient between the air and the snow surface rather than net radiation [50, 51]. During melt in the tundra region of Spitsbergen (Norway), Takeuchi et al. [58] found using a weighing lysimeter and hygrothermometer that an increase in vapor pressure of the air actually favors condensation. Kane et al. [50] found evapotranspiration during snowmelt of 20 to 47 mm (20 to 34% of average snowpack) in a small Alaskan Arctic catchment.

Although multiple freeze-thaw events are possible in the interior plains zone [59], annual volumetric transport during blowing snow events in the Canadian Prairies and the Eurasian steppe zone represents between 15 to 40% of annual snowfall [60, 61], and are typically a much larger term in the winter water budget. Significant sublimation can occur during blowing snow events [62, 63, 64]. The rate of sublimation is largely

dependent on air temperature, humidity and net radiation [63]. The areas of maximum water loss for snow during the cold season were greatest in the north central coastal regions of Russia, the area with the greatest number of blowing snow events [54, 65]. The annual average sublimation across Russia from blowing snow events was between 2.5 to 10 mm with a maximum of 60 mm on the Kamchatka Peninsula [65]. Partial sheltering from the wind by open forest stands in the forest steppe/steppe transition zone in European Russia results in greater average accumulation [66].

Snowmelt in interior Canada and eastern Russia and Siberia generally begins in mid-April and proceeds rapidly often lasting only 1 to 2 weeks. Melt rate is dominated by solar radiation, with turbulent heat exchange playing a lesser role [67]. Evaporation during melt in the forest-steppe to steppe region of northwestern European Russia was estimated to be 15 to 60 mm/yr, increasing to 35 to 90 mm/yr in the forest region [68]. Are and Petropavlovskaya [67] found that the highest evaporation rates preceded the initiation of melt in the steppe region of central Yakutia, Russia.

The boreal zone contains a mosaic of vegetation varying from closed coniferous canopies, through sparsely vegetated clearings and numerous open lakes [69]. The snow season lasts for approximately 6 months, with melt occurring in late April [69, 70]. Mid-winter melt is rare. Solar fluxes dominate melt in the northern extent of the boreal forest, but sensible heat and longwave radiation increase in importance to the south [70].

Interception of snow by boreal forest canopies can store up to 60% of the cumulative winter snowfall [61]. Increased exposure and turbulent transfer can result in sublimation losses from intercepted snow of between 3 to 40% of annual snowfall [68, 71]. The canopy interception capacity is dependent on species, leaf area and snow load, with decreasing interception efficiency for increasing snow load [61, 72].

Vegetation of the alpine zone typically consists of dense conifers extending to the treeline, where shrubs and grasses give way to talus slope and bare rock [25]. Therefore, the alpine zone contains elements of all of the preceding regions. However, it is further characterized by an increase in snow accumulation with elevation due to orographic enhancement of precipitation and decreasing temperature with increasing elevation. The gradient in snow depth increases throughout the snow season, due to continued snowfall at the highest elevations and differential melting in the valleys. The high elevation snowpack generally melts by late July at the southernmost extremes of the Arctic basin [25]. Along the eastern slope of the Rocky Mountains, snowmelt is enhanced by the occurrence of chinooks, strong winds from the south accompanied by elevated temperatures. Golding [73] found potential evaporation rates from the snow of 1.2 to 2 mm/day during chinooks, with a maximum rate of 10.4 mm/day. Snowmelt during the chinooks ranged from 0.4 to 1.6 mm/day [73].

It is unclear how melt from a spatially varying snow pack, which primarily has been studied at small scales, affects runoff from medium to large Arctic rivers. Variability in snow cover extent is important because of the effect on albedo, the area contributing meltwater during spring melt, and its effect on the length of the melt season. However, the initiation of melt in large basins can vary by a month or more from southern headwaters to the mouth due to the difference in latitude alone. Given this large temporal range in meltwater production, differences in runoff rates on the order of several days to weeks due to small-scale snow distribution may be unimportant. At

present, a good understanding of the relative influence of within-basin and between-basin variability in controlling runoff in the major Arctic basins is lacking.

3. Observations of Northern Freshwater Components

The literature reviewed in Section 2 illustrates the unique hydrologic features of the Arctic drainage basin. In Section 3, we explore how such features interact and influence large-scale hydroclimatological trends and the extent to which they are reflected in global data sets essential to hydrologic model forcing and validation. Section 3 utilizes several data sets, as follows:

- **5-minute digital elevation model (DEM):** ETOPO5 DEM (5 minute) from the Earth Resources Observation Systems (EROS) Distributed Active Archive Center (DAAC).
- **2-degree gridded precipitation:** daily station data from Schnur and Lettenmaier [74] adjusted for systematic error using Global Precipitation Climatology Project (GPCP) version 1A gauge precipitation data set [75].
- **Analysis increments and convergence fields:** output from the Goddard Earth Observing System (GEOS-1) data assimilation system of the NASA DAO reanalysis project.
- **Small basin discharge:** mean annual flow computed from the Arctic Runoff Data Base (ARDB) maintained by the GRDC for 100 basins smaller than 7,000 km^2.
- **Spatially distributed basins:** derived Geographic Information System (GIS) dataset of 43 basins in the ARDB delineated from a 30-arcsecond DEM.
- **Weekly snow extent:** provided by the Earth Observing System (EOS) DAAC at the National Snow and Ice Data Center (NSIDC), University of Colorado at Boulder.

3.1. SPATIAL VARIABILITY

The Arctic drainage basin (Figure 1) was delineated from a 5-minute DEM of the world (ETOPO5 data set), obtained from the EROS Data Center DAAC. As shown in Figure 4, 60% of the drainage area lies south of 65° N and there is a higher proportion of area at lower latitudes in Eurasia than in North America. The distribution of land area is critical because latitude and topography strongly influence the land surface hydrology through (a) the seasonal cycle of solar insolation, (b) orographic effects on precipitation, and (c) the distribution of vegetation.

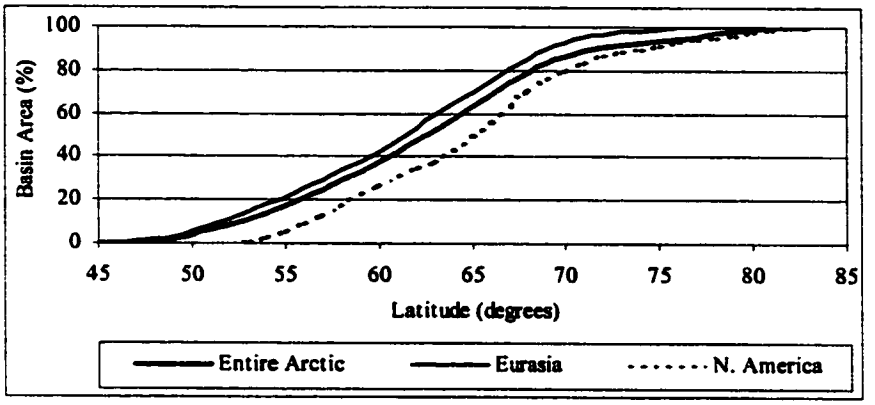

Figure 4. Distribution of Arctic basin area versus latitude.

Figures 5 (Eurasia) and 6 (North America) show the distribution of precipitation, evapotranspiration and runoff with latitude derived from three independent sources. The gridded station precipitation data for 1979 to 1993 from [74] were not corrected for gauge catch deficiencies and therefore probably underestimate precipitation, especially in the cold season. To compensate for this underadjustment, the precipitation data were scaled to match the monthly means from the GPCP station data set. This dataset was corrected (by GPCP) for systematic errors following Legates [76].

We computed evapotranspiration from an atmospheric moisture balance using the gridded precipitation and convergence derived from the GEOS-1 data assimilation system of the NASA DAO reanalysis project [77]. Calculated values for convergence were adjusted by the reported GCM analysis increment, which essentially is the amount of water added to, or extracted from, the atmosphere due to the updating process effected by the data assimilation procedure. The influence of the analysis increment is discussed further later in this section. Runoff from small basins was derived using the mean annual flow from 100 basins in the ARDB data set with drainage areas smaller than 7,000 km^2. The emphasis on smaller catchments facilitated assignment of discharges to the latitude of the gauge locations (which were known), rather than the basin centurions (which were not). The random nature of gauge locations means that limited or no data are available for some latitude bands. In addition, updating of the ARDB is dependent on the response of member countries. Therefore, it was impossible to generate values of mean annual discharge for a consistent time period. In order to maximize the available record, mean annual flow throughout this paper was calculated from the entire record of each basin, which may vary from 10 to 100 years.

Figure 5 shows that in Eurasia, precipitation tends to increase with latitude up to 60-62° N above that it begins to decrease. In contrast, North American precipitation begins to decrease with latitude north of 54-56° N. In general, precipitation exceeds evapotranspiration in North America, but for latitudes less than about 62° N in Eurasia, zonally average P-E is negative. Surprisingly, there is no clear pattern in discharge distribution with latitude. This is partially due to statistical problems associated with small sample sizes and the difficulty of assigning discharge to single latitude bins. In

addition, no discharge data were available north of 73° N (as nearly 95% of the gauged area falls south of 65° N as shown in Figure 7a). The distribution of discharge stations used in Figures 5 and 6, in comparison to the Arctic basin distribution is also shown in Figure 7b.

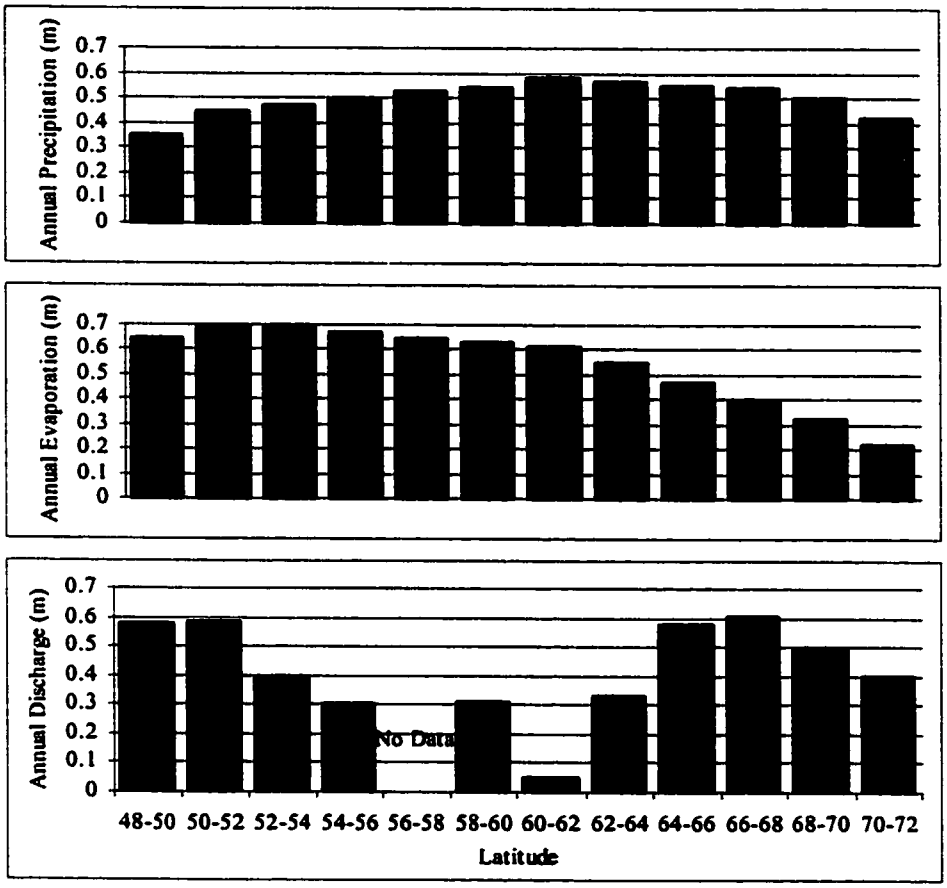

Figure 5. Precipitation, evapotranspiration and discharge versus latitude for Eurasia

Spatial evapotranspiration trends were further analyzed by comparing the evapotranspiration derived from the GEOS-1 data product with the spatial distribution of evapotranspiration derived from basin water balances (Figure 8). Evapotranspiration was calculated as the residual of precipitation and runoff for the 43 spatially distributed ARDB basins delineated from 30-arcsecond DEMs. Mean annual runoff for each of the delineated basins was distributed evenly (as a depth) over the basin area and gridded at a 2° resolution. The runoff depth was subtracted from the precipitation to obtain a gridded average annual evapotranspiration. These same basins are used in Figures 8, 9, 10 and 12 to calculate and display basin average variables.

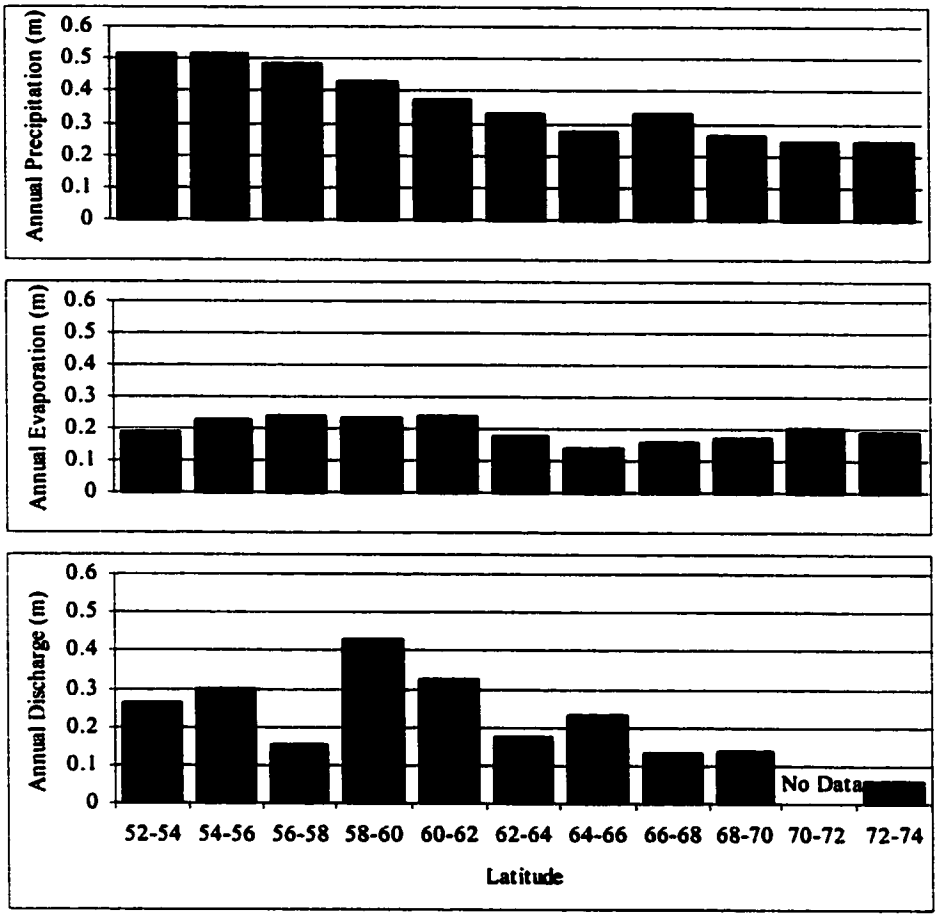

Figure 6. Precipitation, evapotranspiration and discharge versus latitude for North America

The two estimates of evapotranspiration (Figure 8) are roughly equivalent over North America. However, the GEOS-1 derived estimates of evapotranspiration over Eurasia are much higher than those derived from the water balance, particularly over the Ob basin where the estimates differ by several hundred millimeters. These discrepancies have to do in part with the analysis increment of the DAO reanalysis. As described by Molod et al. [17], "The analysis increments (the difference between the model first guess and the analyzed state) are normalized and included as a constant forcing term during model reintegration over the six-hour time span centered on the analysis time". The analysis increment is generally negative for most of the higher latitudes and is often of the same order of magnitude as the other terms. Because it is negative, it acts as an atmospheric sink and extra evapotranspiration is generated by GEOS-1 to fulfill this sink. Calculating evapotranspiration as the residual of precipitation minus divergence plus the analysis increment generates high values for

evapotranspiration, by essentially assigning the entire error term to the evapotranspiration.

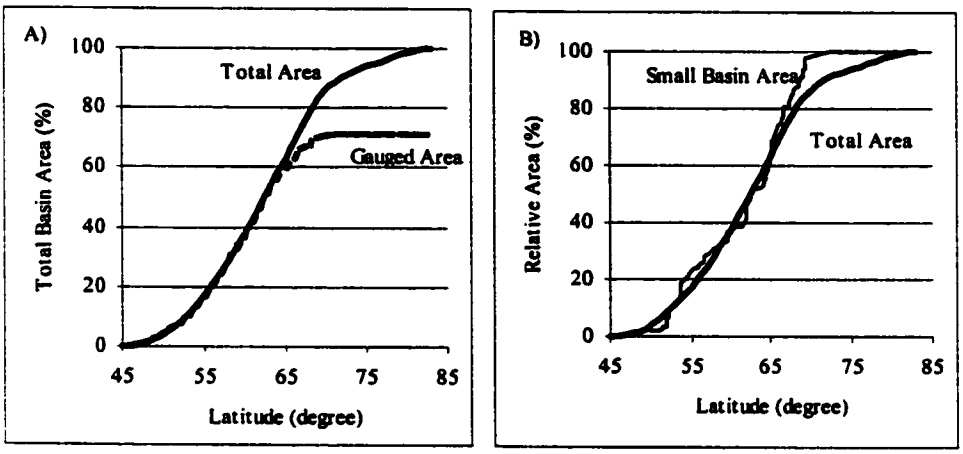

Figure 7. Distribution of A) gauged area versus latitude as a percentage of total basin area and B) area of small basins relative to total small basin area.

The relationship of discharge in the small basins shown in Figures 5 and 6 to geographic factors is further complicated by the effects of topography on the spatial distribution of precipitation. Precipitation maxima for the Arctic drainage basin are over the Rocky Mountains in Canada and the Ural Mountains in western Russia (Figure 9a), creating a strong west-east gradient in precipitation and evaporation in these basins, which somewhat confounds the north-south trend shown in Figures 5 and 6. (See the Hydrological Atlas of Canada [78] for a more complete discussion of the maritime to continental transition in the Mackenzie basin). The distribution of mean annual discharge (Figure 9b) coincides closely with the distribution of precipitation. Relatively high discharge occurs in the Pechora basin, with low discharge in the southern Yenisei basin. Higher discharge occurs in the mountainous areas of the Mackenzie River, although the response relative to precipitation is not as extreme as in the Eurasian rivers, as illustrated by the runoff ratio (annual discharge/precipitation) in Figure 9c. The consistency of the runoff ratio throughout Eurasia confirms the control of precipitation on the spatial variability of runoff generation, notwithstanding a possible increasing northward trend in runoff generation due to reduced evapotranspiration at high latitude (Figure 5).

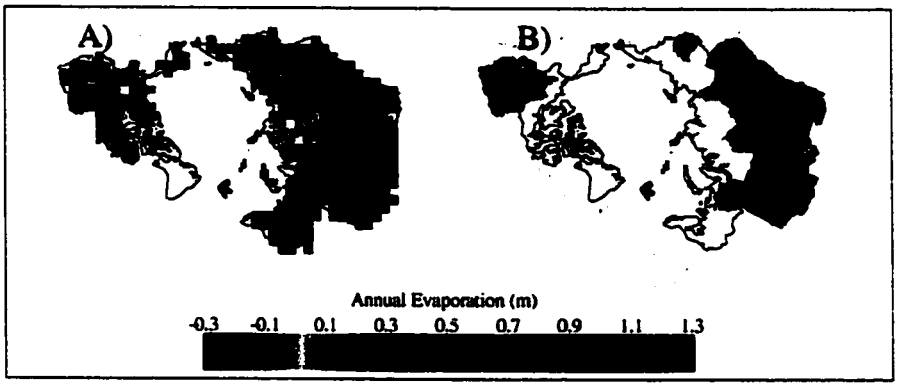

Figure 8. Average annual evaporation computed from A) atmospheric water balance and B) basin water balance

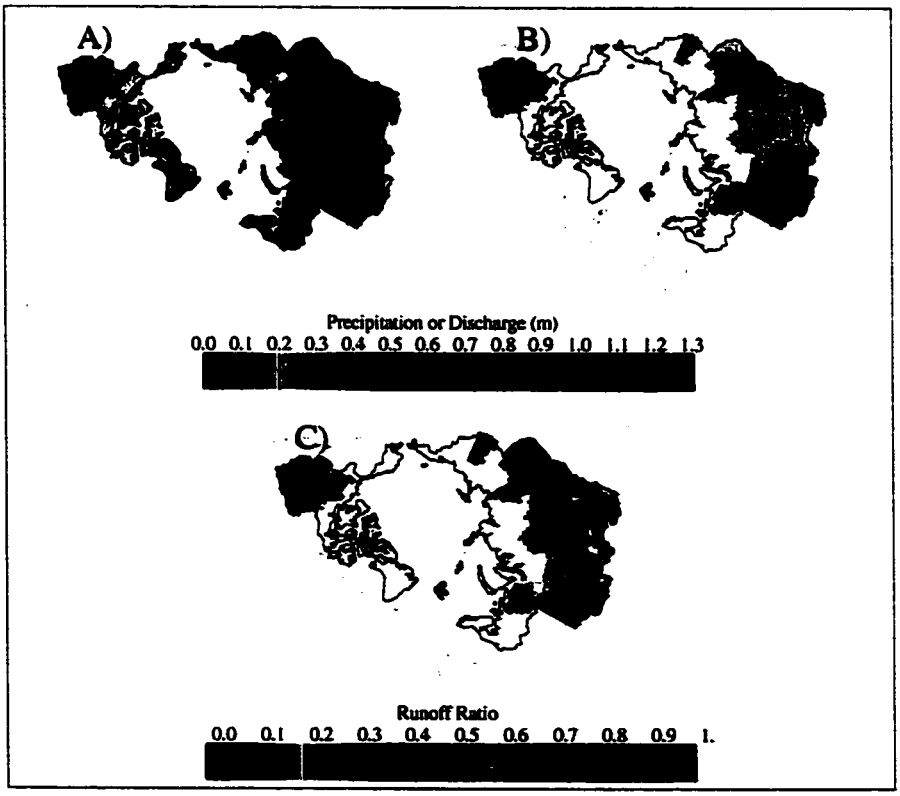

Figure 9. A) Average annual precipitation (1971-1994), B) Average annual discharge (variable records), C) Average annual runoff ratio

3.2. TEMPORAL VARIABILITY

As shown in the previous section, the variability in the discharge of the spatially distributed basins is strongly correlated with variations in latitude and elevation. There is also a large component of interseasonal variability that is associated primarily with latitude and catchment response to snow accumulation and melt. As noted in Section 2.1, Eurasian basins generally are characterized by a very rapid snowmelt response followed by 6 to 7 months of low flow. North American rivers tend to have a lengthier period of seasonal high flow, followed by a shorter period of low flow. This is reflected in the average ratio of minimum monthly discharge/maximum monthly discharge (Figure 10a). The data show quite a bit of scatter, but in general, Eurasian basins have a larger range between maximum and minimum annual discharge (smaller values of min/max discharge).

In Figure 10b the ratio of precipitation occurring as snow to annual runoff is shown. Snow was defined as daily precipitation occurring when the average daily air temperature was below 0° C. Figure 10b is influenced by both the percentage of precipitation which falls as snow (controlled primarily by latitude) and the percentage of meltwater subject to evapotranspiration (controlled by vapor pressure gradient and net radiation) [50, 51]. Although it is somewhat difficult to distinguish from basinwide averages, there appears to be a slight increasing northward trend in Figure 8b due to the increasing fraction of precipitation occurring as snow. In general, the highest (Ob River) and lowest (Lena and Kolyma Rivers) values in Figure 10b correspond with areas of high and low precipitation (Figure 9a), respectively. This is presumably because the higher vapor pressure in the Ob basin suppresses evapotranspiration during melt, yielding a higher percentage of runoff from the snowpack.

Variability of snow extent also plays a large part in determining interannual variability of runoff response. Figure 11 shows the minimum, maximum and average number of days with snow cover throughout the Arctic basin from 1971-1995 derived from snow extent data provided by the EOS DAAC. The largest differences can be seen in coastal areas and the mountainous regions of Asia and North America. Figure 12 illustrates the relationship between snow and discharge interannual variability by plotting the coefficient of variation of discharge versus the average range (max. – min.) of snow covered days from 1971-1994. The number of snow covered days was computed as a spatial average for each of the 43 spatially distributed basins. There is no clear relationship between discharge variability and variability in the annual length of snow cover for basins larger than 100,000 km^2 (Figure 12a). There is a decrease in discharge variability with increasing variation in snow cover, albeit with more scatter, for smaller basins (Figure 12b). This may reflect a greater sensitivity to rainfall variability rather than snow in smaller basins, due to the relatively small-scale of high-intensity rainfall.

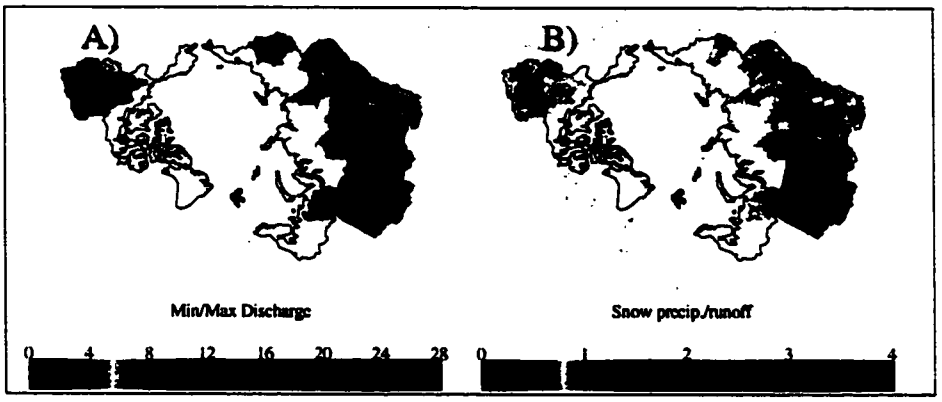

Figure 10. A) Mean ratio of minimum monthly discharge to maximum monthly discharge, and B) Ratio of snow precipitation to runoff

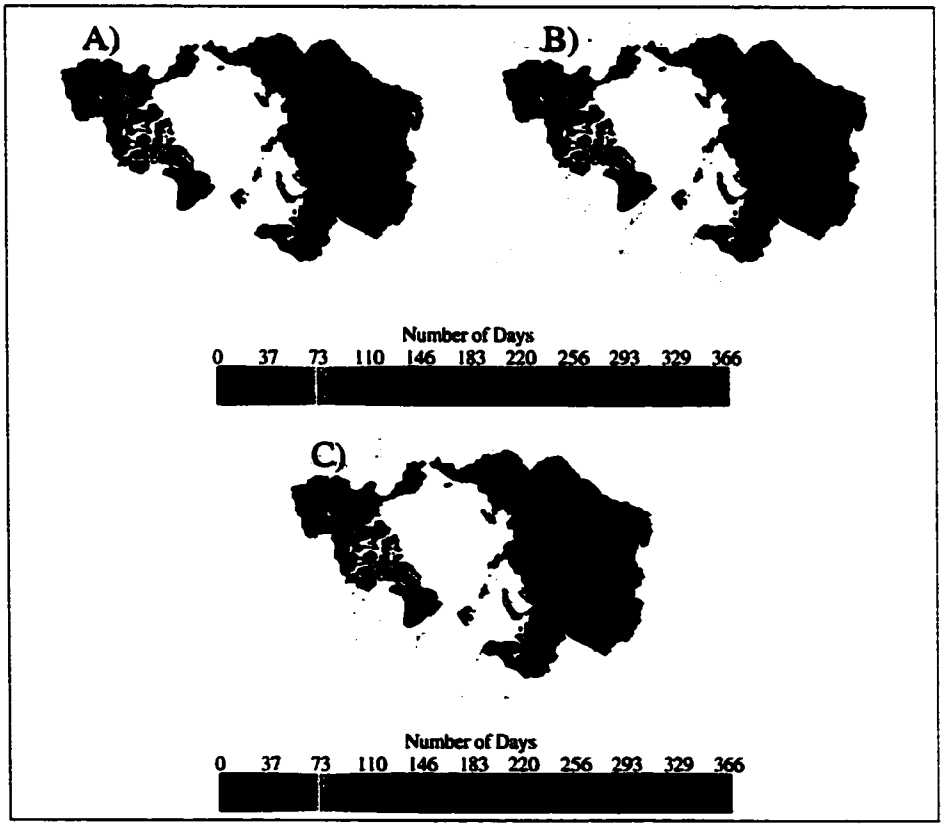

Figure 11. Number of days with snowcover (1971 –1994) A) Minimum B) Average and C) Maximum

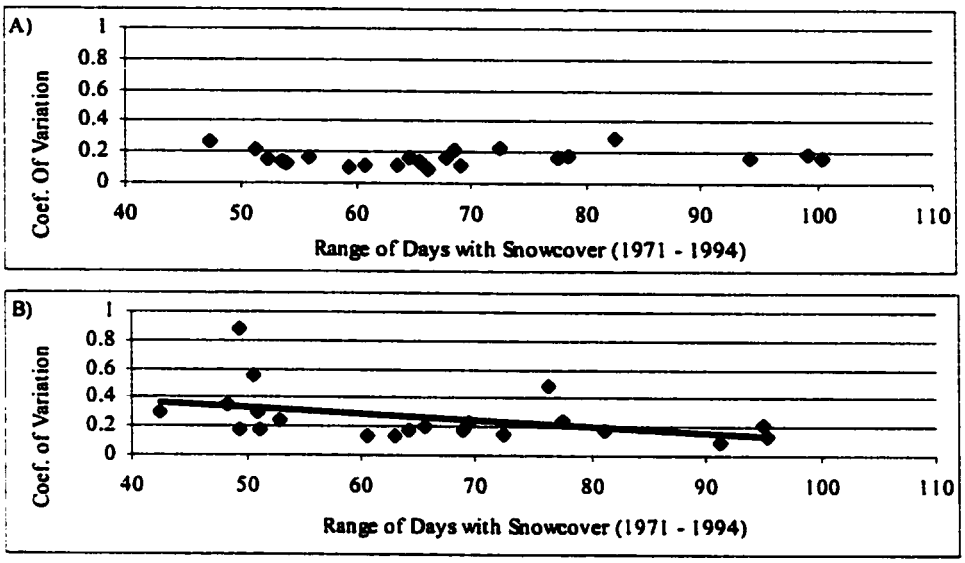

Figure 12. Coefficient of variation of discharge versus the average range of snow covered days: A) basins larger than 100,000 km^2, B) basins smaller than 100,000 km^2

4. Hydrological Modeling

The exploratory data analysis of Section 3, taken together with a knowledge of fundamental northern hydrologic regimes, as reviewed in Section 2, suggests that the most important controls on runoff of medium to large Arctic rivers are latitude, orography and surface storage. However, there remains considerable variability between catchments that could be controlled by a number of possible mechanisms. For instance, it is not clear from the data analysis if discharge variability is more a function of rain than of snow precipitation and how that difference varies over the region. Likewise, the effects of spatial trends in precipitation and albedo on snowcover and runoff generation are not well understood. Such questions further complicate the estimation of freshwater fluxes from the ungauged portion of the Arctic basin. To examine the potential of hydrologic models as diagnostic tools in ungauged portions of the Arctic drainage basins, a macroscale hydrological model, the Variable Infiltration Capacity (VIC) model [79], [80] was applied to the Mackenzie and Ob River basins.

4.1. MODEL DESCRIPTION

4.1.1. VIC Model

The VIC model is a grid-based Soil-Vegetation-Atmosphere Transfer (SVAT) scheme designed both for inclusion in GCMs, and for use as a stand-alone macroscale hydrological model [79, 80]. The model has two modes of operation: a full water and

energy balance mode, in which the surface energy budget is closed by iterating for surface temperature, and a water balance mode, in which surface temperature is assumed to equal air temperature. The water balance mode was used for this application. The model partitions the soil column into multiple soil layers, which allows representation of the rapid dynamics of soil moisture movement during storm events in the upper root zones, and the slower deep interstorm response in the bottom layer. Each grid cell is assigned a partial coverage of a user-specified number of vegetation or bare soil land-use types. The parameters associated with each land-use type are time-varying leaf area index (LAI), the relative fraction of roots in each soil layer, canopy resistance, minimum stomatal resistance, roughness and displacement length. A more complete description of model processes can be found in [79] and [80].

A recent addition to the VIC model incorporates a two-layer energy balance snow model [81, 82]. The model employs two snow layers of variable thickness. The thin surface layer is used to solve the surface energy balance, while the bottom or pack layer is used to simulate deeper snowpacks. The model accounts for the energy advected by rain, throughfall or drip, as well as net radiation and sensible and latent heat. Snow interception by the overstory, if present, is calculated as a function of LAI. Intercepted snow can be removed from the canopy through snow melt, sublimation and mass release. The model does not account for redistribution or sublimation due to blowing snow.

The effects of topography on air temperature and precipitation are represented through snow elevation bands. For each model grid cell, snow accumulation and melt is calculated separately for a variable number of bands. Fractional area, average elevation and the fraction of grid cell precipitation falling in the band are specified for each band. The sum of all fractions must be one to conserve mass. A maximum of five bands was used for this application, with fewer bands in areas of low topographic relief. Each grid cell is divided into equal elevation width bins based on the maximum and minimum elevation at 5-minute spatial resolution. The area and average elevation of the 5-minute cells that fall into each bin are equal to the band elevation and area. Bands that were separated by less than 500 m were merged together for computational efficiency. Temperature was lapsed using a constant lapse rate of 6.5 °C/km. Precipitation was scaled such that higher elevation bands experienced more precipitation, in proportion to the elevation difference between the bands. These elevation bands are the only way in which partial grid cell snow cover is represented. The inherent patchiness of a melting snow cover and resulting effect on area of energy exchange with the snow pack and local advection are not represented by the model.

4.1.2. Routing Model

When the VIC model is implemented over a grid mesh (e.g. watershed), evapotranspiration, energy fluxes, runoff and baseflow are predicted independently for each grid cell. Streamflow is predicted at a specified location by routing surface and subsurface grid cell runoff using the method of Lohmann et al. [83, 84]. To account for differences in travel time from different areas within a cell, the single runoff time-series produced for each cell by VIC is routed to the cell outlet using a triangular unit hydrograph [83, 84]. The hydrographs for the individual cells are routed to the basin

outlet through a channel network, in which cells are connected in the direction of major flow to one of the 8 adjacent cells (Figure 13). All flow from a cell is routed in a single direction. For cells at the edge of the basin, the relative proportion lying within the basin may be specified, allowing the conservation of the true basin area. The routing network for this application was developed manually using GIS overlays of the main river systems on the delineated basins. Flow directions for each grid cell were determined by visual inspection.

The routing model is operated independently from the VIC hydrologic model. Therefore, although the unit hydrograph can be used to control the response time from each model grid cell, it does not represent the ponding and continued evaporation of surface water in low topography areas. The same is true for the effects of large lakes on the inter-cell channel routing scheme. As such, the current model does not explicitly represent the effects of lakes and wetlands.

4.1.3. Model implementation

The VIC model was applied to the Mackenzie and Ob River basins at 2 degree spatial resolution (see Figure 13) and daily temporal resolution. Two southerly sub-basins of the Ob and Mackenzie Rivers, the Irtish and the Athabasca, respectively, were also modeled (hashed in Figure 13). Simulation of smaller sub-basins facilitates model implementation by decreasing computation time at the calibration stage. Also, it allows assessment of the transferability of the more empirical model parameters. In particular, the Irtish and Athabasca sub-basins were selected for their southerly locations and contrasting landforms, as described below.

The Mackenzie River drains an area of 1.66 million km^2 in northern Canada, centered at approximately 115° W and 63° N. It includes the Great Bear Lake, Great Slave Lake and Lake Athabasca, which account for about 4% of the drainage area. Water flows north from latitude 49° N to the mouth at the Beaufort Sea at latitude 69° N. Basin elevations range from over 3500 m in the Rocky and Mackenzie Mountains in the west to sea level. The Athabasca River above McMurray flows east from headwaters in the Rocky Mountains and drains an area of 133,000 km^2. The basin contains some isolated permafrost patches in the mountains and vegetation consists of primarily coniferous and mixed coniferous forest.

The Ob River (basin centroid 78° E and 59° N), drains an area of 2.95 million km^2 of the Siberian plains. The Ural Mountains form the western basin boundary, but because of the relatively flat landscape the eastern boundary is somewhat unclear. The Ob River originates in China at latitude 48° N and flows north to 69° N were it enters the Gulf of Ob. The Irtish River above Omsk drains 321,000 km^2 of wooded steppe and steppe highlands in the southernmost Ob basin. The Irtish basin is not significantly affected by permafrost.

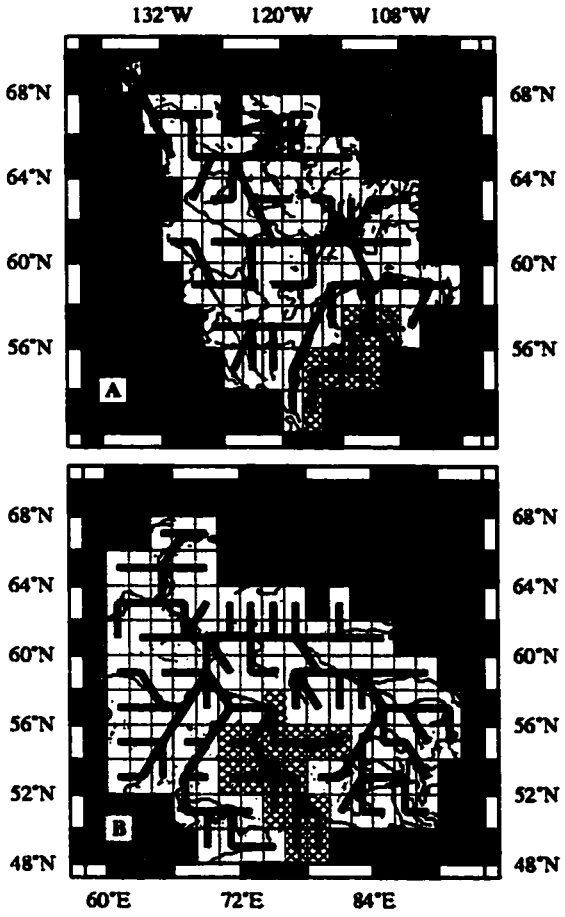

Figure 13. Routing networks for A) the Mackenzie (white) and Athabasca (hashed) Rivers and B) the Ob (white) and Irtish (hashed) Rivers

The required meteorological inputs for the water balance mode of the VIC model are daily minimum and maximum air temperature (also used to infer solar and longwave radiation) and precipitation. Precipitation for the period 1979 to 1993 was taken from [74] and adjusted for gauge catch deficiencies as described in Section 3.1. Gridded minimum and maximum temperature station data were adjusted to match the mean monthly temperature climatology of [85]. A five-year period from January 1979 to December 1983 was used for calibration, however the first year (1979) was used for model initialization and is not shown in subsequent results. The remaining ten years from January 1984 through December 1993 were used for model evaluation. This ten-year period was used in the model interpretation in Section 5.

4.2. MODEL CALIBRATION

Soil and vegetation parameters were based on a data set produced by the International Satellite Land Surface Climatology Project (ISLSCP), also used by [74] in their global simulations. The vegetation parameters were left unchanged, as follows:

- Architectural resistance: 40 s/m (overstory), 10 s/m (understory);
- Minimum stomatal resistance: 80-140 s/m (overstory), 80 s/m (understory);
- Albedo: 20 %; and
- LAI: variable.

Saturated hydraulic conductivity and bulk density were assigned categorical values based on soil texture suggested by the ISLSCP. The maximum velocity of baseflow (D_{smax}) was calculated from average surface slope and saturated hydraulic conductivity. These values were not adjusted during calibration. The most sensitive soil parameters in this work were the infiltration capacity curve shape factor, b_{inf}, the baseflow parameter D_s, the fraction of maximum baseflow at which the baseflow formulation changes from a linear to a nonlinear function of soil moisture W_s, and the upper and lower soil depths. These parameters were changed during calibration. Table 3 shows the values of the parameters used. Constant values were used throughout each of the simulated basins since no coherent procedure was available for adjusting them spatially based on available information. The depth of the top soil layers is realistic only if viewed as a surrogate for surface water storage, which is not represented by the model. Baseflow is only removed from the bottom layer, so moisture retained in the top layer is available for evapotranspiration as it slowly percolates to the bottom layer.

TABLE 3. Model Soil Parameters

Soil parameters	Ob	Irtish	Mackenzie	Athabasca
Infiltration parameter, b_i	0.1	0.1	0.25	0.1
Fraction of maximum soil moisture, Ws	0.99	0.98	0.99	0.8
Fraction of maximum baseflow, Ds	0.008	0.01	0.001	0.0275
Top layer depth (m)	2.0	1.0	1.5	0.8
Bottom layer depth (m)	1.0	0.5	0.5	0.1

The VIC model was calibrated for the Mackenzie and Ob basins, as well as the Athabasca and Irtish sub-basins (Figures 14 and 15). The mean monthly flows for the Mackenzie River from 1980 – 1993 (Figure 14a) indicate that the volume of the snowmelt peak is captured fairly well, although the initial rise is too slow, resulting in an extension of the peak flow into July. This may be due to overcompensation for surface storage effects in the top soil layer, which are actually due to storage in the large lakes of the lower Mackenzie Basin. The constant values of soil storage that are not correlated with true wetland locations prevent quick runoff response from non-wetland areas. In addition, the difference in simulated and observed hydrographs may reflect errors in representation of snowmelt at the highest latitudes. The same problem is not evident in the Athabasca River (Figure 14b) in which the simulated annual peak and recession is too abrupt. It is interesting to note that although the Athabasca sub-basin is at the southern end of the Mackenzie basin and upstream of the three major lakes, the annual peak occurs about one month after that of the Mackenzie. For the most part the

Athabasca basin is not underlain by permafrost, while a significant portion of the Mackenzie Basin is. Another causative factor is the higher average elevation of the Athabasca basin, and hence later snowmelt.

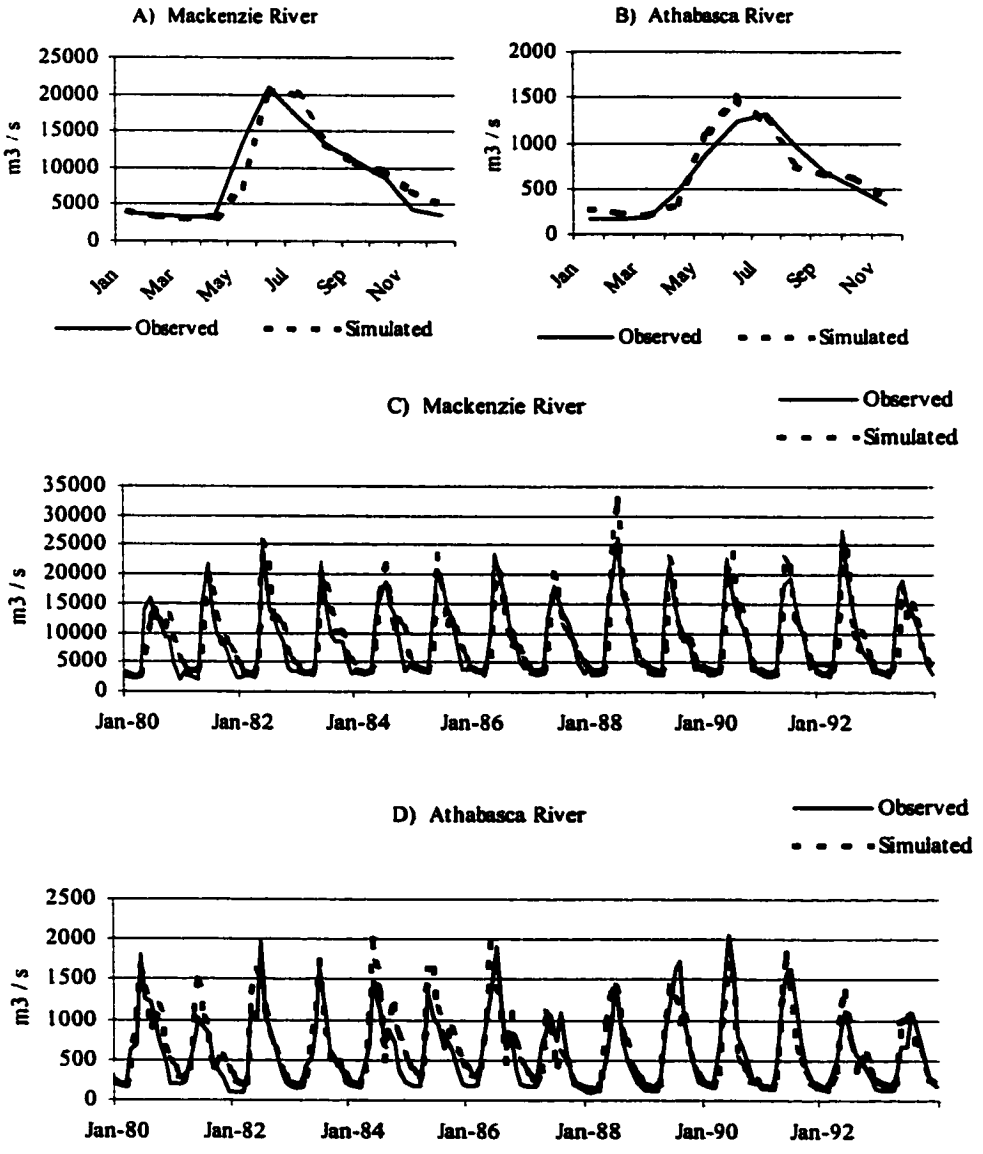

Figure 14. Observed versus simulated hydrographs 1980-1993: A&B) Mackenzie and Athabasca Rivers mean seasonal hydrograph, C&D) Mackenzie and Athabasca monthly hydrographs

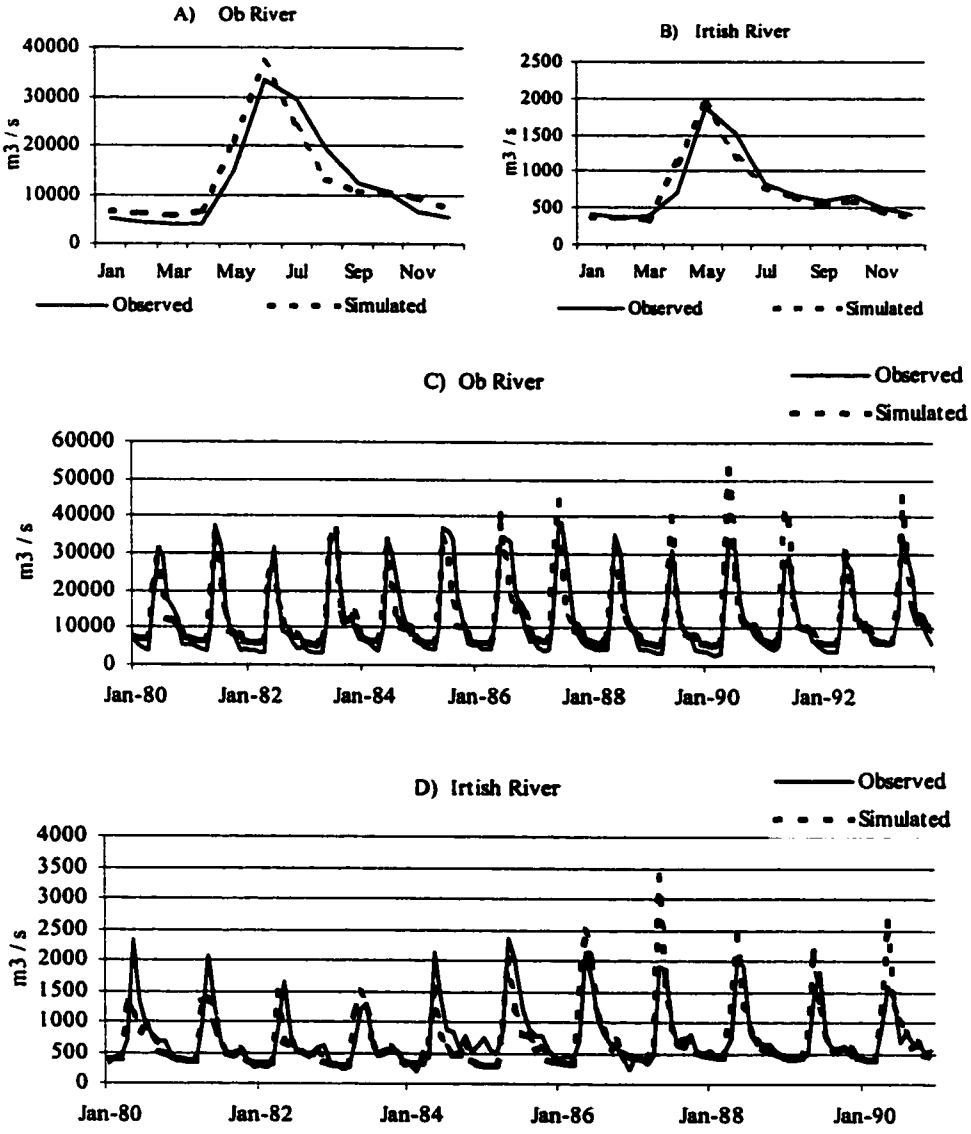

Figure 15. Observed versus simulated hydrographs 1980-1993: A&B) Ob and Irtish mean seasonal hydrographs, C&D) Ob and Irtish monthly hydrographs

Although the timing of the snowmelt peak is well-matched for both the Ob and the Irtish Rivers, Figures 15a and 15b show that in both basins the rising and recession limbs are too steep. Although the Ob basin is not effected by large lake storage to the extent of the Mackenzie basin, it does contain much more extensive wetlands. The overly steep recession may be due to a lack of representation of this storage effect or due

to an over-prediction of the rate of melt of high-altitude snow cover in the southern steppe region. The monthly hydrograph for the Irtish River (Figure 15d) indicates that both the simulated and observed series have more interannual variability than do the other rivers. However, the simulated and observed variability are out-of-phase, which suggests that the model is not entirely representing the over-year storage effects of the natural system.

The observed and simulated mean numbers of days with snow cover are shown in Figure 16. The observed number of days with snow cover were derived from maps of weekly snow extent provided by the EOS DAAC. Because the snow model is a physically-based energy balance model, there is little calibration involved. The maximum temperature at which precipitation can fall as snow and the minimum temperature at which precipitation can fall as rain were fixed at 1.5 and –0.5° C, respectively. Snow surface roughness was fixed at 1 mm. On average, the length of the simulated snow season is slightly over-estimated, but maintains the correct spatial distribution. There appears to be greater spatial variability in the simulated snow cover extent than in the observations (Figures 16 a and b, respectively).

Although sublimation directly from the snowpack and from canopy interception are represented by the VIC snow model, the enhanced rate of sublimation during blowing snow events is not. Modeled sublimation ranged spatially from –9 to 64% of snow precipitation (average of 27%) for the Ob basin and between –6 and 56% (average of 37%) for the Mackenzie basin. Areas of high sublimation coincide with areas of dense forest.

5. Interpretation of Simulation Results

Interpretation of hydrologic model results facilitates analysis of the macroscale hydrology of the Arctic for variables not directly observed at a useful resolution, and also serves as a useful diagnostic tool for existing data sets and global models. For example, Figure 17 shows model-simulated evapotranspiration in comparison to the DAO derived evapotranspiration. The DAO evapotranspiration is probably unrealistically high in the Ob basin, for reasons discussed in part in Section 3. In general, the spatial patterns and magnitudes of evapotranspiration from the hydrology model are more believable, perhaps in part because the model results are constrained by runoff and precipitation, at least at the catchment scale.

Figure 18a shows the percent runoff ratio for the Ob and Mackenzie River basins over the period of simulation. This figure is similar to Figure 9c, but at a higher spatial resolution. It shows that a higher percent of precipitation results in discharge at higher latitudes in the Ob basin than in the Mackenzie basin. In the Ob basin, evapotranspiration is controlled more by latitude than by elevation, due to the low relief of much of the basin. This trend is not clear in the Mackenzie basin, where increased storage creates a lower runoff ratio in the central part of the basin. The maximum rate of baseflow in the model is controlled by the topographic gradient. In the flat, central part of the Mackenzie basin, baseflow is lower, so moisture stored at or near the surface is available for evapotranspiration for a longer time period.

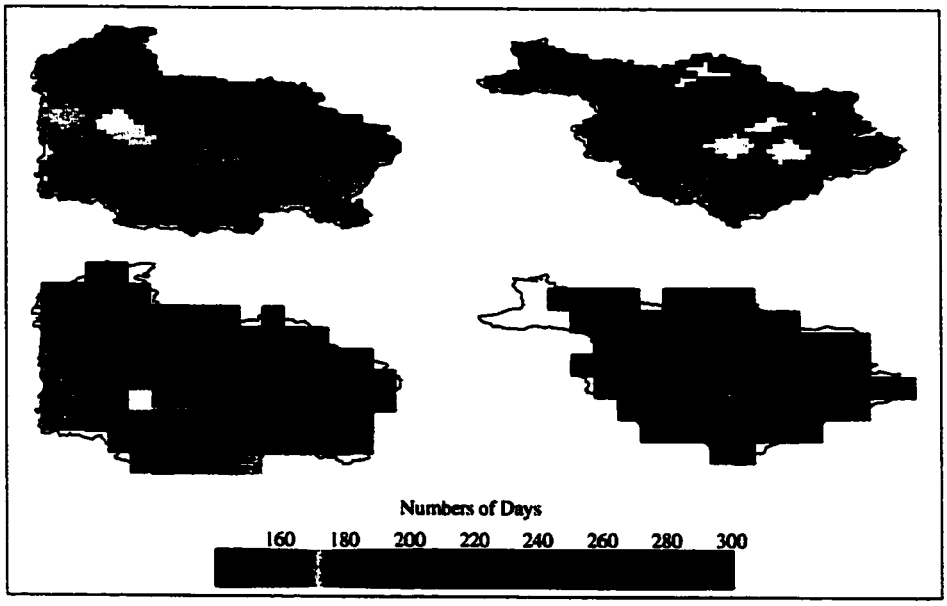

Figure 16. Remotely sensed (top) and simulated (bottom) number of days with snowcover. A) Ob River and B) Mackenzie River

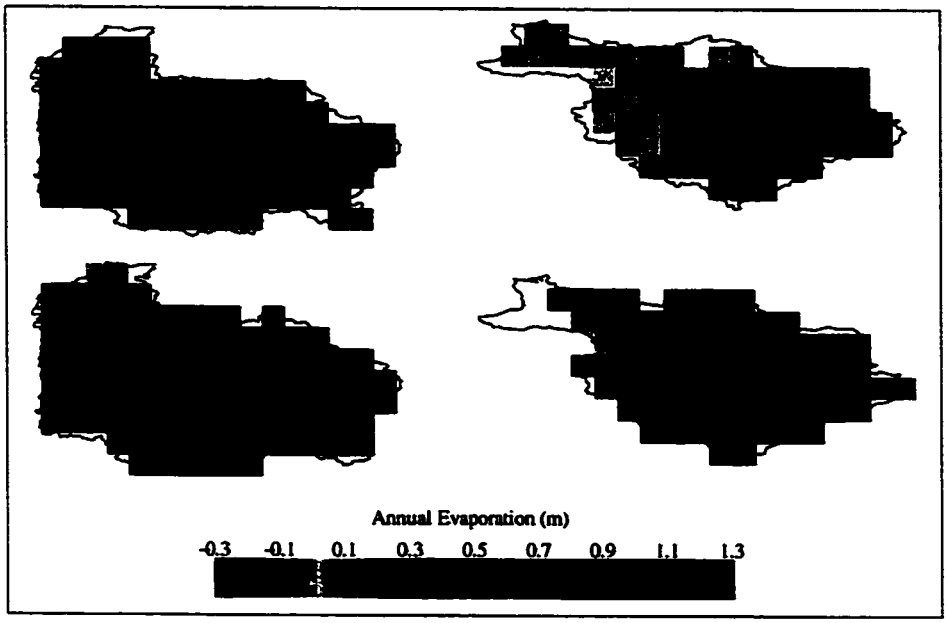

Figure 17. Annual evaporation derived from DAO reanalysis fields (top) and simulated (bottom). A) Ob River and B) Mackenzie River

The percentage of runoff derived from snow (mean maximum snow water equivalent (SWE)/annual runoff) is shown in Figure 18b. These results neglect the effect of infiltration and evapotranspiration of meltwater, and therefore it is possible to have SWE greater than the observed discharge. The greatest percentages of SWE over runoff coincide with the areas of smallest percent runoff in Figure 18a (in particular in the southern steppe region of the Ob basin). Higher values of maximum SWE relative to runoff are expected in low runoff areas, where meltwater is subject to greater evaporation. However, snow accumulations approaching 500% of observed runoff may not be explainable in terms of evaporation alone. The high percentages occur in a region of cold temperatures resulting in a higher proportion of snow accumulation (Figure 18c). The cold areas are also areas of low runoff (Figure 18a), so we are taking ratios of smaller numbers, resulting in large relative changes for small absolute changes. In addition, since this is a non-forested area, it may be subject to significant sublimation from blowing snow. This effect is not represented by the model, so the resulting overprediction of SWE could explain the excessively high percentage of snow accumulation relative to runoff. Figure 18c shows that the mean maximum SWE as a percentage of annual precipitation decreases with latitude in the Mackenzie basin, starting with 50% at the northernmost latitudes. This trend is not as clear in the Ob basin.

The spatial and interannual variability of runoff is explored in Figure 19 through the coefficients of variability of runoff ratio, runoff due to precipitation and runoff due to snowmelt. The average C_v's of runoff ratios in both the Ob (mean = 0.27) and Mackenzie (mean = 0.40) basins are higher than those reported by Grabs et al. [4] for total basin runoff. However, many of the individual grid cell values are consistent with estimates from discharge at the basin outlet and a few regions of high variability elevate the average (Figure 19a). The Mackenzie basin contains an area of very low variability consistent with the low rates of base flow in the approximate location of the Great Bear and Great Slave Lakes. The variability in runoff is predominately due to variation in annual runoff minus the maximum annual SWE (surrogate for runoff due to rain precipitation - Figure 19c). This value is much more variable than the maximum annual SWE (Figure 19b), which corresponds to the runoff due to snowmelt.

6. Conclusions

The Arctic drainage basin is defined as all land surfaces that drain to the Arctic Ocean. It spans 37° of latitude and 360° of longitude and encompasses several mountain ranges, as well as extensive coastal plains and lowland boreal forests. Vegetation varies from boreal forest in the south to sparse Arctic tundra in the north.

The controls on runoff of medium to large Arctic rivers in this vast area were investigated through review of field experiments, exploratory data analysis and interpretation of hydrologic model results. This analysis suggests the following:

- The spatial distribution of runoff production within the Arctic drainage basin is primarily controlled by latitude and orography, as a result of trends in precipitation and evaporation.

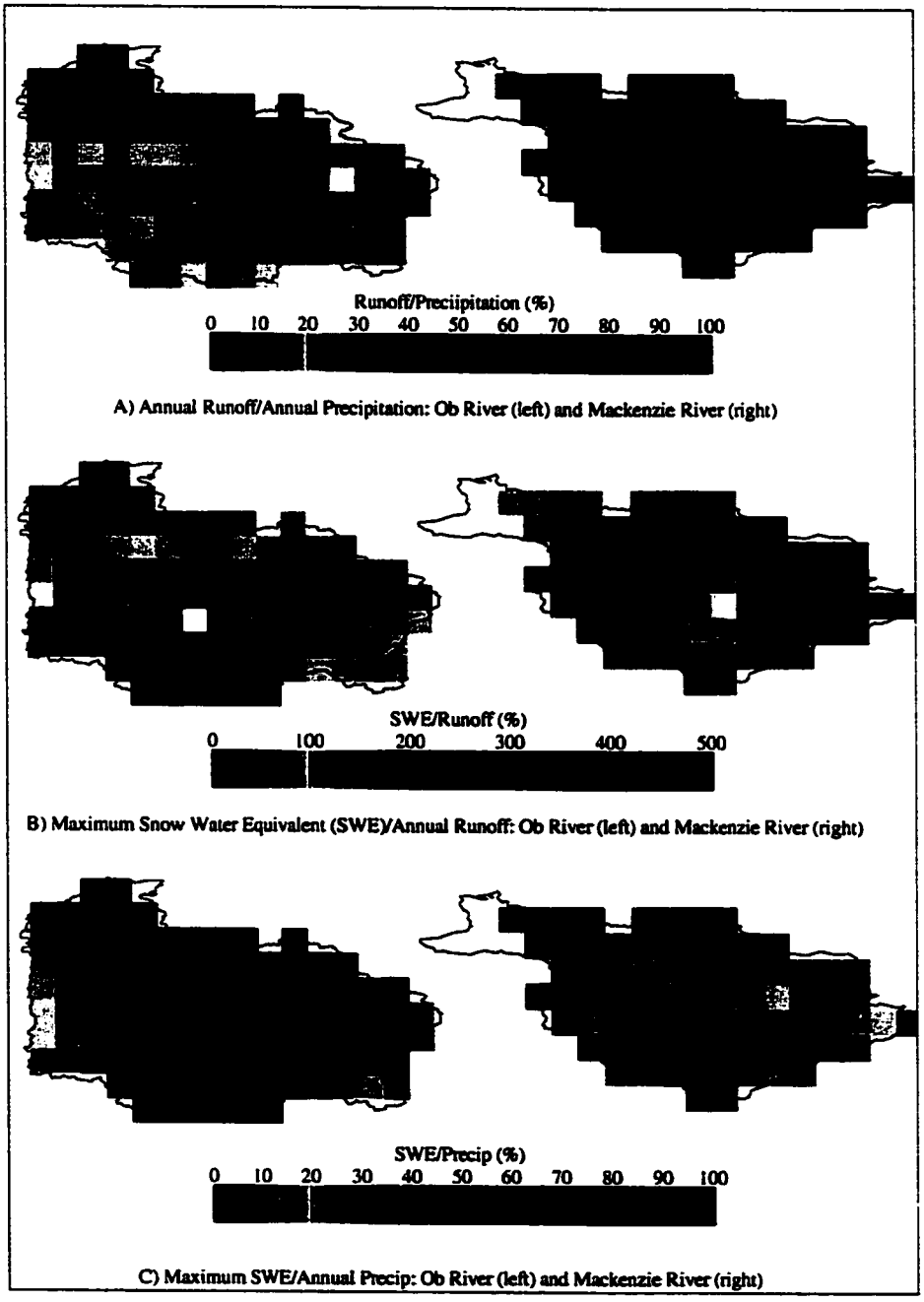

Figure 18. Simulated Water Balance Components

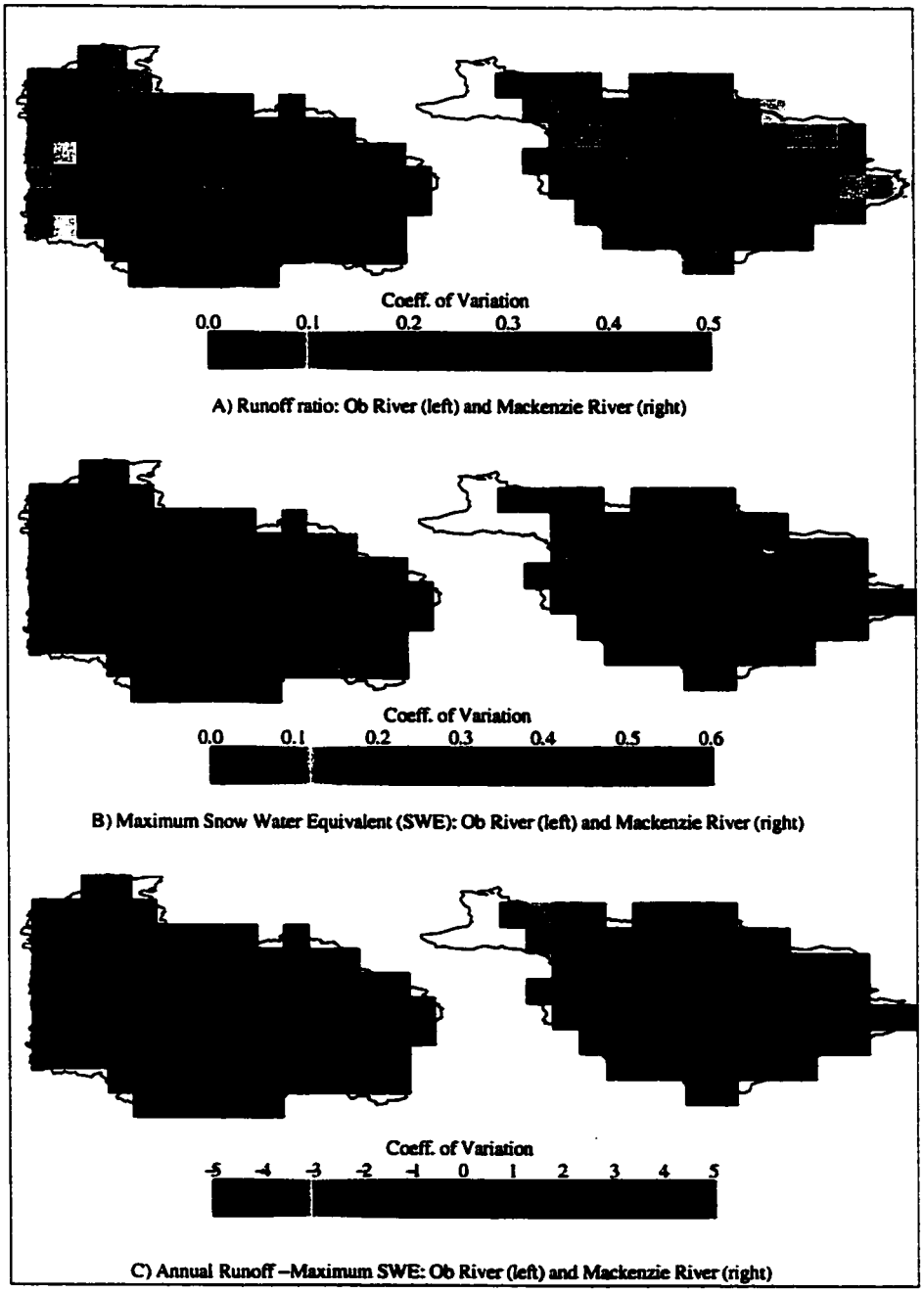

Figure 19. Coefficient of Variation of Simulated Water Balance Components

- Surface storage, primarily in lakes and wetlands, suppresses both the interannual and seasonal variability of North American rivers relative to Eurasian rivers.
- Runoff interannual variability is not related to interannual variability in snow extent for large rivers. The majority of interannual variability in runoff is explained by variations in precipitation for small rivers.
- Preliminary application of a macroscale hydrologic model to the Mackenzie and Ob basins demonstrates the potential of hydrologic models to provide a continuous spatial and temporal trace of hydrologic variables, such as evapotranspiration and snow cover, that can be used as diagnostic tools in data scarce regions. As is the case with atmospheric data assimilation, the results are somewhat model dependent. However, in contrast to atmospheric assimilation methods, the macroscale hydrology model is constrained to preserve a moisture balance at the land surface.
- Exploratory data analysis in Sections 2 and 3 of this paper suggests the importance of physical processes that are not represented by the current model generation. These processes include sublimation from blowing snow, surface storage in lakes and wetlands and infiltration limitation by frozen soils. The extent to which more detailed process representations will improve current model simulations is, however, unclear due to the paucity of observational data.

7. Future Research Priorities

The analysis performed to date has demonstrated that a macroscale hydrologic model can replicate the timing and variability of fresh water fluxes to the Arctic Ocean from large northern river systems. However, it has also illuminated potential concerns, which may increase in importance when transferring the model to the smaller, ungauged catchments of the Arctic drainage basin. Resolution of these concerns points to the following research needs:

- Future work in this area is constrained by the availability of surface meteorological data at appropriate space-time resolutions. The primary need is to assemble a retrospective precipitation data set of the highest possible quality including gauge correction, at least one decade in duration.
- Understanding of land surface processes should be developed from both models and data, with a focus on surface energy exchange, and in particular the snow vapor flux, as well as the water cycle.
- Future modeling must focus on the land surface processes of the entire Arctic basin. The spatial variability of surface water impoundment by lakes and wetlands, and frozen soil cannot be captured by parameterizations that represent spatially averaged processes at the resolution of a model grid cell. Computationally efficient process representations of these processes, perhaps in a derived distribution context, are needed.

8. References

1. Alekseev, G. and Buzuev, A. (1973) On the evolution of the ice-surface layer of the ocean system in the region of drift of the Severniya Polyus-16 station, *Problems of the Arctic and Antarctic* **42**, 37-43.
2. Treshnikov, A.F. (1985) Main stages and prospects of study in the polar regions of the Earth, in *Problems of the Arctic and the Antarctic, Collection of Articles* **57**, 1-19.
3. Aagaard and Carmack (1989) The role of sea ice and other freshwater in the Arctic circulation, *Journal of Geophysical Research*, **94 c**, 14485-14498.
4. Grabs, W.E., Portmann, F., de Couet, T. (1999) Discharge observation networks in Arctic regions: computation of the river runoff into the Arctic Ocean, its seasonality and variability, this volume.
5. WCRP (1996) Report of the fourth session of the WCRP ACSYS scientific steering group, Toronto, Canada, October 11-14, 1995, WCRP informal report N10.
6. WCRP (1994) Arctic Climate System Study (ACSYS) Initial Implementation Plan, WCRP-85, WMO/TD-No. 627.
7. Anisimov, O.A. and Nelson, F.E. (1997) Permafrost zonation and climate change in the northern hemisphere: results from transient general circulation models *Climate Change*, **35**, 241-58.
8. Foster J., Liston, G., Koster, R. Essery, R., Behr, H., Dumenil, L. Verseghy, D., Thompson, S., Pollard, D. and Cohen, J. (1996) Snow cover and snow mass intercomparisons of general circulation models and remotely sensed datasets, *Journal of Climate* **9**, 409-26.
9. Kite, G.W., Dalton, A. and Dion, K. (1994) Simulation of streamflow in a macroscale watershed using general circulation model data, *Water Resources Research* **30**, 1547-1559.
10. Kuhl, S.C. and Miller, J.R. (1992) Seasonal river runoff calculated from a global atmospheric model, *Water Resources Research*, **28**, 2029-2039.
11. Arpe, K., Behr, H. and Dumenil, L. (1996) Validation of the ECHAM4 climate model and re-analyses data in the Arctic region, *Proceedings of the workshop on the implementation of the Arctic Precipitation Data Archive at the Global Precipitation Climatology Centre*, WMO/TD No. 804, 31-40.
12. Hurst, C. and Serreze, M.C. (1997) The utility of NCEP/NCAR reanalysis for Arctic precipitation studies, *Proceedings, Conference on Polar Processes and Global Climate*, Part I of II, 100-102.
13. Serreze, M.C. and Maslanik, J.A. (1997) Arctic precipitation as represented in the NCEP/NCAR reanalysis, *Annals of Glaciology*, **25**.
14. Bromwich, D.H. (1997) The atmospheric moisture budget of the Arctic and Antarctic from atmospheric numerical analyses, *Proceedings, Conference on Polar Processes and Global Climate*, Part I of II, 30-32.
15. Genthon, C. (1997) Convergence of energy and moisture to the Arctic and Antarctic polar caps from ECMWF re-analyses, *Proceedings, Conference on Polar Processes and Global Climate*, Part I of II, 60-62.
16. Oki, T., Musiake, K., Matsuyama, H. and Masuda, K. (1995) Global atmospheric water balance and runoff from large river basins, *Hydrological Processes* **9**, 655-678.
17. Molod A., Helfand, H.M. and Takacs, L.L. (1996) The climatology of parameterized physical processes in the GEOS-1 GCM and their impacts on the GEOS-1 Data Assimilation system, *Journal of Climate* **9**, 764-785.
18. Walsh, J.E. and Kattsov, V. (1996) Data requirements for validation of climate model simulations and reanalyses of arctic precipitation, *Proceedings of the workshop on the implementation of the Arctic Precipitation Data Archive at the Global Precipitation Climatology Centre*, WMO/TD No. 804, 19-25.
19. Woo, M.K. and Winter, T.C. (1993) The role of permafrost and seasonal frost in the hydrology of northern wetlands in North America, *Journal of Hydrology* **141**, 5-31.
20. Anderson, J.R., Hardy, E.E., Roach, J.T. and Witmer, R.E. (1976) A land use and land cover classification system for use with remote sensor data, U.S. Geological Survey Professional Paper 964.
21. Serreze, M.C., Rehder, M.C., Barry, R.G. and Kahl, J.D. (1995) The distribution and transport of atmospheric water vapour over the Arctic basin, *International Journal of Climatology*, **15**, 709-27.
22. Hinzman, L.D., Kane, D.L., Benson, C.S. and Everett, K.R. (1996) Energy balance and hydrological processes in an Arctic watershed, *Ecological Studies* **120**, 131-154.

23. Marsh, P., Quinton, W. and Pomeroy, J. (1994) Hydrological processes and runoff at the Arctic treeline in northwestern Canada, *Proceedings, 10th Inter. Northern Research Basins Symp. And Workshop*, Trondheim, Norway, Norwegian Institute of Technology, 368-397.
24. Moskvin, Y.P. (1989) Runoff from hummocky marshes of western Siberia, *Soviet Meteorology and Hydrology* **3**, 73-80.
25. Storr, D. and Golding, D.L. (1974) A preliminary water balance evaluation of an intensive snow survey in a mountainous watershed, in *Advanced Concepts and Techniques in the Study of Snow and Ice Resources*, Nat. Acad. Sci., Washington, D.C., pp. 294-303.
26. Walsh, J.E., Zhou, X., Portis, D. and Serreze, M.C. (1994) Atmospheric contribution to hydrologic variations in the Arctic, *Atmosphere-Ocean* **32**, 733-755.
27. Brown, J., Ferrians, O.J. Jr., Heginbottom, J.A. and Melnikov, E.S. (1997) Circum-Arctic map of permafrost and ground-ice conditions, United States Geological Survey, Circum-Pacific Map Series, CP-45, Reston, VA, USA.
28. Bjornsson, H., Mysak, L.A. and Brown, R.D. (1995) On the interannual variability of precipitation and runoff in the Mackenzie drainage basin, *Climate Dynamics* **12**, 67-76.
29. Pavlov, V.K. and Stanovoy, V.V. (1997) Climatic signal in the fluctuations of the sea level and river run-off in the Arctic Ocean, *Proceedings, Conference on Polar Processes and Global Climate*, Part II of II, 184-186.
30. Stele, M. (1996) A simple model of the Arctic Ocean freshwater balance, 1979-1985, *Journal of Geophysical Research* **101c**, 20833-20848.
31. Vuglinsky, V.S. (1997) River water inflow to the Arctic Ocean - conditions of formation, time variability and forecasts, *Proceedings, Conference on Polar Processes and Global Climate*, Part II of II, 275-276.
32. Sokolov, A.A. (1965) On the excess of maximum discharges of summer-fall rain floods over discharges of spring high water, *Soviet Hydrology* **5**, 476-482.
33. Woo, M.K. and Steer, P. (1983) Slope hydrology as influenced by thawing of the active layer, Resolute, N.W.T., *Canadian Journal of Earth Sciences* **20**, 978-86.
34. Kane, D.L. and Hinzman, L.D. (1988) Permafrost hydrology of a small Arctic watershed, In: B.A. Senneset-Kaare (ed) , *Permafrost: fifth international conference* **1**, International Conference on Permafrost, Proceedings, pp. 590-595.
35. Roulet, N.T. and Woo, M.K. (1986) Hydrology of a wetland in the continuous permafrost region, *Journal of Hydrology* **89**, 73-91.
36. Untersteiner, N. (1984) The cryosphere, in *Global Climate*, Cambridge, Cambridge, U.K., pp. 121-40.
37. Shea, D. (1986) Climatological atlas: 1950-1979, surface air temperature, precipitation, sea-level pressure and sea-surface temperature (45°S–90°N), *Tech. Note/TN-269+STR*, Natl. Center for Atmospheric Research, Boulder, Colorado.
38. Legates, D.R. and Willmott, C.J. (1990) Mean seasonal and spatial variability in gauge-corrected, global precipitation/*International Journal of Climatology* **10**, 111-27.
39. Cattle, H. (1985). Diverting Soviet rivers: some possible repercussions for the Arctic Ocean, *Polar Record* **22**, 485-498.
40. Marsh, P. and Bigras, S.C. (1988) Evaporation from Mackenzie delta lakesN.W.T., Canada, *Arctic and Alpine Research* **20**, 220-229.
41. Rovansek, R.J., Hinzman, L.D. and Kane, D.L. (1996) Hydrology of a tundra wetland complex in the Alaskan Arctic coastal plain, U.S.A., *Arctic and Alpine Research*, **28**, 311-317.
42. Bigras, S.C. (1990) Hydrological regime of lakes in the Mackenzie delta, Northwest Territories, Canada, *Arctic and Alpine Research* **22**, 163-174.
43. Zoltai, S.C. (1979) An outline of the wetland regions of Canada, in *Proc. workshop on Canadian wetlands* **12**, Environ. Can., Lands Dir., Ecol. Land Classif. Ser., pp. 1-8.
44. Church, M. (1974) Hydrology and permafrost with referece to northern North America, in *Proceedings Workshop Seminar on Permafrost Hydrology*, Can. Nat. Comm., IHD, Ottawa, pp. 7-20.
45. Woo, M.K. (1988) Wetland runoff regime in northern Canada, in *Permafrost: fifth international conference* **1**, Proceedings, International conference on permafrost, pp. 644-649.
46. Woo, M.K. and Xia, Z. (1996) Effects of hydrology on the thermal conditions of the active layer, *Nordic Hydrology* **27**, 129-142.

47. Jacobs, J.D. and Grandin, L.D. (1988) The influence of an Arctic large-lakes system on mesoclimate in south-central Baffin Island, N.W.T., Canada, *Arctic and Alpine Research* **20**, 212-219.
48. Jeffries, M.O., Zhang, T., Frey, K. and Kozlenko, N. (1999) Estimating late winter heat flow to the atmosphere from the lake-dominated Alaskan north slope, *Journal of Glaciology*, in press.
49. Marsh, P. and Pomeroy, J. (1996) Meltwater fluxes at an Arctic forest-tundra site, *Hydrological Processes* **10**, 1383-1400.
50. Kane, D.L., Hinzman, L.D., Benson, C.S. and Liston, G.E. (1991) Snow hydrology of a headwater Arctic basin, I, *Water Resources Research* **27**, 1099-1109.
51. Woo, M.K. (1982). Snow hydrology in the high Arctic, presented at the western Snow Conference, Reno, Nevada, April 20-23.
52. Pomeroy, J.W., Marsh, P. and Gray, D.M. (1997) Application of a distributed blowing snow model to the Arctic, *Hydrological Processes* **11**, 1451-1464.
53. Li, L. and Pomeroy, J.W. (1997) Probability of occurrence of blowing snow, *Journal of Geophysical Research* **102d**, 21955-64.
54. Mikhel, V.M. and Rudneva, A.V. (1967) Regionalization of the USSR according to the transport of snow, *Soviet Hydrology* **5**, 441-449.
55. Shook, K. and Gray, D.M. (1996) Small-scale spatial structure of shallow snowcovers, *Hydrological Processes* **10**, 1283-1292.
56. Woo, M.K., Heron, R., Marsh, P. and Steer, P. (1983) Comparison of weather station snowfall with winter snow accumulation in High Arctic basins, *Atmosphere-Ocean* **21**, 312-325.
57. Woo, M.K. (1976) Hydrology of a small Canadian high Arctic basin during the snowmelt period, *Catena* **3**, 155-168.
58. Takeuchi, Y., Kodama, Y. and Nakabayashi, H. (1995) Characteristics of evaporation in Spitsbergen in the snowmelt season, 1993, *Proceedings of the NIPR Symposium on Polar Meteor. And Glaciol.*, 54-65.
59. Pomeroy, J.W. and Li, L. (1997) Development of the Prairie Blowing Snow Model for application in climatological and hydrological models, in *Proceedings of the Eastern Snow Conference* **54**, pp. 186-197.
60. Pomeroy, J.W., Gray, D.M. and Landine, P.G. (1993) The Prairie Blowing Snow model: characteristics, validation, operation, *Journal of Hydrology* **144**, 165-192.
61. Pomeroy, J.W. and Gray, D.M. (1995) Snowcover accumulation, relocation and management, *National Hydrology Research Institute Science Report No. 7*, NHRI Environment Canada, Saskatoon, 144 pp.
62. Dyunin, A.K. (1959) Fundamentals of the theory of snow drifting, *Izvest. Sibirsk, Otdel, Akad. Nauk. USSR* **12**, 11-24. [English translation by Belkov, G. 1961 Technical Translation 952, National Research Council of Canada, Ottawa.
63. Schmidt, R.A. (1972) Sublimation of wind-transported snow – a model, Research Paper RM-90, USDA Forest Service, Rocky Mountain Forest and Range Experimental Station, Fort Collins, 24 p.
64. Pomeroy, J.W. (1989) A process-based model of snow drifting, *Ann. Glaciol.* **13**, 237-240.
65. Groisman, P.Y., Golubev, V.S., Genikhovich, E.L. and Bomin, S. (1997) Evaporation from snow cover: an empirical study, in *Proceedings, Conference on Polar Processes and Global Climate*, Part I of II, pp. 72-73.
66. Deryugin, A.A. (1990) Snow cover on small forest and field watersheds in the taiga zone of European USSR, *Soviet Hydrology and Meteorology* **1**, 101-105.
67. Are, A.L. and Petropavlovskaya, M.S. (1982) Spring snow melting and evaporation of snow in central Yakutia, *Soviet Meteorology and Hydrology* **2**, 72-76.
68. Krestovskiy, O.I., Postnikov, A.N. and Sergeyeva, A.G. (1972) Evaporation during the snow melting and flood period in spring, *Soviet Hydrology* **5**, 439-451.
69. Harding, R.J. and Pomeroy, J.W. (1996) The energy balance of the winter boreal landscape, *Journal of Climate* **9**, 2778-87.
70. Davis, R.E., Hardy, J.P., Ni, W., Woodcock, C., McKenzie, J.C., Jordan, R. and Li, X. (1997) Variation of snow cover ablation in the boreal forest: a sensitivity study on the effects of conifer canopy, *Journal of Geophysical Research* **102 d**, 29389-95.
71. Pomeroy, J.W. and Schmidt, R.J. (1993) The use of fractal geometry in modelling intercepted snow accumulation and sublimation, in *Proc. Eastern Snow Conference* **50**, pp. 1-10.

72. Hedstrom, N.R. and Pomeroy, J.W. (1998) Measurements and modelling of snow interception in the boreal forest, *Hydrological Processes* **12**, 1611-1625.
73. Golding, D.L. (1978) Calculated snowpack evaporation during chinooks along the eastern slopes of the Rocky Mountains in Alberta, *Journal of Applied Meteorology* **17**, 1647-51.
74. Schnur R. and Lettenmaier, D.P. (1997) A global gridded data set of soil moisture for use in General Circulation Models, Poster presented at the 13th conference on hydrology, 77th AMS annual meeting, Long Beach, CA, February 7.
75. Huffman, G.J., Adler, R.F., Arkin, P.A., Chang, A., Ferraro, R., Gruber, A., Janowiak, J., Joyce, R.J., McNab, A., Rudolf, B., Schnieder, U. and Xie, P. (1997) The Global Precipitation Climatology Project (GPCP) Combined Precipitation data set, *Bulletin of the American Meteorological Society* **78**, 5-20.
76. Legates, D.R. (1987) A climatology of global precipitation, *Climatology* **40**.
77. Schubert, S.D., Rood, R.B. and Pfaendtner, J. (1993) An assimilated data set for earth science applications, *Bulletin of the American Meteorological Society* **74**, 2331-2342.
78. Canadian National Committee for the International Hydrological Decade (1978) *Hydrological Atlas of Canada*, Ottawa, Secretariat, Canadian National Committee for the International Hydrological Decade.
79. Liang, X., Lettenmaier, D.P., Wood, E.F. and Burges, S.J. (1994) A simple hydrologically based model of land surface water and energy fluxes for general circulation models, *Journal of Geophysical Research* **99 d**, 415-428.
80. Liang, X., Lettenmaier, D.P. and Wood, E.F. (1996) One-dimensional statistical dynamic representation of subgrid spatial variability of precipitation in the two-layer Variable Infiltration Capacity model, *Journal of Geophysical Research* **101d**,403-21,422.
81. Cherkauer, K.A. and Lettenmaier, D.P. (1999) Hydrologic effects of frozen soils in the Upper Mississippi River basin, *Journal of Geophysical Research* **104 d**, 19,599-610.
82. Storck, P. and Lettenmaier, D.P. (1999) Predicting the effect of a forest canopy on ground snow accumulationand ablationin maritime climates, in C. Troendle (ed), *67th Western Snow Conference*, Colorado State University.
83. Lohmann, D., Raschke, E., Nijssen, B. and Lettenmaier, D.P. (1998a) Regional scale hydrology: I. Formulation of the VIC-2L model coupled to a routing model, *Hydrological Sciences Journal* **43**, 131-141.
84. Lohmann, D., Raschke, E., Nijssen, B. and Lettenmaier, D.P. (1998b) Regional scale hydrology: II. Application of the VIC-2L model to the Weser River, Germany, *Hydrological Sciences Journal* **43**, 143-157.
85. Jones, P. D. (1994) Hemispheric surface air temperature variations: A reanalysis and an update to 1993, *Journal of Climate* **7**, 1794-1802.

VITA

Laura C. Bowling

Office:
202 A Wilson Ceramics Lab; Box 352700
Department of Civil and Environmental Engineering
University of Washington
Seattle, WA 98195
(206) 685-1796
(206) 685-3836 (fax)

Home:
10736 20th Avenue NE
Seattle, WA 98125
(206) 365-5966

Email: lxb@hydro.washington.edu
WWW: http://www.ce.washington.edu/~lxb/

ACADEMIC PREPARATION

Ph.D. in Civil and Environmental Engineering. University of Washington, Seattle, WA. Expected Summer 2002

- Concentrations: Hydrologic modeling, surface water hydrology, cold season processes
- Dissertation: Estimating the fresh water budget of Arctic land surfaces
- Advisor: Dr. Dennis P. Lettenmaier

M.S.C.E. in Civil and Environmental Engineering. University of Washington, Seattle, WA, 1997.

- Concentrations: Hydrologic modeling, forest hydrology, hillslope processes
- Thesis: Evaluation of the effects of forest roads on streamflow in Hard and Ware Creeks, Washington
- Advisor: Dr. Dennis P. Lettenmaier

B.S.E. in Civil Engineering and Operations Research. Princeton University, Princeton, NJ, 1993.

- Concentrations: Hydrogeology, water resources and systems optimization
- Thesis: Investigation of two-dimensional flow processes and channel erosion, Watt's Branch, Maryland
- Advisors: Dr. James A. Smith and Dr. Eric F. Wood